

UNIVERSITÀ  
DEGLI STUDI  
DI PADOVA

Sede Amministrativa: Università degli Studi di Padova  
Dipartimento di Ingegneria dell'Informazione

SCUOLA DI DOTTORATO DI RICERCA IN: Ingegneria dell'Informazione  
INDIRIZZO: Bioingegneria  
CICLO: XXVIII

# COMBINING MUSCULOSKELETAL MODELING AND FEM IN DIABETIC FOOT PREVENTION

**Direttore della Scuola:** *Ch.mo Prof. Matteo Bertocco*

**Supervisore:** *Ch.mo Prof. Claudio Cobelli*

**Dottorando:**  
*Alessandra Scarton*



To love is to suffer.  
To avoid suffering one must not love.  
But then one suffers from not loving.  
Therefore, to love is to suffer;  
not to love is to suffer;  
to suffer is to suffer.  
To be happy is to love.  
To be happy, then, is to suffer,  
but suffering makes one unhappy.  
Therefore,  
to be happy one must love  
or love to suffer  
or suffer from too much happiness.  
— Woody Allen

Alla mia mamma.





# Acknowledgements

I would like to thank **Dr. Zimi Sawacha** for keeping me in the lab after the master thesis and for proposing me to work on this research project. Thanks for letting me travel and experience the research activity in many different places, both in Europe and in USA. Thanks for your comprehension in the most difficult moments, and in all my existential (PhD) crisis.

I would like to acknowledge **Prof. Claudio Cobelli** as well for supporting my ambitions to move around the world and for founding the activities related to the research. I would like to thank all my colleagues at the *Bioengineering of Movement Laboratory of the University of Padova*, for being my friends, and for not forgetting about me when I was abroad: **Fabiola Spolaor**, **Alice Mantoan**, **Annamaria Guiotto**, **Martina Negretto**, and also **Silvia Del Din** and **Alberto Rigato**. Thanks for your friendship and for all the coffee!

I am also grateful to all the people that welcome me in their lab. First of all, I would like to thank **Prof. Ilse Jonkers** for introducing me in the field of musculoskeletal modeling and for being like another supervisor in my activities. Together with her I would like to thank all the people of the *Human Movement Biomechanics Research Group* of the *Department of Kinesiology* of the *Katholieke Universiteit Leuven* and in particular **Wouter Aerts** for the work that we have done together.

I would like to thank **Dr. Xinshan Li** for helping me with the application of the Principle Component Analysis and all the people of the *INSIGNEO Institute for in silico Medicine, Department of Mechanical Engineering, University of Sheffield*. A special thanks goes to **Roberto Di Marco** that was, and luckily for me, still is always available no matter the time zone.

I would like to thank all my colleagues of the *Motion Analysis Lab at Spaulding Rehabilitation Hospital*, in Boston, for the last year spent together. I learned so much that I am almost surprised when I think about it. A special thanks goes to **Giacomo Severini** for making me smile in my deepest and darkest moments of depression, to **Prof. Ugo Della Croce** for the precious biomechanical hints and of course to **Prof. Paolo Bonato**, for believing in me and giving me the opportunity to start a post doc in a prestigious university as Harvard is.

I would like to thank all the people that I met in these three years, who shared a

## Acknowledgements

---

part of their life with me. In particular **Giovana Maffazioli (and Woody Allen), Isabelle Pitteloud, Gabriela Carvalho, Luc Weydert, Edoardo Bonizzoni, Sofia Ferreira, Daniele Ascani, Iain Hannah, Alessandro Melis, Eugene Chang, Francesca Maria Secchi** and **Ambra Spalletta**. You all know why I nominated you.

A special thanks goes to **Alessia Tagliavini** because after the university we shared again all the doubts of the PhD life and to **Giulia Ginami** because all three together are still "ingegnue".

Finally, I am grateful to my dear family, for being my life and for supporting me both economically and psychologically in all my studies.

## Abstract

Recently the development of Patient-specific models (PSMs) tailored to patient-specific data, has gained more and more attention in clinical applications. PSMs could represent a solution to the growing awareness of personalized medicine which allow the realization of more effective rehabilitation treatments designed on the subject capabilities. PSMs have the potential of improving diagnosis and optimizing clinical treatments by predicting and comparing the outcomes of different approaches of intervention. Furthermore they can provide information that cannot be directly measured, such as muscle forces or internal stresses and strains of the bones. Given the considerable amount of diseases affecting motor ability, PSMs of the lower limbs have been broadly addressed in literature. Two techniques are mostly used in this area: musculoskeletal (MS) modeling and finite element (FE) analysis.

(MS) models represent a valuable tool, as they can provide important information about the unique anatomical and functional characteristics of different subjects, through the computation of human internal variables, such as muscle activations and forces and joint contact forces.

The flexibility and adaptability of FE analysis makes it a perfect solution to model biological geometries and materials and to simulate complicated boundary and loading conditions. Accurate and descriptive FE models would serve as an excellent tool for scientific and medical research. Furthermore they could be used in clinical settings if combined with medical imaging, in order to improve patient care.

Several 3-dimensional (3D) foot FE models were recently developed to analyze the biomechanical behavior of the human foot and ankle complex that is commonly studied with experimental techniques like stereophotogrammetry, force and plantar pressure plates.

In this context, many gait analysis protocols have been proposed to assess the 3D kinetics, kinematics and plantar pressure distribution. This evaluation has shown to be useful in characterizing the foot biomechanics in different pathologies like the diabetic foot.

Diabetic foot is an invalidating complication of diabetes mellitus, a chronic disease frequently encountered in the aging population. It is characterized by the development of ulcers which can lead to amputation. Models for simulations of deformations

## Acknowledgements

---

and stresses in the diabetic plantar pad are required to predict high risk areas on the plantar surface and can be used to investigate the performance of different insoles design for optimal pressure relief.

This work represents a first effort towards the definition of a more complete PSM which combining both a MS model and a FE model, can increase the understanding of the diabetic foot pathology. To achieve this objective, several limitations and issues have been addressed.

As first, MS models of diabetic and control subjects were developed using OpenSim, to estimate muscle forces. The objective was to evaluate whether the diabetic population exhibit lower limb muscle strength deficits compared to the healthy one. Subjects routine gait analysis was performed and lower limb joints kinematics, kinetics, time and space parameters estimated by means of a modified version of the IORgait protocol. 3D lower limb joints kinematics and kinetics was also calculated with OpenSim. Both methodologies were able to highlight differences in joint kinematics and kinetics between the two populations. Furthermore MS models showed significant differences in healthy muscle forces with respect to the diabetic ones, in some of the muscles. This knowledge can help the planning of specific training in order to improve gait speed, balance, muscle strength and joint mobility.

After the use of MS models proved to be applicable in the diabetic population, the next step was to combine them with foot FE models. This was done in two phases. At first the impact of applying the foot joints contact forces (JCFs) obtained from MS models as boundary condition on the foot FE models was verified. Subject specific geometries from MRI were used for the development of the foot FE models while the experimental plantar pressures acquired during gait were used in the validation process. A better agreement was found between experimentally measured and simulated plantar pressure obtained with JCFs than with the experimentally measured ground reaction forces as boundary conditions.

Afterwards the use of muscles forces as boundary condition in the FE simulations was evaluated. Subject-specific integrated and synchronized kinematic-kinetic data acquired during gait analysis were used for the development of the MS models and for the computation of the muscle forces. Muscle insertions were then located in the MRI and correspondent connectors were created in the FE model. FE subject-specific simulations were subsequently run with Abaqus by conducting a quasi-static analysis on 4 gait cycle phases and adopting 2 conditions: one including the muscle forces and one without. Once again the validation of the FE simulations was done by means of a comparison between simulated and experimentally measured plantar pressures. Results showed a marked improvement in the estimation of the peak pressure for the model that included the muscles.

Finally, an attempt towards the definition of a parametric foot finite element model

was done. In fact, despite the recent developments, patient-specific models are not yet successfully applied in a clinical setting. One of the challenges is the time required for mesh creation, which is difficult to automate. The development of parametric models by means of the Principle Component Analysis (PCA) can represent an appealing solution. In this study PCA was applied to the feet of a small cohort of diabetic and healthy subjects in order to evaluate the possibility of developing parametric foot models and to use them to identify variations and similarities between the two populations.

The limitations of the use of models have also been analyzed. Their adoption is indeed limited by the lack of verification and validation standards. Even using subjects' MRI or CT data for the development of FEM together with experimentally acquired motion analysis data for the boundary and loading conditions, the subject specificity is still not reached for what regards all the material properties. Furthermore it should be considered that everything relies on algorithm and models that would never be perfectly representing the reality.

Overall, the work presented in this thesis represents an extended evaluation of the possible uses of modeling techniques in the diabetic foot prevention, by considering all the limitations introduced as well as the potential benefits of their use in a clinical context. The research is organized in six chapters:

- *Chapter 1* - provides a background on the modeling techniques, both FE modeling and MS modeling. Furthermore it also describes the gait analysis, its instrumentation and some of the protocols used in the evaluation of the biomechanics of the lower limbs;
- *Chapter 2* - gives a detailed overview of the biomechanics of the foot. It particularly focuses on the diabetes and the diabetic foot;
- *Chapter 3* - introduces the application of MSs for the diabetic foot prevention after a brief background on the techniques usually chosen for the evaluation of the motor impairments caused by the disease. Aim, material and methods, results and discussion are presented. The complete work flow is described, and the chapter ends with a discussion on new key findings and limitations.
- *Chapter 4* – reports the work done to combine the use of musculoskeletal models with foot FEMs. At first the impact of applying the foot joints contact forces obtained from MS models as boundary condition on the foot FEMs is verified. Then the use of muscles forces (again obtained from MS models) as boundary condition in the FE simulations is evaluated. For both studies a brief background is presented together with the methods applied, the results obtained and a discussion of novelties and drawbacks.

## Acknowledgements

---

- *Chapter 5* – explores the possibility of defining a parametric foot FEM applying the Principle Component Analysis (PCA) on the feet of a small cohort of diabetic and healthy subjects. A background on the importance of patient specific models is presented followed by material and methods, results and discussion of what obtained with this study.
- *Chapter 6* - summarizes the results and the novelty of the thesis, delineating the conclusions and the future research paths.

## Sommario

Recentemente lo sviluppo di modelli specifici di un paziente (PSM), cioè creati a partire dai suoi dati, ha guadagnato sempre più attenzione per le possibili applicazioni cliniche. Questi modelli potrebbero, infatti, rappresentare una soluzione alla crescente consapevolezza che la medicina deve essere personalizzata al fine di ottenere un trattamento riabilitativo più efficace e disegnato ad hoc sulle capacità soggetto. Gli PSM hanno il potenziale di migliorare la diagnosi e di ottimizzare la terapia riabilitativa, data la loro capacità di prevedere e di confrontare i risultati di diversi approcci d'intervento. Inoltre essi sono in grado di fornire informazioni che non possono essere direttamente misurate, quali forze muscolari o tensioni interne alle ossa. Data la notevole quantità di malattie che causano deficit motori, gli PSM sono stati ampiamente affrontati in letteratura. Le due tecniche per lo più utilizzate in questo settore sono la modellazione muscoloscheletrica (MS) e la modellazione agli elementi finiti (FE).

I modelli MS rappresentano uno strumento prezioso, poiché possono fornire importanti informazioni sulle caratteristiche anatomiche e funzionali dei diversi soggetti, attraverso il calcolo di variabili interne come attivazioni muscolari e forze di contatto alle articolazioni.

La flessibilità e l'adattabilità dell'analisi FE la rende una soluzione ideale per modellare geometrie e materiali biologici e per simulare condizioni al contorno e di carico complicate. Modelli FE (FEM) precisi e descrittivi potrebbero dimostrarsi un ottimo strumento per la ricerca scientifica e medica. Inoltre, potrebbero essere utilizzati in ambito clinico se combinati con l'imaging medico, al fine di migliorare la cura del paziente.

Diversi FEM a 3 dimensioni (3D) del piede sono stati recentemente sviluppati per analizzare il comportamento biomeccanico del complesso piede-caviglia che è comunemente studiato con tecniche sperimentali come la stereofotogrammetria, le piattaforme di forza e di pressione.

In questo contesto, sono stati proposti molti protocolli per l'analisi del cammino al fine di valutare la cinematica, la cinetica e la distribuzione della pressione plantare in 3D. Questa valutazione si è dimostrata utile per caratterizzare la biomeccanica del piede in diverse patologie come il piede diabetico.

## Acknowledgements

---

Il piede diabetico è una complicanza invalidante del diabete mellito, una malattia cronica sempre più frequente nella popolazione anziana. Esso è caratterizzato dallo sviluppo di ulcere che possono portare all'amputazione. Modelli per la simulazione di deformazioni e sollecitazioni nel tessuto plantare diabetico devono essere in grado di prevedere quali sono le zone ad alto rischio per la formazione di ulcere sulla superficie plantare e possono essere usati per studiare le prestazioni di diverse solette nell'alleviare la pressione.

Questo lavoro rappresenta un primo sforzo verso lo sviluppo di uno PSM più completo che combinando un modello MS a un FEM, può aumentare la comprensione della patologia del piede diabetico. Per raggiungere quest'obiettivo, numerose limitazioni e problematiche sono state analizzate e risolte.

Innanzitutto, modelli MS di soggetti sani e diabetici sono stati sviluppati usando OpenSim al fine di stimare le forze muscolari. L'obiettivo era di valutare se la popolazione malata presenta deficit di forza muscolare negli arti inferiori rispetto a quella sana. I soggetti sono stati sottoposti a un'analisi del cammino e la cinematica e la cinetica degli arti inferiori sono state stimate per mezzo di una versione modificata del protocollo IORgait. La cinematica e la cinetica 3D delle articolazioni degli arti inferiori sono state calcolate anche con OpenSim. Entrambe le metodologie sono state in grado di evidenziare alcune differenze di cinematica e cinetica articolare tra le due popolazioni. I modelli MS hanno inoltre evidenziato differenze nelle forze muscolari dei soggetti sani rispetto a quelli diabetici. Questa conoscenza può aiutare nella pianificazione di terapie riabilitative specifiche per i pazienti diabetici al fine di migliorare la velocità, l'equilibrio, la forza muscolare, l'andatura e la mobilità articolare.

Dopo aver dimostrato l'applicabilità dei modelli MS nella popolazione diabetica, il passo successivo è stato quello di combinarli con FEM del piede. Ciò è stato fatto in due fasi. In un primo momento l'impatto dell'applicazione delle forze di reazione dell'articolazione del piede, ottenute dai modelli MS, come condizione al contorno per modelli FE del piede è stata verificata. Le geometrie specifiche del soggetto, ricavate da MRI, sono state utilizzate per lo sviluppo dei FEM del piede mentre le pressioni plantari sperimentalmente acquisite durante la deambulazione sono state utilizzate nel processo di validazione. Un miglior accordo tra pressione misurata sperimentalmente e pressione simulata è stato ottenuto utilizzando, come condizioni al contorno, le forze di reazione alla caviglia rispetto alle forze di reazione del suolo sperimentalmente simulate.

Dopodiché l'uso di forze muscolari come condizione al contorno nelle simulazioni FE è stata valutata. Dati di cinematica e cinetica acquisiti in sincrono durante l'analisi del cammino sono stati utilizzati per lo sviluppo di modelli MS e per il calcolo delle forze muscolari. Le inserzioni muscolari sono state poi trovate nelle immagini di risonanza magnetica e i connettori corrispondenti sono stati creati nel FEM. Le simulazioni



FE specifiche del soggetto sono state in seguito eseguite con il software Abaqus conducendo un'analisi quasi statica su quattro fasi del ciclo del passo e adottando due condizioni di carico: una che comprendeva le forze muscolari e una senza. Ancora una volta la validazione delle simulazioni FE è stata fatta per mezzo di un confronto tra le pressioni plantari simulate e misurate sperimentalmente. I risultati hanno mostrato un miglioramento marcato nella stima del picco di pressione nel modello che includeva i muscoli.

Infine è stato fatto un tentativo per la definizione di un modello agli elementi finiti del piede parametrico. Infatti, nonostante i recenti sviluppi, gli PSM non sono ancora stati applicati con successo in un ambiente clinico. Una delle possibili spiegazioni è il tempo necessario per la creazione della mesh, operazione che è di difficile automatizzazione. Lo sviluppo di modelli parametrici mediante l'analisi in componenti principali (PCA) può rappresentare una soluzione accattivante. In questo studio la PCA è stata applicata alla geometria dei piedi di una piccola coorte di soggetti diabetici e sani per valutare la possibilità di sviluppare modelli parametrici del piede e di utilizzarli per identificare varianti e analogie tra le due popolazioni.

Anche i limiti imposti dall'uso di modelli sono stati analizzati. La loro adozione è, infatti, limitata dalla mancanza di standard di verifica e validazione. Anche utilizzando l'MRI per lo sviluppo di un FEM, e dati sperimentali di analisi del movimento per le condizioni al contorno e di carico, la specificità del soggetto non è mai perfettamente raggiunta ad esempio per quanto riguarda le proprietà dei materiali. Inoltre bisognerebbe considerare che tutto si appoggia su algoritmi e modelli che non saranno mai in grado di rappresentare perfettamente la realtà.

Nel complesso, il lavoro presentato in questa tesi rappresenta una valutazione estesa dei possibili usi di tecniche di modellazione nella prevenzione del piede diabetico, considerando tutte le limitazioni introdotte e i potenziali vantaggi del loro utilizzo in un contesto clinico. La ricerca si articola in sei capitoli:

- *Capitolo 1* - fornisce uno sguardo generale sulle tecniche di modellazione, sia modellazione agli elementi finiti sia modellazione muscoloscheletrica. Inoltre descrive l'analisi del cammino, la strumentazione richiesta e i protocolli sviluppati per l'analisi degli arti inferiori.
- *Capitolo 2* - fornisce una panoramica dettagliata della biomeccanica del piede concentrandosi in particolare sul diabete e il piede diabetico;
- *Capitolo 3* - introduce l'applicazione dei modelli MS per la prevenzione del piede diabetico dopo una breve introduzione sulle tecniche più comuni utilizzate nella valutazione dei deficit motori causati dalla malattia. Obiettivi, materiali e metodi, risultati e discussione finale sono presentati. Il flusso di lavoro completo

## Acknowledgements

---

è descritto, e il capitolo si finisce con una discussione sulle nuove scoperte e sulle limitazioni.

- *Capitolo 4* - riporta il lavoro fatto per combinare l'uso di modelli muscoloscheletrici con FEM del piede. In un primo momento è verificato l'impatto dell'applicazione delle forze di contatto all'articolazione del piede, ottenute dai modelli MS, come condizione al contorno nei FEM del piede. Di seguito è valutato l'uso delle forze muscolari (ancora una volta ottenute dai modelli MS) come condizione al contorno nelle simulazioni FE. Per entrambi gli studi è presentata una breve introduzione insieme ai metodi applicati, ai risultati ottenuti e a una discussione sulle novità introdotte e sui limiti.
- *Capitolo 5* - esplora la possibilità di definire un FEM del piede parametrico applicando l'analisi delle componenti principali (PCA) ai piedi di una piccola coorte di soggetti diabetici e sani. Una panoramica sull'importanza di modelli specifici dei pazienti è presentata seguita da materiali e metodi, risultati e discussione di ciò che è stato ottenuto con questo studio.
- *Capitolo 6* - riassume i risultati e la novità della tesi, delineando le conclusioni e i percorsi di ricerca futuri.

# Contents

<b>Acknowledgements</b>	<b>i</b>
<b>Abstract</b>	<b>iii</b>
<b>Sommario</b>	<b>vii</b>
<b>List of figures</b>	<b>xv</b>
<b>List of tables</b>	<b>xxv</b>
<b>1 Introduction</b>	<b>1</b>
1.1 Introduction to Musculoskeletal Modeling . . . . .	1
1.1.1 Software for musculoskeletal modeling . . . . .	4
1.1.2 OpenSim pipeline [13] . . . . .	6
1.2 Introduction to Finite Element Modeling . . . . .	11
1.2.1 Introduction . . . . .	11
1.2.2 Application of the Finite Element Analysis to the biomechanical modeling . . . . .	11
1.3 The Finite Element Method in the analysis of the biomechanics of the foot	19
1.3.1 Summary on the foot FEM . . . . .	25
1.3.2 Software for the Finite Element Analysis . . . . .	26
1.4 Introduction to the Gait analysis . . . . .	28
1.4.1 Gait cycle . . . . .	28
1.5 Gait analysis instrumentation . . . . .	32
1.5.1 Kinematic - Stereophotogrammetric systems . . . . .	32
1.5.2 Kinetic - Ground Reaction Forces . . . . .	33
1.5.3 Plantar pressure [86] . . . . .	35
1.5.4 Protocol for motion analysis . . . . .	36
1.6 Aim of the thesis . . . . .	41
1.7 Outline of the thesis . . . . .	42
	xi

## Contents

---

<b>2</b>	<b>Diabetic foot biomechanics</b>	<b>43</b>
2.1	Introduction . . . . .	43
2.2	Bone Structure . . . . .	43
2.3	Joints[96] . . . . .	45
2.4	Muscles[96] . . . . .	47
2.5	The retinacula . . . . .	54
2.6	Diabetic foot . . . . .	56
2.6.1	Introduction [99] . . . . .	56
2.6.2	Epidemiology . . . . .	57
2.6.3	Complications [107] . . . . .	58
2.6.4	The diabetic foot . . . . .	60
<b>3</b>	<b>Musculoskeletal modeling in diabetic foot prevention</b>	<b>69</b>
3.1	Background & Aims . . . . .	69
3.2	Materials & Methods . . . . .	71
3.3	Results . . . . .	74
3.3.1	Data elaboration through OpenSim . . . . .	74
3.3.2	Experimental data elaboration through routine gait analysis protocol . . . . .	75
3.3.3	Experimental data elaboration through routine gait analysis protocol compared to data elaboration through OpenSim . . . . .	85
3.4	Discussion . . . . .	93
3.5	Acknowledgments . . . . .	95
<b>4</b>	<b>Combining musculoskeletal models and finite element models</b>	<b>97</b>
4.1	Foot finite element models and joint reaction forces . . . . .	97
4.1.1	Background & Aims . . . . .	97
4.1.2	Materials & Methods . . . . .	99
4.1.3	Results . . . . .	103
4.1.4	Discussion . . . . .	109
4.2	Aknowledgments . . . . .	111
4.3	Foot finite element models and muscle forces . . . . .	112
4.3.1	Background & Aims . . . . .	112
4.3.2	Material & Methods . . . . .	112
4.3.3	Results . . . . .	118
4.3.4	Discussion . . . . .	125
<b>5</b>	<b>Towards the definition of a parametric foot finite element model</b>	<b>129</b>
5.1	Background & Aims . . . . .	129
5.2	Materials & Methods . . . . .	131

5.3 Results . . . . .	134
5.4 Discussion . . . . .	143
5.5 Acknowledgments . . . . .	145
<b>6 Conclusion</b>	<b>147</b>
6.1 Summary, achieved results and future developments . . . . .	147
<b>A Appendix</b>	<b>151</b>
A.1 Control of muscle insertions . . . . .	151
<b>Bibliography</b>	<b>195</b>



# List of Figures

1.1	The figure shows the two most popular software used in the field of musculoskeletal modeling, on the left Anybody and on the right OpenSim	5
1.2	The figure shows an example of a scaling in OpenSim	7
1.3	Schematic of the Computed Muscle Control Algorithm Applied to Gait [22]	10
1.4	The figure, inspired by Cheung et al. [33], shows all the steps required for the development of a FE model of the foot	12
1.5	A) 2D model of the heel pad developed by Guiotto et al. [63]. B) 2D model developed by Agic et al. [64]. C) 2D model developed by Erdemir et al.[65]. The Figure on the top shows the model description, the one below the meshed model.	21
1.6	A) 3D coupled foot-boot model developed by Qiu et al. [76]. B) Workflow for the generation of a FEM proposed by Fernandez et al. [77]. C) 3D model developed by Guiotto et al.[78].	25
1.7	Functional divisions of the gait cycle according to Perry and Burnfield [24], [81].	30
1.8	The Bioengineering of Movement Laboratory (DEI - University of Padova) with the streophotogrammetric system and the force plates.	33
1.9	Bertec force plate with its reference system [85].	34
1.10	Winpod Pressure platform and its dimensions [87].	36
1.11	Marker set of the <i>FullBody</i> Protocol [84].	38
1.12	Frontal and lateral view of the marker-set <i>Foot</i> protocol [90].	39
1.13	The figure shows the landmarks where the markers are applied according to the <i>Foot</i> protocol and the three subareas of the foot derived by their vertical projection, [90].	40
2.1	Structures and anatomical division of the foot [95].	44
2.2	Planes of the foot [97].	46
2.3	Possible movements of the foot [97].	47
2.4	Muscles of the leg, front view (adapted from [98]).	49
2.5	Insertions of the muscles of the leg, front view (adapted from [98]).	51
2.6	Insertions of the muscles of the leg, rear view (adapted from [98]).	53

## List of Figures

---

2.7	Sole foot (adapted from [98]). . . . .	55
2.8	Figure a shows the number of people affected by diabetes. Figure b shows the estimated increase by 2035 [105]. . . . .	58
2.9	Schematical representation (on the left) and real pictures (on the right) of claw toes (in the top) and hammer toes (bottom). . . . .	61
2.10	Picture show two ulcers surrounded by callosity, developed in the most typical area underneath the Metatarsal heads [111]. . . . .	62
2.11	Picture shows the typical appearance of a Charcot foot in a later-stage. The rocker-bottom deformity is very pronounced [113]. . . . .	63
2.12	Correlation between plantar pressure and tissue thickness in the forefoot of diabetic subjects [117]. . . . .	65
2.13	Inverse relationship between force (pressure) and time (or repetition). As force (pressure) increases, the duration (time) required to cause tissue injury decrease [116]. . . . .	66
3.1	Gait analysis joints kinematics results of the sagittal plane ( <b>OPENSIM ELABORATION</b> ): comparison between mean joint angles (dashed lines) plus and minus 1 standard deviation of both CS (in blue) and of DNS (in red). Results of two tailed T-Test have been reported in term of the instants of the gait cycle where significant differences were found, and they are represented with the blue asterisk (Level of Significance was set to $p<0.05$ ). . . . .	76
3.2	Gait analysis joints kinematics results of the transverse and frontal planes ( <b>OPENSIM ELABORATION</b> ): comparison between mean joint angles (dashed lines) plus and minus 1 standard deviation of both CS (in blue) and of DNS (in red). Results of two tailed T-Test have been reported in term of the instants of the gait cycle where significant differences were found, and they are represented with the blue asterisk (Level of Significance was set to $p<0.05$ ). . . . .	79
3.3	Gait analysis joints dynamics results of the sagittal plane ( <b>OPENSIM ELABORATION</b> ): comparison between mean joint moments (dashed lines) plus and minus 1 standard deviation of both CS (in blue) and of DNS (in red). Results of two tailed T-Test have been reported in term of the instants of the gait cycle where significant differences were found, and they are represented with the blue asterisk (Level of Significance was set to $p<0.05$ ). . . . .	80



3.4	Gait analysis joints dynamics results of the transverse and frontal planes ( <b>OPENSIM ELABORATION</b> ): comparison between mean joint moments (dashed lines) plus and minus 1 standard deviation of both CS (in blue) and of DNS (in red). Results of two tailed T-Test have been reported in term of the instants of the gait cycle where significant differences were found, and they are represented with the blue asterisk (Level of Significance was set to $p < 0.05$ ). . . . .	81
3.5	Gait analysis joint kinematic results of the sagittal plane. Comparison between mean joint angles (dashed lines) plus and minus 1 standard deviation of both CS (in blue) and of DNS (in red). Results of two tailed T-Test have been reported in term of the instants of the gait cycle where significant differences were found, and they are represented with the blue asterisk (Level of Significance was set to $p < 0.05$ ). . . . .	82
3.6	Gait analysis joint kinematic results of the frontal plane. Comparison between mean joint angles (dashed lines) plus and minus 1 standard deviation of both CS (in blue) and of DNS (in red). Results of two tailed T-Test have been reported in term of the instants of the gait cycle where significant differences were found, and they are represented with the blue asterisk (Level of Significance was set to $p < 0.05$ ). . . . .	82
3.7	Gait analysis joint kinematic results of the transverse plane. Comparison between mean joint angles (dashed lines) plus and minus 1 standard deviation of both CS (in blue) and of DNS (in red). Results of two tailed T-Test have been reported in term of the instants of the gait cycle where significant differences were found, and they are represented with the blue asterisk (Level of Significance was set to $p < 0.05$ ). . . . .	83
3.8	Gait analysis joint kinetic results of the sagittal plane: comparison between mean joint moments (dashed lines) plus and minus 1 standard deviation of both CS (in blue) and DNS (in red). Results of two tailed T-Test have been reported in term of the instants of the gait cycle where significant differences were found, and they are represented with the blue asterisk (Level of Significance was set to $p < 0.05$ ). . . . .	83
3.9	Gait analysis joint kinetic results of the frontal plane: comparison between mean joint moments (dashed lines) plus and minus 1 standard deviation of both CS (in blue) and DNS (in red). Results of two tailed T-Test have been reported in term of the instants of the gait cycle where significant differences were found, and they are represented with the blue asterisk (Level of Significance was set to $p < 0.05$ ). . . . .	84

## List of Figures

---

- 3.10 Gait analysis joint kinetic results of the transverse plane: comparison between mean joint moments (dashed lines) plus and minus 1 standard deviation of both CS (in blue) and DNS (in red). Results of two tailed T-Test have been reported in term of the instants of the gait cycle where significant differences were found, and they are represented with the blue asterisk (Level of Significance was set to  $p<0.05$ ). . . . . 84
- 3.11 Gait analysis joint kinematic results of the sagittal plane: comparison between mean joint angles (dashed lines) plus and minus 1 standard deviation of both CS estimated with OpenSim (in blue) and of CS estimated with the modified Leardini et al. 2007 (in red). Results of two tailed T-Test have been reported in term of the instants of the gait cycle where significant differences were found, and they are represented with the blue asterisk (Level of Significance was set to  $p<0.05$ ). . . . . 86
- 3.12 Gait analysis joint kinematic results of the transverse and frontal planes: comparison between mean joint angles (dashed lines) plus and minus 1 standard deviation of both CS estimated with OpenSim (in blue) and of CS estimated with the modified Leardini et al. 2007 (in red). Results of two tailed T-Test have been reported in term of the instants of the gait cycle where significant differences were found, and they are represented with the blue asterisk (Level of Significance was set to  $p<0.05$ ). . . . . 87
- 3.13 Gait analysis joint kinetic results: comparison between mean joint moments (dashed lines) plus and minus 1 standard deviation of both CS estimated with OpenSim (in blue) and of CS estimated as in [146] (in red). Results of two tailed T-Test have been reported in term of the instants of the gait cycle where significant differences were found, and they are represented with the blue asterisk (Level of Significance was set to  $p<0.05$ ). . . . . 88
- 3.14 Gait analysis joint kinematic results of the sagittal plane: comparison between mean joint angles (dashed lines) plus and minus 1 standard deviation of both DNS estimated with OpenSim (in blue) and of DNS estimated with the modified Leardini et al. 2007 (in red). Results of two tailed T-Test have been reported in term of the instants of the gait cycle where significant differences were found, and they are represented with the blue asterisk (Level of Significance was set to  $p<0.05$ ). . . . . 89

3.15 Gait analysis joint kinematic results of the transverse and frontal planes: comparison between mean joint angles (dashed lines) plus and minus 1 standard deviation of both DNS estimated with OpenSim (in blue) and of DNS estimated with the modified Leardini et al. 2007 (in red). Results of two tailed T-Test have been reported in term of the instants of the gait cycle where significant differences were found, and they are represented with the blue asterisk (Level of Significance was set to $p < 0.05$ ). . . . .	90
3.16 Gait analysis joint kinetic results: comparison between mean joint moments (dashed lines) plus and minus 1 standard deviation of both DNS estimated with OpenSim (in blue) and of DNS estimated as in [146] (in red). Results of two tailed T-Test have been reported in term of the instants of the gait cycle where significant differences were found, and they are represented with the blue asterisk (Level of Significance was set to $p < 0.05$ ). . . . .	91
3.17 The figure shows the results of the analysis of the SEMG regarding the POP. On the x-axis the name of the muscles is reported while in the y-axis there is the percentage of the gait cycle. DNS are in red while CS are in blue. . . . .	92
4.1 Workflow of the development of MSMs and simulations. . . . .	101
4.2 Healthy (top) and Neuropathic (bottom) subject specific predicted and experimental PP values for the whole foot at the initial contact, loading response, midstance and push off. . . . .	104
4.3 Healthy (top) and Neuropathic (bottom) subject's errors (difference between the simulated and the experimental values) for the peak of pressure in the different phases of the gait cycle expressed in percentage of the experimental value. On the left errors between experimental PP values and simulated with GRFs ones. On the right errors between experimental PP values and simulated with JCFs ones. . . . .	105
4.4 Healthy (top) and Neuropathic (bottom) subject's errors (difference between the simulated and the experimental values) for the contact surface in the different phases of the gait cycle expressed in percentage of the experimental value. On the left errors between experimental PP values and simulated with GRFs ones. On the right errors between experimental PP values and simulated with JCFs ones. . . . .	105
4.5 Comparison of the GRFs (top) and of the JCFs (bottom) used as boundary conditions for the FE simulations of the neuropathic and the control subjects in the different instants of the stance phase of the gait cycle expressed in percentage of the body weight. All the values are expressed in percentage of the BW. Kruskal Wallis, * $p < 0.05$ . . . . .	106

## List of Figures

---

4.6	Healthy (top) and Neuropathic (bottom) subject's X coordinate of the peaks of pressure position expressed in percentage of the foot length. Comparison between experimental values (EXP), values of the simulation with the GRF (SIMUL-GRF) and values of the simulations with the joint reaction forces (SIMUL-JFC) in the different subareas of the foot in the Loading Response. Kruskall Wallis, * p<0.05. . . . .	107
4.7	Healthy (top) and Neuropathic (bottom) subject's Y coordinate of the peak of pressure expressed in percentage of the foot length. Comparison between experimental values (EXP), values of the simulation with the GRF (SIMUL-GRF) and values of the simulations with the joint reaction forces (SIMUL-JCF) in the different subareas of the foot in the Loading Response. Kruskall Wallis, * p<0.05. . . . .	107
4.8	Healthy (top) and Neuropathic (bottom) subject's X coordinate of the peaks of pressure expressed in percentage of the foot length. Comparison between experimental values (EXP), values of the simulation with the GRF (SIMUL-GRF) and values of the simulations with the joint reaction forces (SIMUL-JCF) in the different subarea of the foot in the Midstance. Kruskall Wallis, * p<0.05. . . . .	108
4.9	Healthy (top) and Neuropathic (bottom) subject's Y coordinate of the peaks of pressure expressed in percentage of the foot length. Comparison between experimental values (EXP), values of the simulation with the GRF (SIMUL-GRF) and values of the simulations with the joint reaction forces (SIMUL-JCF) in the different subarea of the foot in the Midstance. Kruskall Wallis, * p<0.05. . . . .	108
4.10	DNS' foot FEM: example of a critical area. . . . .	115
4.11	On the left the DNSM: frontal, posterior and lateral views. On the right the HSM: frontal posterior and lateral views. . . . .	116
4.12	The Figure shows the distribution of the DNS' plantar pressure on the platform, experimentally and simulated in C1 and C2. . . . .	118
4.13	The Figure shows the distribution of the HS' plantar pressure on the platform, experimentally and simulated in C1 and C2. . . . .	119
4.14	On the left, the peak of pressure of the HS, experimental and simulated in C1 and C2. On the right, the peak of pressure of the DNS, experimental and simulated in C1 and C2. . . . .	119

4.15	On the left, the error calculated as the difference between simulated and experimental peak of pressure values and expressed in percentage of the experimental ones for both the condition C1 and C2 and for the HS. On the right, the error calculated as the difference between simulated and experimental peak of pressure values and expressed in percentage of the experimental ones for both the condition C1 and C2, and for the DNS.	120
4.16	On the left, the HS' contact surface experimentally acquired and in both the condition C1 and C2, for all the phases simulated, is reported. On the right, the DNS' contact surface experimentally acquired and in both the condition C1 and C2, for all the phases simulated, is reported. . . .	120
4.17	On the left, the error calculated as the difference between simulated and experimental contact surface and expressed in percentage of the experimental ones for both the condition C1 and C2 and for the HS. On the right, the error calculated as the difference between simulated and experimental contact surface and expressed in percentage of the experimental ones for both the condition C1 and C2, and for the DNS.	121
4.18	The Figure shows the Von Mises stresses in the DNS' bones during the different phases simulated. From the top to the bottom (INITIAL CONTACT, LOADING RESPONSE, MIDSTANCE and PUSH OFF). On the left column, results of C1 and on the right results of C2. . . . .	122
4.19	The Figure shows the Von Mises stresses in the HS' bones during the different phases simulated. From the top to the bottom (INITIAL CONTACT, LOADING RESPONSE, MIDSTANCE and PUSH OFF). On the left column, results of C1 and on the right results of C2. . . . .	123
4.20	The Figure shows the Von Mises stresses values in the DNS' and HS' bones during the different phases simulated and in the two conditions.	124
5.1	Meshes of the first metatarsal bone of all the subjects used for the PCA. The first row shows the three diabetic subjects and the second one shows the three healthy subjects. . . . .	133
5.2	Meshes of the skin without toes used for the PCA. The first row shows the three diabetic subjects and the second one the three healthy subjects.	133
5.3	Workflow of the computation of the PCA. The name of the software used for every step is indicated in italic. . . . .	135

## List of Figures

---

5.4	FMTB hypothesized models generated by means of Equation 5.1 for all six subjects. For each principal mode, the variation was illustrated by varying the value of the constant $c$ from -3 to +3. Positive $c$ values represent shape variation in the positive direction, whereas negative $c$ values represent shape variation in the opposite direction. The larger the magnitude of constant $c$ , the more substantial is the shape variation represented. . . . .	136
5.5	FMTB shape variations generated by means of Equation 5.1 considering only the diabetic subjects. For each principal mode, the shape variations were shown by varying the constant $c$ from -3 to +3. . . . .	137
5.6	FMTB shape variations generated by means of Equation 5.1 considering only the healthy subjects. For each principal mode, the shape variations were shown by varying the constant $c$ from -3 to +3. . . . .	138
5.7	hypothesized models generated by means of Equation 5.1 considering the meshes of the skin without toes of all the subjects. For each significant principal component 6 different models were obtained, according to the constant $c$ which varied from -3 to +3. . . . .	139
5.8	hypothesized models generated by means of Equation 5.1 considering the meshes of the skin without toes of the diabetic subjects. For each significant principal component 6 different models were obtained, according to the constant $c$ which varied from -3 to +3. . . . .	140
5.9	hypothesized models generated by means of Equation 5.1 considering the meshes of the skin without toes of the healthy subjects. For each significant principal component 6 different models were obtained, according to the constant $c$ which varied from -3 to +3. . . . .	141
5.10	hypothesized models generated by means of Equation 5.1 considering the meshes of the skin without toes of all the HSs plus the first DB subject. For each significant principal component 6 different models were obtained, according to the constant $c$ which varied from -3 to +3. . . . .	141
5.11	hypothesized models generated by means of Equation 5.1 considering the meshes of the skin without toes of all the HSs plus the second DB subject. For each significant principal component 6 different models were obtained, according to the constant $c$ which varied from -3 to +3. . . . .	142
5.12	hypothesized models generated by means of Equation 5.1 considering the meshes of the skin without toes of all the HSs plus the third DB subject. For each significant principal component 6 different models were obtained, according to the constant $c$ which varied from -3 to +3. . . . .	142
A.1	Insertion of the Tibialis Anterior on the first metatarsal bone. (ScanIP)	152
A.2	Insertion of the Tibialis Anterior on the medial cuneiform bone. (ScanIP)	152

A.3	Insertion of Hallucis Extensor on the dorsal surface of the base of the phalanx of the hallux. (ScanIP) . . . . .	153
A.4	Insertion of the Extensor Digitorium on the base of the second distal phalanx. (ScanIP) . . . . .	154
A.5	Insertion of the Extensor Digitorium on the base of the second medial phalanx. (ScanIP) . . . . .	155
A.6	Insertion of the Extensor Digitorium on the base of the third distal phalanx. (ScanIP) . . . . .	155
A.7	Insertion of the Extensor Digitorium on the base of the third medial phalanx. (ScanIP) . . . . .	156
A.8	Insertion of the Extensor Digitorium on the base of the fourth distal phalanx. (ScanIP) . . . . .	156
A.9	Insertion of the Extensor Digitorium on the base of the fourth medial phalanx. (ScanIP) . . . . .	157
A.10	Insertion of the Extensor Digitorium on the base of the fifth distal phalanx. (ScanIP) . . . . .	157
A.11	Insertion of the Extensor Digitorium on the base of the fifth medial phalanx. (ScanIP) . . . . .	158
A.12	Insertions of the Peroneus Longus on the tuberosity of the first metatarsal bone. (ScanIP) . . . . .	159
A.13	Insertion of the Peroneus Longus on the medial cuneiform bone. (ScanIP)	160
A.14	Insertions of the Peroneus Brevis on the tuberosity of the fifth metatarsal bone. (ScanIP) . . . . .	161
A.15	Insertion of the Achilles tendon on tuberosity of the calcaneus. (ScanIP)	163
A.16	Insertion of the Tibialis Posterior on the fourth metatarsal bone. (ScanIP)	164
A.17	Insertion of the Tibialis Posterior on the third metatarsal bone. (ScanIP)	165
A.18	Insertion of the Tibialis Posterior on the second metatarsal bone. (ScanIP)	165
A.19	Insertion of the Tibialis Posterior on the third cuneiform bone. (ScanIP)	166
A.20	Insertion of the Tibialis Posterior on the second cuneiform bone. (ScanIP)	166
A.21	Insertion of the Tibialis Posterior on the first cuneiform bone. (ScanIP)	167
A.22	Insertion of the Tibialis Posterior on the navicular bone. (ScanIP) . . .	167
A.23	Insertion of the plantar fascia on the first phalanx. (ScanIP) . . . . .	168
A.24	Insertion of the plantar fascia on the second phalanx. (ScanIP) . . . . .	169
A.25	Insertion of the plantar fascia on the third phalanx. (ScanIP) . . . . .	169
A.26	Insertion of the plantar fascia on the fourth phalanx. (ScanIP) . . . . .	170
A.27	Insertion of the plantar fascia on the fifth phalanx. (ScanIP) . . . . .	170
A.28	Insertion of the plantar fascia on the tuberosity of the calcaneus. (ScanIP)	171





# List of Tables

1.1	Technical details of the force plates-item 4060-80 (Data sheet [85]). . .	35
1.2	Technical details of the force plates-item 4060-80 (Data sheet [85]). . .	35
1.3	Structural characteristics of the plantar pressure systems [87]. . . . .	36
1.4	Electronic characteristics of the plantar pressure systems [87]). . . . .	37
2.1	Action of the muscles on the ankle joint . . . . .	52
3.1	Results of the SO run with OpenSim. Phase of the gait cycle where the muscle activation of DNS showed a statistically significant difference with respect to the CS and P-values are reported . . . . .	77
3.2	Results of the SO run with OpenSim. Phase of the gait cycle where the muscle force of DNS showed a statistically significant difference with respect to the CS and P-values are reported. . . . .	78
4.1	Demographic and clinical data of the diabetic neuropathic subject (DNS1) and the healthy subject (HS1) whose foot geometries were used for the development of the FEMs. . . . .	99
4.2	Demographic and clinical data of the healthy and the neuropathic subjects. # = Number of subjects. . . . .	100
4.3	Clinical data of the DNS . . . . .	113
4.4	Podiatric examination of the DNS . . . . .	113
5.1	Demographic and clinical data of the healthy and the neuropathic subjects. # = Number of subjects . . . . .	132
5.2	Parameters of the MRI and data of the subjects. (HS= healthy subject, DB= diabetic subject) . . . . .	132
5.3	Eigenvalues computed with the PCA run on the meshes of the metatarsal bones (HS = healthy subjects, DB = diabetic subjects). First column shows the eigenvalues of PCA run on all the 6 meshes, second column shows the eigenvalues of PCA run on 3 HS, third column shows the eigenvalues of the PCA on 3 DB, fourth, fifth and sixth columns show the eigenvalues of the PCA run on 3 HS plus each time a different DB. .	137

**List of Tables**

---

5.4 Eigenvalues computed with the PCA run on the meshes of the skin without toes (HS = healthy subjects, DB = diabetic subjects). First column shows the eigenvalues of PCA run on all the 6 meshes, second columns the eigenvalues of PCA run on 3 HS, third column the eigenvalues of the PCA on 3 DB, fourth, fifth and sixth columns the eigenvalues of the PCA run on 3 HS plus each time a different DB. . . . . 140

# 1 Introduction

## 1.1 Introduction to Musculoskeletal Modeling

When humans and animals perform a motor skill, they use their brain to activate and coordinate the muscles and limbs involved in it. This paradigm is called motor control [1]. In order to determine the appropriate set of muscle forces and joint activations that produces a desired movement, sensory information about the environment and the state of the body at a certain time is integrated [2]. The central nervous system (CNS) and the musculoskeletal system are required to work together in this process [3].

Many muscles act at the same time on multiple joints [4]. They are force generators and so responding to the neural drive, they develop forces that are transmitted by tendons to the body segments to which they are attached, causing the generation of joint moments [5]. The consequence is an acceleration of joints and segments, and quite simply the movement.

It is clear that muscles and tendons act together as an interface between the CNS and the body segments, but the mechanism underneath the accomplishment of the role is complex [4]. The movement of multiple joints requires the coordination of many muscles, that contribute to accelerate even joints that are not actually spanned [6]. But in particular, the nervous system can use different strategies to produce the same desired motion, as there are more muscles than mechanical degrees-of-freedom (DOFs) [7]. This is a fundamental property of the neuromusculoskeletal system, known as redundancy, which has for long been a central problem in biomechanics and neural control [8]. The challenge is to know how the CNS selects muscle coordination patterns from a theoretically infinite set of possibilities [9]. Controlling this ability could make it possible to intervene in cases where there is a deficit. However, an experimental direct measurement of the individual muscle forces contribution to the movement is not feasible in most cases, unless by applying invasive techniques [10].

## Chapter 1. Introduction

---

This has led to the development of non-invasive methods based on models.

To investigate the biomechanics of human movement and to estimate muscle forces, two opposite approaches are generally pursued: forward and inverse dynamics (ID) ([11], [12], [13]). ID assumes that the position and the external forces acting on a body are known parameters. Thanks to the gait analysis, joint kinematics data and ground reaction forces are easily measurable and thus this technique has become widely popular [1]. ID allows the estimation of joint moments, but since each of them represents the resultant action of all muscles spanning a joint, the contribution of each single muscle remains unknown. This approach implies some main limitations:

- the calculation of muscle forces from joint moments leads to a large set of possible solutions, as multiple muscles span each joint. It is thus not possible to estimate the contribute of each muscle;
- information about co-contraction of agonist and antagonist muscles cannot be derived;
- even supposing that muscle forces can be determined, there are not algorithms that enables to do the reverse, from muscle forces to muscle activations.

The minimization of an objective function, appropriately selected with respect to the movement under analysis, has been proposed to address the problem of the redundancy. As a consequence optimization methods, such as static optimization, combined with a model of the musculoskeletal geometry of the human body, have extensively been applied ([14], [15], [13], [16]) . They have a closed-loop structure which keeps tracking the joint moments obtained from ID and distributes them to the individual muscles crossing a specific joint. The assumption behind this is that each muscle contributes according to a predefined objective function. Presuming that the chosen criterion is generalizable across subjects and motor tasks, forces and activation are thus estimated [15]. It is evident that this approach is based on the physiological validity of the objective function, as it makes a priori assumptions about how muscles are recruited to produce a given movement [17]. The hypothesis is even more questionable in the clinical field, since it has been proved that muscle excitations strategies are determined by the personal history of training and pathology of the subject [18]. Furthermore, as already stated, the co-contraction of muscles cannot be accounted. This aspect is fundamental and its lack should not be underestimated since that it can lead to a great inaccuracy in the predictions, as co-contraction of muscles is very common ([19], [20]). All these consideration make clear that the differences highlighted by an ID-based optimization approach, in an individual's neuromuscular

## 1.1. Introduction to Musculoskeletal Modeling

---

control system, especially when affected by motor impairments, should be evaluated with caution. It is in fact not recommended to ascertain how a muscle contributes to the observed movement of body joints and segments ([11], [12],[21]).

As stated above, the problem of estimating muscle forces can be addressed also by exploiting a forward dynamics approach ([22], [23]). In contrast to ID where the motion of the model was known, in forward dynamics, the input is a measure or estimate of the neural drive, which is transformed with three steps in order to obtain joint moments.

- Firstly, a model of the underlying muscle activation dynamics transforms the neural signal into a time varying measure of the muscle activation ranging from zero to one;
- then, a model of the muscle that accounts for the muscle contraction dynamics allows the transformation of the muscle activation into muscle force. The tendon, coupled with the muscle, transfers the developed force from the muscle to the bone.
- at the end the joint moments are computed. A moment for each degree of freedom (DOF) is obtained as the sum of all the musculotendon forces that contribute to that moment, multiplied by their respective moment arms. A model of the musculoskeletal geometry and information about joint angles is required to determine the muscles moment arms (that change as a function of joint angles). Once joint moments are attained, joint movements can be derived through the equations of motion.

The process herein described is meant to reproduce how the body actually generates movement as it is usually done by the neuromusculoskeletal system which transforms the neural commands into movement [23]. This approach requires providing estimates of the neural commands which can be obtained either with optimization methods or with the use of surface electromyography (EMG) data experimentally recorded [24]. EMGs are small electrical signals generated in the muscles that induce contraction according to the neural stimulation. They have the potential to reveal the actual activated muscles and their pattern of activation [25]. They can be detected on the surface of the skin through sensors attached on the body. This strategy allows overcoming the indeterminacy of the neuromusculoskeletal system while accounting for co-contraction and without the need to make any assumption on how the forces applied to a joint are partitioned. Furthermore there is no need to satisfy any constraints imposed by a single objective function [26].

### 1.1.1 Software for musculoskeletal modeling

The need to create software for the simulation of the movement, arose from the interest of fully understand how the nervous system controls human movement, in both healthy and impaired subjects, and to establish a scientific basis for rehabilitation treatments of pathological movements. The aim was to overcome the limitation imposed by the experimental approach, namely the inability to measure the forces generated by the muscles and the impossibility of establishing a precise cause-effect relationship in a complex dynamic system, as the human body is [27].

For these reasons, many laboratories began developing simulation software which allow the creation of musculoskeletal models. The human body has a very complex structure, consisting of bones, muscles, tendons and joints. To have a good mechanical representation of it, a model should contain more than 1000 muscles that are activated independently. Several simulation software have been developed. Among them, the most popular are **OpenSim** and **AnyBody Modeling System** ([28],[29]) (see Figure 1.1).

**AnyBody Modeling System** was designed at the University Of Aalborg (DK) with the purpose to reconstruct the mechanics of the human body during any movement, under the influence of the surrounding environment. The environment is intended as something within (implant, e.g. knee or hip devices), something attached to (exoskeleton, e.g. knee brace) or something interacting (e.g. automotive seat, wheelchair) with the human body. Everything in a STL (STereo Lithography) format can be imported, used and analyzed in AnyBody. The system is believed to be able to analyze any musculoskeletal system but it comes with a full body human model containing most bones, joints and muscles in the human physiognomy. The model can be adapted to the user needs, by changing dimensions (height, weight etc.), muscle strength, or even importing subject specific bone geometries. As input it uses motion which can be recorded with a motion capture (MoCap) system, or defined by the user by describing initial joint angles and joint velocities manually. The external forces are used to simulate the internal loads in the body. Using these inputs, AnyBody calculates the activations of the individual muscles responsible for a given motion with an ID approach. AnyBody indeed uses an optimization process, a muscle recruitment solver to solve what muscles (each single fascicle) will do [30]. As output it is thus possible to get muscle forces, activations and joint reaction forces and moments during this motion. Additionally, each model can be setup to obtain forces and moments in any point of interest.

In the early 90s, Delp and Loan introduced a musculoskeletal modeling software called SIMM (Software for Modeling Interactive Muskuloskeletal), in order to evaluate the different structures of the musculoskeletal system [31]. In the following years

## 1.1. Introduction to Musculoskeletal Modeling



Figure 1.1 – The figure shows the two most popular software used in the field of musculoskeletal modeling, on the left Anybody and on the right OpenSim

numerous computer models of the musculoskeletal system were created which were capable of simulating movements such as walking, running and cycling. However, the software presented limits, such as the inability to calculate the excitations produced during a complex movement and the limited number of tools available that would allow analyzing the results of the dynamic simulations. Over the past decade, thanks to the advent of more powerful computers and the creation of a simulation open-source environment called **OpenSim**, some limits have been exceeded [32]. OpenSim is indeed an open-source musculoskeletal simulation software used for modeling and analysis. It allows sharing the musculoskeletal models between researchers, in such a way that they are reproducible in different laboratories and improvable according to the specific requirements. The plug-in architecture that characterizes it encourages users to extend the functionality of the software with the personal development of models and simulations, thus providing a tool for rapid dissemination and consultation. The software provides the ability to scale a model, to solve kinematic and/or ID problems, to solve forward dynamic problems (and to generate a simulation based on it) and to analyze and display the results obtained as output with graphics. OpenSim is used in several laboratories all around the world, thanks also to the workshops and courses organized with the purpose to promote its use in different context and for different kind of simulations. The library provides both models of the lower and of the upper limbs. Furthermore a forum is active in the website allowing users to discuss about problems and new key findings. The software interacts as well with the most common programming languages, like Python and C++. Finally an integration with Matlab is also implemented which makes easier running simulations in batch processing and analyzing the outputs of the simulations.

## Chapter 1. Introduction

---

By considering that in the present thesis musculoskeletal modeling simulations have been performed in OpenSim, a detailed description of Opensim pipeline has been reported in the following sections.

### 1.1.2 OpenSim pipeline [13]

A typical pipeline in OpenSim consists of the following steps:

- Scaling, which means adapting a generic musculoskeletal model to the anthropometric measures of the subject under analysis;
- Inverse Kinematic, that is the determination of the coordinate values (angles and positions of the markers on the virtual space) of the model that best reproduces the movement acquired experimentally through MoCap system.
- Inverse Dynamic;
- Joint Reaction analysis, which estimates the reaction forces at each joint;
- Static Optimization, which determines the action of the individual muscle forces in a movement at any instant of time.
- Computer Muscles Control, which compute a set of muscle excitations that will drive a dynamic musculoskeletal model to track a set of desired kinematics in the presence of applied external forces. This tool allows to constraint the activation of the muscles using the experimental EMG signals. In addition to the Static Optimization it implements a proportional-derivative control [22].

#### 1.1.2.1 Scaling

Scale a model means adapting a generic musculoskeletal model to the anthropometric measures of the specific subject under analysis (see Figure 1.2). This is done by using the measured distances between marker locations and with manually-specified scale factors. The marker locations are usually obtained using motion capture equipment, better if with a static trial. The not-scaled model has a set of virtual markers placed in the same anatomical locations as the experimental markers. This set of marker can be defined according to the protocol used during the data collection. The dimensions of each segment in the model are adjusted so that the distances between the virtual markers match the distances between the experimental markers. Manual scale factors, which may come from other anthropometric analyses, can also be used as an



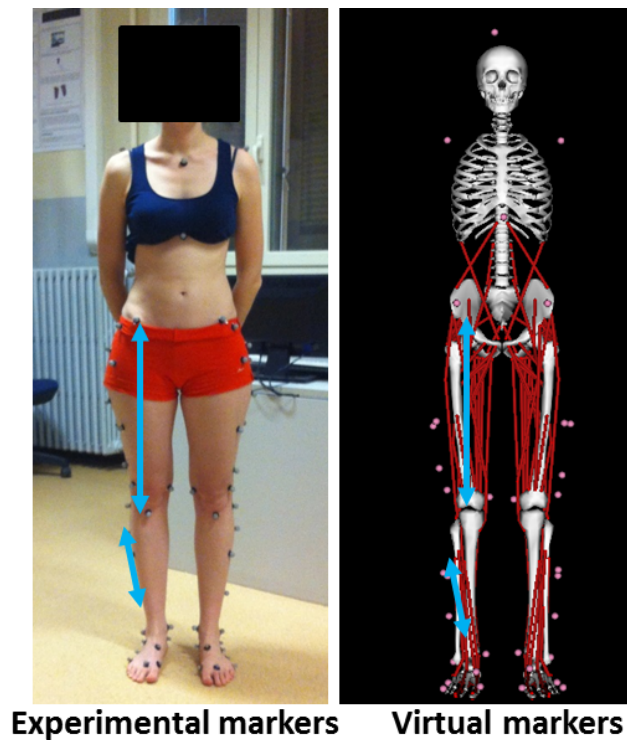


Figure 1.2 – The figure shows an example of a scaling in OpenSim

alternative. With this procedure, taking into account the weight of the subject, the masses of the generic bone segments will be scaled in proportion to the real subject [28].

### 1.1.2.2 Inverse Kinematic

Inverse kinematic (IK) refers to the study of the movement of a subject or object, without considering the forces and moments produced during the entire movement. IK is used to determine the values of the coordinates (angles and positions of the markers on the virtual space) of the model that better reproduce the movement experimentally acquired through MoCap. To obtain this, it is necessary to minimize the differences between the positions of the experimental markers and the positions of the correspondent virtual markers belonging to the model at each frame. Mathematically, the "best match" is expressed as a weighted least squares problem, whose solution aims to minimize the distance between an experimental marker and the corresponding marker on the model. The weighted least squares problem solved by IK represented

by the equation 1.1:

$$\min_{\mathbf{q}} \left[ \sum_{i \in \text{markers}} w_i \| \mathbf{x}_i^{\text{exp}} - \mathbf{x}_i(\mathbf{q}) \|^2 + \sum_{j \in \text{unprescribed coords}} (\omega_j)(\mathbf{q})_j^{\text{exp}} - \mathbf{q}_j)^2 \right] \quad (1.1)$$

$\mathbf{q}_j = \mathbf{q}_j^{\text{exp}}$  for all prescribed coordinates  $j$

where  $\mathbf{q}$  is the vector of generalized coordinates being solved for,  $\mathbf{x}_i^{\text{exp}}$  is the experimental position of marker  $i$ ,  $\mathbf{x}_i(\mathbf{q})$  is the position of the corresponding marker on the model (which depends on the coordinate values),  $\mathbf{q}_j^{\text{exp}}$  is the experimental value for coordinate  $j$ . Prescribed coordinates are set to their experimental values.

### 1.1.2.3 Inverse Dynamic

The ID determines the generalized forces (e.g., net forces and torques) at each joint responsible for a given movement. The inputs required are the kinematics describing the movement of a model and a portion of the kinetics (e.g., external loads) applied to the model. In OpenSim the ID solves the classical equations that mathematically expresses the mass-dependent relationship between force and acceleration,  $\mathbf{F} = m\mathbf{a}$ . The output would thus be the net forces and torques at each joint which produce the movement.

The equation can be written as:

$$\mathbf{M}(\mathbf{q})\ddot{\mathbf{q}} + \mathbf{C}(\mathbf{q}, \dot{\mathbf{q}}) + \mathbf{G}(\mathbf{q}) = \boldsymbol{\tau}$$

Where  $N$  is the number of degrees of freedom;

$\mathbf{q}, \dot{\mathbf{q}}, \ddot{\mathbf{q}} \in \mathbf{R}^N$  are the vectors of generalized positions, velocities, and accelerations, respectively;

$\mathbf{M}(\mathbf{q}) \in \mathbf{R}^{N \times N}$  is the system mass matrix;

$\mathbf{C}(\mathbf{q}, \dot{\mathbf{q}}) \in \mathbf{R}^N$  is the vector of Coriolis and centrifugal forces;

$\mathbf{G}(\mathbf{q}) \in \mathbf{R}^N$  is the vector of gravitational forces;

And  $\boldsymbol{\tau} \in \mathbf{R}^N$  is the vector of generalized forces.

### 1.1.2.4 Joint Reaction analysis

OpenSim offers a tool to perform a joint reaction analysis which provides resultant forces and moments at each joint of interest. Specifically, it calculates the joint forces and moments transferred between consecutive bodies as a result of all loads acting on the model. These forces and moments correspond to the internal loads carried by the joint structure. These loads represent the contributions of all un-modeled joint

## 1.1. Introduction to Musculoskeletal Modeling

---

structures that would produce the desired joint kinematics, such as cartilage contact and any omitted ligaments.

### 1.1.2.5 Static Optimization

Static Optimization (SO), is the tool of OpenSim which uses the musculoskeletal geometry and assumptions about the distribution of external forces, to estimate the individual muscle forces which allow the achievement of the desired acceleration by the body segments connected to those particular muscles, at any instant of time. It is called "static" because the optimization criterion is limited to the amount that can be calculated at any point in time during a simulation. The muscle forces are resolved by minimizing the sum of squared (or other power) muscle activations. SO uses the known motion of the model to solve the equations of motion for the unknown generalized forces (e.g., joint torques) subject to one of the following muscle activation-to-force conditions:

ideal force generators:  $\sum_{m=1}^n (a_m F_m^0) r_{m,j} = \tau_j$  or,

constrained by force-length-velocity properties:  $\sum_{m=1}^n [a_m f(F_m^0, l_m, v_m)] r_{m,j} = \tau_j$

while minimizing the objective function:  $J = \sum_{m=1}^n (a_m)^p$

where  $n$  is the number of muscles in the model;  $a_m$  is the activation level of muscle  $m$  at a discrete time step;  $F_m^0$  is its maximum isometric force;  $l_m$  is its length;  $v_m$  is its shortening velocity;  $f(F_m^0, l_m, v_m)$  is its force-length-velocity surface;  $r_{m,j}$  is its moment arm about the  $j^{th}$  joint axis;  $\tau_j$  is the generalized force acting about the  $j^{th}$  joint axis; and  $p$  is a user defined constant. Note that for static optimization  $f(F_m^0, l_m, v_m)$  computes the active fiber force along the tendon assuming an inextensible tendon and does not include contribution from muscles' parallel elastic element.

### 1.1.2.6 Computer Muscle Controls

Computed Muscle Control is another tool used to compute a set of muscle excitations (or, more generally, actuator controls) that will drive a dynamic musculoskeletal model to track a set of desired kinematics in the presence, when applicable, of applied

**Chapter 1. Introduction**

external forces. It combines SO with a proportional-derivative control [22] (see Figure 1.3. It gives the possibility to place constraints on the upper and lower bounds of the

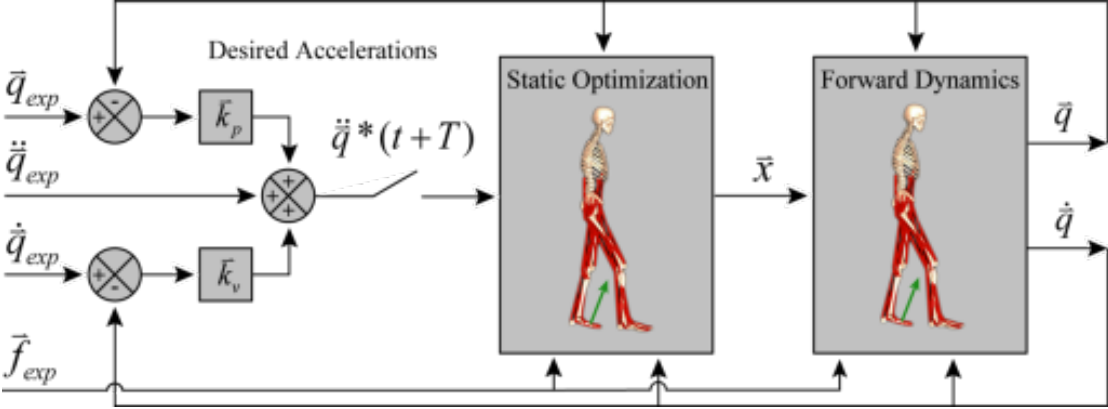


Figure 1.3 – Schematic of the Computed Muscle Control Algorithm Applied to Gait [22]

controls which can be defined using the EMG signals.

## 1.2 Introduction to Finite Element Modeling

### 1.2.1 Introduction

The finite element analysis (FEA) is a simulation technique used in engineering applications. Its greatest power is given by the Finite Element (FE) Method, a numerical technique which searches for approximate solutions to problems described by partial differential equations. The technique comes from the need to solve problems ruled by equations which are too complex to be directly solved in an analytical way. The approach to reach the solution consists in breaking down a very complex issue in the sum of many elementary problems. It applies to physic bodies which are divided into a number of elements of small shape (usually tetrahedrons, hexahedrons, triangles or quads) and dimensions. Each element in the model represents a discrete portion of the physical structure and it is connected to other elements by shared nodes. The collection of all the elements and nodes is called the mesh and it is generally only an approximation of the actual geometry of the structure. The element type, shape, and location, as well as the overall number of elements, affect the results obtained. The number of elements per unit of length, area, or in a mesh is referred to as the mesh density. The greater it is, the more accurate the results. Anyway as the mesh density increases, the computer time required for the analysis increases.

### 1.2.2 Application of the Finite Element Analysis to the biomechanical modeling

The human musculoskeletal system is a complex structure whose primary function is the transmission of mechanical forces. The deficits that can arise are related to biomechanical factors, which play an important role as regards the etiology, treatment and prevention. In order to study the mechanical forces, different techniques have been developed, such as stereophotogrammetry, force platforms, surface electromyography, musculoskeletal models and methods for image segmentation. With them it is possible to derive the three-dimensional (3D) joints kinematics and kinetics, in dynamic conditions. From this information the internal stresses and strains can be derived. The latter are essential, and a direct measurement would be almost impossible without an appropriate computational model. The FE method is in fact considered as a valuable experimental tool in order to predict the load distribution between the different structures, both at the body or at an organ level. FE models (FEMs) can perform static and/or dynamic analysis, modeling structures with irregular geometry and composed of materials with complex properties. Furthermore they can easily simulate situations with particular loads and boundary conditions. The first step

towards the development of a FEM is the creation of the geometry, based on the volume reconstruction of the Computer Tomography (CT) or Magnetic Resonance Imaging (MRI) images of the foot in non-weight-bearing condition. Once collected, the images are segmented in order to separate each part of the foot complex. They are thus processed into a CAD environment to obtain the volume of interest in the form of a mesh. Starting from this and using a software for FEA, it is possible to develop the model and to perform all the simulation of interest. All the steps are summarized in Figure 1.4.

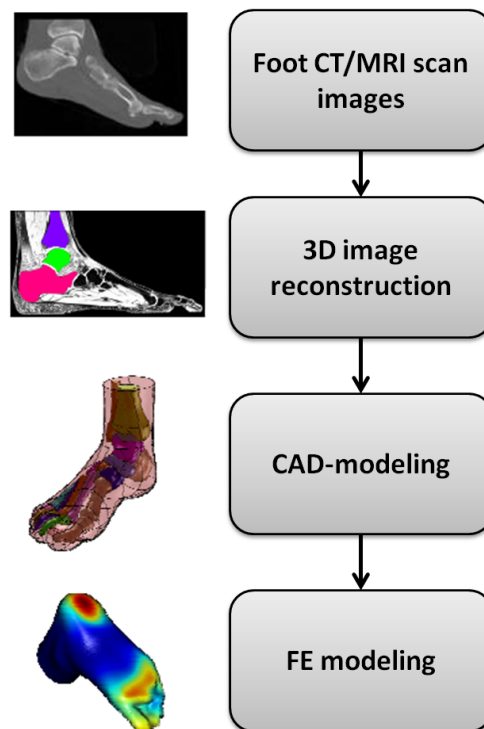


Figure 1.4 – The figure, inspired by Cheung et al. [33], shows all the steps required for the development of a FE model of the foot

### 1.2.2.1 Computed tomography and Magnetic Resonance Imaging for the acquisition of the subject specific geometry

CT or MRI scan images are usually the choice for the 3D reconstruction of the geometries of the foot. Being different methods, they produce different results. **MRI** is a medical imaging technique used in radiology, to visualize the internal structures of the body in detail [34]. The principle behind it, is that body tissue contains lots of water (and hence protons) which gets aligned to large magnetic field to produce net average magnetic moment vector. The decay of the latter is detected as MR signal.

## 1.2. Introduction to Finite Element Modeling

---

MRI has a very high ability to distinguish the differences between two similar, but not identical, tissues. Behind this aptitude, there is a complex library of pulse sequences that the modern medical MRI scanner offers. Each one is optimized to provide image contrast based on the chemical sensitivity of MRI. A good segmentation for a good geometry reconstruction requires obtaining the best images. Different parameters can be adjusted to improve the final result. Echo time (TE) and repetition time (TR) are the two basic parameters of image acquisition. With particular values of those, a sequence takes on the property of T2-weighting. On a T2-weighted scan, water- and fluid-containing tissues are bright and fat-containing tissues are dark. The reverse is true for T1-weighted images. In a typical MRI examination 5-20 sequences are used. Each one is chosen in order to provide a particular type of information about the subject's tissues. Other parameters that have to be considered are the distance between the slices, usually around 2 mm, and the accuracy that is possible to obtain. **CT scan** makes use of computer-processed combinations of many X-ray images taken from different angles, to produce cross-sectional images of the area of interest of a scanned object. X-ray slice data is generated using an X-ray source that rotates around the object. Characteristics of its internal structure such as dimensions, shape, presence of defects, and density are readily available from CT images because of its high-contrast resolution. Tissues that differ in physical density by less than one can in fact be distinguished. The interval between two slides varies from 1 mm to 2 mm. In contrast to other techniques, MRI scan is harmless to the patient. It uses strong magnetic fields and non-ionizing radiation in the radio frequency range, unlike CT scans and traditional X-rays, which use ionizing radiation. However the average cost of a MRI acquisition is higher than the CT. For a FEM model, the choice of the techniques should be made considering the necessity of having a good definition of all the different tissues and a good spatial resolution. MRI is usually preferred since it is less invasive and it allows a greater accuracy in acquiring the musculoskeletal anatomy of patients alive.

### 1.2.2.2 Segmentation

Segmentation is the process of subdividing a digital image into several portions. The result is a set of segments that collectively cover the entire image. The two-dimensional case (2D) has to be distinguished from the 3D one. The first is generally adopted when the object of interest is considered approximately symmetrical, both in term of geometries and of materials, along one axis. However the state of the art prefers now 3D models.

As stated above, the construction of the geometric model originates from digital images like CT or MRI images. Different software have been developed for the seg-

mentation of the images and some of them are able to directly generate the mesh for the FE simulations. Others are able to segment the geometry of the tissues automatically and to supply the surface in STL format which can then be imported into specific software for the generation of the mesh. Within the volume of interest (VOI), voxels have to be divided in appropriate groups (bones, muscles, tendons, etc.). Available techniques try to climb over the manual drawing of the voxels through the use of methods for the identification of the contours [35]. Generally, the segmentation algorithms are based on one of the two fundamental properties of the levels of intensity of the voxel, discontinuity and similarity. The first partitions the image on the basis of the changes of the gray levels, such as the contours and edges, while the second based partitioning into regions that are similar according to a set of criteria predefined. Thresholding is a segmentation technique of the second type whose main action is that of searching for the voxel with intensity greater or lesser than a predetermined threshold. It is commonly use with CT images where the contrast among different tissues is very high and so a manual pixel-level user input is required only to define some suboptimal delineated border. MRI images instead have a larger grayscale and so segmentation required more manual work by an expert user. For this reason the geometry obtained with MRI images is sometimes less accurate than the one from CT images. Furthermore techniques that do filtering in the spatial or in the frequency domain may be adopted for the improvement of the quality of the image and for the extraction of the contours. In the spatial domain, an example is the Laplacian Of Gaussian Filter (LOG), where the strong high-pass characteristic of the Laplacian operator requires the use of a low-pass prefiltering of the image which ensures a good robustness against noise.

Clearly, accuracy of the final model is function not only of the resolution of the image, but also of innumerable other factors such as noise, poverty contrast between tissues, motion artifacts and also the interpretation of different operators. A suitable compromise for the development of an accurate FEM of the musculoskeletal system would be the combination of a subject-specific model with scaled models which derive, for example, the shape of the bones and the points of insertion of the muscles from the height and weight of the subject. This would involve applying an automatic segmentation of the points of interest and then to scale the other bones from a generic mesh through one of the available methods, thus reducing the costs of the development of the model.

### 1.2.2.3 Mesh

After the image segmentation, the geometry has to be converted in a 3D volume mesh which should have a smooth surface as closer as possible to reality. The accuracy



## 1.2. Introduction to Finite Element Modeling

---

of the mesh heavily depends on the algorithm used for the segmentation, while the quality of the mesh influences the FEA. The spatial discretization must have adequate extent, quality and shape in order to obtain an accurate solution.

Current methods applied for generating a subject-specific mesh are the following:

- **marching cubes** of Lorensen and Cline [36]: The algorithm proceeds through the scalar field, taking eight neighbor locations at a time thus forming an imaginary cube. Then it determines the polygon(s) needed to represent the part of the isosurface that passes through this cube. The individual polygons are finally fused together into the desired surface.
- **NURBS**, that is the use of B-splines;
- **regridding methods**, starting from an initial mesh of surface that can also not be optimal;
- **mapping methods**, where the surface is mapped in a triangulated plane, producing a high-quality 2D mesh;
- **mesh-cosmetic operations** that convert an initial mesh into one that is viable for the computation.
- **voxel approach** [35], which combines the search for the geometry and the mesh generation in a single step so that each segmented voxel is exported as a hexahedron.

Different types of elements are available to discretize the geometry of interest. For a 2D model triangular or quadrilateral elements are usually preferred. For 3D models the best choices are tetrahedral or hexahedral finite elements. It has been proved that in 2D FE modeling, quadrilaterals are always to be preferred. Triangles are quite convenient for mesh generation, mesh transitions and rounding up corners, but in FEA characterized by several degrees of freedom, 4-noded quadrilateral elements proved to give better results than 3-noded triangular elements [37].

In 3D FE modeling instead the preference is for the hexahedral elements. The tetrahedral mesh is fully automated and it allows the quick generation of millions of elements. Hexahedral mesh instead is only partially automated, it usually requires user intervention and it is labor intensive. In general the complexity of the geometry of the foot does not allow the use of hexahedral elements that usually provide better accuracy and lower computational costs. As a result most foot FEMs are built using tetrahedral

elements ([38], [39], [40], [41], [42]) which are more versatile in capturing the irregularities of the geometry of the bony structures [43].

Another interesting approach is represented by the use of quadratic tetrahedral elements. They have a high number of nodes, indeed they are also called ten nodes tetrahedron. It has been proved that they performed as well as the hybrid hexahedral elements in terms of contact pressure and contact shear stress predictions. The limit is given by the fact that the simulations are more computationally expensive than the hexahedral element simulations [44].

As already said the greater the mesh density is, the more accurate the results. A relatively fine discretization should thus be used in regions where a rapid variation of strains and/or stresses is expected. Examples are the surrounding area of concentrated loads or the sharply curved edges typical of the geometry of the bones. FEA software usually provides a section for the construction of the mesh but several dedicated software have been proposed. An example is given by *IA-FEMesh*, a freely available software toolkit developed by the University of Iowa in an attempt to facilitate anatomic FE model creation [45].

### 1.2.2.4 Boundary Conditions

At this stage of the analysis it is very important to define the regions of the model which require certain load conditions and how they interact with the physical structure of the model. In order to study the musculoskeletal system, variables easily measured by means of stereophotogrammetry and pressure platforms during a gait evaluation can be used. These are for example ground reaction forces and the positions of the specific joints of interest. For an improved accuracy it is also possible to acquire the movement of the joint by means of radiographic techniques. For example Banks and Hodge [46], followed then by others, used an iterative method of 3D alignment based on the match of shapes. They obtained the 3D movement of the joints by projecting the solid model obtained from MRI on the radiographic images. In this way the positions of the bones were well identified from the fluoroscopic images. However it must be remembered that this is an invasive technique and therefore little used. Where the subject specific loading conditions are not available, it is possible to obtain them from the literature.

### 1.2.2.5 Properties of the materials

The assignment of the properties of the materials of the tissues represents a fundamental step in the generation of FEMs. However, they are not always available and cannot be determined for any tissues, such as bones, ligaments and soft tissues, as standard and preliminary procedure to the simulations. In this case they can be obtained from

## 1.2. Introduction to Finite Element Modeling

---

literature. In 3D models, biological soft tissues are generally represented with isotropic hyperelastic models employing a second order polynomial strain energy potential. The formulation is the following (Equation 1.2):

$$U = \sum_{i+j=1}^2 C_{ij}(I_1 - 3)^i(I_2 - 3)^j + \sum_{i=1}^2 \frac{1}{D_i}(J_{el} - 1)^{2i} \quad (1.2)$$

Where  $U$  ( $Nm^{-2}$ ) is the strain energy density, and  $I_1$ ,  $I_2$ , and  $J_{el}$  (dimensionless) are the first and second deviatoric strain invariants and elastic volume ratio, respectively. The coefficients  $C_{ij}$  ( $Nm^{-2}$ ) and  $D_i$  ( $m^2 N^{-1}$ ) correspond to material characteristics [47].

Usually bones and cartilages are assumed to be homogeneous, isotropic, and linearly elastic. Young's modulus and Poisson's ratio are the only parameters requested and for bone structures, they can be estimated by averaging the values for the cortical and the trabecular parts in terms of their volumetric contribution. However, when such data are obtained from the literature, it should be considered that the mechanical properties of bones vary by subject, anatomical location, orientation, biological processes and time. When developing subject-specific FEMs, the mechanical properties can be obtained from a CT analysis. For example, Carter and Hayes reported a method to derive the distribution of mechanical properties in bone tissues from CT data, showing a linear correlation between the values of CT with the density of skeletal bone [48]. The same authors highlighted, through empirical studies, the relationship between bone density and mechanical properties. Finally, due to the high biological variability, the definition of the mechanical properties must often resort to the idealizations. For this reason it is recommended to conduct preliminary sensitivity tests to have information about the accuracy of the simulation.

### 1.2.2.6 Post-processing

When the simulation is done, the following step is of post-processing, or data analysis. To do so it is necessary that the FE mesh is constructed by taking into account the will of the analysis, or the type of results sought. For example, if the aim is to estimate forces or moments, one-dimensional elements are fine, but on the other hand, if the focus is on force fields or on displacements, 2D or 3D elements become necessary. The most frequently used variables in biomechanical analysis are the displacements of the nodes of the mesh, as well as the rotations. When 2D or 3D elements are used, force fields and displacements are calculated from the strain gradients and the properties of the materials. The estimation of the errors is a measure of the accuracy obtained with a given mesh or discretization time. It is generally good to run more than a

single FEA using different discretizations in space and time to highlight the possible influence of these aspects in simulation. For example, Cheung et al. [41] use a mesh of 50,964 tetrahedral elements while Chen et al. [38] built the model using 83.180 and 162.602 respectively tetrahedral elements for skeleton and soft tissues of the foot. They subsequently perform a sensitivity analysis to guarantee the convergence in the numerical results.

### 1.2.2.7 Validation

Finite element modeling is an approximation technique therefore it is necessary to demonstrate the validity of the solutions obtained. This validation process is divided into two parts: validation of the mesh and validation of the model. In biomechanics, the usual validation techniques for the mesh (test of convergence) are not applicable in the classic manner due to the large number of elements and for the irregular geometry of the structures. In these cases a test of general convergence it is usually carried out. Several alternative meshes with progressively increasing resolution are exploited while avoiding the systematic subdivisions typical of simple geometries. Actis et al. [49] obtained the numerical solution by subdividing the solution domain into elements and assigning polynomial degrees (p-level) to the approximating elemental shape functions that describe the displacement components within each element. Goske et al. [50] increased the density of the mesh until the peak plantar pressure was not exceeding 2% by decreasing the size of the elements. Alternatively a model validation can be used. In this case it is essential to know the source of information. For example, if a kinematic validation is chosen, it will be based on the comparison between points of displacement or speed of the model with those experimentally measured through stereophotogrammetry or fluoroscopy. An example of the validation of the model is provided by Chen et al. (2001) [51] who, given the absence of experimental results of the same subject under analysis, compared the results obtained with previous work of Soames [52] and Brown et al. [53]. Soames used the measurement of plantar pressure obtained from the gait analysis, and found that the highest average plantar pressure is situated under the third metatarsal head with values around 550-590 KPa. Brown et al. instead derived the dynamic plantar pressure using the FSCAN system during a normal walking with different foot orthoses. They found for the averaged peak of the plantar pressure, values of 1136 KPa in the forefoot and of 435 KPa in the five metatarsal heads. When-Ming Chen et al. [54] validate their model with subject specific geometry and boundary condition, comparing the predicted foot pressures with the experimental measurements. In particular with regard to the central metatarsal heads (second, third and fourth metatarsal) they reported a mean difference of 14.1% which they considered acceptable. Wei et al. [55] conducted two tests of validation of the model.

### **1.3. The Finite Element Method in the analysis of the biomechanics of the foot**

---

The first regarded the deformation of the ligaments. They recreated the experimental study conducted on the corpses by Colville et al. [56] on the deformations of the lateral ligaments of the human ankle. The second test recreated the study of corpses of Wei et al. [57] on the damage caused by excessive external rotation of the foot. Tao et al. [58] conducted sensitivity tests to evaluate the impact of using different modules of elasticity for bone, soft tissue, plantar fascia, ligaments and cartilage, in the prediction of the model. They used as principle index, the relationship between the strength of the plantar arch and the vertical displacements of the support plate. However, a statistical comparison between the FE results and experimental measurements within a certain range of usability can be considered an acceptable compromise [59].

#### **1.2.2.8 Errors**

Besides the choice of the validation process, it is important to be aware that in the FEA applied in a biomechanical context, there are always sources of error. The work of Anderson et al. [59] gives an accurate description of the most important sources of error that can influence musculoskeletal FEMs. In their work errors are classified as either numerical errors or errors of the model. The numerical errors refer to those coming from the resolution of mathematical equations through technical computational (discretization errors, incomplete convergence). The errors of the model are related to those simplifications, both physical and physiological, applied to the FEM (approximations in the geometries, properties of materials, boundary condition, etc.). Some errors can be decreased by using subject specific geometries and materials. Besides approximation errors or tolerances in convergences are difficult to prevent. Finally the human error, due to man-machine interaction, must be taken into account.

### **1.3 The Finite Element Method in the analysis of the biomechanics of the foot**

The first application of FEA in biomechanics appeared about 30 years ago. Since then, a significant acceleration in the development of mathematical models, software and tools has been observed, which provided a major precision and speed in the simulations. Recently, in the field of biomechanics, different studies have been published focusing both on 2D (see Figure 1.5), and 3D analysis (see Figure 1.6). A further distinction can be done within 3D models depending on whether they represent only a part of the foot or they consider the foot as a whole.

### 1.3.0.1 2D models of the foot

One of the first 2D models was created by Patil et al [60] in 1993. By using a radiographic analysis as a reference, they modeled the arc of an average human foot. The latter consisted of a membrane in two dimensions where two forces were acting: one at the heel in order to simulate the action of the Triceps Surae, the other in correspondence of the cuneiform-metatarsal bones simulating the effect of the Tibialis Anterior muscle. They analyzed the stresses inside the foot during three quasi-static walking phases: heel-strike, mid-stance and push-off. The results served as guidance for the following higher level of complexity models. In 1997 Lemmon et al. developed a more complex model with the aim of overcoming the trial-and-error process for the design of foot orthoses. They elaborated a 2D FE model of a slice of the second metatarsal bone and the underlying soft tissue. Alterations in pressure distribution correlated to insole and tissue thickness were investigated. The reduction of plantar stresses in the simulations with the insole (approximately 2 KPa for each millimeter of thickness of the insole) was demonstrated. Furthermore they reported that the use of an insole in a foot with reduced tissue, resulted in a reduction of the peak pressure by approximately  $6\text{KPa}\text{mm}^{-1}$  [61]. The already mentioned Goske et al. (2006) [50], studied the effects of the properties of the insoles in reducing plantar pressures, by building a 2D model of a foot with a thick section of 55 mm. The geometry was obtained from a coronal MRI of the right heel of an adult male patient. Bones were assumed as a hard tissue while the heel soft tissue was modeled with a hyperelastic energy function and meshed with quadrilateral elements. Halloran et al. in 2010 [62] presented a study which combined a 2D musculoskeletal model with a 2D FE model of the foot. The first contained seven body segments: trunk, thighs, shins and feet. The joints were modeled as ideal hinges. Furthermore eight muscles were considered including Gastrocnemius, Soleus and Tibialis Anterior, each one represented by a three elements Hill's muscle model. A descriptive model of the friction was also added. The second model instead represented the geometry of bones and tissues of the foot with a sagittal section along the second radius. The bones were represented as rigid tissues while soft tissues were modeled with an Ogden formulation with properties of material obtained from indentation test. The bones of the phalanges were combined together. A more recent study that uses gait analysis data to drive simulations of foot 2D FE models was proposed by Guiotto et al. in 2015 [63]. The purpose was to develop two finite element models of the hindfoot, of healthy and diabetic neuropathic subjects for the diabetic foot prevention.

In the 2D models the level of simplification and the number of assumptions are high. However they represent a fast compromise for analysis limited to a part of the foot, in case of symmetric geometries and for feasibility studies.

### 1.3. The Finite Element Method in the analysis of the biomechanics of the foot

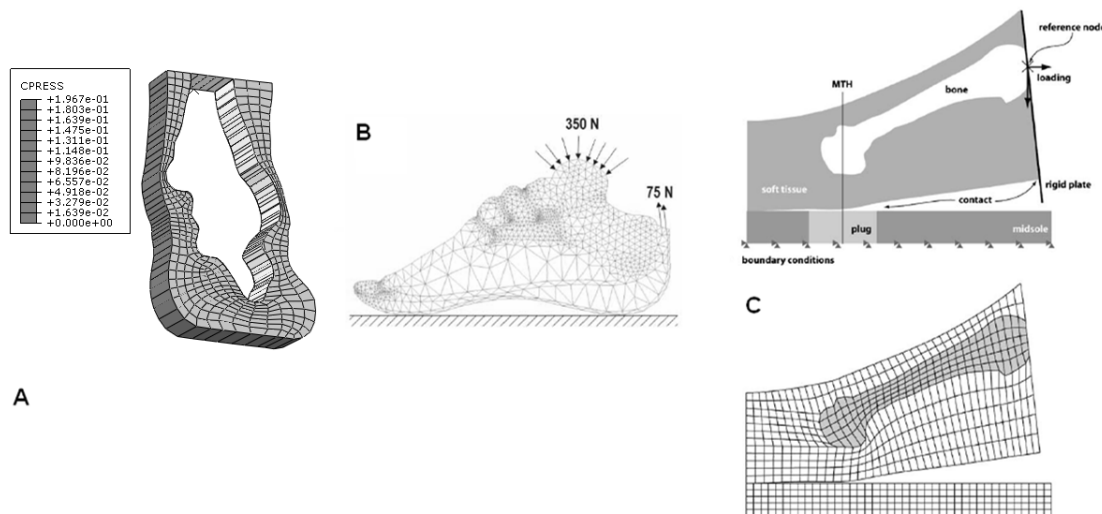


Figure 1.5 – A) 2D model of the heel pad developed by Guiotto et al. [63]. B) 2D model developed by Agic et al. [64]. C) 2D model developed by Erdemir et al. [65]. The Figure on the top shows the model description, the one below the meshed model.

#### 1.3.0.2 3D models of the foot

3D FE modeling is more adequate than the 2D one because it considers the real geometry and boundary conditions allowing a more accurate prediction of the stress-strain behaviour of the heel pad [65]. The development of 3D models of the feet, gave indeed new insights into the internal load distribution. As previously said, some of those models considered the foot as a whole, while other analyzed only part of it as done for example in 2007 by Budhabhatti et al. They developed indeed a 3D FE model for the evaluation of the effect of orthopedic surgery on the first ray of the foot [66].

The first 3D foot FEM can be considered the one of Chu et al. **in 1995** even though the geometry and the FE formulation were very simple. They presented an asymmetric 3D FE model for analysis of the effects of ankle-foot orthoses [67].

**In 2000**, Gefen et al [42] developed the first 3D model which incorporated realistic geometry and material properties of both skeletal and soft tissue components of the foot. They integrated the optical Contact Pressure Display (CPD) method for plantar pressure measurements with the Digital Radiographic Fluoroscopy (DRF) instrument for the acquisition of skeletal motion during gait. The latter allows the knowledge of kinematics and dynamics of the foot during the analysis. The model was built for individual parts. The tridimensionality of each bone was obtained using a software for the surface generation (SURFdriver), and afterwards the relative position of the bones was determined thanks to a sagittal MRI of the subject. The model consisted of 17 bones, connected by cartilage; also in this case the proximal phalanges, both medial and distal, were unified for simplification. Also 38 ligaments were included together

## Chapter 1. Introduction

---

with the plantar fascia and the soft tissue. Bone and cartilages were assumed to be homogeneous, isotropic and linearly elastic materials. Ligaments, plantar fascia and soft tissue were instead not linear. Some muscles forces obtained from literature were also added and adapted through a process of convergence in order to get a correlation between simulated and experimentally acquired data. An add-in of this study with was that the model simulations were run over a series of six sequential characteristic subphases of the stance. For the validation of the model, the same authors developed new technique for dimensionless characterization of the Foot-Ground Pressure Pattern evolution.

**In 2001** Chen WP et al. proposed a [51] a less accurate model, with a simplified geometry and a mesh characterized by a low number of elements. For the sake of model simplification and to reduce computational complexity, the bones of the five phalanges were modeled as five integrated parts and the rest of the metatarsals and tarsal bones were modeled with two rigid columns. The authors introduced important novelties like, for example, the possibility of moving the support according to 3D linear and angular displacement of the foot with respect to the ground acquired with a stereophotogrammetric system during gait. The mesh adopted was tetrahedral. All the elements were assumed to be homogeneous, and the materials were modeled as linear elastic materials with properties chosen from previous literature. The main drawbacks were the lack of patient specificity (both in terms of material properties and of the plantar pressures used for the validation, which were derived from literature) and the excessive simplifications on the structures and mesh. However the same model was used by the authors in 2003, to study the effect of total contact insoles on high plantar pressure [68].

**In 2005** Cheung et al. proposed a highly detailed model of the human foot and ankle that incorporated realistic geometry of both bony and soft tissue components. The geometry of the model was obtained from the reconstruction of the MRI of a right foot of a healthy adult male subject. The model included 28 bone segments, 72 ligaments and the plantar fascia, all wrapped in soft tissue. The structures were meshed with a total of 50,964 tetrahedral elements and contact surfaces were defined in order to allow the relative movement of the joints. Ligaments were defined with tension-only truss elements. All tissues were considered as homogeneous, isotropic, and linearly elastic and the characteristics of the materials were taken from literature. The ground support, where the GRF was applied, was simulated with a rigid bottom layer. The foot-insole interface was modeled using contact surfaces with a friction coefficient of 0.6. Only simulations in balance standing condition were performed, applying to the ground a load of half-body-weight and an Achilles tendon force of half of the ground-load. The superior surface of the soft tissue, distal tibia, and fibula was fixed throughout the whole analysis. To validate the model, the subject specific plantar



### 1.3. The Finite Element Method in the analysis of the biomechanics of the foot

---

pressures were measured during barefoot standing and compared to the simulated ones. The authors demonstrated that the custom-molded shape is more important in reducing peak plantar pressure than the stiffness of the insole material.

**In 2008** Cheung and Nigg [69] improved the model to analyze the internal stresses and deformations, which were unlikely to be measured with other methods certainly more invasive and expensive. They added the action of 9 extrinsic muscles which strength was obtained from electromyography. The reaction force was applied to a supporting horizontal plane whose angle was established by kinematic boundary conditions. With this model they analyzed the effect of the hardness of the soft tissues, the influence of the forces applied to the Achilles tendon, the load distribution in the case of a Tibialis Posterior dysfunction, the effects of merging first and second metatarsal heads with the medial cuneiform bone and the plantar pressure distribution when using an insole which was also developed in the FE environment and modeled with different material properties.

Tao et al **in 2009** [58] built a foot FE model a healthy subject from a MRI. The model consisted of 30 bones (28 bones in the foot and the distal segments of the tibia and fibula), 53 ligaments, plantar fascia and cartilage, all covered by soft tissue. The joints of the tarsus and metatarsus were simplified because of their reduced mobility. The plantar fascia was simulated using five connectors. All tissues were defined homogeneous, isotropic and linearly elastic with mechanical properties taken from the literature. The same subject was subjected to an analysis in which they recorder the plantar strength, the plantar pressures and the deformation of the surface, during six different loading conditions. This analysis was conducted through the use of markers and radiography.

**In 2010**, by considering only the forefoot, Gu et al. developed a 3D FE model to investigate the effect of inversion positions on stress distribution and concentration within the metatarsals [70]. The importance of well positioning the foot with respect to the ground in the FE simulations was highlighted.

Iaquinto and Wayne [71] built a 3D model from a CT of a cadaveric foot from which they derive the anatomy of bones, ligaments and muscle insertions. The strength of this study was the possibility of obtaining physical parameters not measurable with in vivo experiments. The validation was performed by comparing the model results with two different experimental studies (Arch Stability range and Release). Even Qian et al [72] and Antunes et al [73] created a model from CT images, but in this case the subject was an alive adult. Through the images they reconstructed the skeleton of the foot. With an MRI, Qian et al. placed also the muscles. Antunes instead defined the plantar fascia (geometrically simplified in five rays) and the Achilles tendon using axial connectors. In addition, they fixed the upper surface of the foot, the tibia and the fibula, with a boundary constraint. The mechanical properties were obtained from

literature.

**In 2010** Chen WM et al. developed a model with the purpose to predict both the foot 3D, internal, plantar soft-tissue deformation and stress. The principal novelty was in this case represented by the introduction of an accurate soft tissue model with isotropic, incompressible, hyperelastic second order polynomial formulation. Furthermore they represented relative articulating movements with surface-to-surface contact elements between adjacent bones. This allows the bones to slide over one another without friction and transmitting only compression forces. Phalanges were merged together with the cartilage as done by Cheung, Mphil and Zhang [33] and Cheung and Nigg [69]. Tendons were considered isotropic linearly elastic materials with Young's modulus of 816 MPa (Achilles) and 450 MPa (for other tendons) and a Poisson's ratio of 0.3. Subject-specific acquired plantar pressures were used for the validation of the model: good predictions were shown. [38].

**In 2011**, Natali et al. [74] contribute to the field by defining an appropriate hyper-elastic constitutive model of adipose tissues and plantar fascia. This was done by considering that their mechanical behavior is a determinant factor in the changes of distribution of the plantar pressure. However no cartilage elements, nor tendons or ligament, with the exception of the plantar fascia, were added to the model.

**In 2012** the authors improved their model in order to analyze the role of the Gastrocnemius-Soleus complex in a gait analysis [75]. The work was based on the previous developed 3D FE model of a human foot with the addition of some muscles, such as the Gastrocnemius-Soleus complex, Tibialis Posterior, Flexor Digitorum Longus, Peroneus Brevis and Longus, which were created using a linear approximation. Subject-specific peak plantar pressures were again acquired for the model validation. In order to study the effect of the variation of the Gastrocnemius-Soleus complex, a multi-step analysis, in which the force was progressively reduced of 10%, was adopted.

In the same year, Fernandez et al [77] built a foot FE model starting from the Visible Human male [79]. The geometries were developed by the "*International Union of Physiological Sciences Physiome project*", which made sharing through the scientific community easier. The database thus obtained included bones, soft tissue and other structures such as arteries and nerves. The foot was later adapted in order to capture the shape of the foot of the subject, using the images obtained with an MRI. The distribution of fibers, derived from each muscle, was then added, creating a continuum with the mesh. Using a specific algorithm, also the main nerves pathways were added. A quasi-static analysis was performed and the ground reaction force at heel-strike, midstance and toe-off was applied by means of a horizontal plane that interacted with the sole of the foot. The aim of the work was the evaluation of the influence of the tissue stiffness in the contact pressures and the internal stresses in the case of diabetic foot. They based the study on a single subject of whom they acquired the

### 1.3. The Finite Element Method in the analysis of the biomechanics of the foot

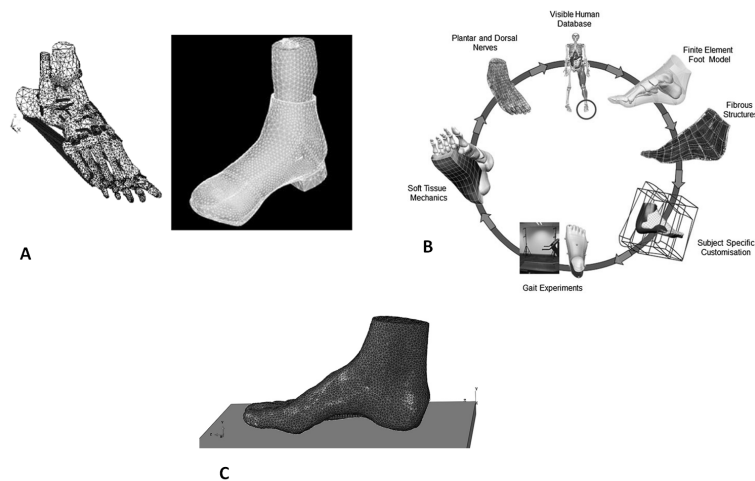


Figure 1.6 – A) 3D coupled foot-boot model developed by Qiu et al. [76]. B) Workflow for the generation of a FEM proposed by Fernandez et al. [77]. C) 3D model developed by Guiotto et al.[78].

foot geometry, kinematics, kinetics and pressures. The results obtained were similar to those of the work previously presented by Chen et al, Gefen et al, and Cheung and Nigg.

A more recent work has been conducted by Guiotto et al [78] **in 2014**. They compared a model of a healthy person with a model of a diabetic subject. Both were derived from MRI images in which the 30 bones were merged into three subgroups: forefoot, which included the metatarsal bones and the sesamoid bones, the midfoot which included the cuboid and the cuneiform bones and the hindfoot which contained the talus and the calcaneus. The phalanges were free to move with respect to the metatarsal bones in order to allow the dorsiflexion. The properties of the materials were taken from the literature; bones, ligaments and plantar fascia were assumed to have a linear isotropic behavior. The soft tissue was represented by a second order polynomial formula. The plantar fascia was simulated with not-compressible axial connectors according to their physiology. During the FEA the upper part of the tibia-fibula and the soft tissues was fixed in order to simulate the effect of the overlying tissues.

#### 1.3.1 Summary on the foot FEM

In the previous paragraph, a large part of the various techniques adopted for the creation of a FEM, has been reported. In summary, the images can be acquired via CT ([42], [71], [72], [73]) and/or MRI ([50], [69], [71], [72], [58], [78]) and meshed with tetrahedral elements. It is also possible to use models already prepared and to customize them, as done in the work of Fernandez et al. [77]. The foot structure can be

made by the individual bones but often phalanges and related cartilages are unified for the sake of simplification, considering the few degrees of freedom ([62], [75], [33], [69], [78]). The same applies to the joints of tarsal and metatarsal bones [58], [78]. As regards to the properties of the materials and the muscles, especially in the analysis of subjects *in vivo*, they are usually taken from literature. In particular, the bones are assumed rigid with a Young's modulus of about 7300 MPa and a Poisson ratio of 0.3. The soft tissue can be modeled with a first order Ogden formulation ([62], [75]) or in general as an incompressible hyperelastic and isotropic material with Young's modulus about 0.45 MPa and Poisson ratio 0.45. Cartilages are represented with the Young's modulus of about 1 MPa and the Poisson index of 0.4; for ligaments and the plantar fascia, respectively, the Young's modulus is 250 MPa and 350 MPa [78]. In general muscles are modeled as axial connectors, with forces obtained from the literature, in most cases, or through electromyography. Remarkable improvements were made in few years. Most of these works, however, while being of great importance and significance, have some limitations including the not complete subject-specificity in deriving muscular forces or the geometries of the foot. Furthermore walking velocities, kinematics and ground reaction forces of the healthy subjects are often assumed to be similar to the ones of pathological subjects, which is not true especially in the case of advanced diabetes. The above are the main limitations that this thesis proposes to overcome.

### 1.3.2 Software for the Finite Element Analysis

The implementation of a FEM requires the use of different software. In this thesis, the segmentation was done using **ScanIP**, one of the three platforms of *Simpleware* for managing 3D images. It provides a working environment rich of tools to view and to segment the regions of interest from 3D volumetric data, such as MRI and CT. The segmented images can be exported as STL format for CAD analysis. *Simpleware* also offers the package **ScanFE** by which it is possible to convert 3D segmented images in volumetric or superficial meshes. The third platform is *ScanCad* which allows to import and to interactively place CAD models.

*Simulia* **ABAQUS**, a package for engineering simulations, was used for the creation of the FEM. It can solve problems that range from the simplest linear cases to the most complex not-linear analysis. It is characterized by an extensive library of FE, virtually able to model any geometry, by a considerable number of models for the description of the behavior of materials (metals, rubbers, polymers, composites, etc.) and by the possibility of simulating a good number of physical phenomena: structural problems, heat transfer etc. It is divided in more products (ABAQUS/Standard, ABAQUS/Explicit, ABAQUS/CFD, ABAQUS/CAE). In this thesis ABAQUS/CAE (Abaqus Complete

### **1.3. The Finite Element Method in the analysis of the biomechanics of the foot**

---

Environment) was used given its possibility to implement the pre-processing and post-processing and to monitor the results.

### 1.4 Introduction to the Gait analysis

The previous paragraph highlighted that biomechanical factors play a crucial role in the etiology, treatment and prevention of diabetic foot ulcers. Before the application of any treatment, it is indispensable to understand the biomechanics of the foot. To evaluate the conditions of a diabetic patient a study of his gait is usually performed. Different aspects are analyzed:

- **Kinematic**, which studies the positions of the body segments in space, their velocity, acceleration and joint angles through stereophotogrammetric systems, electrogoniometers or inertial sensors;
- **Kinetic**, which includes the study of ground reaction forces and moments recorded through force plates;
- **Electromyography**, which studies the muscle activation through an EMG device;
- **Plantar pressure distribution** acquired with pressure mats or pressure insoles.

The evaluation of all or of part of these variables is called gait analysis.

#### 1.4.1 Gait cycle

During walking, one limb acts as a mobile source of support, while the other moves forward to the next support; subsequently the two limbs reverse their roles. During the transfer of the weight from one to the other, both feet are in contact with the ground. A single sequence of these functions by one limb is called *gait cycle*. Since each action is directly concatenated with the next, it is difficult to determine the start and the end point. Conventionally the beginning is identified in the moment of contact of the foot with the ground. Healthy individuals begin ground contact with the heel strike, but since not all the patients have this capability, the generic term initial contact is preferred to indicate the onset of the gait cycle.

Each cycle is divided in two periods (See Figure 1.7):

- **stance**, interval during which the foot is in contact with the ground, usually it occupies the 60% of the entire cycle;
- **swing**, the time in which the foot is lifted from the ground for the advancement of the limb; it occupies the remaining 40% of the cycle;

## 1.4. Introduction to the Gait analysis

---

The stance phase is furthermore subdivided into three intervals (See Figure 1.7):

- **initial double stance** is the start of the cycle. It corresponds to the moment in which both feet are on the floor after the initial contact;
- **single limb support**, begins when the opposite foot is lifted from the ground ready for its swing phase; in this time all the weight rests on one leg. Its duration is thus a good indicator of the limb's support capability;
- **terminal double stance**, begins when the opposite foot ends its swing phase and rests on the ground. It then continues until the original stance limb is lifted for swing.

Rancho Los Amigos gait analysis committee developed a generic terminology for the functional phases of gait, in order to create a common standard to share in the clinical and research community [80]. The terminology directly reflects the functional meaning of the different movements at the single joints level. The sequential combination of the phases enables the limb to accomplish three basic tasks:

- **weight acceptance** which begin the stance period and includes the two first phases of it;
- **single limb support**, which continues stance with the next two phases;
- **limb advancement**, which starts from the final phase of stance and then continues through the three phases of swing.

The functional phases of gait are eight (See Figure 1.7):

1. **Initial Contact:** 0-2% of the gait cycle; includes the time at which the foot is in contact with the ground. The limb is positioned so that it can begin the full support through the heel rocker.
2. **Loading Response:** 2-10% of the gait cycle, practically coincides with the range of the initial double support. The impact of the contact with the floor is absorbed and the body under load is stabilized.
3. **Mid-stance:** 10-30% of the gait cycle, it is the first half of the single limb support interval. Ends upon reaching the stability of the limb and torso as the weight of the body is aligned on the forefoot.

## Chapter 1. Introduction

4. **Terminal stance or push off:** 30-50% of the gait cycle; final phase of the single support. The weight of the body is transferred over the forefoot.
5. **Pre-swing:** 50-60% of the gait cycle; it coincides with the terminal double stance. In this phase the load transfers from one limb to the other in order to predispose the limb that was in stance for the swing.
6. **Initial swing:** 60-73% of the gait cycle, it is the first third of the swing phase. It has the objective to raise the foot from the ground and to advance the limb to a position parallel to the limb in support.
7. **Mid-swing:** 73-85% of the gait cycle; second phase of the oscillation period. It ends when the swinging limb is forward and the tibia is vertical (equivalence between flexion of the hip and knee).
8. **Terminal swing:** 85-100% of the gait cycle, is the final phase of the oscillation. Leading to the full advancement of the limb (leg is in front of the thigh), it ends when the foot touches the ground.

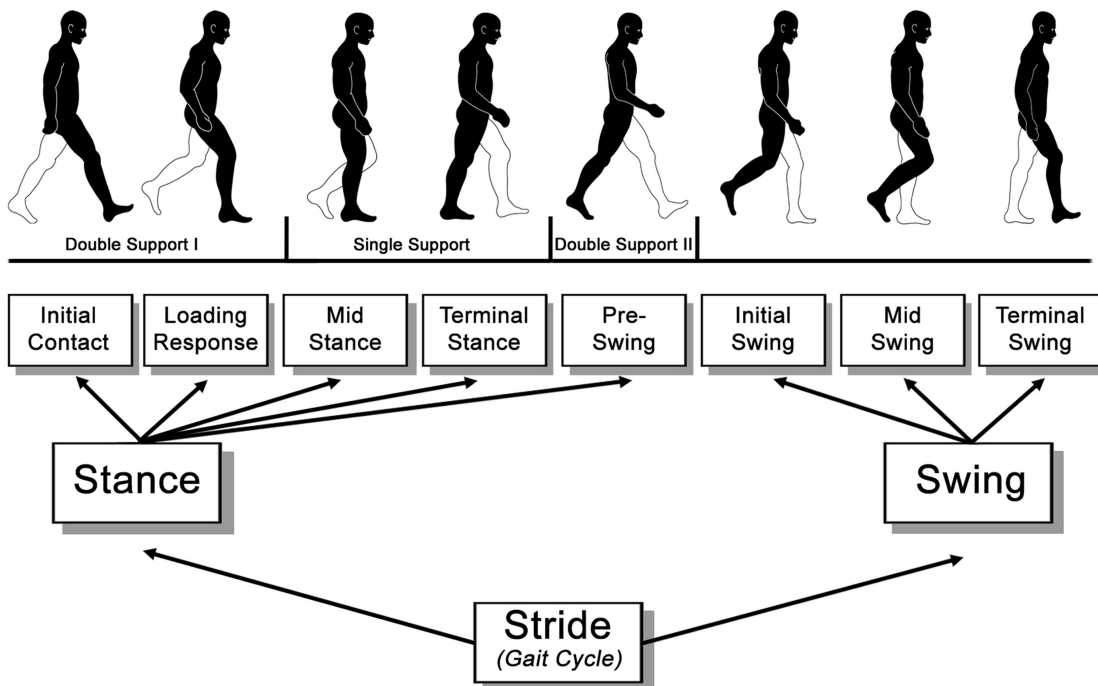


Figure 1.7 – Functional divisions of the gait cycle according to Perry and Burnfield [24], [81].

The main spatial-temporal parameters of the gait cycle are [24]:



- **Gait Cycle:** the period of time between an event and its next occurrence in the same foot [s].
- **Gait Stride:** the distance between the initial contact of a foot and the next initial contact of the same foot [m].
- **Stance phase:** the period of time when the foot is in contact with the ground [s].
- **Swing phase:** the period of time during which the foot is not in contact with the ground [s]. In the case where the foot does never lift from the ground (drag foot), it is defined as the phase in which all the parts of the foot are moving forward.
- **Double support:** the period of time in which both feet are in contact with the ground [s]. It happens twice in a gait cycle.
- **Single support:** is the period of time when only one foot is in contact with the ground [s]. It coincides with the swing phase of the other foot.
- **Step length:** the distance between a contact point of a foot with the ground (usually the heel) and the same point of contact with the ground of the other foot [m].
- **Step period:** is the time needed for the step length [s].
- **Speed:** the linear velocity along the direction of progression of one or more measured steps [m/s].
- **Cadence:** number of steps per minute [steps/min].

### 1.4.1.1 Muscle control during the gait cycle

The activity of the flexor muscles starts during pre-swing. The first muscle to contract is the extensor of the big toe, which is active throughout the pre-swing. Immediately after, during the mid-swing, the Tibialis Anterior and the Extensor Digitorum Longus are active. The intensity of the contraction of the Tibialis Anterior grows fast during initial swing. In the terminal swing it increases more gradually, in order to position the foot for the support. The action of the Extensor Digitorum Longus is parallel to that of the Tibialis Anterior, but with amplitude lightly lower. The action of the Soleus muscle starts at the end of the loading response and remained constant throughout the mid stance to take a quick and marked peak from the 45% of the gait cycle. Subsequently the intensity decreases with a similar speed, to stop at the beginning of double support (pre-swing). The medial head of the Gastrocnemius is activated in parallel with the Soleus, while the beginning of the lateral head can be delayed until the midstance.

The other perimalleolar muscles show modest plantarflexor efficiency, since their alignment gives them a different primary role in the gait: the control of foot joints. The Tibialis Posterior becomes active at initial contact and continues throughout the individual support. The contact of the opposite foot (50% of the gait cycle) represents the signal for the relaxation of the Tibialis Posterior. The action of the peroneal muscles begins early during the gait cycle and ends in pre-swing (55-58% of the gait cycle) [24].

### 1.5 Gait analysis instrumentation

In this paragraph only the instrument setup and protocols adopted for this thesis is presented.

#### 1.5.1 Kinematic - Stereophotogrammetric systems

The study of human movement involves the measurement of variables that describe the kinematics and the kinetics of anatomical segments. The kinematic variables (positions, velocities and accelerations) are obtained through MoCap systems, while the kinetic variables (forces, moments) are obtained indirectly by the measurement of the external forces acting on the subject. Different commercial systems are available for the measurement of kinematic quantities. They are characterized by heterogeneous technologies and different degrees of invasiveness:

- electrogoniometers and accelerometers;
- electromagnetic systems;
- systems based on acoustic sensors;
- optoelectronic systems.

Current research is moving in the direction of developing methodologies for estimating the human movement, with simpler and relative cheap devices like inertial sensors. However the most commonly used systems for the estimation of human movement are still the optoelectronic ones that use cameras operating in the range of the visible or near infrared. They ensure high accuracy even though they can provide only an estimate and not the direct measure of the kinematic variables.

The use of cameras with infrared emitters together with passive markers is called stereophotogrammetry. [82]. Passive markers are small plastic balls covered with reflector film. In contrast to the active ones they do not have a led that generates light,

## 1.5. Gait analysis instrumentation

thus they need an additional lighting device with specific wavelengths (780-820 nm). Their spherical shape provides the best reflection of infrared rays and with cameras equipped with an appropriate optical filter, they are immediately recognizable from the background. When setting up a laboratory the location of the cameras has to be decided considering the motion that has to be studied. Before starting the acquisition the cameras have to be calibrated so their geometrical parameters have to be settled. Furthermore the volume of interest where the subject is going to move has to be defined together with the reference system of the laboratory. When a data collection is performed, data are processed by an elaboration software that using different algorithms to detect the markers locations in the 3D space. For this thesis, a stereophotogrammetric system was adopted and passive markers were double-side taped to the skin of the subjects at various anatomical landmarks of the body and of the feet, according to the protocol described in [83] and in [84]. The Bioengineering of Movement Laboratory (DEI - University of Padova) is indeed equipped with a 60-120 Hz 6 cameras stereophotogrammetric system (BTS S.r.l, Padova) (See Figure 1.8). Sensors of the cameras are CCD (1/2" F 1.4/4.5 mm) with IR filters. The video resolution is 640 x 480 pixels while the lenses are 3.5mm and 6-12mm.

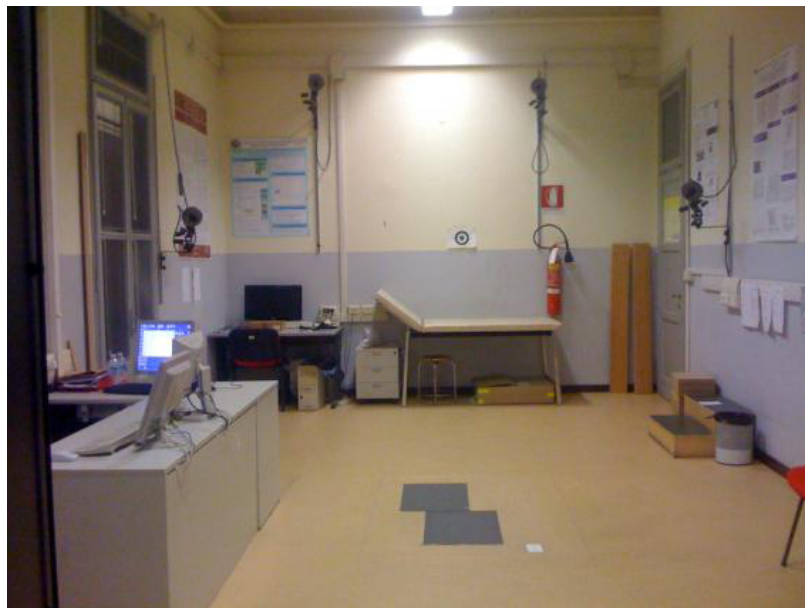


Figure 1.8 – The Bioengineering of Movement Laboratory (DEI - University of Padova) with the stereophotogrammetric system and the force plates.

### 1.5.2 Kinetic - Ground Reaction Forces

The analysis of human movement is intended to gather quantitative information not only on the kinematics, but also on the kinetic of the act. In fact, the human body

## Chapter 1. Introduction

---

moves under the action of internal forces, namely the action of the muscles within the constraints of the joints, and external forces, exchanged from the body with the environment. Locomotion and upright posture can be studied both in the living environment, through wearable technologies, and in the laboratory, providing walkways properly instrumented and trying not to interfere with the free expression of the motor act. Force platforms embedded in the walkway of the laboratory represent the gold standard in this area. Force platforms are measuring instruments that detect the GRFs generated by a body standing on or moving across them, to quantify balance, gait and other parameters of biomechanics. The detection of the GRFs is enabled by trans-

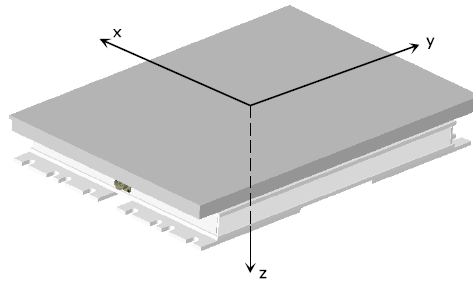


Figure 1.9 – Bertec force plate with its reference system [85].

ducers that rely on the effects of the mechanical deformation, directly proportional to the intensity of the forces they bear and they have to measure. The quality of the measurement is mainly influenced by the elastic response of the transducer, which ideally should be linear and without phase distortion across the field amplitudes and speed. The two technologies most commonly uses are based on piezoelectric crystals or on strain gauges. The first solution is not suitable for measuring static loads, because the electric charge disperses over time. The strain gauge sensors have a frequency response lower than the piezoelectric crystals but they are cheaper and they can be used for the posturographic examination Measures are given according to the reference system associated with the platform and usually provided by the constructor. More advanced and most commonly used devices measure the 3D components of the single equivalent force applied to the surface and its point of application, usually called the centre of pressure, as well as the vertical moment of force. For this thesis two strain gauge force platform (FP4060-10, Bertec Corporation, USA) have been used [85] (see Figure 1.9). The technical characteristics of the platforms are reported in Table 1.1 and Table 1.2.

## 1.5. Gait analysis instrumentation

Table 1.1 – Technical details of the force plates-item 4060-80 (Data sheet [85]).

Size [mm]			Weight (kg)	Rated Load (KN)			Natural Frequency (Hz)		
L	W	H		Fx	Fy	Fz	Fx	Fy	Fz
600	400	83	28	5	5	10	550	540	340

Table 1.2 – Technical details of the force plates-item 4060-80 (Data sheet [85]).

	Fx	Fy	Fz	Mx	My	Mz
<b>Rated Load (KN,KN*m)</b>	5	5	10	3	2	1.5
<b>Overload Factor (%)</b>	50	50	50	50	50	50

### 1.5.3 Plantar pressure [86]

During locomotion the forces exchanged between the human body and the ground are spread on the support structures of the foot. Knowing how they are distributed is very important (e.g. in the pathology of the diabetic foot) and the only measure of the GRFs provided by the force platforms is not enough. Recently, low cost technologies have made possible the realization of devices which measure only the vertical component of the force through matrix of sensors. Since the active area of the single device is known, it is possible to express the response in pressure, as the average force on area ( $F/A$ ). These measuring systems thus provide the distribution of the pressures on a surface with a good detail which is set according to the application needs. Typically the individual pressure sensors are arranged in matrices to form pressure platforms or insoles. The latter have the advantage that they can be inserted inside a shoe thus allowing moving from the laboratory environment and measuring within shoes foot pressures. However they are less accurate than the pressure platforms due to deformation that can occur on the sensors while adapting to the shoe shape and to possible movements or misplacements inside the shoe. The relevant characteristics that should be considered when using a pressure system are:

- spatial resolution, which is the distance between the centers of two adjacent sensors. It is important in order to obtain information under the smallest structures of the foot, such as the metatarsal heads;
- area of the sensor. Ideally, sensors should be point given that the greater the surface is, the greater is the resulting error;
- sampling frequency. It should be the highest possible but usually the limit is in the in the large amount of data that has to be registered.

## Chapter 1. Introduction

---

- type of sensors. They are usually either resistive or capacitive. The first ones have to be avoided in case of postural examinations, due to the presence of the phenomenon of creep [86]. The second one are usually more accurate but more expensive as well.

The Bioengineering of Movement Laboratory (DEI - University of Padova) is equipped with two plantar pressure systems (Imagortesi, Piacenza, produced by Medicapteurs, France, Figure 1.10), whose technical characteristics are shown in Table 1.3 and 1.4.

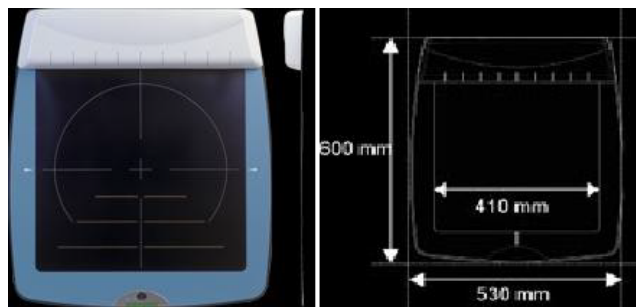


Figure 1.10 – Winpod Pressure platform and its dimensions [87].

Table 1.3 – Structural characteristics of the plantar pressure systems [87].

<b>Size (length/depth/height)</b>	530 x 600 x 45mm
<b>Thickness of the sensors</b>	4mm
<b>Detectable area</b>	382 x 382mm
<b>Weight</b>	6,8kg

### 1.5.4 Protocol for motion analysis

In motion analysis protocols are used to make clinically interpretable kinematic and dynamic parameters of the pelvis and the lower limbs. A protocol defines a biomechanical model and the procedures to acquire process and analyze the data, in order to get some information from them. The synchronization between different instruments is a delicate and mandatory step in order to provide a comprehensive analysis of the movement of body segments. The various protocols can be distinguished for the marker-set and the acquisition procedures adopted as well as for the proposed biomechanical model.

In this thesis two protocols proposed by Sawacha et al. were used: a *FullBody* and a *Foot* model. The existent motion analysis protocols are indeed not suitable for the analysis of the diabetic patients. They include the use of rigid plates applied with

## 1.5. Gait analysis instrumentation

Table 1.4 – Electronic characteristics of the plantar pressure systems [87]).

<b>Sensors type</b>	Resistive
<b>Sensor size</b>	8mm x 8mm
<b>Sensor thickness</b>	0,15mm
<b>Number of sensors in the platform</b>	2304 = 48 x 48
<b>Resistor</b>	>1M
<b>Sensor accuracy</b>	±5%
<b>Rise time</b>	1 to 2ms
<b>Operating temperature</b>	-40 to +85°C
<b>Average life time of sensors</b>	>1 M of activations
<b>Minimum pressure detectable</b>	4 $N/cm^2$
<b>Maximum pressure detectable/sensor</b>	100 $N/cm^2$
<b>PC connection</b>	USB
<b>Power supply</b>	External transformer 12V DC
<b>Frame rate (sampling frequency)</b>	≤ 150Hz
<b>Analogical/digital conversion</b>	8 bit, 255 values

elastic bandages and long calibration procedures which are not easily applicable to patients affected by neuropathies ([88], [89]). Also models that consider the foot as a single segment, or that do not consider the relative movement of the midfoot with respect to the adjacent bone segments, can not fully describe the kinematic complications arising from the disease. The *FullBody* model is a modification (Sawacha et al. [90]) of the protocol of Leardini et al. [91] done in order to study the gait changes in the patients with diabetes mellitus. It requires the direct application of 24 markers on anatomical landmarks distributed among the head, torso, thigh, leg and foot, and of additional 24 markers for the composition of the six clusters of the pelvis, thigh and leg (Figure 1.11). The center of the femoral head is reconstructed either using the method of Harrington [92], that means using anthropometric tables, or with the functional method [93], according to the ability of the subjects to move. The second approach indeed calculates the center of the best sphere described by the trajectory of markers placed on the thigh during several trials of hip rotations. It is thus mandatory that the subject under analysis can rotate the hip without major complications.

The *Foot 3D* 4-segment protocol consists in the application of marker directly on the skin in correspondence of the anatomical landmarks. The distribution of the 13 anatomical markers is the following (Figure 1.12 and 1.13):

Tibia:

- Tibial Tuberosity (TT)



Figure 1.11 – Marker set of the *FullBody* Protocol [84].

- Head of Fibula (HF)
- Lateral Malleolus (LM)
- Medial Malleolus (MM)

Hindfoot:

- Calcaneus (CA)
- Peroneal Tubercle (PT)
- Sustentaculum Talii (ST)

Midfoot:

- Navicular Tuberosity (NT)
- Cuboid (C)
- Fifth Metatarsal Base (VMB)



Forefoot:

- Fifth Metatarsal Head (VMH)
- First Metatarsal Head (IMH)
- Proximal epiphysis of Second Toe phalanx (IIT)

The model of the three subareas in which the foot is divided is obtained by projecting the anatomical landmarks, identified by its marker, on the footprint (Figure 1.13). The three sub-areas that result are:

- **Hindfoot:** the area between the line connecting both the vertical projection of the sustentaculum tali and the peroneal tubercle and the vertical projection of calcaneus;
- **Midfoot:** the area between the anterior reference line of the hindfoot and the line connecting the vertical projection of the first and fifth metatarsal head;
- **Forefoot:** the area between the anterior reference line of the midfoot and the end of the anterior border of the footprint.

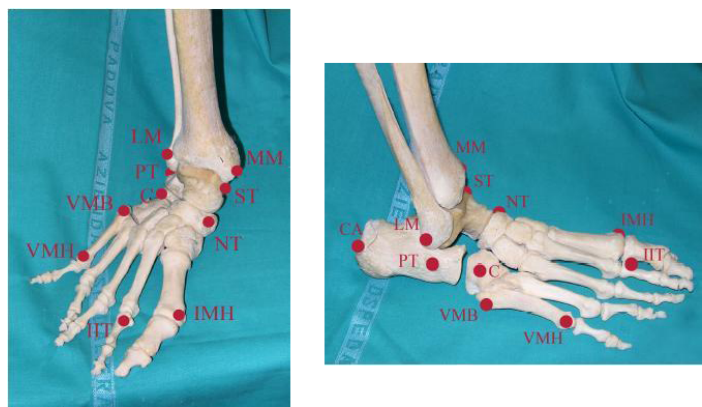


Figure 1.12 – Frontal and lateral view of the marker-set *Foot* protocol [90].

The subdivision of the plantar surface allows calculating the GRFs of each subarea, defined as the sum of the vertical forces measured by each sensor of the pressure platform which belong to the same subarea. Antero-posterior and mid-lateral forces are instead calculated assuming that they are proportionally distributed with respect to the vertical. This assumption had been previously performed in Winter et al. [1] and Uccioli et al. [94], and lead to successful results. The computational details of this methodology can be found in [83].

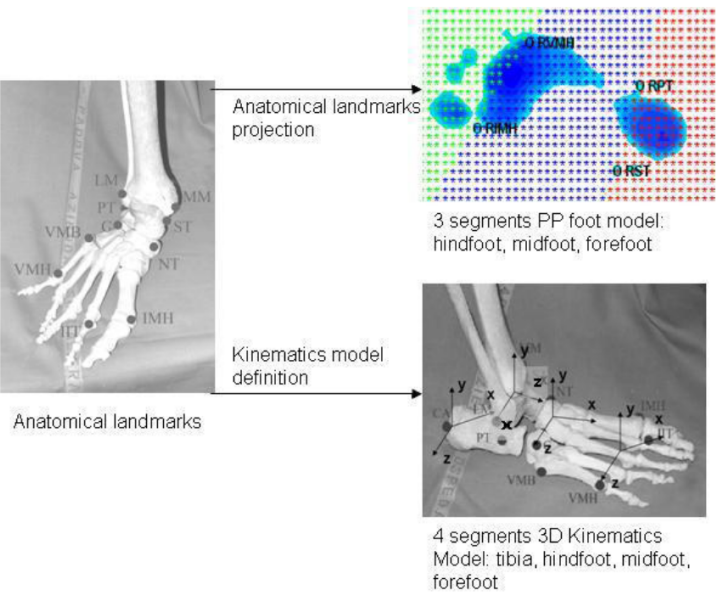


Figure 1.13 – The figure shows the landmarks where the markers are applied according to the *Foot* protocol and the three subareas of the foot derived by their vertical projection, [90].

## **1.6 Aim of the thesis**

The aim of this thesis was to extensively evaluate the possible application of modeling techniques in the diabetic foot prevention, by considering all the limitations introduced as well as the potential benefits of their use in a clinical context. The rationale behind this idea is provided by the big attention that the development of Patient-specific models tailored to patient-specific data, has recently gained not only in the research environment but also in clinical applications. Following the current state of the art, two techniques have been explored: MS modeling and FEA. MS models are considered a valuable tool, as they can provide an estimation of human internal variables, such as muscle activations and forces and joint contact forces. In this thesis their use was extensively evaluated by developing MS models of both diabetic and healthy subjects. Lower limb joints kinematics and kinetics during gait were estimated by means of a modified version of the IORgait protocol. 3D lower limb joints kinematics and kinetics was also calculated with OpenSim. Comparisons between populations and between simulated and experimental data were performed. Both methodologies were able to highlight differences and MS models proved to be able to analyze also the changes in healthy muscle forces with respect to the diabetic ones. This knowledge could be helpful in the development of specific training to improve biomechanical deficit of diabetic subjects in terms of balance, muscle strength and joint mobility. The outputs provided by MS models were then used as boundary conditions in FEA. The flexibility and adaptability of FEA made it become a first choice in modeling biological geometries and materials and in the simulations of complicated boundary and loading conditions. Its application in medical research is considered promising even more in clinical settings, in order to improve patient care. In this thesis this was evaluated in two steps. At first the impact of applying the foot joints reaction forces obtained from MS models as boundary condition on the foot FE models was verified. Subject specific geometries from MRI were used for the development of the foot FEMs while the experimental plantar pressures acquired during gait were used in the validation process. Then the use of muscles forces as boundary condition was also assessed. Subject-specific integrated and synchronized kinematic-kinetic data acquired during gait analysis were used for the development of the MS models and for the computation of the muscle forces. Muscle insertions were located in the MRI and correspondent connectors were created in the FE model. FE subject-specific simulations were subsequently run with Abaqus and once again the validation was done by means of a comparison between simulated and experimentally measured plantar pressures. Finally, an attempt towards the definition of a parametric foot finite element model was done. In fact, despite the recent developments, patient-specific models are not yet successfully applied in a clinical setting probably because of the

long time required for mesh creation. In this thesis the application of the Principle Component Analysis was proposed as a solution. It was applied to the feet of a small cohort of diabetic and healthy subjects and it proved to be able to successfully describe features in the foot, and to highlight differences in the shape of healthy and diabetic subjects.

### 1.7 Outline of the thesis

The research presented in this thesis is organized in five chapters:

*Chapter 2* - gives a complete and detailed overview of the biomechanics of the diabetic foot.

*Chapter 3* - introduces the application of MSs for the diabetic foot prevention. At first, it presents a brief background on the techniques usually chosen for the evaluation of the motion abilities and impairments typically seen in diabetic subjects. Then, with the aim of explaining while the application of musculoskeletal models could improve the knowledge and the information on the disease, it reports a study on diabetic and healthy subjects. Aim, material and methods, results and discussion are presented. The complete work flow is described, and the chapter ends highlighting its major limitations.

*Chapter 4* – reports the work done to combine the use of musculoskeletal models with foot FEMs. The chapter is divided in two parts which represent the two steps performed. At first the impact of applying the foot joints reaction forces obtained from MS models as boundary condition on the foot FEMs is verified. Then the use of muscles forces (again obtained from MS models) as boundary condition in the FE simulations is evaluated. For both studies a brief background is presented together with the methods applied, the results obtained and a discussion of novelties and drawbacks.

*Chapter 5* – explores the possibility of defining a parametric foot FEM. An attempt in overcoming the time required for the mesh creation was done by applying the Principle Component Analysis (PCA) to the feet of a small cohort of diabetic and healthy subjects. A background on the importance of patient specific models is presented followed by material and methods, results and discussion of what obtained with this study.

*Chapter 6* - summarizes the results and the novelty of the thesis, delineating the conclusions and the future research paths.

## 2 Diabetic foot biomechanics

### 2.1 Introduction

The human foot is the terminal segment of the lower limb; it is a complex anatomical structure with skeletal organization similar to that of the hand, but with particular differences that makes it suitable to fulfill different functions. It acts transmitting force with the ground, allowing stable ambulation and stance. During gait the foot functions as a flexible shock-absorber, deforming to uneven surfaces before undergoing a series of biomechanical changes which allow it to act as a rigid lever to exert force [94].

### 2.2 Bone Structure

The skeleton of the foot may be divided into three parts (see Figure 2.1):

- **the hindfoot:** it is composed of the Talus and the Calcaneus. The two long bones of the lower leg, the Tibia and Fibula, are connected to the top of the Talus to form the ankle. The calcaneus, the largest bone of the foot, is connected to the Talus at the subtalar joint and it is cushioned at the bottom by a layer of fat.
- **The midfoot:** it consists of five irregular short bones, the Navicular bone (or Scaphoid), the Cuboid bone and the three Cuneiform bones. Together they form the arches of the foot which serves as a shock absorber. The midfoot is connected to the hindfoot and forefoot by the muscles and the plantar fascia.
- **The forefoot** is composed of five long bones called the first, second, third, fourth and fifth Metatarsal bone and by the Phalanges. The latter can be furthermore distinguish in the first Phalanges (or proximal Phalanges), second Phalanges (or medial Phalanges) and third Phalanges (or distal Phalanges). The first toe (or

## Chapter 2. Diabetic foot biomechanics

Hallux) has only two Phalanges and it lies on the same level as the other toes (differing in this from the thumb), so it does not have a lot of independence movements. The joints between the Phalanges are called interphalangeal and those between the metatarsus and Phalanges are called metatarsophalangeal.

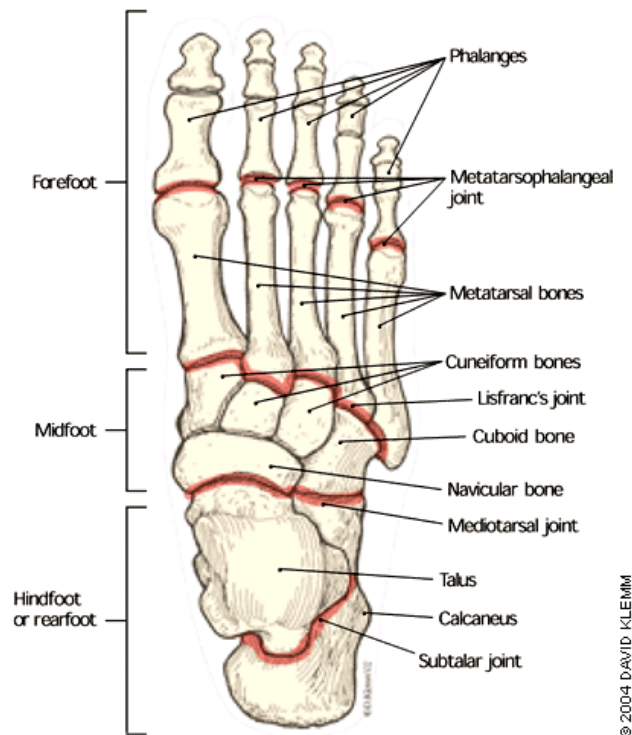


Figure 2.1 – Structures and anatomical division of the foot [95].

**The astragalus**, or Talus bone, is a short bone transmitting the weight of the body on the foot; It has an irregularly Cuboid shape in which it is possible to recognize a head, a neck and a body. Most of its surface is covered with hyaline cartilage due to the articulation with several bones.

**The calcaneus** is the biggest short bone of the tarsus; It has an elongated anteroposterior shape which articulates on the top with the Talus and in the front with the Cuboid.

**The Navicular**, or Scaphoid bone, is a short bone, with an oval flattened, located in the middle of the tarsus, in front of the Talus and behind the three Cuneiform bones.

**The Cuneiform bones** are three short bones in the shape of a triangular prism, which are distinguished by their conformation and position. The medial one is the most voluminous, the middle one is the smallest, and the side one has an intermediate size.

**The Cuboid bone** is a short bone, which has an almost cubical shape, placed at the side of the tarsus, in front of the calcaneus and lateral to the Cuneiform bones.

**The Metatarsal bones** are long bones which are numbered from one to five in the

mediolateral direction. The Metatarsal bones have a proximal base, a body and a distal head.

**Phalanges** form the skeleton of the toes and, as for the hand, they are in three: the proximal, medial, distal from the second to the fifth toes. In the Hallux they are two: the proximal and the distal. Phalanges have a decreasing length and volume from the proximal to the distal direction. They are long bones which have a body, a base and a head.

Finally there can be many **sesamoid bones** near the metatarsophalangeal joints, although they are usually present only in the distal portion of the first Metatarsal bone.

## 2.3 Joints[96]

The conjunction between bones is permitted by the presence of joints that are stabilized by robust segments of fibrous tissue (ligaments). They are classified into two broad categories: synarthrosis (or joints for continuity) and diarthrosis (joints or for contiguity). In the first one, the surface of the bones which form the joint are not in direct contact, but they are held together by a layer of connective tissue and cartilage. The second type allows wider movements. They consist of joint surfaces of varying shape which are covered by a layer of cartilage, an articular capsule and an articular cavity. The latter is filled with a liquid called synovial fluid, which facilitates scrolling. The whole foot-ankle complex is characterized by several joints. The principal are reported below:

**Ankle joint:** situated between the Tibia, Fibula and Talus it is a diarthrosis thus the articular heads are held together by a fibrous capsule, internally lined by a capacious synovial membrane (containing the eponymous liquid), which is inserted on the top in the Tibia and the Fibula and in the bottom in the Talus. The capsule is loose because it needs to ensure the movement of dorsi/plantar flexion.

**Subtalar joint:** is the conjunction between the astragalus and the calcaneus. It adds mobility in the frontal and transverse planes in addition to what provided in the sagittal plane at the level of the ankle joint.

**Transverse tarsal joint** (or midtarsal joint): it includes the calcaneoCuboid and the talo-calcaneo-Navicular joints. The joint participate in the lateral and medial rotation of the foot. This movement contributes to the absorption of the impact of the foot to the ground.

**Intertarsic joints:** examples are the cuneoNavicular joint, the interCuneiform and the Cuboid-Cuneiform joints. They allow small sliding movement.

## Chapter 2. Diabetic foot biomechanics

---

**Tarsal-Metatarsal joints:** they are diarthrosis and they connect the Metatarsal bones at some of the midfoot bones (Cuboid and Cuneiform bones). These joints allow small movements of flexion, extension and laterality assuring thus foot shape adjustments and modification of the plantar arch.

**Metatarsophalangeal joints:** they are diarthrosis which tie the Metatarsal heads to the proximal Phalanges. They allow flexion and extension of the toes on the Metatarsal bones. They represent the point of bending of the toes, which allows the foot rotation on the Metatarsal heads rather than on the tips of the toes.

**Interphalangeal joints:** they are nine diarthrosis that connect the head of the Phalanges with their bases. They allow flexion and extension movements of the Phalanges.

These joints allow the foot to adapt during gait according to the roughness of the underlying soil and to perform a movement characterized by three axes, and three degrees of freedom. The movements are defined according to the plan (sagittal, frontal and transverse) in which they take place (Figure 2.2):

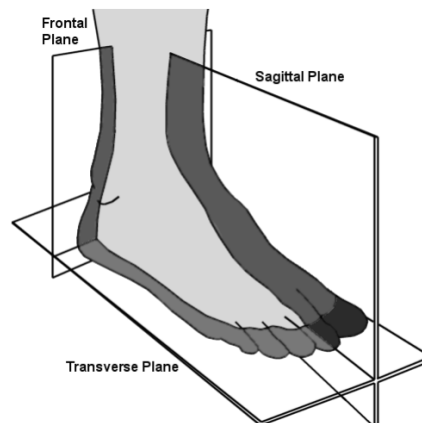


Figure 2.2 – Planes of the foot [97].

- **dorsi/plantar flexion of the foot**, which is the up and down movement of the foot in the sagittal plane. The angle described by the plantar surface varies between  $20^{\circ}$  to  $30^{\circ}$  in dorsiflexion and between  $30^{\circ}$  to  $50^{\circ}$  in plantar flexion, starting from the position of perpendicularity to the axis of the leg (Figure 2.3).
- **inversion (supination) and eversion (pronation):** the inversion consists in the rotation of the ankle so that the plantar surface looks medially, i.e. towards the other foot, while the eversion brings the surface to look sideways. The entity of the movement is of about  $50^{\circ}$  in supination, and between  $20^{\circ}$ - $25^{\circ}$  in pronation (Figure 2.3).



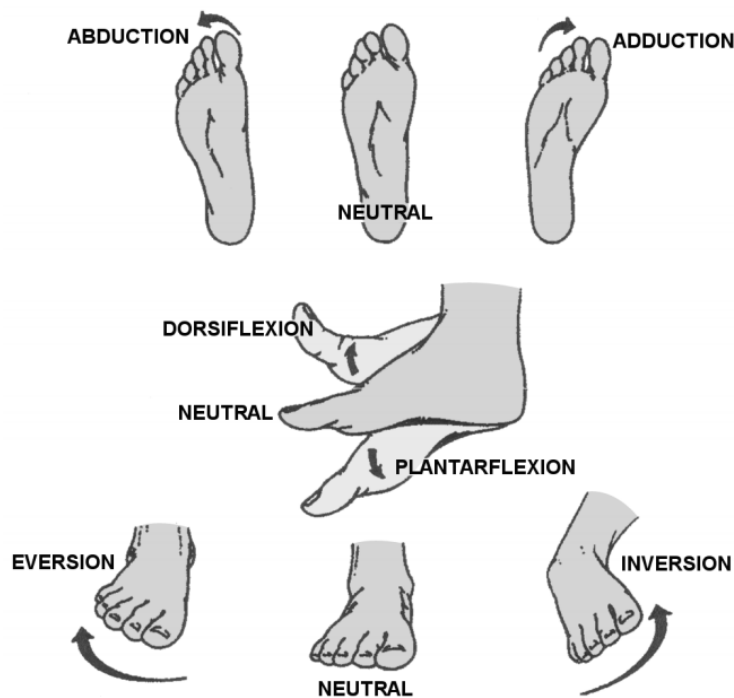


Figure 2.3 – Possible movements of the foot [97].

- **abduction-adduction**, around the longitudinal axis of the leg during which the forefoot, respectively, approaches and moves away from the medial axis. The amplitude of these movements varies between 35°-45° but it can increase up to 90° if the rotations of the knee and hip are added (Figure 2.3).

## 2.4 Muscles[96]

The leg-ankle-foot complex has many muscles which allow the whole foot, and its subsegments, to move. The muscles of the leg (Figure 2.4), as the muscles of the forearm, have a proximal big volume, while distally they are represented by long tendons. They can be divided into posterior, lateral and anterior muscles. The anterior muscles of the leg are disposed in a single layer and they have a mediolateral direction. They allow the dorsiflexion and they all are innervated by the deep peroneal nerve. Three major muscles are included in this section, with the addition of the Peroneus Tertius which is an inconstant auxiliary of the Extensor Digitorum. Since the two muscles are tied and share the tendon side, the action of the Peroneus Tertius is assumed to be equivalent to that of the Extensor Digitorum Longus [24]:

## Chapter 2. Diabetic foot biomechanics

---

The other muscles are:

- **Tibialis Anterior** (Figure: 2.5,2.6): placed closed to the lateral face of the Tibia, it is characterized by a prismatic and triangular shape and, with a long tendon, it terminates to the medial edge of the foot. It originates from the lateral side of the Tibia, from the interosseous membrane and from the crural fascia, it is directed downward and, in correspondence of the lower part of the leg, it continues with a sturdy tendon. The latter goes deeply to the top and bottom retinacula of the extensor muscles inserting into the area of the medial Cuneiform bone and the base of the first Metatarsal bone. It acts flexing the foot (Figure 2.4);
- **Extensor Hallucis Longus** (Figure 2.5): it is deeply located between the Tibialis Anterior and the Extensor Digitorum Longus. It originates from the middle third of the medial aspect of the Fibula and the interosseous membrane, and then it continues with a flattened tendon, which after passing top and bottom retinacula of the extensor muscles, fits over the surface of the dorsal base of the phalanx of big toe. It is responsible for the flexion of the big toe and it participates to the foot dorsiflexion by lifting its medial edge (supination);
- **Extensor Digitorum Longus** (Figure 2.5) is a robust flattened muscle placed between the Tibialis Anterior the Extensor Hallucis Longus. It connects the Tibia and the Fibula to the last four toes. It originates from the lateral condyle of the Tibia, the interosseous membrane, the head and anterior margin of Fibula and the crural fascia. The muscular belly runs distally and continues in a tendon which, after passing the top and bottom retinacula of the extensor muscles, divides into four secondary tendons for the last four fingers. Each of the secondary tendons is divided into three parts of which, the middle one is inserted at the base of the middle phalanx, the other ones at the base of the distal phalanx. It is responsible for the dorsal flexion of the last four toes. Furthermore it participates in the dorsiflexion of the foot by lifting the lateral margin (pronation).

The lateral muscles of the Fibula go to the foot and are both innervated by the superficial peroneal nerve. They are considered as part of the internal flexor muscles group, more specifically among the perimalleolar muscles, together with the Tibialis Posterior. They are relatively small and they closely surround the medial and lateral malleolus [24]:

- **Peroneus Longus** (Figure: 2.5, 2.6) is a stretched muscle that is superficially located in the lateral aspect of the leg. It extends from the Fibula to the first

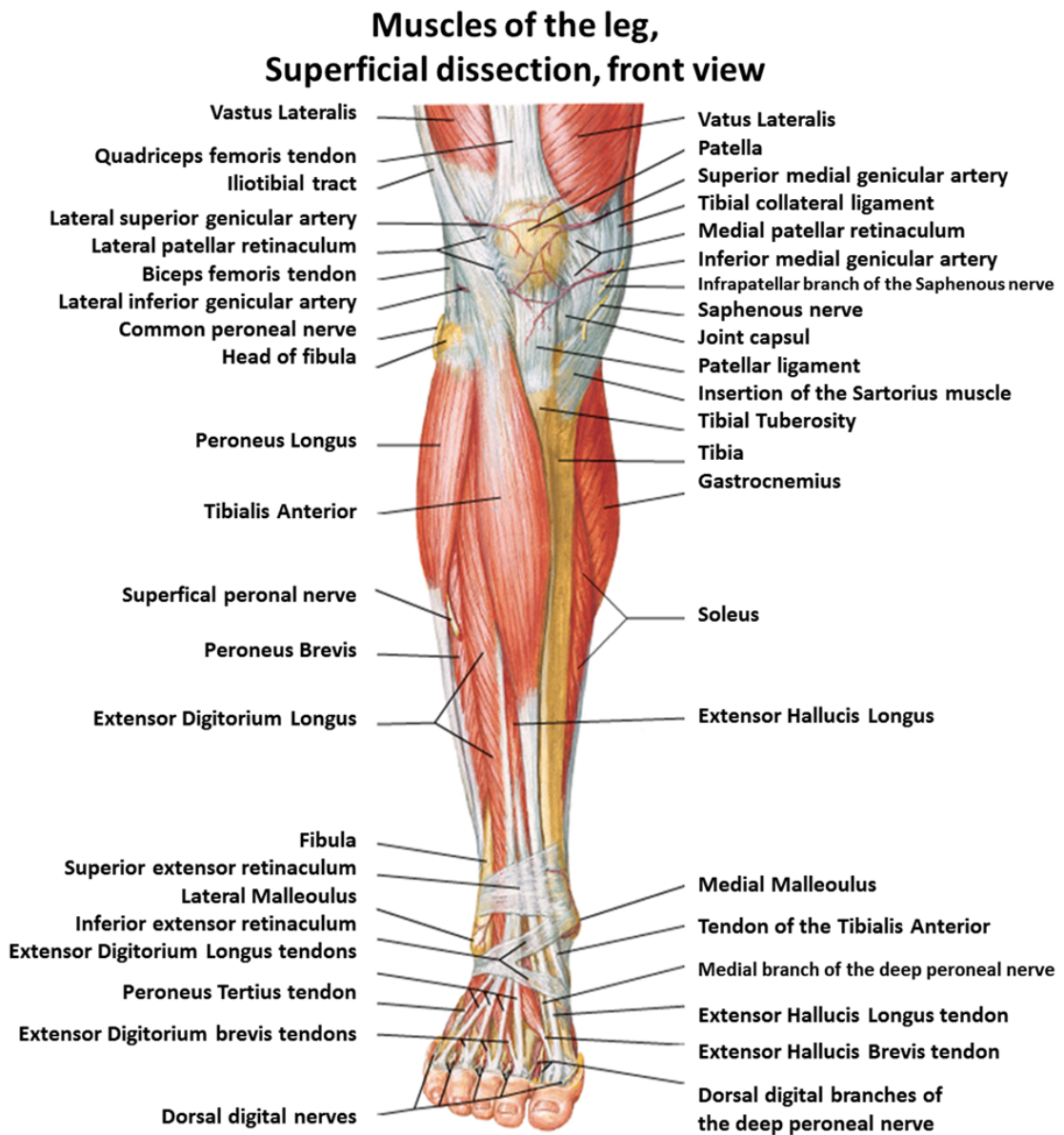


Figure 2.4 – Muscles of the leg, front view (adapted from [98]).

## Chapter 2. Diabetic foot biomechanics

---

Metatarsal bone. It originates from the head and the lateral side of the Fibula. After reaching the half of the leg, its muscle bundles continue in a long tendon that passes behind the lateral malleolus and deeply in the top retinacula of the extensor muscles. The tendon then goes forward, passing deeply to the lower retinacula of the extensor muscles, and moves to the sole of the foot. Here it runs forward and medially, deeply into the plantar muscles, and reaches the medial edge of the foot where it fits in the medial Cuneiform and the tuberosity of the first Metatarsal bone. It lowers the medial side of the foot by exerting a strong pronation action.

- **Peroneus Brevis** (Figure 2.5) is placed deeply in the Peroneus Longus and it connects the Fibula to the fifth Metatarsal bone. It originates from the third middle of the lateral side of the Fibula and it continues with a tendon that runs along with that of the Peroneus Longus, behind the ankle and deeply into the top and bottom retinacula of the extensor muscles. From the lateral aspect of the calcaneus, the tendon reaches the lateral border of the foot and it inserts into the tuberosity of the fifth Metatarsal bone. Along with the Peroneus Longus it contributes to the pronation of the foot by lifting the lateral margin.

The posterior muscles of the leg are arranged in two superimposed layers. They are all innervated by the Tibial nerve and they are also defined as plantar flexor muscles. The Soleus and the Medial and Lateral Gastrocnemius have the advantage of the wide size and of a lever arm equal to the entire length of the heel[24]:

- **The triceps surae muscle** (Figure 2.6). It is a voluminous muscle which consists of three parts, two more superficial, the medial and lateral **Gastrocnemius** and a deep one, the **Soleus** muscle. The triceps surae distally unifies into a long rugged calcaneal tendon (Achilles tendon) that attaches to the heel. The medial head of the Gastrocnemius originates from the epicondyle and from the rear surface of the femur medial condyle. The Lateral Gastrocnemius is detached from the corresponding areas of the lateral condyle of the femur. Both also originate from the posterior aspect of the knee joint capsule. The two muscles move downwards converging and defining the popliteal fossa. Then in the third middle of the leg, they come together to create a broad aponeurosis which continues distally in the calcaneal tendon. The Soleus muscle has a fibrous origin from the head and the posterior side of the Fibula, the line of the soleus muscle of the posterior surface of the Tibia and from the fibrous archway stretched between the head of the Fibula and the line of the soleus. From these broad origins, a large flattened belly originates which continues in a large aponeurosis descending downwards.

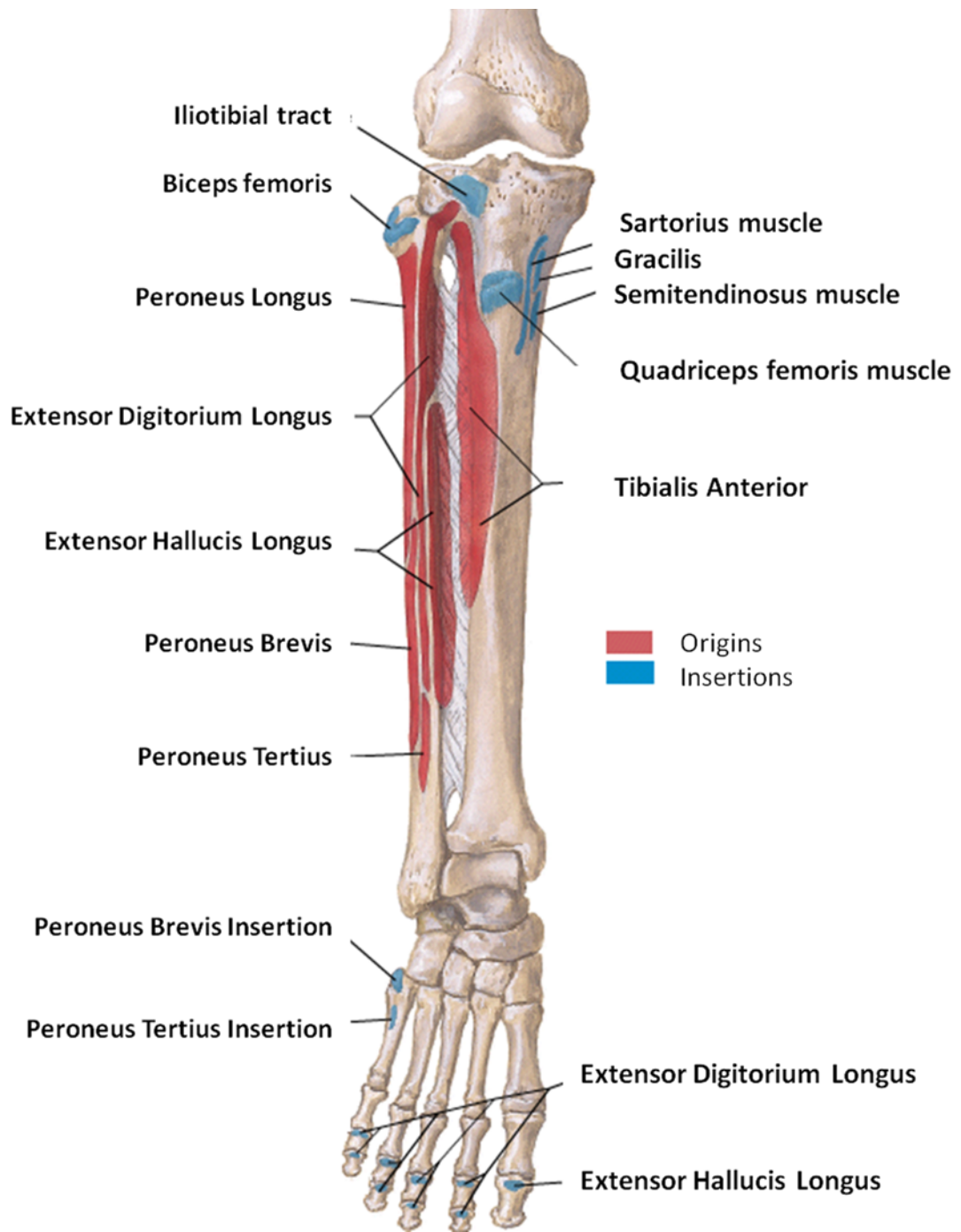


Figure 2.5 – Insertions of the muscles of the leg, front view (adapted from [98]).

## Chapter 2. Diabetic foot biomechanics

In the lower third of the leg it joins the deep face of the aponeurosis of the Gastrocnemius Muscle forming the calcaneal tendon. The latter reaches the foot and it attaches to the tuberosity of the calcaneus. The triceps surae muscle determines the flexion and the supination of the foot. Moreover, it flexes the leg on the thigh. In a standing position, it stretches the leg on the foot and it plays a decisive role in maintaining posture, in walking, running and jumping.

- **Tibialis Posterior** (Figure 2.6) is the deeper of the posterior muscles of the leg and it is located in an intermediate position with respect to long flexors. It originates from the rear end of the Tibia, below the origin of the Soleus, the interosseous membrane and the medial aspect of the Fibula. The muscle bundles are directed downward and medially to continue in a tendon which runs behind the medial malleolus, deeply to the retinaculum of the flexor muscles. The tendon then goes forward, on the medial aspect of the Talus, to reach the soles of the feet. It fits to the Navicular tuberosity and to the plantar surface of the three Cuneiform bones. It is responsible of the plantar flexion of the foot and of the supination. In a standing position, it participates in the maintenance of an upright posture and in the gait by approaching the leg to the heel bone.

Table 2.1 summarize the role of the muscles in the movements of the foot.

Table 2.1 – Action of the muscles on the ankle joint

Action	Muscles	Innervation
<b>Plantar flexion</b>	Gastrocnemius Soleo	Tibialis Nerve
<b>Dorsiflexion</b>	Tibialis Anterior Extensor Hallucis Longus Extensor Digitorum Longus Peroneus Anterior	Deep Peroneal Nerve
<b>Pronation</b>	Peroneus Longus Peroneus Brevis Extensor digitorum longus	Superficial Peroneal Nerve Deep Peroneal Nerve
<b>Supination</b>	Tibialis Anterior Extensor Hallucis Longus Extensor Digitorum Longus Peroneus Anterior  Tibialis Posterior Flexor Digitorum Longus Flexor Hallucis Longus	Deep Peroneal Nerve     Tibialis Nerve

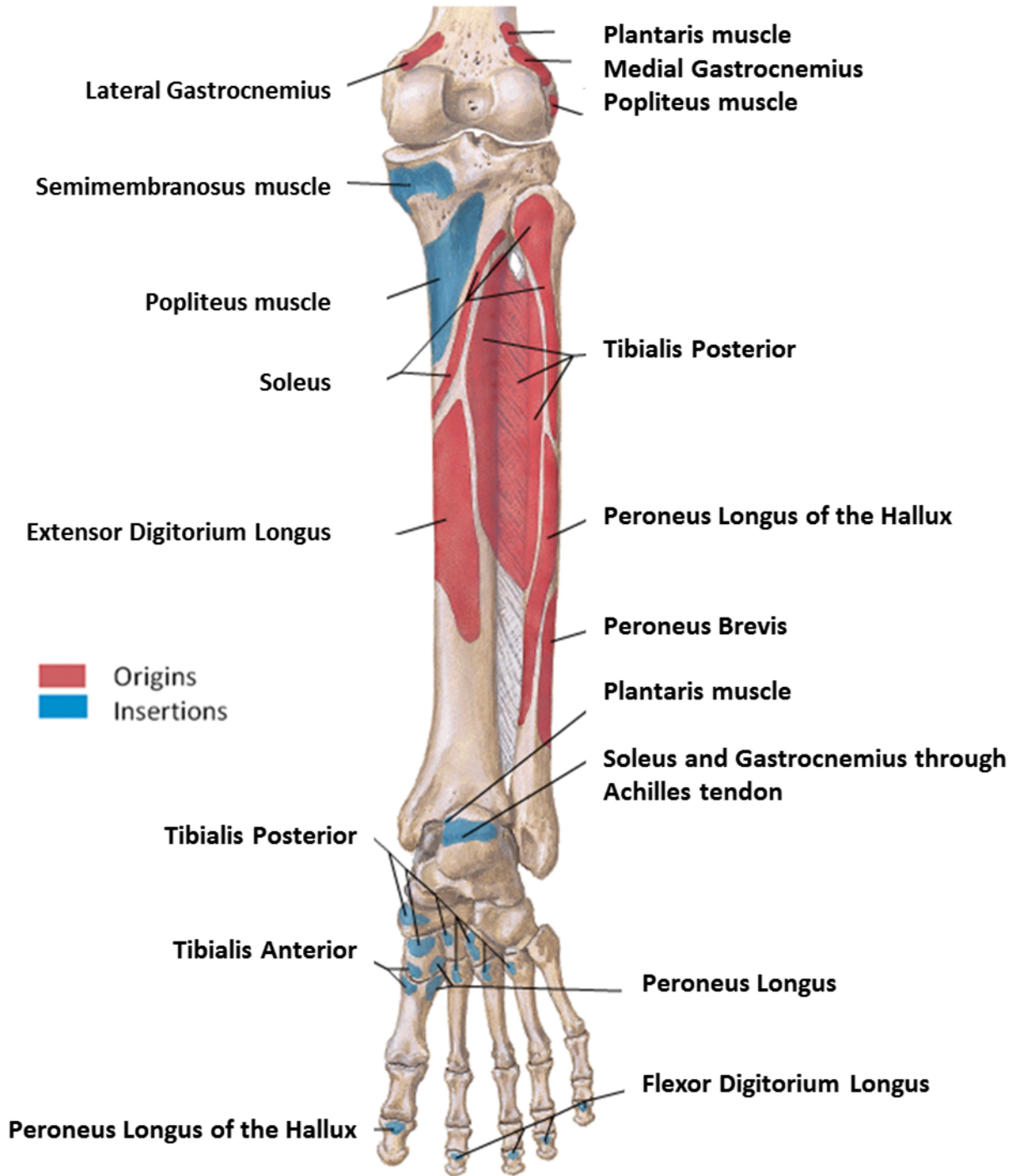


Figure 2.6 – Insertions of the muscles of the leg, rear view (adapted from [98]).

### 2.5 The retinacula

**The retinacula of the extensor muscles** are divided into superior or inferior. The superior one is located superficially to the tendons of the anterior muscles of the leg and it attaches to the front edge of the Tibia and the lateral margin of the Fibula. The lower one is stretched between the lateral aspect of the calcaneus, the medial malleolus, the medial Cuneiform bone and the Navicular.

**The retinaculum of the flexor muscles** is stretched between the posterior edge of the medial malleolus and the medial aspect of the calcaneus.

**The retinacula of the peroneal muscles** are separated into superior and inferior. Both retinacula are tense between the lateral malleolus and the lateral aspect of the calcaneus.

**The plantar fascia** (Figure 2.7) is a thickening of the superficial fascia characterized by a triangular shape with the front base that covers the sole. It originates in the proximity of the tuberosity of the calcaneus with longitudinal beams that are directed forward to reach the toes, at the level of the metatarsophalangeal joints.



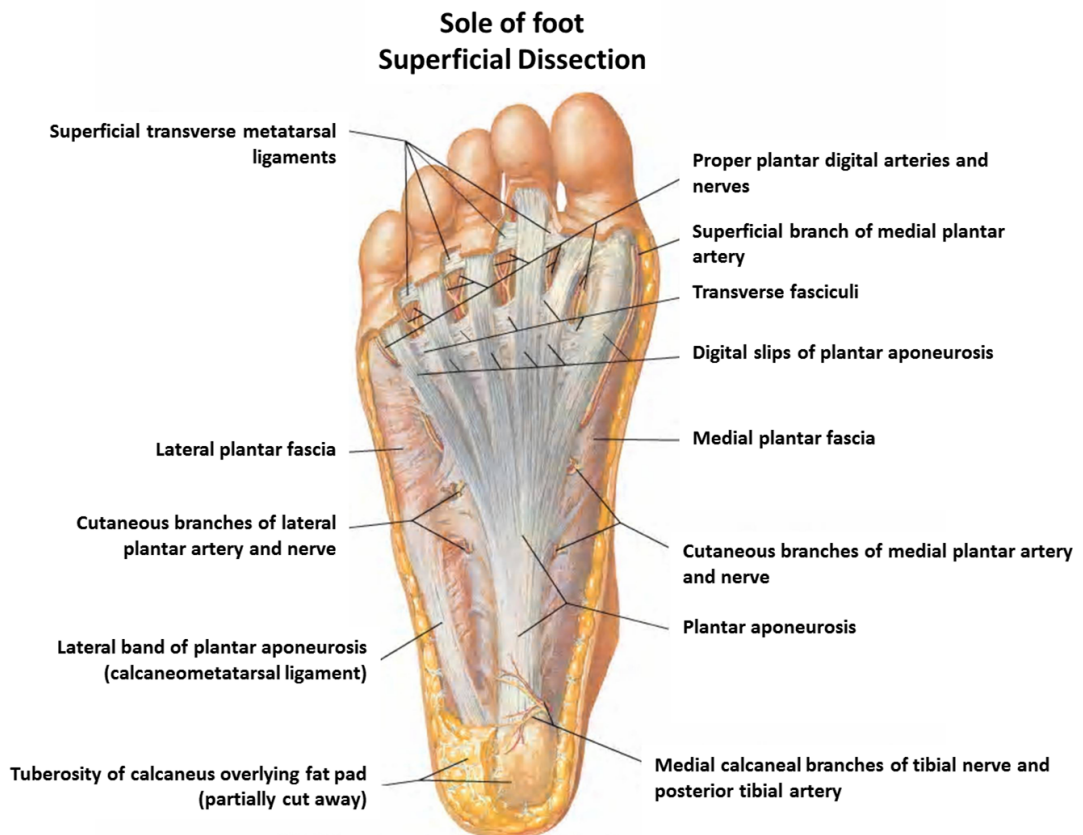


Figure 2.7 – Sole of foot (adapted from [98]).

## 2.6 Diabetic foot

### 2.6.1 Introduction [99]

Diabetes mellitus is one of the most common endocrine disorders characterized by the presence of high concentrations of blood glucose (hyperglycemia) and other metabolic disorders, which are consequent of an absolute deficiency (type 1 diabetes) or relative (type 2 diabetes) of the insulin, the hormone primary regulator of metabolism [100]. Glycemia measures the concentration of glucose in the blood. In healthy individuals, with a regular life and a proper diet, sugar levels are maintained between 60 and 130 mg/dl. At fasting, blood glucose levels may vary from 70 to 110 mg/dl. A glycemia between 110 and 125 mg/dl instead represent the Impaired Fasting Glucose (IFG) [101]. In this condition patients should pay more attention to their lifestyle and, in particular, to their diet. American Diabetes Association reported that blood glucose levels greater than or equal to 126 mg/dl have to be likely considered symptoms of diabetes [102]. A firm diagnosis of Diabetes is established when glycemia has a value of 200 mg/dl at any time of the day or two hours after a glucose load. Glucose values comprised between 140 to 200 mg/dl after a glucose load of 75mg, defined instead an Impaired Glucose Tolerance (IGT). IFG and IGT can evolve over time to overt Diabetes [103].

There are three main types of diabetes mellitus:

- **Type 1 diabetes mellitus**, results from the failure of the pancreas to produce insulin because of the destruction of the  $\beta$ -cellules of the islets of Langerhans which are the producer of that hormone. The affected subjects need lifetime insulin injection to overcome the lack and, for this reason, the disease is also referred to as insulin-dependent diabetes mellitus. The rate of destruction of the  $\beta$ -cells is quite variable, so that the onset of the disease can occur quickly in some people, usually in children and adolescents, and more slowly in adults. Given the higher percent of young people affected, the disease is also called juvenile diabetes.
- **Type 2 diabetes mellitus** is the most common form of diabetes, accounting for approximately 90 % of the cases. It results from insulin resistance, a condition in which cells fail to use insulin properly, although the pancreas is still able to produce it. Typically, the disease occurs after 30-40 years and several risk factors have been recognized as associated to its onset. These include: familiarity for diabetes, low physical exercise, drugs and toxic agents, viral infection, overweight or obesity and membership to certain ethnic groups. The disease

is not genetically predestined, but an increased susceptibility can be inherited [104]. Furthermore genetic factors may have to be modified by environmental factors for diabetes mellitus to become overt. Type 2 diabetes is also referred to as non insulin-dependent diabetes mellitus or adult-onset diabetes.

- **Gestational diabetes** is a condition in which pregnant women, who have never had diabetes before, have a high blood glucose level during pregnancy. This event turns out to be quite transient and easily treatable but can cause problems for the infant ranging from an increased weight at birth until death of the unborn. For the mother it represents an important risk factor for developing type 2 diabetes mellitus.

Finally there are other forms of diabetes mellitus as for instance congenital diabetes. All forms of diabetes have been treatable since insulin became available in 1921, and type 2 diabetes may be controlled with medications but both types 1 and 2 are chronic conditions that usually cannot be cured.

### 2.6.2 Epidemiology

Diabetes is rapidly emerging as a global health care problem that threatens to reach pandemic levels. In 2007 Hossain et al. reported that the number of people with diabetes worldwide was projected to increase from 171 million in 2000 to 366 million by 2030 [102]. The estimation was probably too optimistic since that the International Diabetes Atlas declared in a report of 2013, 382 million of diabetics in the world. The future increase is estimated to be most noticeable reaching the level of 592 million of people suffering from the disease in 2035 [105] (Figure 2.8). Adeghate et al. in 2006 reported that the incidence of type I diabetes ranged from 1.9 to 7.0/100,000/yr in Africa, 0.13 to 10/100,000/yr in Asia, 4.4/100,000/yr in Australasia, 3.4 to 36/100,000/yr in Europe, 2.62 to 20.18/100,000/yr in the Middle East, 7.61 to 25.7/100,000/yr in North America, and 1.27 to 18/100,000/yr in South America. The epidemiology of type II diabetes was equally bleak. The prevalence of type II diabetes ranged from 0.3 to 17.9% in Africa, 1.2 to 14.6% in Asia, 0.7 to 11.6% in Europe, 4.6 to 40% in the Middle East, 6.69 to 28.2% in North America, and 2.01 to 17.4% in South America [104].

In US, the *National Diabetes Statistics Report* of 2014 [106], reported that 29.1 million Americans, 9.3% of the population, had diabetes. Of them 21.0 million were diagnosed, and 8.1 million were undiagnosed. 87% of these patients had type II diabetes and the prevalence was directly proportional to the age of the subjects. Diabetes remained the 7th leading cause of death in the United States in 2010, both alone or as associated with other diseases. The burden of diabetes is enormous, both in human and financial

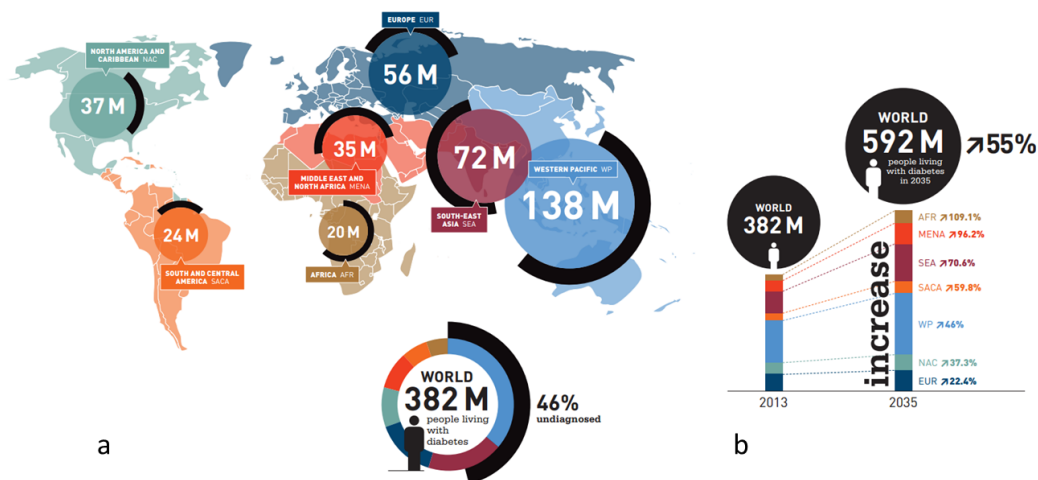


Figure 2.8 – Figure a shows the number of people affected by diabetes. Figure b shows the estimated increase by 2035 [105].

terms. It indeed provokes 5.1 million deaths taking up some USD 548 billion dollars in health spending (11% of the total spent worldwide) in 2013. In 2035 it is estimated that at least 627 billion dollars will be spent for diabetes [105]. It is clear that the increasing number of diabetic patients will strain the capabilities of healthcare providers the world over thus making the research on the prevention becoming crucial.

### 2.6.3 Complications [107]

Diabetes can cause acute or chronic complications. Acute complications are more frequent in type 1 diabetes and are related to the almost total lack of insulin. Acute Hyperglycemic Syndromes are the Diabetic Ketoacidosis (DKA) and the Hyperosmolar State. The subject usually presents an increased urination and thirst along with nausea, vomiting, abdominal pain, dehydration, weakness, and dizziness. The most severe scenario for patients with DKA is the diabetic coma which is due to the accumulation of the products of altered metabolism, the ketones. Hyperosmolar hyperglycemic syndrome differs from DKA in the more dramatic degree of dehydration, higher serum glucose, lack of acidosis, advanced patient age, and much higher mortality. Hypoglycemia can also be dangerous because of its possible detrimental effects on the central nervous system, and consequent cognitive dysfunction.

In type 2 diabetes acute complications are rare, but on the other hand chronic complications are very frequent and affecting different organs and tissues, including eyes, kidneys, heart, blood vessels and peripheral nerves. Most common chronic

complications are:

- **Diabetic retinopathy** is a damage of the retina caused by complications of diabetes, which can eventually lead to blindness as it usually affects both eyes. Its best predictor is the duration of the disease. Among younger-onset patients with diabetes, the prevalence of any retinopathy was 8% at 3 years, 25% at 5 years, 60% at 10 years, and 80% at 15 years. The precise mechanism resulting in diabetic retinopathy remains unknown even though several metabolic pathways have been implicated in its pathogenesis. It is characterized by changes in the blood vessels of the retina which in some people may swell and leak fluid while in other they experience an abnormal grow on the surface of the retina. At first a subject suffering from the disease may not notice changes to his vision but over time, diabetic retinopathy can get worse and cause vision loss.
- **Nephropathy.** Diabetic nephropathy is a progressive reduction of the filter function of the kidney which, if untreated, can lead to renal failure until the need for dialysis or kidney transplant. It is the second most common cause of kidney failure. As the name suggests, the clinical picture is caused by the pathophysiological changes associated with diabetes. Since diabetic nephropathy does not develop in every diabetic patient, genetic factors are believed to play a determinant role.
- **Peripheral vascular disease (PVD).** PVD is an expression of a process of atherosclerosis which is localized in the lower limbs. In diabetic subject it represents one of the most frequent manifestations in terms of development of chronic complications due to poor glycemic control. Vascular disease also occurs in non-diabetic elderly men, but in a patient with diabetes mellitus it has particular characteristics. First of all the frequency of occurrence is nearly similar in both diabetic male and female. Furthermore both legs are usually involved and the pain is localized to the feet instead that to the calves where it is more common in non-diabetics subjects.
- **Neuropathy.** Neuropathies in diabetes are a heterogeneous group of disorders with different mechanisms accounting for the various forms of neuropathy. They are the most common late complication and may lead to a significant burden of disability for the patient. They originate from microangiopathic which causes a narrowing of the small blood vessels that carry blood and therefore oxygen and nutrients to the relative tissues: the peripheral nerves, the retina and kidneys. Symptoms have difference intensity depending on the fibers affected and the entity of the lesion. A neuropathy can cause numbness, pain of varying intensity and limb injuries, requiring amputation in severe cases [108]. It can also lead

to malfunctions of the heart, eyes, stomach and it is a major cause of male impotence.

### 2.6.4 The diabetic foot

The diabetic foot is one of the most serious complications of diabetes mellitus as it compromises the function and structure of the foot. Depending on whether it is the result of neuropathies or of the PVD, it is respectively called neuropathic foot or ischemic foot. Furthermore it could develop the Charcot disease which causes the fragmentation and destruction of the joint and the surrounding bones resulting in a severe foot deformity. Neuropathic and ischemic foot are deeply different, however in most subjects especially at advanced age, they coexist.

#### 2.6.4.1 Neuropathic foot

Diabetic neuropathy is defined as a damage of the peripheral nervous, somatic or vegetative system, merely attributable to diabetes. It may manifest with different clinical pictures but the most common form is the one that underlies the neuropathic foot and causes the impairment of all three components: sensory, motor and vegetative. The sensory neuropathy affects the nerve fibers that send sensations to the brain. It is initially manifested by the gradual loss of vibratory sensitivity. The compression of the bigger sensitive fibers leads to a decrease of the proprioceptive and tactile sensitivity, while the impairment of fibers of small caliber reduces pain and heat sensitivity. The most serious consequence is the reduction of the pain threshold that may have different levels of severity: some patients have feet less sensitive than the normal, others can endure surgery without anesthesia. The deficit initially manifests at the toes level involving hereinafter the whole foot and the leg. More rarely, it manifests also at the level of the hands and arms. The loss of sensitivity is the leading cause of injury to the foot in diabetic patients, since there is a minor response to external harmful agents. Motor neuropathy affects the nerve fibers affects the nerves that innervate the muscles of the foot and are responsible for directing the commands of the brain to the muscles, thus leading the movement. When a nerve is injured, the muscle itself suffers manifesting hypotrophy or hypertrophy. Typically in motor neuropathy, the balance between the extensor and flexor muscles is lost with consequences in the tendons and the joints: a patient may sometimes not be able to walk due to the concomitant activation of antagonist muscles. In addition, when a muscle withdraws because it atrophies, its tendon pulls back the articulation on which it is inserted. Interosseous and lumbrical muscles, which normally act to stabilize the Phalanges on the Metatarsals, are often involved in this process resulting in deformations of the

foot. Typical is the formation of claw toes, (Figure 2.9 top), hammer toes (Figure 2.9 bottom), or the accentuation of the cavus foot. All these deformities can coexist in the same foot and, in some cases, exacerbate those already present. Changes in the foot structure determines alteration of the bearing surface of the foot that will shrink to some particular points thus subjected to very high pressures (usually Metatarsal heads and heel). The body, in an attempt to defend itself from this excess load, strengthens the more superficial layer of the skin with callosities. The process is referred to as hyperkeratosis, but it provides a weak defense: if there is not intervention the formation of ulcers is inevitable.



Figure 2.9 – Schematical representation (on the left) and real pictures (on the right) of claw toes (in the top) and hammer toes (bottom).

Diabetic neuropathy patients also show an increase of the stiffness of the plantar soft tissue (especially in correspondence of the Metatarsal heads). This effect may be attributed to the accumulation of collagen molecules, but a fundamental role is also played by some products of the glycosylation (e.g. glycated hemoglobin) [109]. Literature showed that ulcers develop under the sites of greatest load, but not only the vertical forces play a leading role in the pathogenesis of neuropathic diabetic foot [110]. Also the tangential forces developed at the contact with the ground should indeed be considered.

This because, not all the areas with high plantar pressure develop callosity and, above all, not all ulcers develop in sites of maximum pressure (Figure 2.10). A significant increase of tangential forces was identified in the Metatarsal region of neuropathy patients with past history of ulceration. This suggested that the tangential forces may



Figure 2.10 – Picture show two ulcers surrounded by callosity, developed in the most typical area underneath the Metatarsal heads [111].

have an important role in assessing the risk of ulcerating again [94].

### 2.6.4.2 Ischemic foot

The poor blood supply (ischemia) is a consequence of the narrowing of blood vessels that occurs in the ischemic diabetic foot due to plaque lipids and other substances that accumulate in the vessel lumen, restricting the gauge. PVD is twice as common in people with diabetes than in people without, and it is also a major risk factor for lower extremity amputation [112]. The normal pathophysiology do not greatly differ in patients with or without diabetes and it is characterized by endothelial damage followed by platelet aggregation, lipid deposition and proliferation of smooth muscle with the formation of plaques. The risk of PVD clearly increases with age, and therefore with the duration of the disease, but also with the habit of smoking, the high blood pressure, the presence of dyslipidemia and the altered platelet functions. Although many of these risk factors are present in massive form in the diabetic population, a full explanation of the excess of PVD in it needs further investigations. In this population it usually affects both legs and especially the arteries below the knee. The small caliber of the latter makes it difficult to intervene. If specific therapies are not applied, the clinical situation can worsen quickly to produce a state of total difficulty in walking and, in the worst cases, requiring the amputation of the affected limb. This because diabetics' arteries are often calcified with a prevalence of multiple occlusions. When circulation is compromised, the foot is less able to react to situations such as cold, infections and trauma, and it is more susceptible to dry skin. The earliest symptom of PVD is the claudication but this is absent in the diabetic population. It is caused by the arteries of the leg which stenotic or occluded, receive little blood and fail to increase the blood flow needed during exercise. The number of steps that the patient may be able to accomplish is extremely variable and, if the disease is severe, it can be reduced even in a few units. The absence of claudication in diabetic is explained



by the concomitant presence of sensory neuropathy: the pain will be muted or even absent and the patient will be unaware of suffering PVD in the legs. This makes also difficult the diagnosis of PVD. There is a real risk that its first manifestation is a non-healing ulcer or, in the most severe cases, a gangrene of the tissue. Vascular diseases are responsible for more than 70% of deaths in patients with type 2 diabetes.

### 2.6.4.3 Charcot foot [113]

The most serious manifestation of neuropathic complications in the foot is the Charcot neuropathic osteoarthropathy, commonly referred to as the Charcot foot. In the earliest phase the condition is characterized by inflammation which is then followed by destruction, fragmentation and remodeling of the foot and ankle complex. The architecture of the foot is compromised resulting in a serious deformation. The etiology of this particular disease is not fully understood, but what is certain is the contemporary action of several component factors: diabetes, sensory-motor neuropathy, autonomic neuropathy, trauma, and metabolic abnormalities of bone.



Figure 2.11 – Picture shows the typical appearance of a Charcot foot in a later-stage. The rocker-bottom deformity is very pronounced [113].

Two theories have been proposed to explain its development. The first one has a neuro-traumatic approach, as it attributes the destruction of the bones to the loss of proprioception and sensitivity to pain combined with mechanical trauma undergone by the foot during walking. Unperceived trauma, together with the loads that a limb already wounded has to carry, may lead to fractures and thus to the destruction of joints. The second has a neuro-vascular approach, as it suggests that the collapse of the structures is a secondary effect of an autonomic vascular reflex. This reflex causes vascular hyperemia (increased amount of blood) and osteopenia (low bone mass) that, thanks also to the contribution of trauma during walking, allows the formation of

fractures. The hallmark deformity associated with this condition is a midfoot collapse, described as “rocker-bottom” (Figure 2.11).

### 2.6.4.4 Application of the biomechanical analysis to the diabetic foot [114]

The foot has three main functions: shock absorption during the contact with the ground, maintenance of the balance and of the stability, and progression during walking or running [24]. Peripheral neuropathy can undermine one or more of these functions, determining a reduction or loss of sensitivity and changes in foot structure. The modification of the morphology of the foot causes an alteration of the joints biomechanics and of the ground reaction forces (GRF) ([83], [115]) has been demonstrated that the deformities of the foot, as the bony prominences, were predictive of increased plantar pressure and ulceration of the foot. Furthermore, a strong correlation between the amount of soft tissue and the distribution of plantar pressure was confirmed [116].

Figure 2.12 illustrates this relationship at the level of the Metatarsal head: a higher pressure was noticed on sites with reduced thickness of the plantar tissue. In addition, recent studies have demonstrated that:

- Patients with diabetes are less active;
- the steps are shorter with a wider base of support. The gait is slower and the double support time longer.
- Muscle weakness is always present.
- Muscle weakness is always present.
- Joints, muscles, tendons and plantar tissues are all characterized by an increased stiffness. They all undergo changes due to diabetes as happen to the bones.
- there is an absence of compensatory mechanisms of dysmetria with a proprioceptive deficit that causes unbalances of the body; this is in agreement with the typical reduction of vibration and tactile sensitivity that affects patients with polyneuropathy together with a significant loss of the sense of the position of the lower limbs.
- gait is characterized by anteversion of the pelvis; this was considered strange given that the patients with a cavus foot which is typical of the pathology, should show a pelvic tilt. This anomaly would explain however why both people with

## 2.6. Diabetic foot

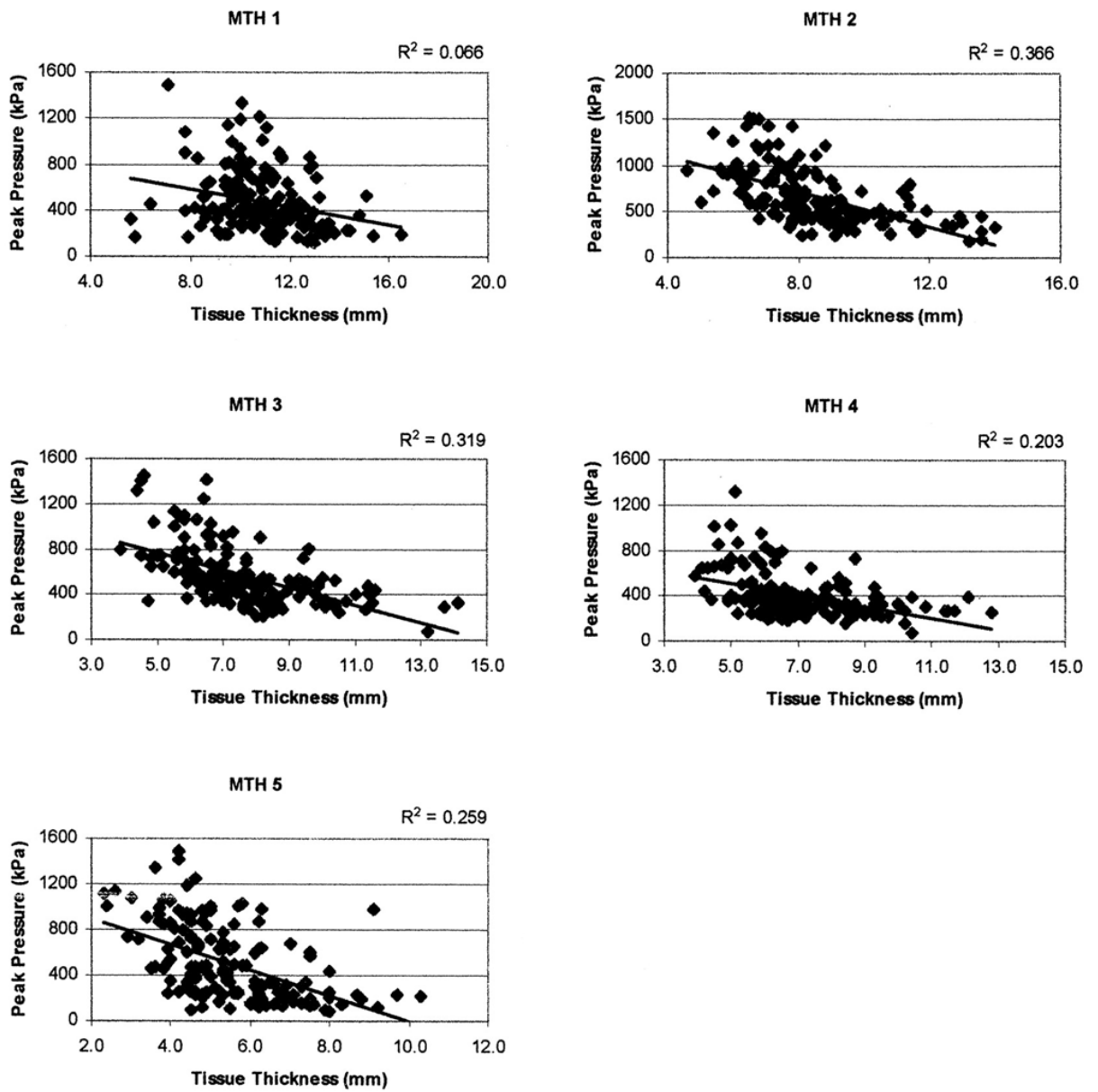


Figure 2.12 – Correlation between plantar pressure and tissue thickness in the forefoot of diabetic subjects [117].

## Chapter 2. Diabetic foot biomechanics

---

cavus and flat feet have similar gait patterns in terms of plantar pressure distribution and position of the center of pressure (COP). The condition is also due to the thickening of the plantar tissue caused by tissue glycation.

- the increased plantar pressures due to changing in the bearing surface of the foot and to hyperloads, is concentrated only in certain areas (usually midfoot and toes) [118].
- there is an increase of tangential forces in the plantar midfoot. Their exact role in the etiology of diabetic foot is not yet fully understood. Anteroposterior forces decrease with the worsening of the disease, while the medium-lateral forces are related to the site of ulceration [83];

From the evidences reported above it becomes clear how the analysis of the biomechanics of the foot is very important in the diagnosis and especially in the prevention of ulcers. Many of these are in fact detected without the presence of the typical evidence of neuropathy or vascular disease [119]. A study that deeply evaluates the kinematics, the GRFs and the plantar pressures may give significant information on the possibility of development of ulcers, thus defining a method of classification for the patient “at risk” whose need a timely intervention.

### 2.6.4.5 Plantar pressure measurement [19] [114]

Breakdown of the plantar tissues can be initiated by two main mechanisms:

1. increased duration of pressures, which includes application of relatively low pressures for a long period of time. Diabetic patients developing foot ulcers seem indeed to have less cumulative plantar stress than those that do not develop foot ulcers [110].
2. increased magnitude of pressures which implies the application of hyper loads in a short period of time.

An inverse relationship between time and pressure that leads to injuries has been demonstrated and it is shown in Figure 2.13.

The definition of a universal peak plantar pressure (PP) threshold for ulceration is not possible. Given that different PP measurement devices give data that are not directly comparable with other devices, normal pressure ranges has to be obtained each time that a new system is used. Furthermore there are significant limitations

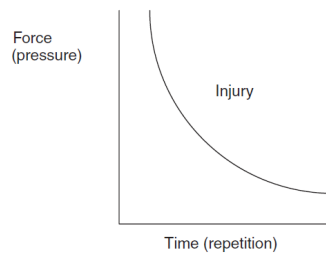


Figure 2.13 – Inverse relationship between force (pressure) and time (or repetition). As force (pressure) increases, the duration (time) required to cause tissue injury decrease [116].

in using a single critical level of PP to identify patients at risk for neuropathic foot ulceration because different areas experience different pressures and might have different thresholds. Peak PP can be difficult to interpret because they depend also on other factors such as gait speed. For example, while an increase in walking speed may be deemed a functional improvement, it could result in increased peak PP that would traditionally be viewed as detrimental. Some authors proposed instead the evaluation of a pressure gradient, defined as a spatial change in plantar pressure around the peak pressure location, as a possible predictor of foot ulcer. The impossibility of the PP to become an index of the risk of ulceration reflexes the fact that surface pressures are not representative of the complex mechanical stresses that developed inside the subcutaneous plantar soft-tissue, which are more likely the cause of tissue breakdown. Anyway ulceration would not happen without an additional trauma to neuropathy and vascular diseases [120]. A trauma may be intrinsic or extrinsic. In the first case it is due for example to repeated stress from high pressure or calluses. In the second case it is due to external effects like, for instance, the rubbing on the skin of an object inside the shoe. The body responds to high pressures or to repeated micro-trauma with callus formation to protect the skin from further damage. However if the callus becomes excessive it also contribute to an increase in pressure and must therefore be removed at regular intervals.



## 3 Musculoskeletal modeling in diabetic foot prevention

*Diabetes mellitus is a chronic disease, highly invalidating. Diabetes neuropathy and vasculopathy are two of its major complications that can lead to diabetic foot disease, which worst consequences are plantar ulcers and lower limb amputations. Regardless of the type of diabetes, regular physical activity plays a primary role in: preventing the development of obesity; promoting the glucose uptake by the muscles thus reducing the effect of the damages caused by hyperglycemia; promoting a proper musculoskeletal response thus improving load distribution and avoiding the concentration of high plantar pressures. The objective of this study was to define a methodology for estimating muscle forces in subjects with diabetes that allows identifying differences with respect to a population of healthy subjects matched for age and BMI. Furthermore the possibility of defining a common platform that enables comparison of OpenSim outcomes variables with experimental gait analysis parameters was explored. Musculoskeletal models of diabetic and control subjects were developed in OpenSim to obtain their muscle forces. Subjects routine gait analysis was performed and lower limb joints kinematics and kinetics estimated by means of a modified version of Leardini et al. 2007 [91]. 3D lower limb joints kinematics and kinetics were also calculated in OpenSim. Both methodologies were able to highlight differences in joints kinematics and kinetics between the two populations. Significant differences were observed between lower limb muscle forces of diabetic and healthy subjects. This knowledge can help either planning or estimating the benefit of specific training programs aiming at improving muscle strength and joints mobility.*

### 3.1 Background & Aims

Diabetes mellitus is a chronic disease caused by a deficiency in the production of insulin by the pancreas, or by the ineffectiveness of the insulin produced. This deficit

### Chapter 3. Musculoskeletal modeling in diabetic foot prevention

---

results in increased concentrations of glucose in the blood, which in turn damage the blood vessels and nerves [100]. Approximately 382 million people have diabetes mellitus worldwide, and this number may almost double by the year 2035. Diabetic neuropathy is the most common complication of diabetes which affects up to 50% of people with diabetes [105]. Diabetic peripheral neuropathy (DPN) and peripheral arterial disease are disabling complications of diabetes. They are both involved in the pathogenesis of diabetic foot complications, which significantly limits mobility [121]. In the last decade several studies have investigated diabetic subjects' biomechanics by means of instrumented motion analysis. These studies have contributed to identify patients at higher risk for the development of diabetic complications ([83],[122], [123], [124]). It has been reported that DPN significantly decreases the ability to walk and causes alterations of foot posture and function (See ). The result is an impaired balance and gait which increases the risk of falls ([90], [125], [126]). Biomechanical alterations may serve as markers that trace the consequences of diabetes and DPN on foot loading. These include limited foot flexibility and a restrained forward progression of the body weight during the stance phase of gait ([83],[127]). Other important alterations were demonstrated in hip, knee, ankle joints and trunk moment patterns over the entire stance phase of gait in both DPN and without DPN subjects (NoDPN) ([90],[128], [127]). In particular, the altered rollover process varies the plantar pressure distribution with areas that have to bear higher pressures and that can be more subjected to the formation of ulcers [129], [130]). Diabetes also accelerates age-related decreases in muscle mass [131], a condition related to insulin resistance. In this context a few authors have reported lower limb muscle electromyographic abnormalities in diabetic subjects with and without neuropathy during gait analysis ([122], [123],[132]). Muscle strength significantly contributes to lower limb joints loading during walking and recently attention has been focused on specific training in order to improve gait speed, balance, muscle strength and joint mobility in diabetic patients [133]. The idea is to combine strengthening, stretching and functional training program to improve gait biomechanics and foot function ([133], [134]). This approach could partially substitute the use of insoles for the reduction of the stress in the plantar tissue, which might induce some changes in the muscular control during gait.

Regardless of the type of diabetes, regular physical activity plays a primary role in preventing the development of obesity and in particular it contributes to avoid the occurrence of type 2 diabetes. Recent studies have indeed demonstrated a close relationship between BMI and type 2 diabetes incidence [135]. Combined aerobic and resistance training has been reported to enhance insulin sensitivity and to improve glycemic control, lipid profile and blood pressure ([136], [137], [138], [139], [140], [141], [142]). State of the art of quantitative muscle strength evaluation relies on isokinetic



dynamometry [133], but a comprehensive biomechanics evaluation should integrate joints kinematics and muscle function during gait. This result can be achieved by means of multi-body simulations based on musculoskeletal models (MSMs) that, in the past decades, have proliferated in the biomechanics research community. MSMs allow the computation of muscles forces starting from data experimentally acquired during gait analysis. **The first objective of this study was the identification of a methodology for estimating muscle forces in subjects with diabetes that allows identifying differences with respect to a population of healthy subjects matched for age and BMI.** This was done by analyzing their muscle forces computed with the software OpenSim. **A second aim was the definition of a common platform in order to enable Comparison of OpenSim outcomes variables with Experimental gait analysis parameters.** Results of the present study might be useful for evaluating the benefit of exercise treatment in diabetic subjects.

## 3.2 Materials & Methods

### 3.2.0.1 Subjects

Twenty subjects were enrolled [10 control subjects (CS) (mean  $\pm$  SD age  $62.8 \pm 7.1$  and BMI  $24.3 \pm 2.9$ ) and 10 diabetic neuropathic subjects (DNS) (mean  $\pm$  SD age  $57.2 \pm 4.1$ , BMI  $24.16 \pm 1.8$ )] at the University Clinics of Padova Hospital. A written informed consent was obtained from all subjects and the protocol has been approved by the local Ethic Committee of the University Clinic of Padova. DNS' inclusion criteria were: type 1-2 diabetes, no lower limb surgery, no orthopedic problems, no history of ulcers or neurological disorders (DPN excluded) and no cardiovascular disease. Walking ability without any additional aids was also required. They underwent the following screening: a neurological evaluation which included the Michigan Neuropathy Screening Instrument [143] and the assessment of symptoms and signs compatible with peripheral nerve dysfunction, and a physical examination as in Sawacha et al. [119]. Each patient had at least one measure of urinary albumin to creatinine ratio (0–30 mg/g normal, 30–300 mg/g microalbuminuria, 4300 mg/g macroalbuminuria), one ophthalmologic examination, a 12-leads electrocardiogram collected in the three months preceding the study, a carotid artery Doppler ultrasound examination and HbA1c values from the preceding ten years. CS were enrolled among hospital personnel.

### 3.2.0.2 Experimental set up

A 60 Hz 6 cameras stereophotogrammetric system (BTS S.r.l, Padova) synchronized with 2 force plates (FP4060-10, Bertec Corporation, USA) and a 16 channels Pocket EMG (1000 Hz, BTS S.r.l, Padova) was used to perform a routine gait analysis and lower limb joints kinematics and kinetics were estimated by means of a modified version of Leardini et al.[91] as in [84]. The protocol provides for a full-body marker set [84]. 24 reflective markers were placed on the subjects at specific anatomical landmarks (ALs), while other 24 reflective markers were used for the six clusters following the anatomical calibration technique proposed by Cappozzo ([89], [144])(each formed by four markers bilaterally on shanks, thighs and pelvis, see Figure 1.11). Some markers were placed directly on the ALs through double sided tape and anatomical calibration performed through a static acquisition as in [84] as follows: right and left acromions, spinous process of 7th cervical vertebrae, spinous process of 5th lumbar vertebrae, right and left lateral malleolus, foot right and left calcaneus, right and left first metatarsal head, right and left second metatarsal head, right and left fifth metatarsal head, right and left medial epicondyle, right and left tibial tuberosity, right and left head of the fibula, right and left medial malleolus). Others ALs which were calibrated with the aid of a pointer with respect to a local cluster of markers as in [89]: pelvis right and left anterior superior iliac spine, right and left posterior superior iliac spine, right and left greater trochanter. The center of the femoral head was assumed to coincide with the center of the acetabulum and it was reconstructed by means of a functional method as in [145]. Data collection consisted of some preliminary static trials for the anatomical calibration followed by several gait trials. A static acquisition was performed asking the subjects to stand on the force platform without shoes, with the heels jointed, and with the feet 30° separated [84]. During the dynamic acquisition, the subject was asked to walk at a self-selected speed, along a 10 m walkway, so that the target foot would naturally land on the force plates. At least three left and right foot strikes were acquired. Anatomical reference frames for the body segments were defined according to previous work ([89], [91], [84], [144]) and standard coordinate systems were adopted for each joint. Joint moments were determined according to [146]. The electrical activity of 6 muscles for each lower limb were collected by means of a portable SEMG system (POCKETEMG, 16 channels, BTS Padova). Surface EMG signals of the following muscles were recorded at 1000 Hz: Rectus Femoris, Gluteus Medius, Tibialis Anterior, Gastrocnemius Lateralis, Peroneus Longus, Extensor Digitorum Communis. Sensors were positioned as in [132] after appropriately cleaning and preparing the skin. Sensors were 3 cm of diameter and positioned 1 cm apart.

### 3.2.0.3 Musculoskeletal models

A generic musculoskeletal model with 10 rigid bodies, 23 degrees of freedom and 92 musculotendon actuators was scaled to match each subject's dimensions and inertial properties ([28], [31]) by using the experimentally measured body mass and the position of markers placed on ALs during the static trial. The scaled models were then used to generate and analyze walking simulations of each subject's trials in OpenSim (v.3.2). The following pipeline was run: scaling, inverse kinematics (IK), inverse dynamics (ID) and static optimization (SO) (See Section 1.1).

### 3.2.0.4 Statistical Analysis

Statistical analysis was done according to ([119], [84]). Regarding 3D joint rotation angles and moments, each subject's variables were represented by the mean from three representative walking trials. Intra-class correlation (ICC) was used to aid in selecting each subject's representative walking trial that could be included in the computation of the mean; thus, the ICC coefficient was calculated for each subject's kinematic parameter. Walking trials whose kinematics variables were found with an ICC coefficient less than 0.75 (75%) were excluded from the statistical analysis ([119], [84]). With respect to the knee joint, only its motion on the sagittal plane was reported as in ([119], [84]), by considering the large impact of skin artifact on knee rotations on the other planes. The average kinematic data, were plotted over one gait cycle and the 2 tailed Student's T-test was used, after evidence of normality (Kolmogorov-Smirnov Test), to compare the data of the 2 populations as ([119], [84]). Joint kinematics and kinetics derived from the modified Leardini et al. 2007 [91] were used as ground truth for evaluating the simulations results of ID and IK, and Person correlation coefficient between curves estimated.

The following comparisons have been performed:

- OpenSim joint kinematic output of CS vs. OpenSim joint kinematic output of DNS;
- OpenSim joint kinetic output of CS vs. OpenSim joint kinetic output of DNS;
- OpenSim SO output (muscles' force and activation) of CS vs. OpenSim SO output of DNS;
- Experimental gait analysis joint kinematic output of CS vs. Experimental gait analysis joint kinematic output of DNS;

### Chapter 3. Musculoskeletal modeling in diabetic foot prevention

---

- Experimental gait analysis joint kinetic output of CS vs. Experimental gait analysis joint kinetic output of DNS;
- Experimental gait analysis joint kinematic output of CS vs. OpenSim joint kinematic output of CS;
- Experimental gait analysis joint kinetic output of CS vs. OpenSim joint kinetic output of CS;
- Experimental gait analysis joint kinematic output of DNS vs. OpenSim joint kinematic output of DNS;
- Experimental gait analysis joint kinetic output of DNS vs. OpenSim joint kinetic output of DNS.

Afterword SEMG envelope, envelope peak values and position of the envelope peak values with respect to the gait cycle [132], estimated directly from the experimental data, were used as ground truth for static optimization outcome measures. The recorded signals were band pass filtered between 10 and 450 Hz with a 5th order Butterworth filter and full wave rectified. The envelope was computed by low-pass filtering the signals with a 4th order Butterworth filter and a cut off frequency of 5 Hz [122]. The right and left muscle activation patterns were analyzed and the envelope of the signal computed (the peak and the position of the peak (POP) during the gait cycle). The envelope of the signals during the stance phase was selected and normalized on the mean signal in this time interval. In order to determine the gait cycle the heel marker trace together with the ground reaction force curve were used. Hence phases of normal activation for each signal in the gait cycle were defined as in [132]. The same analysis was performed for each signal in the gait cycle considering both phase of normal and non normal activation (Matlab R2008b). The time of peak muscle activity occurrence was evaluated as a function of the gait cycle.

### 3.3 Results

Both methodologies were able to highlight differences in joint kinematics and kinetics between DNS and CS on some of the joints' angles and moments ( $P < 0.05$ ). Furthermore also SEMG analysis results were evaluated.

### 3.3.1 Data elaboration through OpenSim

#### 3.3.1.1 OpenSim joints kinematic output of CS vs. OpenSim joints kinematic output of DNS

Diabetic subjects displayed statistically significant differences on the pelvic rotation ( $0.013 < P < 0.044$ ) and on the hip flexion/extension (flex/ext) at the end of gait cycle ( $0.022 < P < 0.049$ ). Significant differences were also revealed on the ankle flex/ext ( $0.014 < P < 0.043$ ) and on the pelvic obliquity ( $0.042 < P < 0.049$ ) during the loading response (Figures 3.1, 3.2).

#### 3.3.1.2 OpenSim joint kinetic output of CS vs. OpenSim joint kinetic output of DNS

DNS displayed statistically significant differences on pelvic rotation moment ( $0.039 < P < 0.043$ ) around the midstance and on the hip flexion moment at the end of stance phase of the gait cycle ( $0.035 < P < 0.043$ ). Statistically significant differences were registered also at the beginning and end of the gait cycle both on hip abduction/adduction (ab/ad) moment ( $0.012 < P < 0.050$ ) and hip internal external (int/ext) rotation moment ( $0.012 < P < 0.048$ ). Finally a difference was found on knee flex/ext even though only for one instant in the swing phase of the gait cycle (Figures 3.3, 3.4).

#### 3.3.1.3 OpenSim SO output (muscles' force and activation) of CS vs. OpenSim SO output of DNS

##### *Muscle Forces*

DNS showed statistically significant differences in correspondence of the force exerted by several muscles either in the stance or in the swing phase of the gait cycle. Values were reported in Table 3.1.

##### *Muscle Activations*

DNS showed statistically significant differences on the activation of several muscles either in the stance or in the swing phase of the gait cycle. Values were reported in Table 3.2.

**Chapter 3. Musculoskeletal modeling in diabetic foot prevention**

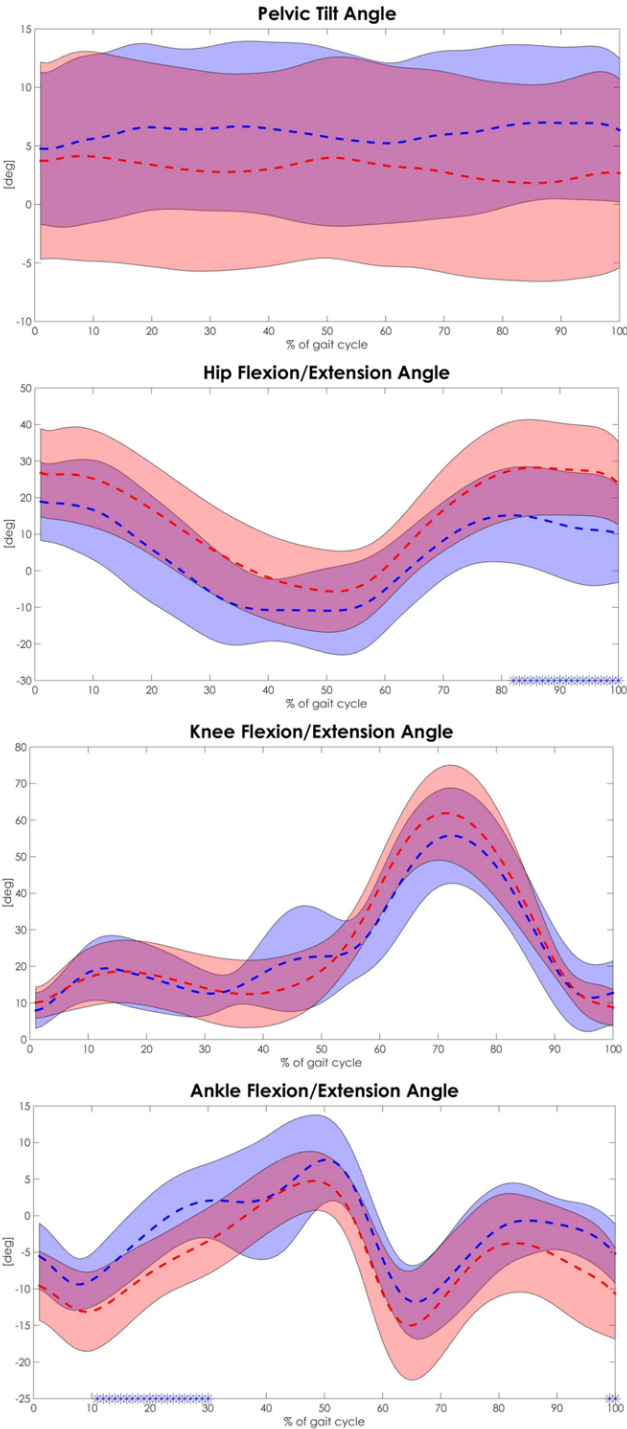


Figure 3.1 – Gait analysis joints kinematics results of the sagittal plane (**OPENSIM ELABORATION**): comparison between mean joint angles (dashed lines) plus and minus 1 standard deviation of both CS (in blue) and of DNS (in red). Results of two tailed T-Test have been reported in term of the instants of the gait cycle where significant differences were found, and they are represented with the blue asterisk (Level of Significance was set to  $p < 0.05$ ).

Table 3.1 – Results of the SO run with OpenSim. Phase of the gait cycle where the muscle activation of DNS showed a statistically significant difference with respect to the CS and P-values are reported

<b>Stance</b>	<b>Swing</b>	<b>P- Value</b>
<b>Adductor Magnus</b>	<b>Adductor Magnus</b>	0.016 <P <0.043
	<b>Extensor Hallucis</b>	0.010 <P <0.049
	<b>Extensor Digitorum</b>	0.015 <P <0.036
<b>Flexor Digitorum</b>	<b>Flexor Digitorum</b>	0.001 <P <0.049
<b>Flexor Hallucis</b>		0.036 <P <0.050
<b>Gemellus</b>	<b>Gemellus</b>	0.011 <P <0.045
<b>Gluteus Maximus</b>	<b>Gluteus Maximus</b>	0.018 <P <0.037
	<b>Gluteus Medius</b>	0.010 <P <0.041
	<b>Gluteus Minimus</b>	0.008 <P <0.025
<b>Gracilis</b>	<b>Gracilis</b>	0.021 <P <0.048
	<b>Iliacus</b>	0.019 <P <0.040
	<b>Lateral Gastrocnemius</b>	0.016 <P <0.042
	<b>Long Head of Biceps Femoris</b>	P <0.048
<b>Pectoralis</b>		0.026 <P <0.046
<b>Peroneus Brevis</b>	<b>Peroneus Brevis</b>	0.027 <P <0.049
<b>Peroneus Longus</b>		0.032 <P <0.049
<b>Psoas</b>		0.034 <P <0.048
<b>Quadratus Femoris</b>	<b>Quadratus Femoris</b>	P <0.046
<b>Rectus Femoris</b>		0.029 <P <0.048
<b>Soleus</b>	<b>Soleus</b>	0.003 <P <0.045
<b>Tibialis Anterior</b>	<b>Tibialis Anterior</b>	0.015 <P <0.047
<b>Tibialis Posterior</b>	<b>Tibialis Posterior</b>	0.007 <P <0.050
<b>Vastus Intermedius</b>		0.026 <P <0.030
<b>Vastus Medius</b>		0.028 <P <0.038

### Chapter 3. Musculoskeletal modeling in diabetic foot prevention

---

Table 3.2 – Results of the SO run with OpenSim. Phase of the gait cycle where the muscle force of DNS showed a statistically significant difference with respect to the CS and P-values are reported.

<b>Stance</b>	<b>Swing</b>	<b>P- Value</b>
<b>Adductor Brevis</b>		0.026 <P <0.034
	<b>Adductor Magnus</b>	0.016 <P <0.024
<b>Extensor Digitorum</b>	<b>Extensor Digitorum</b>	0.002 <P <0.048
<b>Flexor Digitorum</b>		P <0.045
<b>Flexor Hallucis</b>		0.011 <P <0.048
	<b>Gluteus Maximus</b>	0.010 <P <0.024
	<b>Gluteus Medius</b>	0.012 <P <0.040
	<b>Gluteus Minimus</b>	0.002 <P <0.025
	<b>Iliacus</b>	0.013 <P <0.047
	<b>Lateral Gastrocnemius</b>	0.018 <P <0.045
	<b>Medial Gastrocnemius</b>	0.013 <P <0.041
<b>Psoas</b>		0.037 <P <0.045
	<b>Rectus Femoris</b>	P <0.043
<b>Soleus</b>	<b>Soleus</b>	P <0.049
<b>Tibialis Posterior</b>		0.001 <P <0.039
	<b>Vastus Intermedius</b>	P <0.042
	<b>Vastus Lateralis</b>	0.015 <P <0.049
	<b>Vastus Medius</b>	P <0.043



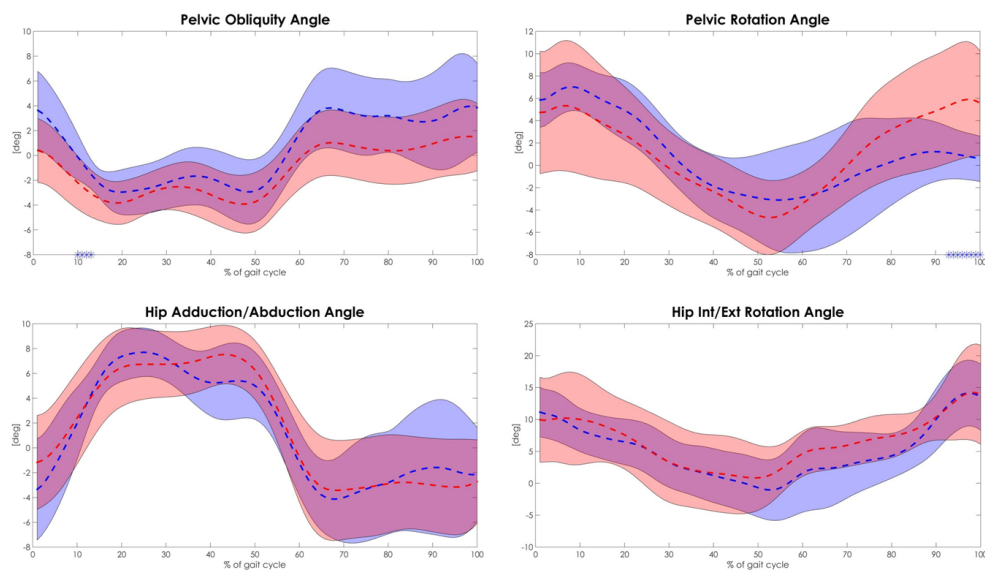


Figure 3.2 – Gait analysis joints kinematics results of the transverse and frontal planes (**OPENSIM ELABORATION**): comparison between mean joint angles (dashed lines) plus and minus 1 standard deviation of both CS (in blue) and of DNS (in red). Results of two tailed T-Test have been reported in term of the instants of the gait cycle where significant differences were found, and they are represented with the blue asterisk (Level of Significance was set to  $p < 0.05$ ).

### 3.3.2 Experimental data elaboration through routine gait analysis protocol

#### 3.3.2.1 Experimental joint kinematic output of CS vs. experimental joint kinematic output of DNS

DNS displayed statistically significant differences on the trunk ab/ad ( $0.036 < P < 0.045$ ) and int/ext rotation angles ( $0.018 < P < 0.048$ ) around the end of the stance phase and at the beginning of the swing phase of the gait cycle. Pelvic rotation angle displayed statistically significant differences in swing ( $0.030 < P < 0.042$ ) while pelvic obliquity ( $0.008 < P < 0.047$ ) and hip ab/ad angle ( $0.003 < P < 0.045$ ) were found statistically different in loading response and in the second half of the gait cycle. The first half of the gait cycle was characterized by statistically significant differences on the hip int/ext rotation angle ( $0.009 < P < 0.046$ ), knee ab/ad angle ( $0.032 < P < 0.050$ ), and ankle int/ext rotation angle ( $0.008 < P < 0.044$ ). The last two angles showed differences also during the swing phase of gait. (Figures 3.5, 3.6, 3.7) .

**Chapter 3. Musculoskeletal modeling in diabetic foot prevention**

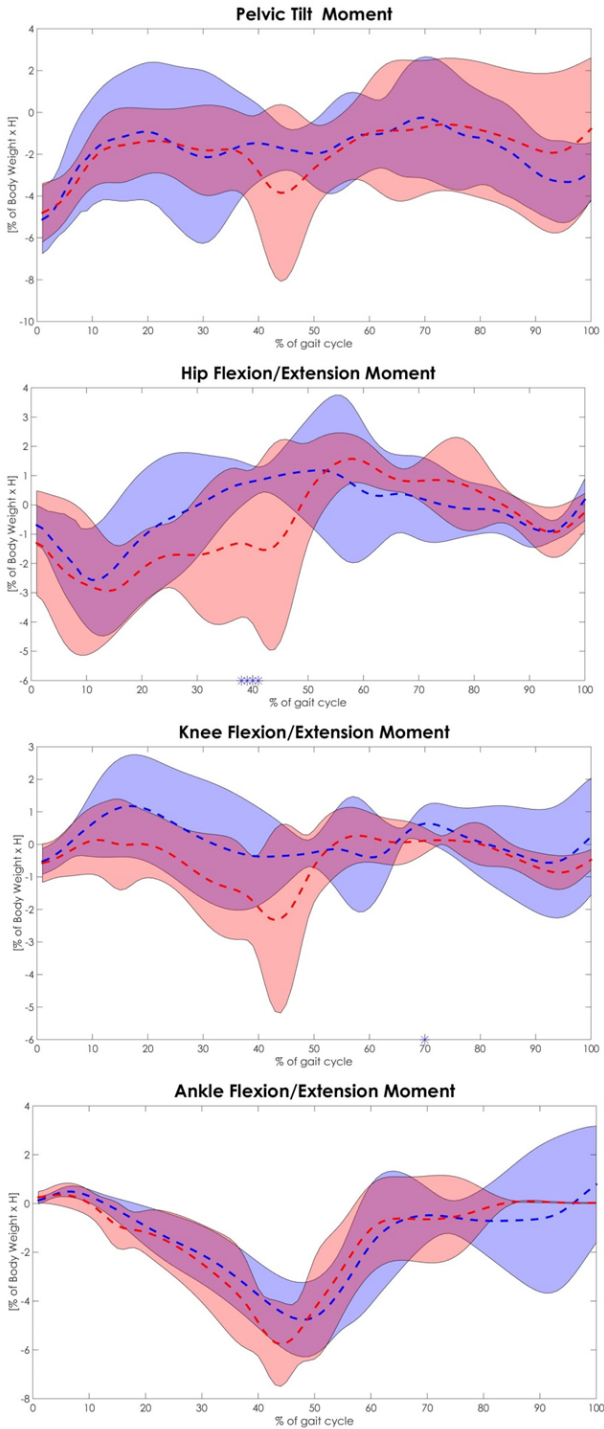


Figure 3.3 – Gait analysis joints dynamics results of the sagittal plane (**OPENSIM ELABORATION**): comparison between mean joint moments (dashed lines) plus and minus 1 standard deviation of both CS (in blue) and of DNS (in red). Results of two tailed T-Test have been reported in term of the instants of the gait cycle where significant differences were found, and they are represented with the blue asterisk (Level of Significance was set to  $p < 0.05$ ).

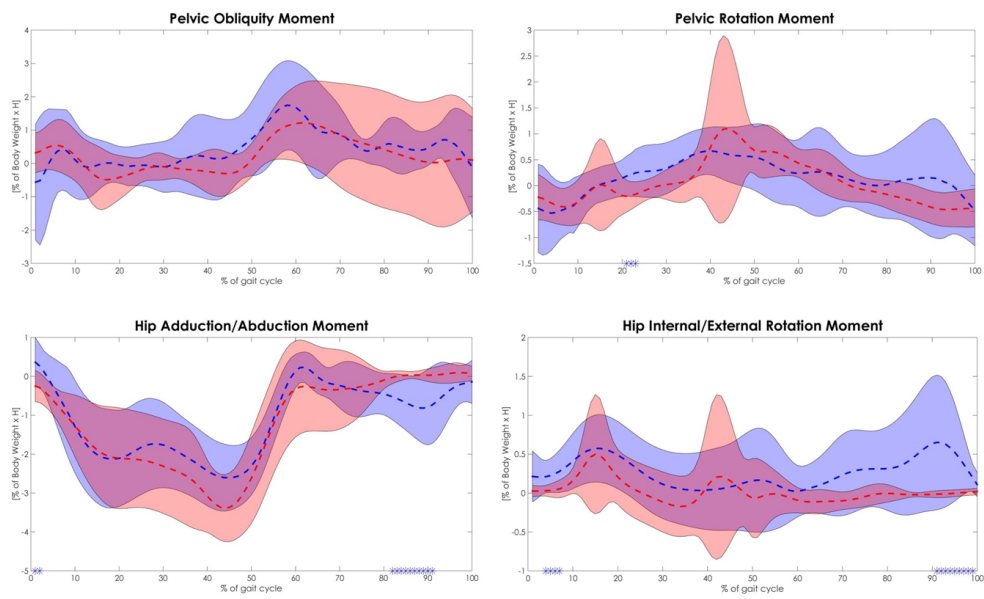


Figure 3.4 – Gait analysis joints dynamics results of the transverse and frontal planes (**OPENSIM ELABORATION**): comparison between mean joint moments (dashed lines) plus and minus 1 standard deviation of both CS (in blue) and of DNS (in red). Results of two tailed T-Test have been reported in term of the instants of the gait cycle where significant differences were found, and they are represented with the blue asterisk (Level of Significance was set to  $p < 0.05$ ).

**Chapter 3. Musculoskeletal modeling in diabetic foot prevention**

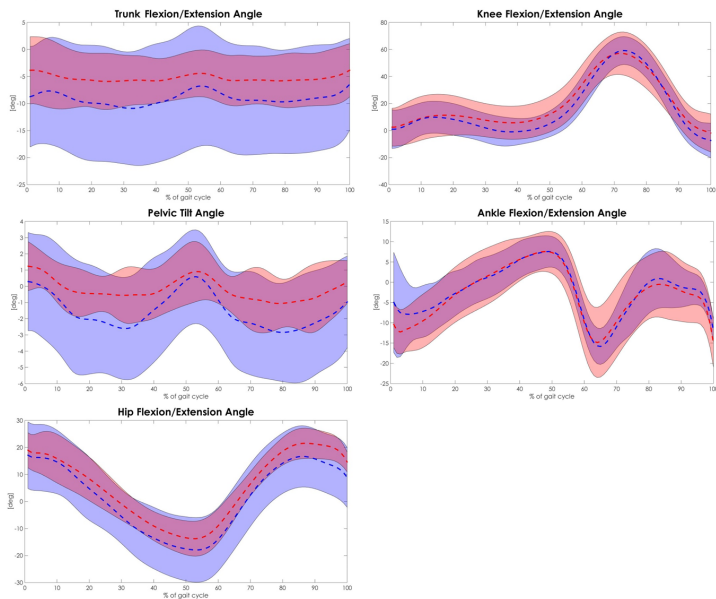


Figure 3.5 – Gait analysis joint kinematic results of the sagittal plane. Comparison between mean joint angles (dashed lines) plus and minus 1 standard deviation of both CS (in blue) and of DNS (in red). Results of two tailed T-Test have been reported in term of the instants of the gait cycle where significant differences were found, and they are represented with the blue asterisk (Level of Significance was set to  $p < 0.05$ ).

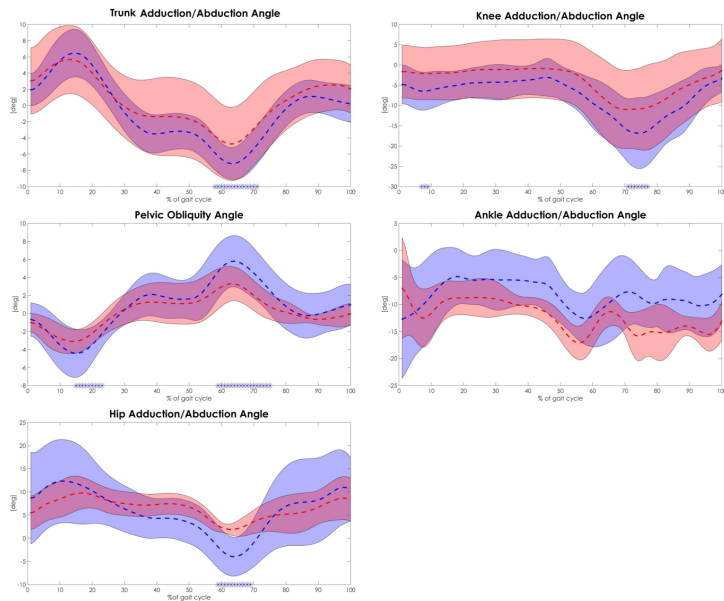


Figure 3.6 – Gait analysis joint kinematic results of the frontal plane. Comparison between mean joint angles (dashed lines) plus and minus 1 standard deviation of both CS (in blue) and of DNS (in red). Results of two tailed T-Test have been reported in term of the instants of the gait cycle where significant differences were found, and they are represented with the blue asterisk (Level of Significance was set to  $p < 0.05$ ).

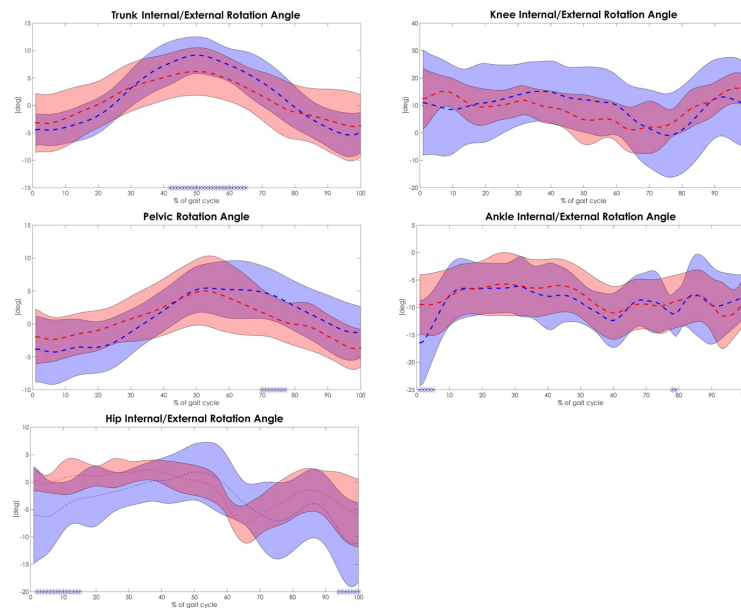


Figure 3.7 – Gait analysis joint kinematic results of the transverse plane. Comparison between mean joint angles (dashed lines) plus and minus 1 standard deviation of both CS (in blue) and of DNS (in red). Results of two tailed T-Test have been reported in term of the instants of the gait cycle where significant differences were found, and they are represented with the blue asterisk (Level of Significance was set to  $p < 0.05$ ).

### 3.3.2.2 Experimental joint kinetic output of CS vs. Experimental joint kinetic output of DNS

The stance phase of the gait cycle was characterized by statistically significant differences on the DNS trunk int/ext rotation moment ( $0.003 < P < 0.048$ ), hip int/ext rotation moment ( $0.010 < P < 0.044$ ) and ankle ab/ad moment ( $0.002 < P < 0.047$ ). On the other hand, swing phase showed a difference in the DNS trunk ab/ad moment ( $0.015 < P < 0.049$ ) and in the hip flex/ext moment ( $0.047 < P < 0.049$ ) (Figures 3.8, 3.9, 3.10).

### 3.3.3 Experimental data elaboration through routine gait analysis protocol compared to data elaboration through OpenSim

#### 3.3.3.1 Experimental joint kinematic output of CS vs. OpenSim joint kinematic output of CS

The comparison between CS' angles calculated with OpenSim and CS' angles calculated with modified Leardini et al. 2007, displayed statistically significant differences at the heel strike on the pelvic tilt ( $0.030 < P < 0.040$ ) and during almost all the stance

### Chapter 3. Musculoskeletal modeling in diabetic foot prevention

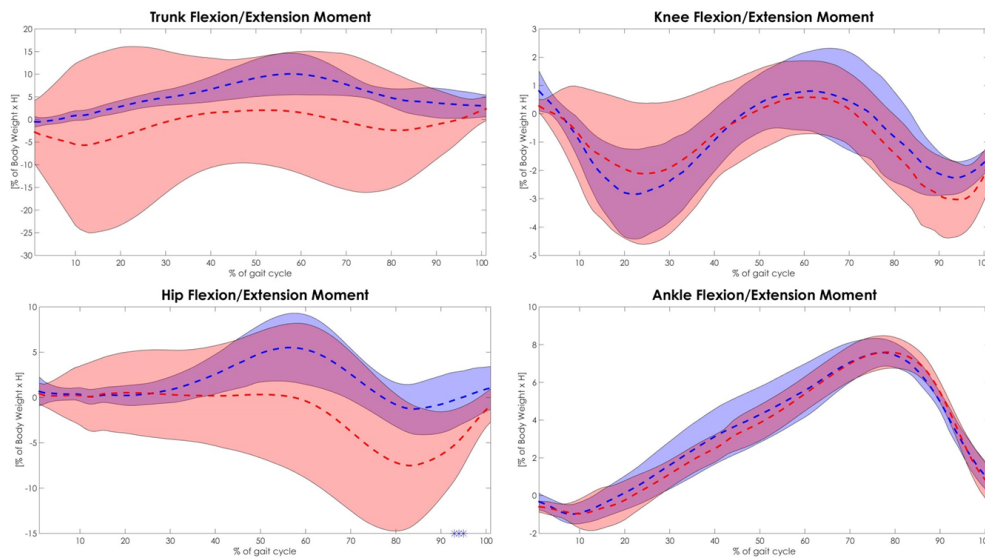


Figure 3.8 – Gait analysis joint kinetic results of the sagittal plane: comparison between mean joint moments (dashed lines) plus and minus 1 standard deviation of both CS (in blue) and DNS (in red). Results of two tailed T-Test have been reported in term of the instants of the gait cycle where significant differences were found, and they are represented with the blue asterisk (Level of Significance was set to  $p < 0.05$ ).

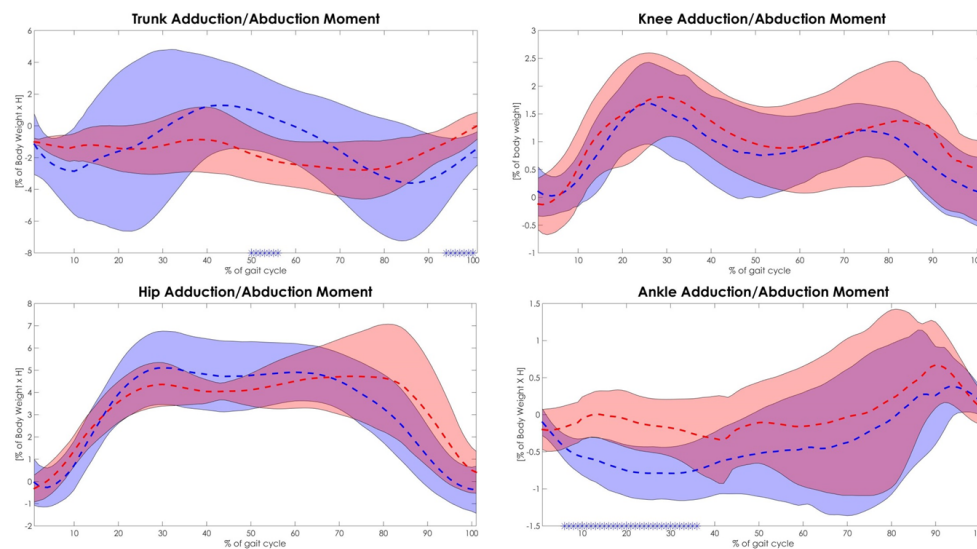


Figure 3.9 – Gait analysis joint kinetic results of the frontal plane: comparison between mean joint moments (dashed lines) plus and minus 1 standard deviation of both CS (in blue) and DNS (in red). Results of two tailed T-Test have been reported in term of the instants of the gait cycle where significant differences were found, and they are represented with the blue asterisk (Level of Significance was set to  $p < 0.05$ ).



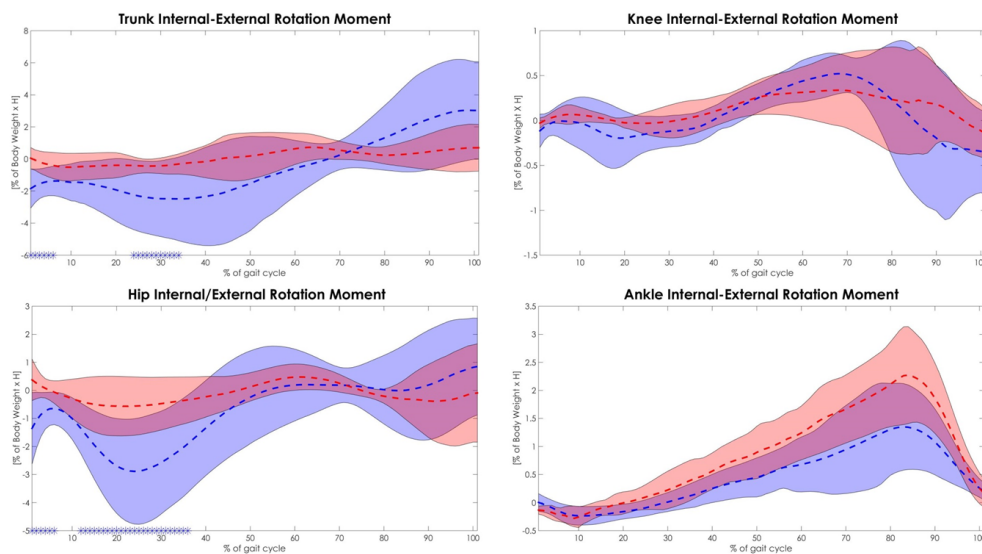


Figure 3.10 – Gait analysis joint kinetic results of the transverse plane: comparison between mean joint moments (dashed lines) plus and minus 1 standard deviation of both CS (in blue) and DNS (in red). Results of two tailed T-Test have been reported in term of the instants of the gait cycle where significant differences were found, and they are represented with the blue asterisk (Level of Significance was set to  $p < 0.05$ ).

phase of gait on the pelvic list ( $0.003 < P < 0.041$ ). A significant difference was registered also on the knee ( $0.005 < P < 0.046$ ) and on the ankle ( $P < 0.034$ ) flex/ext. Furthermore hip ab/ad angle differed in the two approaches at the beginning and at the end of the gait cycle ( $P < 0.043$ ). (Figures 3.11 3.12).

### 3.3.3.2 Experimental joint kinetic output of CS vs. OpenSim joint kinetic output of CS

All CS' joint moments calculated with OpenSim showed statistically significant differences with respect to the ones calculated directly from the experimental data as in [146] (Figure 3.13). Hip flex/ext moment displayed significant differences ( $0.001 < P < 0.041$ ) during the loading response and in the transition between stance and swing phase. Hip ab/ad was found statistically significant different during almost all the swing phase and the central part of the stance ( $P < 0.050$ ); hip int/ext rotation moment displayed significant differences only during the loading response and during the midstance ( $0.008 < P < 0.0047$ ). Knee flex/ext moment ( $0.002 < P < 0.046$ ) together with ankle flex/ext moment ( $P < 0.048$ ) differed significantly during both the stance and the swing phases.

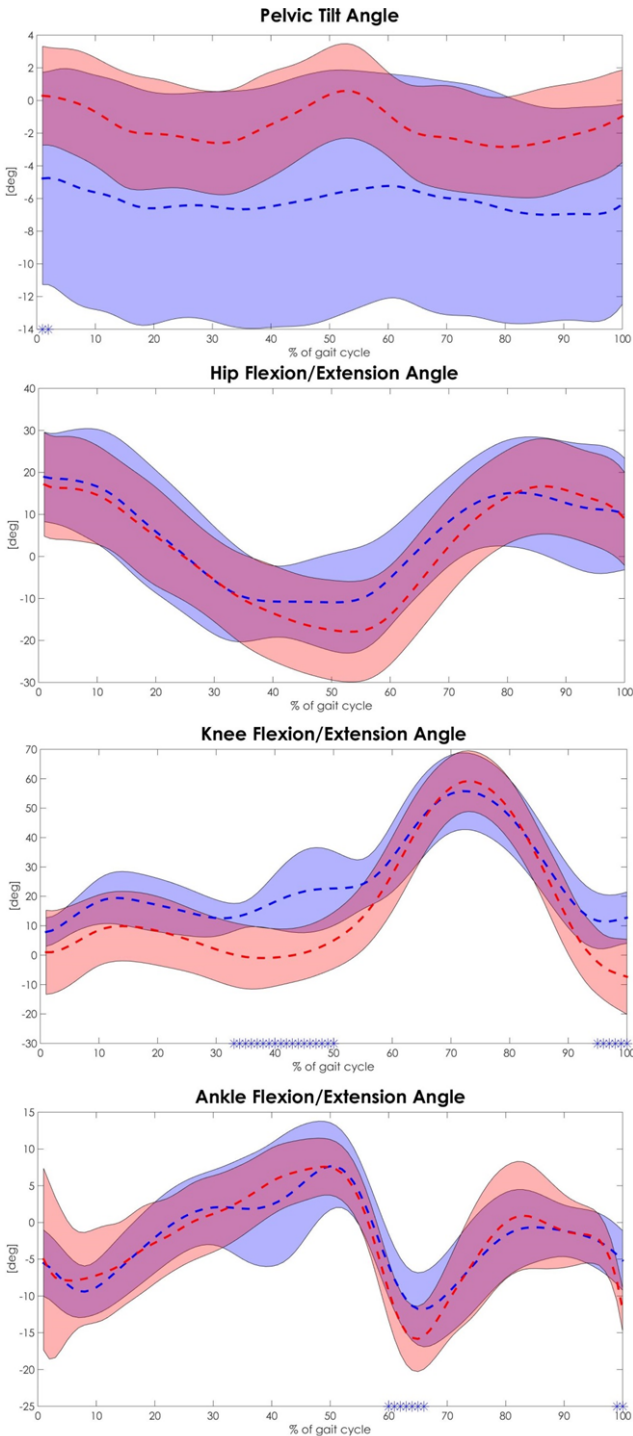


Figure 3.11 – Gait analysis joint kinematic results of the sagittal plane: comparison between mean joint angles (dashed lines) plus and minus 1 standard deviation of both CS estimated with OpenSim (in blue) and of CS estimated with the modified Leardini et al. 2007 (in red). Results of two tailed T-Test have been reported in term of the instants of the gait cycle where significant differences were found, and they are represented with the blue asterisk (Level of Significance was set to  $p < 0.05$ ).



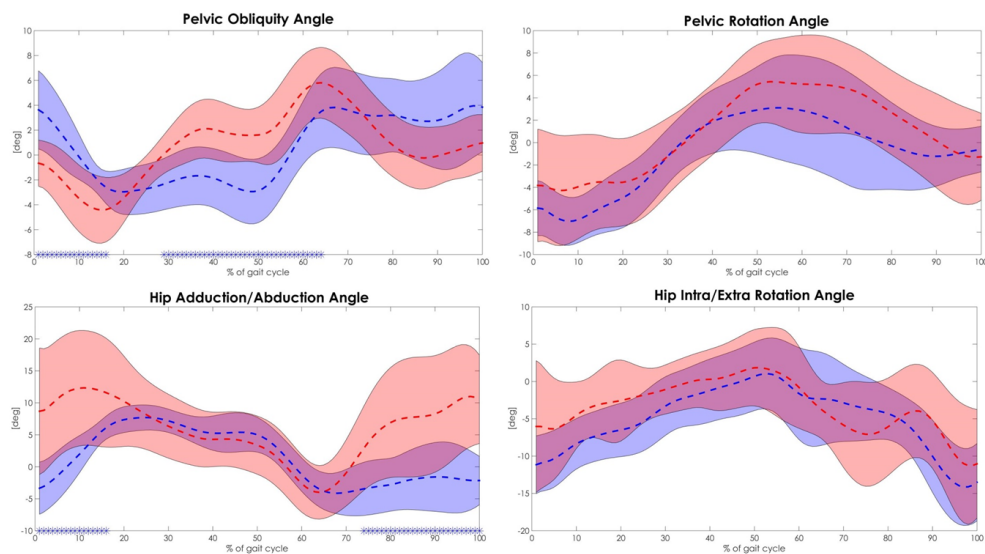


Figure 3.12 – Gait analysis joint kinematic results of the transverse and frontal planes: comparison between mean joint angles (dashed lines) plus and minus 1 standard deviation of both CS estimated with OpenSim (in blue) and of CS estimated with the modified Leardini et al. 2007 (in red). Results of two tailed T-Test have been reported in term of the instants of the gait cycle where significant differences were found, and they are represented with the blue asterisk (Level of Significance was set to  $p < 0.05$ ).

### 3.3.3.3 Experimental joint kinematic output of DNS vs. OpenSim joint kinematic output of DNS

DNS Joints kinematics computed with OpenSim differed significantly from the one computed with the modified Leardini et al. 2007 on the pelvis obliquity during the second part of the stance phase and at the beginning of the swing ( $0.001 < P < 0.036$ ). Hip flex/ext moment differed significantly at the end of the stance phase ( $0.036 < P < 0.050$ ), hip ab/ad moment at the heel strike and during the swing ( $0.001 < P < 0.050$ ), hip rotation at the beginning and at the end of the gait cycle. Finally knee flex/ext differed significantly between the end of the stance and the beginning of the swing and at the end of the gait cycle ( $0.039 < P < 0.050$ ). (Figures 3.14 3.15).

### 3.3.3.4 Experimental joint kinetic output of DNS vs. OpenSim joint kinetic output of DNS

DNS' joints kinetics calculated with OpenSim differed significantly on the hip flex/ext moment at the end of the gait cycle ( $0.005 < P < 0.042$ ). Hip ab/ad moment was found statistically different during the swing phase ( $0.004 < P < 0.046$ ) together with the ankle flex/ext moment ( $P < 0.033$ ). The latter showed significant differences also during the

**Chapter 3. Musculoskeletal modeling in diabetic foot prevention**

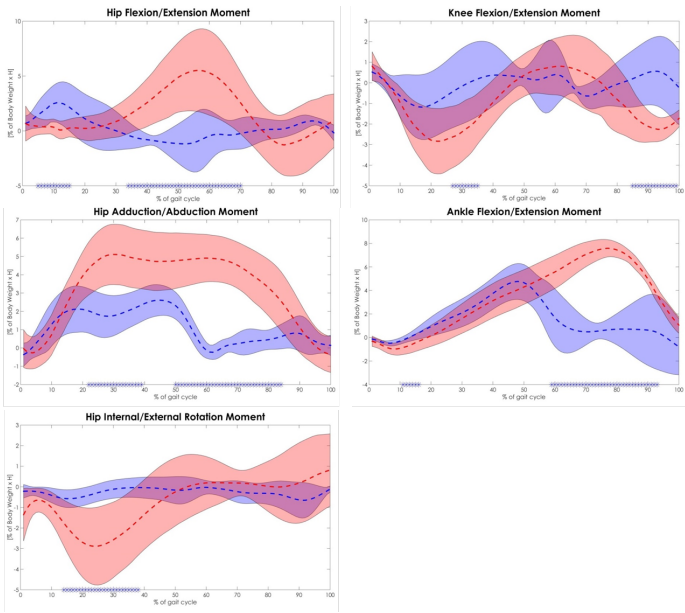


Figure 3.13 – Gait analysis joint kinetic results: comparison between mean joint moments (dashed lines) plus and minus 1 standard deviation of both CS estimated with OpenSim (in blue) and of CS estimated as in [146] (in red). Results of two tailed T-Test have been reported in term of the instants of the gait cycle where significant differences were found, and they are represented with the blue asterisk (Level of Significance was set to  $p < 0.05$ ).

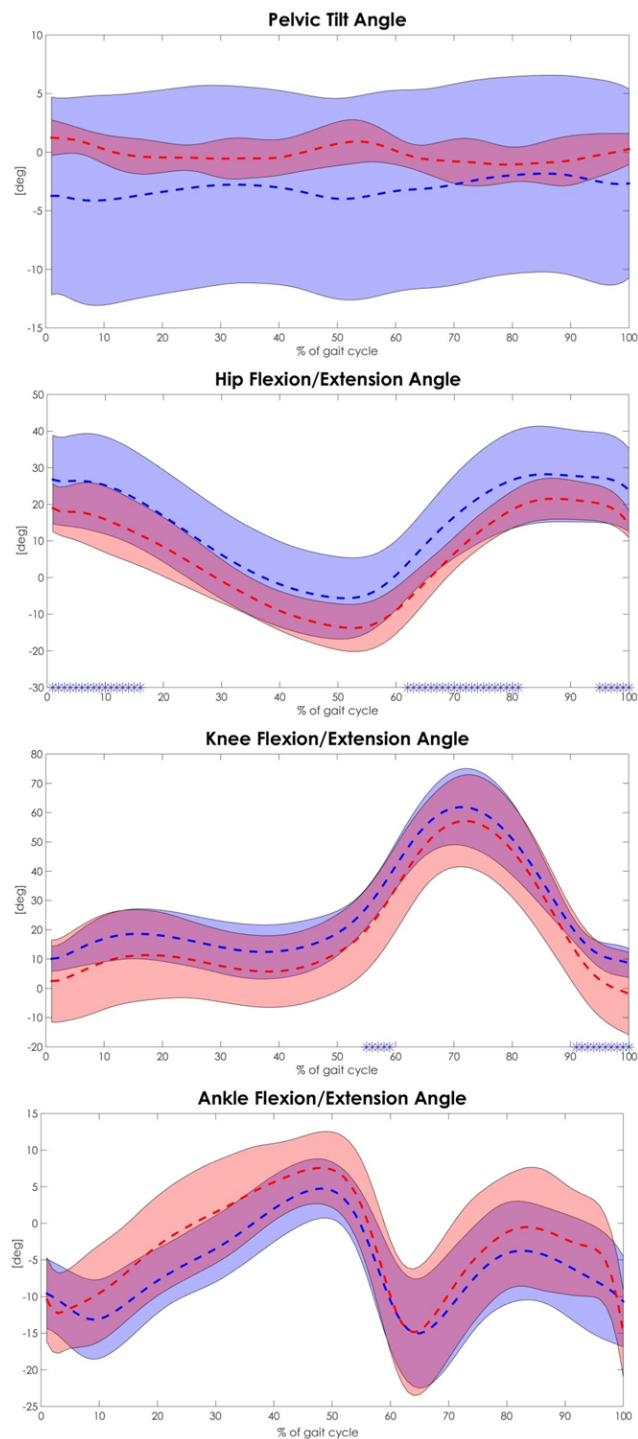


Figure 3.14 – Gait analysis joint kinematic results of the sagittal plane: comparison between mean joint angles (dashed lines) plus and minus 1 standard deviation of both DNS estimated with OpenSim (in blue) and of DNS estimated with the modified Leardini et al. 2007 (in red). Results of two tailed T-Test have been reported in term of the instants of the gait cycle where significant differences were found, and they are represented with the blue asterisk (Level of Significance was set to  $p < 0.05$ ).

**Chapter 3. Musculoskeletal modeling in diabetic foot prevention**

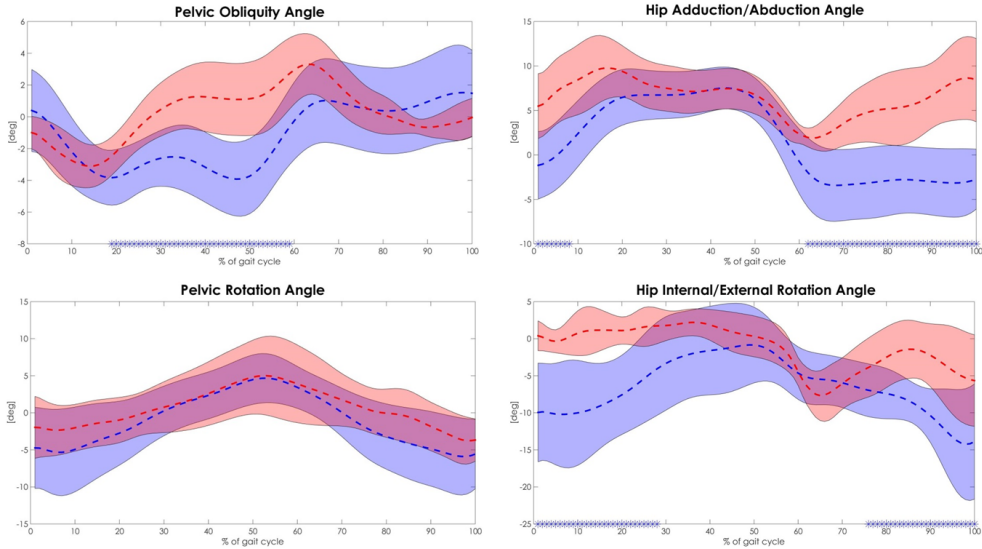


Figure 3.15 – Gait analysis joint kinematic results of the transverse and frontal planes: comparison between mean joint angles (dashed lines) plus and minus 1 standard deviation of both DNS estimated with OpenSim (in blue) and of DNS estimated with the modified Leardini et al. 2007 (in red). Results of two tailed T-Test have been reported in term of the instants of the gait cycle where significant differences were found, and they are represented with the blue asterisk (Level of Significance was set to  $p < 0.05$ ).

stance as well as the knee flex/ext moment ( $P < 0.048$ ). Figure 3.16.

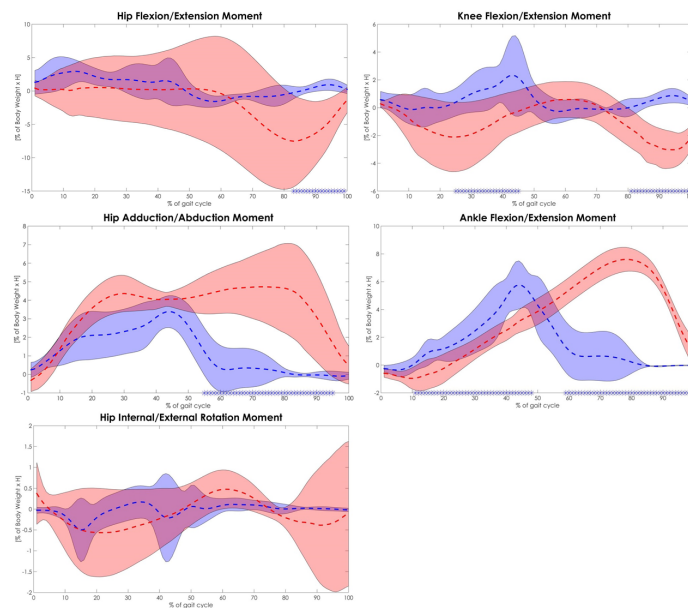


Figure 3.16 – Gait analysis joint kinetic results: comparison between mean joint moments (dashed lines) plus and minus 1 standard deviation of both DNS estimated with OpenSim (in blue) and of DNS estimated as in [146] (in red). Results of two tailed T-Test have been reported in term of the instants of the gait cycle where significant differences were found, and they are represented with the blue asterisk (Level of Significance was set to  $p < 0.05$ ).

### 3.3.3.5 Experimental muscle activations measured with SEMG

In Figure 3.17 the values of the POP with respect to the gait cycle are reported. The histogram highlighted a delay of the DNS' peaks of activation in the following muscles:

- Gluteus Medius (~20% of the gait cycle);
- second activation of the Rectus Femoris (~60% of the gait cycle);
- Lateral Gastrocnemius (~40% of the gait cycle);
- second activation of the Tibialis Anterior (~80% of the gait cycle);
- both the activations of the Extensor Digitorius (~5% and ~80% of the gait cycle).

On the other side an anticipated peak of activation was highlighted in the following muscles:

**Chapter 3. Musculoskeletal modeling in diabetic foot prevention**

- first and third activation of the Rectus Femoris (~5% and ~95% of the gait cycle);
- first activation of the Tibialis Anterior (~5% of the gait cycle);
- Peroneus Longus (~35% of the gait cycle).

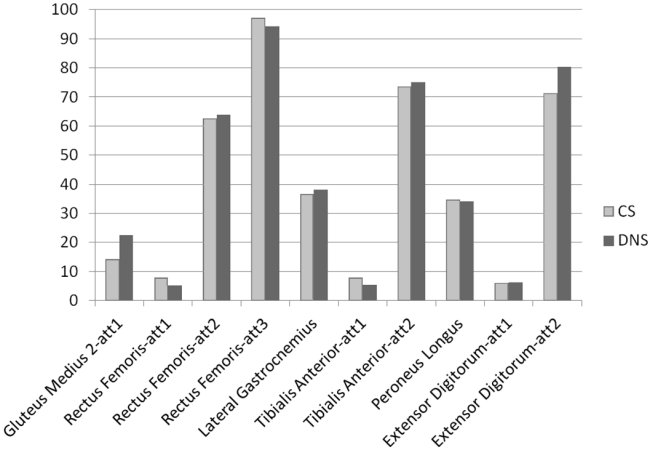


Figure 3.17 – The figure shows the results of the analysis of the SEMG regarding the POP. On the x-axis the name of the muscles is reported while in the y-axis there is the percentage of the gait cycle. DNS are in red while CS are in blue.

### 3.4 Discussion

By analyzing OpenSim simulations results and standard gait analysis output in a diabetic population, this study offers new key findings. The use of OpenSim demonstrated to be complementary to the standard gait analysis performed as in [84]. In this study it indeed enabled the evaluation of muscles forces in the DNS and CS, highlighting the differences between them. Furthermore the comparison between joint kinetic and kinematic results obtained with the two methods, provided us with an idea of how good modeling techniques are and on how they can be use to integrate clinical findings. A comparison between CS and DNS kinematic and kinetic variables and muscle forces was indeed done. All the gait cycle was considered. Routine gait analysis variables [84] gives a more complete overview of the subjects kinematics and kinetics, given the reduced number of degree of freedom (DOF) available in the generic OpenSim model ([31], [28]). Besides differences in the joint embedded frames definitions ([91], [84], [89], [144],[145], [31], [28]) this might in part explain why statistically significant differences between DNS and CS were highlighted with both approaches, but not always on the same joints rotations or moments. State of the art in DNS gait analysis revealed the presence of several gait alterations in this population of subjects ([90], [119], [132], [147], [83], [148], [149], [150],[151], [152],[153], [128], [154], [155],[156], [157], [158],[159]). In particular their association with neuropathy has been demonstrated ([90], [119], [132], [147], [83], [148], [149], [150],[151], [152],[153], [128], [154], [155],[156], [157], [158],[159]) (See section ).Different authors found an increased gait variability [151] characterized by a general decrease of the mobility and changes in movement of the ankles ( [83], [156], [90], [152]) and in the ground reaction forces during walking [153]. OpenSim kinematics results identified a decreased mobility in the sagittal plane at the hip joint in DNS accompanied by a higher value of the pelvic rotation angle at the end of the gait cycle. At the same time both the activation and the force of the Iliacus and Gracilis were found significantly lower indicating the presence of differences in the hip flexor muscles for this specific population of subjects in agreement with the literature ([132], [148], [154], [122], [160], [147]). Furthermore a significant difference on the ankle flex/ext angle was found during the stance phase. The estimation of activations and forces of muscles implicated in the ankle plantar flexion revealed significant differences during the same gait cycle phases. In particular Flexor Hallucis and Flexor Digitorum revealed significant weaker forces in the DNS as previously reported in the literature with the aid of SEMG ([132], [122], [160], [147]). DNS also showed a significantly minor activity of the Extensor Digitorum. On the other hand differences in joints kinematics revealed with the standard gait analysis protocol might indicate an enhanced joint stiffness in DNS, as already pointed out in other studies ([155], [156]). In particular, this phenomenon was highlighted on

### Chapter 3. Musculoskeletal modeling in diabetic foot prevention

---

pelvic obliquity and pelvic rotation where the range of motion of DNS appeared to be limited. No significant differences were found on the ankle flex/ext of DNS with respect to the CS, although several studies reported a deficiency in the flexibility of this joint during all the gait cycle, even before the development of the neuropathy ([119], [91], [157]). However, a change was found at the ankle int/ext rotation angle.

The results of the static optimization showed significant differences both in the activation and in the force of the Tibialis Posterior between DNS and CS. Tibialis Posterior plays a key role in ankle stabilization and it also act at the ankle level to produce inversion and assists in the plantar flexion of the foot (See section 2.4). Furthermore it has a major role in supporting the medial arch of the foot [158]. Its dysfunction can determine the development of the flat foot, thus leading to an irregular distribution of the load on the plantar surface. This will influence the localization of the ulcers as already reported in the literature. Sawacha et al. identified excessive plantar pressures and ground reaction forces in a population of DNS, which were accompanied by a reduction in the contact surface of the mid foot [90]. Furthermore diabetic subjects without neuropathy showed an alteration in mid foot and forefoot kinematics during most of the gait cycle [157]. The weakness of the Tibialis Posterior is often associated with an irregular behavior of the Gastrocnemius, but this was not revealed in the present study. This can be explained with the fact that muscles properties in the standard OpenSim model has not been changed according to the specific populations of subjects (DNS). In the literature important differences in DNS muscles tissue properties have been recorded and this should be taken onto account in future works [161]. However significant differences were found in the force of the Peroneus Longus which, together with the Lateral Gastrocnemius, is responsible for the plantar flexion of the ankle. The development of excessive plantar pressure can thus be linked to this specific finding. It should be mentioned that a delay of the peak of activation of the Peroneus Longus experimentally measured with the SEMG, was observed at the end of the midstance and at the beginning of the terminal stance phases. This finding could be responsible for the deficit in the ankle mobility revealed in DNS. For what regards the inverse dynamics, OpenSim allowed identifying significant differences on each hip joint moments (flex/ext, and/add, int/ext). Experimentally derived joints moments instead allowed identifying significant changes on the pelvis rotation and obliquity and on the hip rotation moment: these results might indicate a deficit in the mobility and in the stability of the related joints. The results concerning muscle forces have been reflected in the position of the peak of the envelope of the muscles activations experimentally recorded. The SEMG analysis indeed reported during stance an early activation of the Tibialis Anterior and of the Peroneus Longus in DNS with respect to the CS. This seems to confirm results obtained with the OpenSim simulations. When comparing the outputs of the two modeling approaches, in both CS and DNS popula-



tions, the largest discrepancies were found on the pelvis and on the hip joint angles. When the comparison was made between the inverse dynamic estimated with the two approaches more divergences were found. This can be explained by the different algorithms that are underneath the computation. The experimental approach uses "Table A2.6" e "Table A2.7" in the appendix of Zatsiorsky et al. 1990 [162] to compute the masses of the different segments while OpenSim uses the position of the markers in the static acquisition to scale the masses of the generic model. Overall, results of the present work might be used in planning specific exercise protocols for DNS, aiming to decrease the alteration of the lower limb muscles, strengthening the deficient muscles and stretching the ones too tense. This is in order to decrease the joint rigidity and to improve the load distribution on the foot, avoiding the formation of hyper pressures in certain area. This finds agreement with Sartor et al. who successfully proposed the adoption of these protocols in order to prevent the formation or the worsening of the peripheral neuropathy, decreasing the risk of injury, wounds and ulcers which can lead to amputation of the feet in the most serious cases [133]. The limit of state of the art physical therapy is the absence of a quantitative method for evaluating its effectiveness. Motion analysis integrated with musculoskeletal simulations performed with OpenSim proved to be a good technique to diagnose alterations in the musculoskeletal system. For this reason it can be used to evaluate the validity of different protocol of exercise, looking at the posture and at the muscles of the subjects. OpenSim demonstrated its ability to obtain results similar to those obtained from the standard gait analysis, providing as well data not experimentally measurable. The limited number of subjects and of muscles analyzed constitutes the main limitation of the study. This will be object of future developments, with the aim to deepen the knowledge of musculoskeletal abnormalities present in diabetic patients with and without neuropathy and to evaluate the effectiveness of different protocol of exercises suitable to their needs.

### 3.5 Acknowledgments

I acknowledge Prof. Ilse Jonkers for welcome me in the *Human Movement Biomechanics Research Group* of the *Department of Kinesiology* of the *Katholieke Universiteit Leuven* and for introducing me to field of musculoskeletal modeling. This work would not have been possible without her collaboration.



## 4 Combining musculoskeletal models and finite element models

### 4.1 Foot finite element models and joint reaction forces

*Foot ulcerations are one of the most common and invalidating complications that affect diabetic foot patients and can lead to amputations. Biomechanical factors play an important role in the etiology and treatment of the disease. A foot finite element model (FEM) can improve the experimental findings offering information that is not directly measurable. Motion capture and force plate data are generally used as boundary conditions, while plantar pressure data are used to verify the validity of FEM solutions. The aim of this work was to verify the impact of applying the foot joints contact forces (JCFs) obtained from musculoskeletal modeling as boundary condition, on the foot FEM simulations. Two musculoskeletal models (MSMs) were then developed in OpenSim using one healthy and one neuropathic subjects gait analysis data. The subjects' foot geometries were used for the development of two 3D foot FEMs. To test the importance of the subject-specificity, MSMs of 10 neuropathic and 10 healthy subjects were also created and their JCFs were used as input for the two FEMs. A better agreement was found between experimentally measured and simulated plantar pressure obtained with JCFs than with the GRFs as boundary conditions. The average error at the stance phase of gait, calculated as the difference between simulated and experimental values and expressed in percentage of the experimental ones, was of 17% in GRFs driven simulations while it was of -3.34% in the JCFs ones for the healthy model; it was respectively of 30% and 14% for the diabetic model.*

#### 4.1.1 Background & Aims

Diabetic patients are often affected by foot ulcerations that are one of the most common complications and can lead to amputations. It has been reported that the lifetime

risk of diabetic patients developing a foot ulcer could be as high as 25% [163]. Although the awareness of this problem among health care professionals has recently risen, it remains one of the most ordinary causes for hospital admission among diabetic patients [164]. Avoiding this complication would result in a decrease of medical, personal, social, and economic costs. Diabetic foot ulceration has a multifactorial pathophysiology, but diabetic peripheral neuropathy (DPN) is thought to be responsible for most cases. DPN is a sensorimotor neuropathy responsible for changes in foot structure and function ([83], [119]) and dryness of the skin which is the cause of excessive callus formation. Several authors have demonstrated a close relationship between neuropathy and foot biomechanical alterations that leading to an increased plantar foot pressure ([165], [115], [166], [116]), might determine plantar ulcerations ([167], [65], [126], [168], [169], [170]). Biomechanical analysis have been traditionally carried out using both experimental techniques, i.e. motion analysis, and computational methods, i.e. Finite Element (FE) simulations or MSMs. While experimental analysis can only assess variables at the interface between surfaces, reliable numerical models can provide the insight on internal stresses and strains tolerated by the plantar tissue ([170]). Different foot FEMs have been reported in literature for their ability to take into account critical aspects of the diabetic foot, namely the movement, the morphology, the tissue properties and the loads ([54], [39], [77], [171]). Several assumptions were made, such as: a simplified or partial foot shape, linear material properties and boundary conditions that were never subject specific. The validity of the models was then assessed by comparing the simulation outputs with experimentally measured plantar pressures [172]. An attempt towards the reduction of these simplifications has been performed in our laboratory [78] with the development of a geometrically detailed and subject specific 3D FE model of the diabetic neuropathic foot and ankle combined with subject specific gait analysis data. Together with FEMs, the use of MSMs has proliferated in the biomechanics research community thanks to its ability to reveal muscle forces and joint contact forces (JCFs) for a wide range of motions ([28], [173], [174]). Several studies have therefore already tried to combine gait analysis to MS modeling in order to get a deeper understanding of motion dysfunction ([175], [176], [177], [178]). The aim of this work was to verify the possibility of improving foot FEM by applying the foot joints contact forces obtained from MSMs as boundary conditions. The validity of the approach was evaluated by comparison between simulated and experimentally measured foot plantar pressures. The biomechanical behavior of both a healthy subject (HS) and a diabetic neuropathic subject's (DNS) feet were assessed in order to predict the area exposed to excessive stresses on the plantar surface which, in the case of a DNS, can lead to the development of foot ulcers. Specific MSMs were developed allowing the determination of joint kinematics and kinetics that were used as input for two foot FEMs previously developed (case A)

## 4.1. Foot finite element models and joint reaction forces

[78]. A comparison between the simulated plantar pressure and the subject-specific experimental ones during different phases of the stance phase of gait was performed in order to validate the FE simulations. A further aim of this study was to assess the validity of the models when driven by JCFs of 10 healthy and 10 diabetic neuropathic subjects, in order to verify the possibility of extending the results of the subject specific FEMs to a wider population (case B). Also in this case experimental plantar pressure data were used as gold standard to validate the results of the simulations.

### 4.1.2 Materials & Methods

#### 4.1.2.1 Subjects

**Case A:** FEMs were developed based on the data of one healthy subject (HS1) and one diabetic subject with peripheral neuropathy (DNS1) (Table 4.1) [78].

**Case B:** 10 HSs and 10 DNSs (Table 4.2) underwent a gait analysis during which data were acquired as in ([83], [90]). DNS' inclusion criteria were: type 1-2 diabetes, no history of ulcers or neurological disorders (apart from neuropathy), no lower limb surgery, no orthopedic problems, no cardiovascular disease and with walking ability. HSs were enrolled among hospital personnel. A written informed consent was obtained from all subjects. The protocol was approved by the local Ethic Committee of the University Clinic of Padova. In both cases (case A and B) the DNS underwent the following screening: a neurological evaluation which included the assessment of symptoms, and signs compatible with peripheral nerve dysfunction, the Michigan Neuropathy Screening Instrument ([179]); and a physical examination as in Sawacha et al. [119]. Each patient had at least one measure of urinary albumin-to-creatinine ratio (0–30 mg/g normal, 30–300 mg/g microalbuminuria, 4300 mg/g macroalbuminuria), one ophthalmologic examination, a 12-leads electrocardiogram collected in the three months preceding the study, a carotid artery Doppler ultrasound examination and HbA1c values from the preceding ten years.

Table 4.1 – Demographic and clinical data of the diabetic neuropathic subject (DNS1) and the healthy subject (HS1) whose foot geometries were used for the development of the FEMs.

Condition	Sex	Age	Weight	Height	BMI	Foot size	Type of foot
HS1	F	27	61	174	20.1	40	Normal
DNS1	M	61	79	175	25.8	42.5	Cavus

## Chapter 4. Combining musculoskeletal models and finite element models

Table 4.2 – Demographic and clinical data of the healthy and the neuropathic subjects.  
# = Number of subjects.

Groups	HS		DNS	
	# or Mean	SD	# or Mean	SD
<b>Subjects [#]</b>	10		10	
<b>Sex [# of males]</b>	7		6	
<b>BMI</b>	24.6	2.3		
<b>Hypertensive disease</b>				
<b>Age [years]</b>	62.2	4.8		
<b>Peripheral neuropathy [#]</b>	-	-	10	
<b>Diabetic retinopathy [#]</b>	-	-	6	
<b>Microalbuminury [#]</b>	-	-	2	
<b>Vasculopathy [#]</b>	-	-	3	
<b>Vasculopathy (peripheric) [#]</b>	-	-	2	
<b>Vasculopathy (TSA) [#]</b>	-	-	5	
<b>Vasculopathy (coronary) [#]</b>	-	-	1	
<b>Type of diabetes [#]</b>	-		Type 1: 6; Type 2: 4	
<b>Hb A1c</b>			8	1.3
<b>Years of disease</b>			29	12.3
<b>Cavus foot [#]</b>	4		9	12.3
<b>Flat foot [#]</b>	0		1	
<b>Hallux valgus [#]</b>	2		5	
<b>Foot deformities [#]</b>	4		4	
<b>Plantar callosity [#]</b>	1		5	

## 4.1. Foot finite element models and joint reaction forces

### 4.1.2.2 Experimental set up

The gait analysis was carried out using a 60 Hz 6 cameras stereophotogrammetric system (BTS S.r.l, Padova), 2 force plates (FP4060-10, Bertec Corporation, USA), and 2 pressure platform systems (410 x 410 x 0.5 mm,  $0.64\text{cm}^2$  resolution, 150 Hz, Imagortesi, Piacenza). The signals from all systems were synchronized in post-processing as in [83]. A four segments 3D foot kinematic model, which was previously validated in the author's laboratory, was adopted. It allows the 3D evaluation of ankle, hindfoot, midfoot and forefoot kinematics ([83], [90]), [119]) as well as sub-segment forces and PP. A static trial and at least three gait cycles of each limb while walking at a self-selected speed were included in the motion analysis acquisitions.

### 4.1.2.3 Musculoskeletal models

Using the experimentally measured body mass and the position of markers placed on anatomical landmarks during standing trial, a generic musculoskeletal model with 10 rigid bodies, 23 degrees of freedom and 92 musculotendon actuators was scaled to match each subject's dimensions and inertial properties [31]. The scaled models were then used to generate and analyze walking simulations of each subject's trials in OpenSim [28]. The lower-limb JCFs were calculated using the Joint Reaction analysis. These JCF are the resultant force acting on the joint, and is determined based on the kinematics and ground reaction forces. The workflow is shown in Figure 4.1.

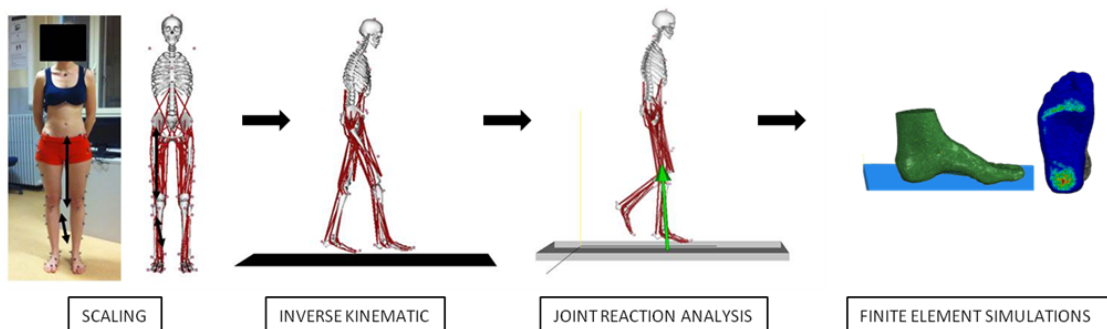


Figure 4.1 – Workflow of the development of MSMs and simulations.

### 4.1.2.4 Finite element models

Both the healthy subject (3DHSM) and the neuropathic subject (3DNSM) models used for the simulations were previously developed by the authors starting from the MRI of the right unloaded feet that were acquired with 1.5 T devices (Philips Achieva and Siemens Avanto, Spacing between slides: 0.6-0.7mm, Slice thickness: 1.2-1.5mm,

multi-fast-field-echo sequence). For details please refer to [78].

### 4.1.2.5 Simulations

For the FE simulations of both the 3DHSM and the 3DNSM, four instants of the stance phase when critical loads occur were chosen. This choice allows to cover the range of foot contact over the ground: the heel strike (the 1% of the stance), the loading response (first peak of the hindfoot vertical force), midstance (minimum height of the markers of the foot from the floor) and the push off (peak of the forefoot vertical force) [180]. Two different boundary conditions were investigated. The first one included the whole foot vertical ground reaction force together with the 3D angular position of the whole foot relative to the global reference system. We will refer to this condition as GRF simulations. The second one considered the 3D angular position of the foot relative to the global reference system but the JCFs at the ankle, determined with MSM in the same instants of interest, were applied. We will refer to this condition as JCF simulations. In GRF simulations the vertical GRF was applied to the FE plate while in the JCF simulations the vertical JCF was applied in the node correspondent to the midpoint between the lateral and the medial malleolus towards the simulated force plate. This choice is in line with the definition of the ankle coordinate system origin [181]. In the GRF simulations of the midstance phase, the gastrocnemius-soleus muscle force acting through the Achilles tendon, which insertion was detected from the MRI, was applied by a force vector equal to the 50% of the ground load as in [182]. All the simulations were performed in non-linear condition and the foot initial position was defined according to the ankle joint rotation [90] as derived from the experimental gait trails in the corresponding specific instant of the gait cycle. FE analyses were performed in Abaqus (Simulia, v.6.12) altering the FEMs loading characteristics and kinematics according the following two cases.

**Case A:** FE simulations were ran using both the subject specific JCFs and GRFs of the subjects whose foot geometry was used to develop the models. **Case B:** FE simulations were driven by the data of the 10 HSs and the 10 DNSs using the 3DHSM for HSs and the 3DNSM for the DNSs.

### 4.1.2.6 Model validation

The contact pressures simulated at the nodes of the plate were used for the experimental validation of the model by considering the agreement between model predicted and experimental plantar pressure (PP). The value of the peak of pressure was considered. Furthermore also the position of the peak of pressure was determined and



## 4.1. Foot finite element models and joint reaction forces

---

compared between experimental and simulated PP maps. In order to do this a reference frame was defined with the origin being the projection on the floor of the marker on the Calcaneus prominence. The X axis was defined from the origin to the projection on the floor of the marker on the 5th Metatarsal head prominence and the Y axis was perpendicular to X, lying on the floor plane, directed towards the medial part of the foot. This reference frame was calculated in the midstance phase in agreement with [83]. The foot was subdivided in three areas, hind foot, mid foot and fore foot as defined in [83]. Finally also the difference in the experimental and simulated contact area was evaluated as well as the one between GRFs and JCFs of HSs and DNSs.

### 4.1.3 Results

#### 4.1.3.1 Case A

The maximum contact PP values predicted by the 3DHSM are reported in Figure 4.2 (top). Positive values indicate that FE simulations overestimated the experimental ones, while the negative values indicate that FE simulations underestimated them. The GRF simulations underestimated the peak PP in all instances except for the push off. The average error between all the phases calculated as the difference between simulated and experimental values and expressed in percentage of the experimental ones, was -17%. The JCF simulations instead showed an overestimated value in the loading response while it underestimated the PP in the other phases with an averaged error value of -3.34%. The maximum contact PP values predicted by the 3DNSM are reported in Figure 4.2 (bottom). In this case the GRF simulations always overestimated the peak pressure values with an average error of 30%. On the other hand, the JCF simulations overestimated the peak PP values in the first three instances but not in the push off phase. The average error was 14%.

#### 4.1.3.2 Case B

The differences between the simulated and the experimental PP values estimated by the 3DHSM, driven with the HS group data as boundary conditions, are reported in Figure 4.3 (top). They are expressed in percentage of the experimental values. The averaged error was of 30.09% for the GRF simulations and of 35.98% for the JCF simulations. Furthermore the difference between simulated and experimental contact surface area is reported in Figure 4.4 (top). The GRF simulations ran with the data of the 10 HS, underestimated the PP in all the instants of the stance phase while the JCF simulations overestimated the PP at initial contact and loading response but underestimated them at midstance and push off. The contact surface was always

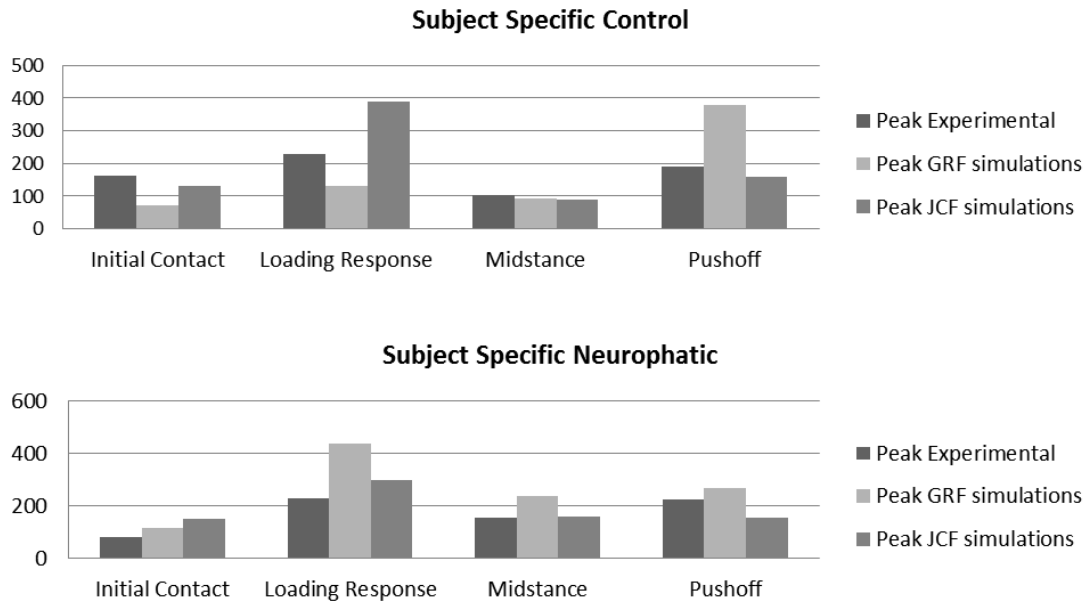


Figure 4.2 – Healthy (top) and Neuropathic (bottom) subject specific predicted and experimental PP values for the whole foot at the initial contact, loading response, midstance and push off.

overestimated in both simulations types, one exception found for the loading response in the JCF simulations.

The differences between the simulated and the experimental PP values estimated by the 3DNSM, driven with the DNS group data as boundary conditions, are reported in Figure 4.3 (bottom). They are expressed in percentage of the experimental values. The averaged error was of 37.12% for the GRF simulations and of 31.65% for the JCF simulations. Furthermore the difference between simulated and experimental contact area is reported in Figure 4.4 (bottom). The GRF simulations ran with the data of the DNS overestimated the PP at loading response and midstance but underestimated them at initial contact and push off. The JCF simulations overestimated the PP at initial contact and loading response but underestimated them in the other two phases. The contact area was always underestimated except for the initial contact in both boundary conditions. The experimental and simulated peak pressure positions for HSs' PP and the DNSs' PP are reported in Figures 4.6, 4.7, for the X and Y directions at loading response, and in Figures 4.8, 4.9, for midstance. A Kruskal Wallis test was used to determine statistically significant differences between the values (Matlab v.2013b). The values are expressed as a percentage of foot length. The loading response simulations ran with the JCFs can locate the X coordinate of the position of PP with no statistically significant differences throughout the foot area, divided as in [83], with

## 4.1. Foot finite element models and joint reaction forces

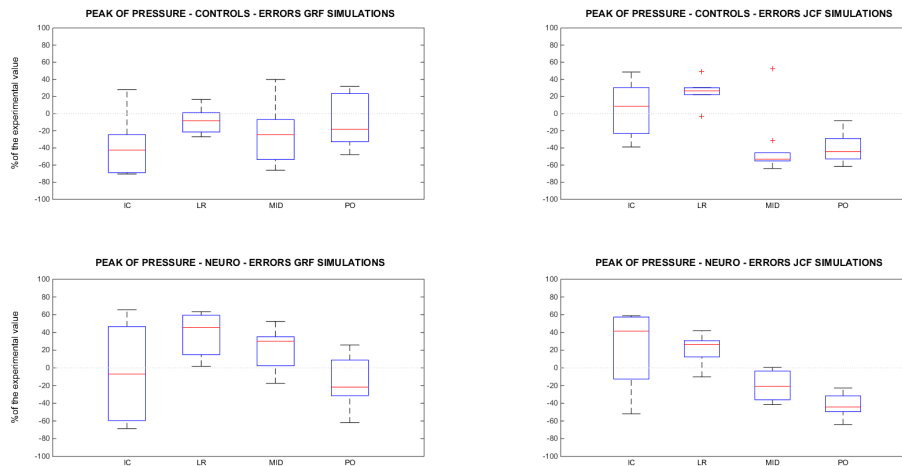


Figure 4.3 – Healthy (top) and Neuropathic (bottom) subject's errors (difference between the simulated and the experimental values) for the peak of pressure in the different phases of the gait cycle expressed in percentage of the experimental value. On the left errors between experimental PP values and simulated with GRFs ones. On the right errors between experimental PP values and simulated with JCFs ones.

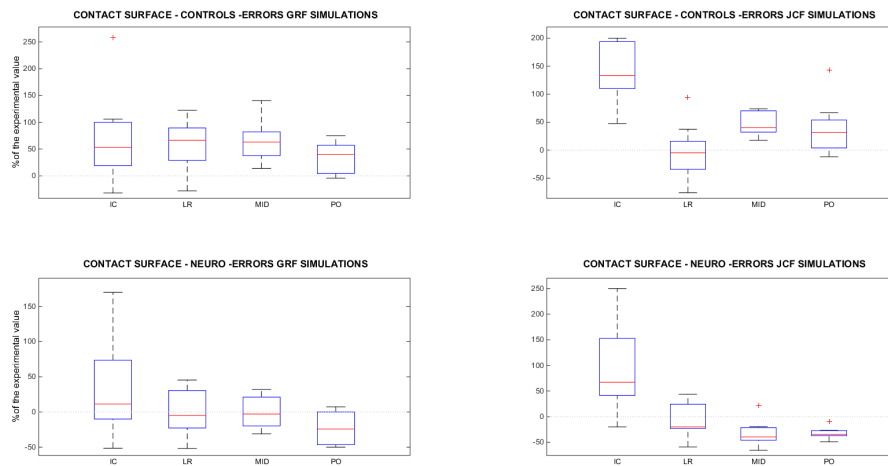


Figure 4.4 – Healthy (top) and Neuropathic (bottom) subject's errors (difference between the simulated and the experimental values) for the contact surface in the different phases of the gait cycle expressed in percentage of the experimental value. On the left errors between experimental PP values and simulated with GRFs ones. On the right errors between experimental PP values and simulated with JCFs ones.

## Chapter 4. Combining musculoskeletal models and finite element models

an exception made when considering the whole foot in HSs. In the GRF simulation a statistically significant difference in the estimated X position has been found in the forefoot of DNSs. Same consideration applies for the Y coordinate with slight differences. In midstance the JFC simulations seem to have a higher error with respect to the GRF simulations in particular in the X coordinate. The results of the comparison of the GRFs and of the JCFs between the two groups was made and is reported in 4.5. The Kruskal Wallis test was used to determine statistically significant differences between the groups (Matlab v.2013b). The values are expressed as a percentage of the Body Weight (BW).

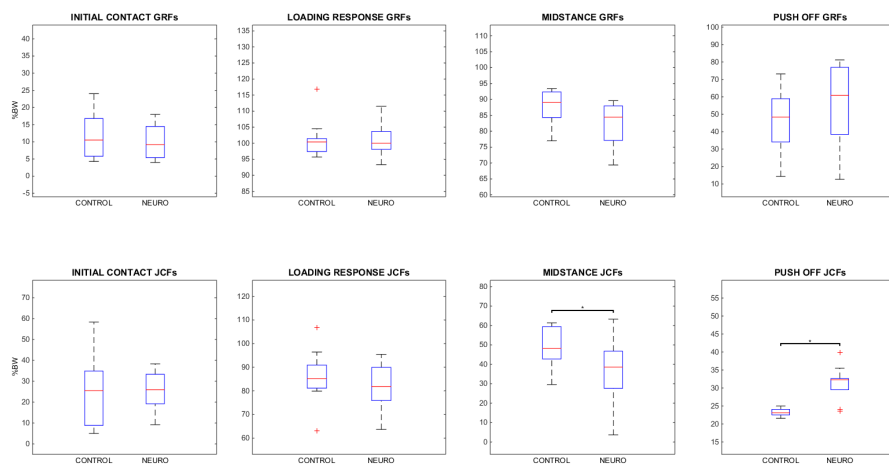


Figure 4.5 – Comparison of the GRFs (top) and of the JCFs (bottom) used as boundary conditions for the FE simulations of the neuropathic and the control subjects in the different instants of the stance phase of the gait cycle expressed in percentage of the body weight. All the values are expressed in percentage of the BW. Kruskal Wallis, \*  $p < 0.05$ .

## 4.1. Foot finite element models and joint reaction forces

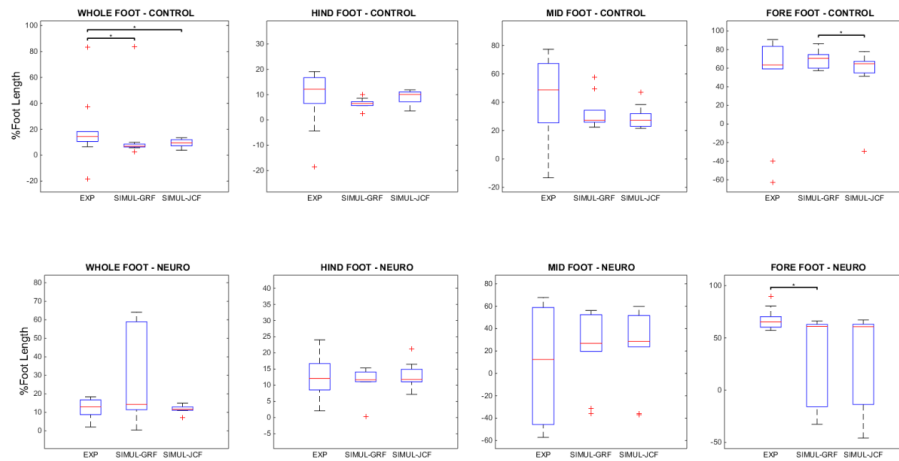


Figure 4.6 – Healthy (top) and Neuropathic (bottom) subject's X coordinate of the peaks of pressure position expressed in percentage of the foot length. Comparison between experimental values (EXP), values of the simulation with the GRF (SIMUL-GRF) and values of the simulations with the joint reaction forces (SIMUL-JCF) in the different subareas of the foot in the Loading Response. Kruskal Wallis, \*  $p < 0.05$ .

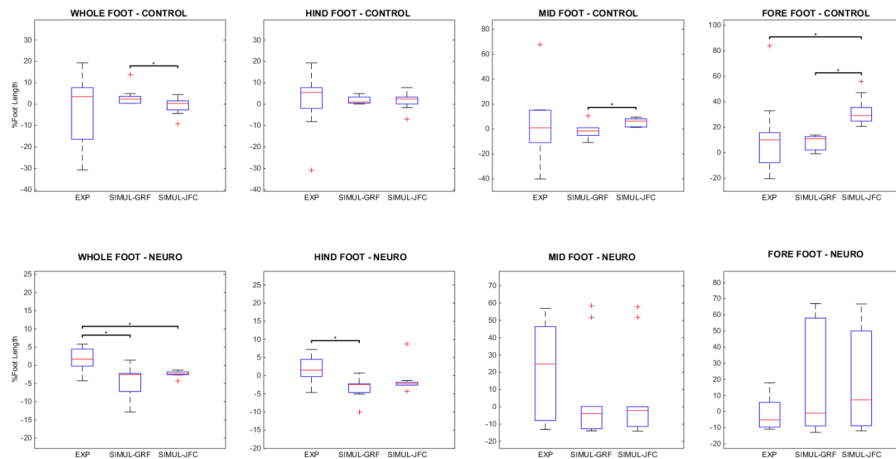


Figure 4.7 – Healthy (top) and Neuropathic (bottom) subject's Y coordinate of the peak of pressure expressed in percentage of the foot length. Comparison between experimental values (EXP), values of the simulation with the GRF (SIMUL-GRF) and values of the simulations with the joint reaction forces (SIMUL-JCF) in the different subareas of the foot in the Loading Response. Kruskal Wallis, \*  $p < 0.05$ .

**Chapter 4. Combining musculoskeletal models and finite element models**

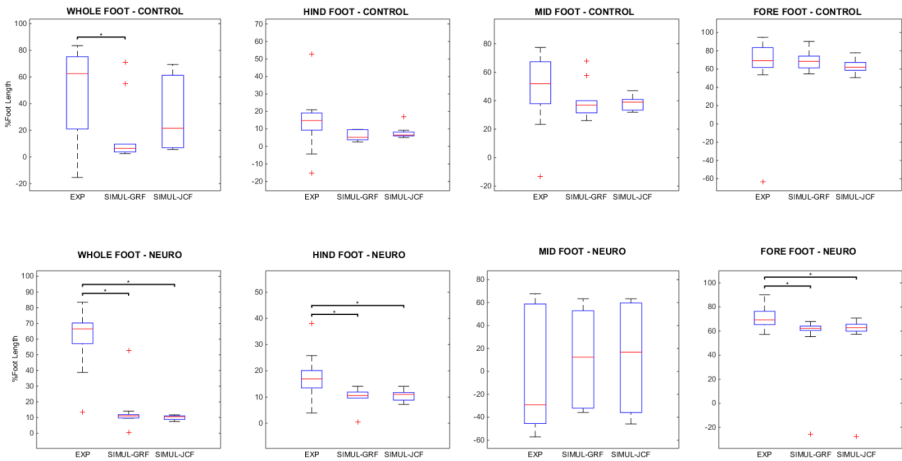


Figure 4.8 – Healthy (top) and Neuropathic (bottom) subject’s X coordinate of the peaks of pressure expressed in percentage of the foot length. Comparison between experimental values (EXP), values of the simulation with the GRF (SIMUL-GRF) and values of the simulations with the joint reaction forces (SIMUL-JCF) in the different subarea of the foot in the Midstance. Kruskal Wallis, \* p<0.05.

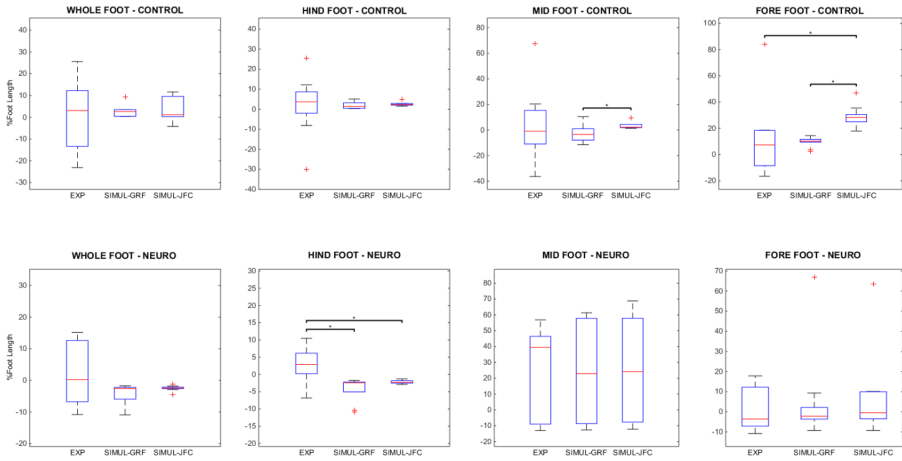


Figure 4.9 – Healthy (top) and Neuropathic (bottom) subject’s Y coordinate of the peaks of pressure expressed in percentage of the foot length. Comparison between experimental values (EXP), values of the simulation with the GRF (SIMUL-GRF) and values of the simulations with the joint reaction forces (SIMUL-JCF) in the different subarea of the foot in the Midstance. Kruskal Wallis, \* p<0.05.

### 4.1.4 Discussion

The novelty of this study is represented by the integration of different methodologies namely MS modeling, FE analysis and gait analysis, for the development of both healthy and diabetic subjects' foot FEM. Two 3D anatomical FE models of both a HS1's foot and a DNS1's one, based on MRI, were previously developed and validated by our group ([78]). In order to customize the results of the simulations, these models were driven by the kinematic-kinetic data of the subjects whose underwent the MRI acquired during gait. In this study JCFs calculated by means of MSMs were used to drive FE simulations by either subject-specific (case A) or group (case B) data. The validation of the procedure was done by comparing the experimental PP recorded with pressure platforms and the PP obtained with the simulations, in agreement with the state of the art of foot FE analysis ([172], [54], [39], [77]). The value of the peak of pressure and its position was considered as well as the dimension of the contact area. Improvements obtained with the methodology proposed herein were verified through comparison between GRFs and JFCs simulation results. Computational modeling and simulations of the musculoskeletal system enable researchers to study the complex dynamics of the human motion which is not experimentally recordable, but the lack of verification standards limits their adoption and use ([173]). The validation process is thus a very important issue and has to be carried out to assess the reliability of a model. In this work, for each subject, model predictions of contact PP were within the range of the experimental platform measurements for the same subject. In the 3DHSM the simulated peak values for the whole foot in midstance (90.9 KPa for the GRFs simulations and 90 KPa for the JCFs ones) were consistent with values reported in literature (131 KPa) (PJ Antunes, 2008) when considering the different weight of the subject. In the 3DHSM the simulated peak values for the whole foot in midstance (277.323 KPa) for the GRF simulations and 299.570 KPa for the JCFs ones) showed a good agreement with the work of Actis et al. [49] (279 KPa) and Fernandez et al. (240 KPa) ([77]). Several studies ([183], [184], [126], [185]) highlighted the influence of the foot morphology on foot function in terms of kinematics, kinetics and plantar pressure distribution. Furthermore, in computational modeling, the importance of patient-specific geometries together with subject-specific boundary conditions has been emphasized [77]. This is confirmed by the fact that the average errors in the estimation of the PP are lower in the subject-specific case A than in type-specific case B and it can also explain the errors in the determination of the contact surface area. However MRI acquisitions are expensive and the process of segmenting them in order to obtain the mesh is computationally expensive too. Keeping in mind that foot geometry may change notably between healthy and pathological conditions, group data simulations ran using the two models previously validated can be useful to quantify the errors that this assumption implies. While interpreting the results it

## Chapter 4. Combining musculoskeletal models and finite element models

---

should be considered that a number of simplifications have been applied during the development of the foot models and of the MSMs. To calculate the JCFs, an inverse dynamic approach was used which solved a different optimization problem at each instant of movement. The validity of the results depends on the accuracy of the data recorded during the gait data collection, namely the position of the markers placed on the subjects, and errors associated with skin artifact in stereophotogrammetry which cannot be neglected [186]. A wrong calculation of net joint torques and forces is thus possible given the difficulty in accurately estimating velocity and accelerations from position measurements [187]. However in this study a standard approach, already validated in literature, was used [28]. It has been reported that DNSs and HSs show differences in the biomechanics of walking ([125], [132], [116]). According to this, also JCFs in midstance and push off have shown a significant difference between HSs and DNSs. Muscle forces have a really predominant role in the different steps of the gait cycle and the complex relationship among muscular control, internal joint movement, and plantar loading transfer needs to be considered [54]. Models developed including the muscle forces and ankle joint loads have already been published and show good results but they only adapted values reported in literature and so they were not completely subject-specific [188]. Their absence in our models, together with the fact that also plantar ligaments and fascia were inserted only as straight node-to-node link elements with no cross-sectional areas, may explain the discrepancy in the simulated and experimental positions of the peak of pressure. The prediction of the position of the peak of pressure would be very helpful in preventing the occurrence and recurrence of foot ulceration in diabetic subject allowing for the prescription of better footwear and orthotic devices which can provide a different pressure distribution. FE models may also be adopted to study the mechanical interaction between the foot and the insole [189] allowing to test the effects of a change of insole shape, thickness or material stiffness. In this study the ability of locating the peak of pressure was tested and the error in the estimation can be attributed to the non subject specific geometries as well as to the further simplification that the use of another model in the pipeline implies. However the results seem to indicate the possibility of locating the position of the peak of pressure. At the present state these models may have a significant impact in providing a basic but useful tool in studying the influence of therapeutic interventions that adopt plantar support for stress redistribution. In conclusion despite the limitations and the approximations, the workflow adopted herein to connect FE simulations and MSMs can be considered satisfactory and could be further explored with the insertion of subject specific muscle forces in the developed FEMs. The data obtainable with gait analysis experiments provide a quantitative description of kinetic and kinematic of the body-segment motion but they are not able to explain how the muscles work together to produce a determined movement



[190]. On the contrary MSMs can provide an estimation of the muscle forces during different kinds of motion. In the context of diabetes these models may become a useful tool for subject specific therapeutic solutions and interventions.

## 4.2 Acknowledgments

I would like to thank Gabriella Guarneri and Angelo Avogaro for providing the diabetic subjects, and Imago Ortesi (Piacenza) for providing the plantar pressure systems. Furthermore a special thanks goes to Prof. Ilse Jonkers and to Wouter Aerts from the *Human Movement Biomechanics Research Group* of the *Department of Kinesiology* of the *Katholieke Universiteit Leuven*, who collaborated with me in the development of this project.

### 4.3 Foot finite element models and muscle forces

*After evaluating the impact of applying the foot JCFs obtained from musculoskeletal modeling as boundary condition on the foot FEM simulations, the use of muscles forces was evaluated. Subject-specific integrated and synchronized kinematic-kinetic data acquired during gait analysis were again used for the development of the MSMs and for the computation of the muscle forces of two subjects, a healthy and a diabetic one. Muscle insertions were located in the MRI of the subject (used as well for the geometries of the FEM) and correspondent connectors were created in the FE model. FE subject-specific simulations were subsequently run with Abaqus by conducting a quasi-static analysis on 4 gait cycle phases and adopting 2 conditions: one including the muscle forces and one without. Once again the validation of the FE simulations was done by means of a comparison between simulated and experimentally measured plantar pressures. Results showed a marked improvement in the estimation of the peak pressure for the model that included the muscles. In particular the simulations with the healthy model showed an error (expressed in percentage of the experimental value) on the estimation of the peak of pressure as small as 4% in loading response, while in the diabetic model simulations the smallest error was of 9% in push off.*

#### 4.3.1 Background & Aims

Diabetic foot may lead to plantar ulcers: their etiology has been investigated with different techniques (See section 3.4). Gait analysis allows kinematics and kinetics estimation during walking while FE modeling enables computing internal stresses and strains acting on the foot. Furthermore MSMs can provide an estimation of muscle forces (see Section 1.1). The aim of this study was to improve a previously developed FE model [78] adding muscle forces obtained with OpenSim as boundary condition for the prevention of foot ulcers.

#### 4.3.2 Material & Methods

An informed consent was signed for the participation to the study by a DNS (age 71, BMI  $37 \text{ kg/m}^2$ ) and a HS (age 31, BMI  $20.15 \text{ kg/m}^2$ ). DNS underwent a clinical examination which is reported in Table 4.3 and 4.4.

### 4.3. Foot finite element models and muscle forces

Table 4.3 – Clinical data of the DNS

<b>Sex</b>	Male
<b>Age [years]</b>	71
<b>BMI [kg/m<sup>2</sup>]</b>	37
<b>Shoe Size [EU]</b>	43
<b>Phenotype</b>	Normal
<b>BP humeral</b>	160/80
<b>Neuropathy</b>	Yes
<b>Autonomic Neuropathy</b>	Instrumental signs not clear
<b>Vasculopathy</b>	Peripheral
<b>Disease Duration [years]</b>	16
<b>Type of diabetes (1 or 2)</b>	2
<b>Glicata (HbA1c)</b>	8.6
<b>Pelvic simmetry</b>	Normal
<b>Shoulder-girdle simmetry</b>	L: swing
<b>Lower limb length [cm]</b>	Left leg >1.2
<b>Pelvic structure</b>	L: translates, R: rotates
<b>Hip joint mobility</b>	Normal
<b>Right and left knee position</b>	Normal

Table 4.4 – Podiatric examination of the DNS

<b>Podiatric examination</b>	<b>Right foot</b>	<b>Left foot</b>
<b>Foot type</b>	Roman	Roman
<b>Podological type</b>	Cavus	Cavus
<b>Heel (varus, valgus)</b>	Valgus	Valgus
<b>Hallux (valgus, rigid)</b>	Normal	Normal
<b>Overlapping fingers</b>	Normal	Normal
<b>Hammertoes</b>	Normal	Normal
<b>Claw toes</b>	2°- 3°- 4° toe	2°- 3°- 4° toe
<b>V finger (normal, adduct)</b>	Normal	Normal
<b>Plantar evaluation</b>	Scarring and calluses under the Metatarsal heads	Scarring and calluses under the Metatarsal heads

### 4.3.2.1 Gait analysis

The experimental setup consisted of a 6 cameras BTS stereophotogrammetric system, synchronized with 2 Bertec force plates and 2 plantar pressure systems (Imagortesi) (Figure 1.8). Gait analysis was then carried out as in Sawacha et al. [83] and Del Din et al. [84], by applying two different marker protocols previously described, a FullBody protocol and a Foot protocol (see Section 1.5.4). The first one was useful both for the OpenSim scaling and for the determination of the points of insertion of the muscles, the second one for the determination of the position of the model of the foot with respect to the ground.

### 4.3.2.2 Musculoskeletal models (Section 1.1.2)

Experimentally measured body mass and position of markers placed on Anatomical Landmarks (ALs) during a static trial, were used to scale a generic musculoskeletal model with 10 rigid bodies, 23 degrees of freedom and 92 musculotendon actuators. This in order to match subject's dimensions and inertial properties [31]. Scaled models were then used to generate and analyze walking simulations of each subject's trials in OpenSim (v.3.2) [28]. The following steps were performed: scaling, inverse kinematics and static optimization [28].

### 4.3.2.3 Finite Element Models

HS and DNS right foot MRI were acquired with 1.5 T devices (Philips Achieva and Siemens Avanto, spacing between slides: 0.6–0.7 mm and slice thickness: 1.2–1.5 mm, sequence 3D mFFE and T2 3D MEDIC, TE/TR 9/33 and 14/32). The right feet under analysis were not subjected to any loading condition during acquisition. An angle between foot and leg of 90° was maintained with the help of pillows on the sides of the limb. The grey-scale-images were then segmented using the software Simpleware-ScanIP (v.5.0) to obtain the geometries of 30 bones and of the skin as contour of the homogenous mass of foot soft-tissues [78]. The DNS model (DNSM) was developed as in [78] while the HS one (HSM) was the one already developed in that work. According to the procedure followed in [78], the most used tools for the segmentation were the Threshold, to define thresholds of gray which represented the structures of interest, the Paint, to manually select the relevant pixel and the FloodFill to choose an entire area first defined with the Paint. Before meshing the model, basic filters were applied on the masks representing bones and the skin. The tool Smoothing - Recursive Gaussian, which applies a Gaussian Filter, was used to make the volumes contours smoother while Morphological Filters were used to adjust

### 4.3. Foot finite element models and muscle forces

the size of the volumes. Once all the masks were obtained, a simplification was done according to what already published in literature [78]. In particular some of the masks were grouped together:

- the Phalanges of each toes together with its cartilage;
- the Sesamoid bones with the first Metatarsals head;
- the Metatarsal and Sesamoid bones to define the forefoot;
- the Navicular, Cuboid and Cuneiform to define the midfoot;
- the Astragalus and the Calcaneus to constitute the hindfoot.

The Phalanges were kept separated from the Metatarsals to allow the dorsiflexion during the push-off phase of the gait cycle. The space between the bones was segmented with cartilage. The mesh was thus generated from the bitmapped data with the Simpleware- ScanFE module. Tetrahedral elements were obtained. In the most critical areas a densification was allowed (Figure 4.10).

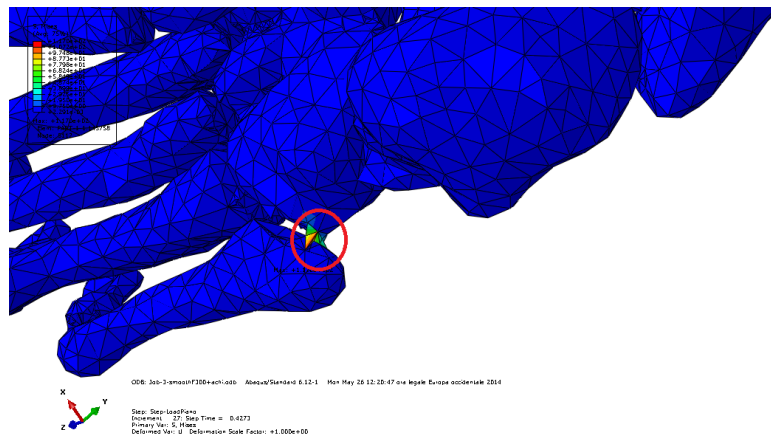


Figure 4.10 – DNS' foot FEM: example of a critical area.

These settings have led to a mesh of 34800 elements for the HSM and 63309 elements for the DNSM in accordance with the literature [182], [54]. The geometries were then imported in Abaqus where the FEMs were created as in [78]. The force platform was reconstructed by drawing a rectangle with the correspondent size: 384x384x20 mm. Material properties were assigned for each element, values where obtained from the literature as in [78]. Muscle insertions previously located in the MRI were inserted in both the FE models by creating the correspondent connectors. In order to give more stability to the model of the foot, Tibialis Anterior, Tibialis Posterior, Peroneus

## Chapter 4. Combining musculoskeletal models and finite element models

brevis, Peroneus Longus, Medial and Lateral Gastrocnemius, Soleus, Toes and Hallux Extensors were added, together with some ligaments (calcaneo-navicular, long plantar and calcaneo-cuboid) and the plantar fascia (Figure 4.11).

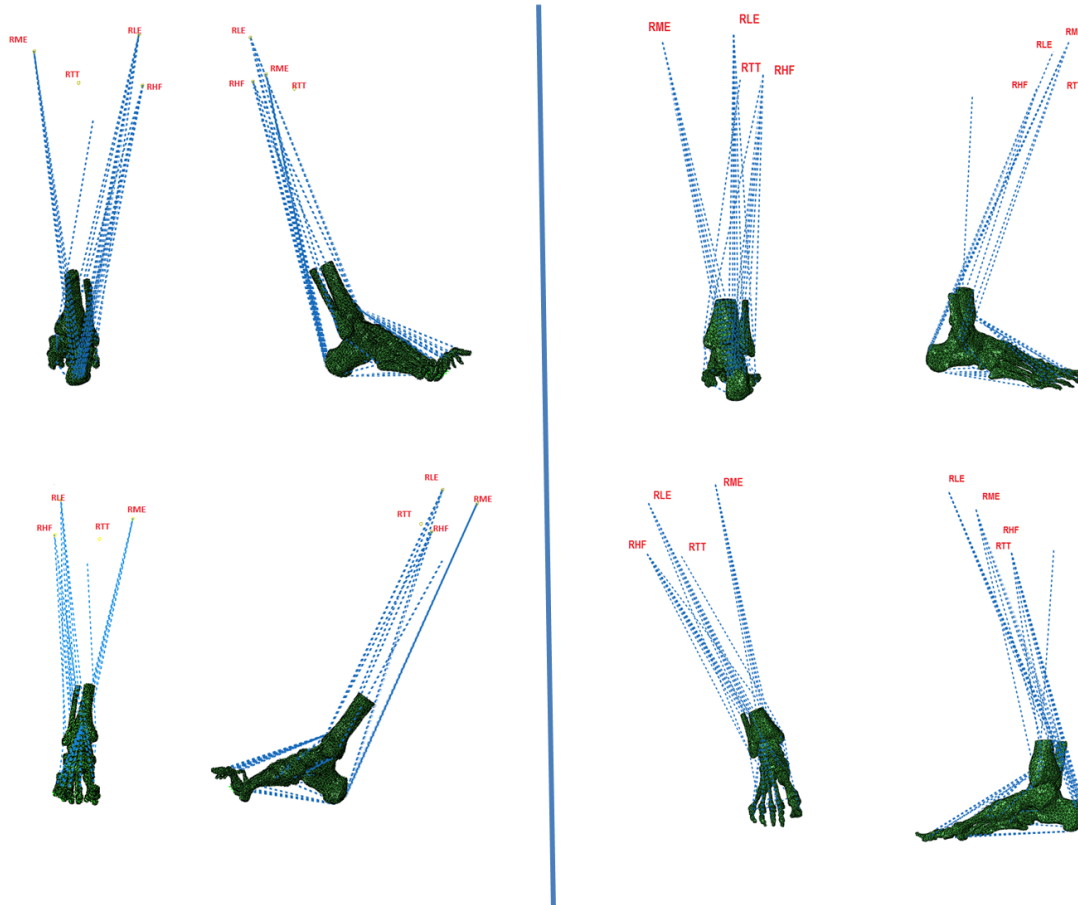


Figure 4.11 – On the left the DNSM: frontal, posterior and lateral views. On the right the HSM: frontal posterior and lateral views.

The identification of the point of insertion of the muscles was determined in the MRI by using two anatomical atlases ([191], [192]) as a reference (Appendix A).

In Abaqus, muscles and ligaments were represented using disjunct and concatenated connectors. Muscles such as the Soleus and Gastrocnemius fit into the heel via the Achilles tendon, which is characterized by a large area of insertion. A connector in Abaqus can be inserted in only one vertex of an element and thus it cannot mimic by itself the properties of the Achilles tendon. The approach of Cheung et al. [193], who used five connectors to evenly spread the loads in the Calcaneus, was thus applied. The same was done for the plantar fascia. In order to correctly insert the above mentioned muscles in the foot and leg, the coordinates of the ALs placed on the patient's knee were needed. This information was available thanks to the gait eval-

### 4.3. Foot finite element models and muscle forces

---

uation done on the subject, after a transformation between reference systems. A local reference frame was indeed defined using the coordinates of RIIT, RMM and RLM (See section subsec:protocol) referred to the global reference frame of each environment: experimental of the gait laboratory, and computational of Abaqus and ScanIp. ALs in Abaqus and in ScanIp were identified miming the procedure of palpation usually performed on a patient. The position of muscle and tendon insertions and of the ALs, with respect to this new local frame defined, was then computed thus making it possible to identify the various points in all the systems. The computation was done with Matlab R2014b.

After the definition of the model, a quasi-static analysis was performed considering 4 instants of the gait cycle (in brackets the percentage of the cycle is reported):

- Initial contact (1% for the DNS, 1% for the HS)
- Loading response (31% for the DNS, 30% for the HS)
- Midstance (52% for the DNS, 50% for the HS)
- Push Off (93% for the DNS, 82% for the HS)

The position of the foot over the platform was determined using the coordinates of the foot ALs experimentally acquired with the procedure above explained (see also Section 1.5.4). At first the foot was placed on the platform miming its position in standing. Then at the beginning of each simulation, an initial rotation was applied in order to replicate each subject's foot position experimentally recorded during the different gait phases. Simulations were run for each phase of the stance in two different conditions:

- **C1**; applying muscle forces computed with OpenSim together with GRFs as in [194];
- **C2**; without muscle forces, applying only GRFs.

In the second case the connectors representing muscles and tendons were eliminated and, with them, all the forces associated. The load was thus only represented by the ground reaction force.

### 4.3.3 Results

#### 4.3.3.1 Pressures

Once the quasi-static analysis in the four phases previously indicated in both conditions C1 and C2 was performed, the simulated pressures were compared to the experimental ones considered as the gold standard. Figure 4.12 shown the distribution of the plantar pressure on the platform for the DNS subject, while Figure 4.13 shown the distribution of the plantar pressure on the platform for the HS subject.

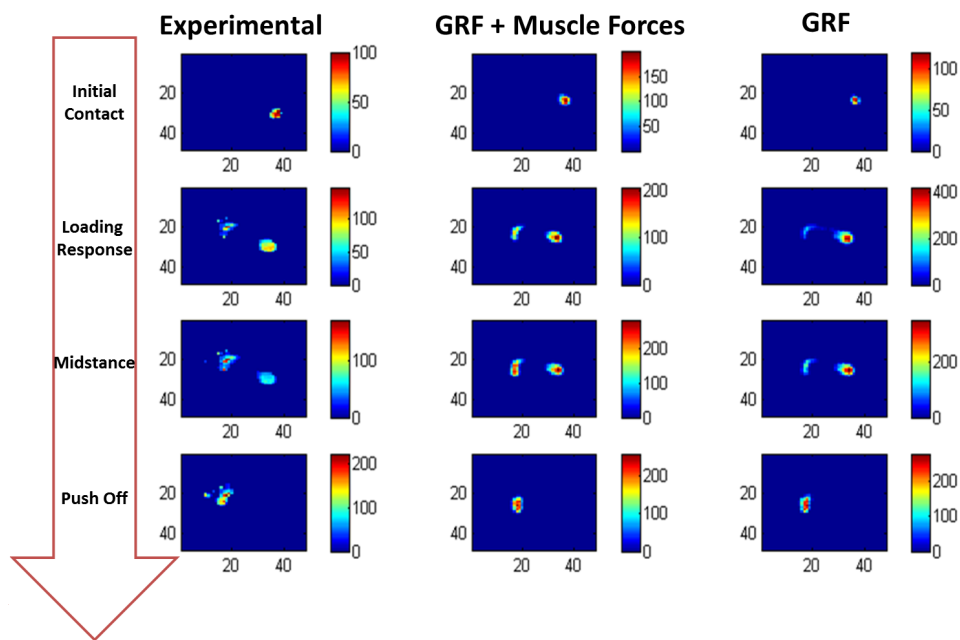


Figure 4.12 – The Figure shows the distribution of the DNS’ plantar pressure on the platform, experimentally and simulated in C1 and C2.

Figure 4.14 shows the values of maximum pressure [KPa] for both subjects, in each of the four phases of the gait cycle analyzed: experimental values, values of C1 and C2 simulations.

Figure 4.15 shows the error calculated as the difference between simulated and experimental peak of pressure values and expressed in percentage of the experimental ones for both the condition C1 and C2 for both subjects.

Figure 4.16 shows the contact surface of both subjects, in each of the four phases of the gait cycle analyzed: experimental values, values of C1 and C2 simulations.

Figure 4.17 shows the error calculated as the difference between simulated and exper-



### 4.3. Foot finite element models and muscle forces

#### WHOLE FOOT - Pressure

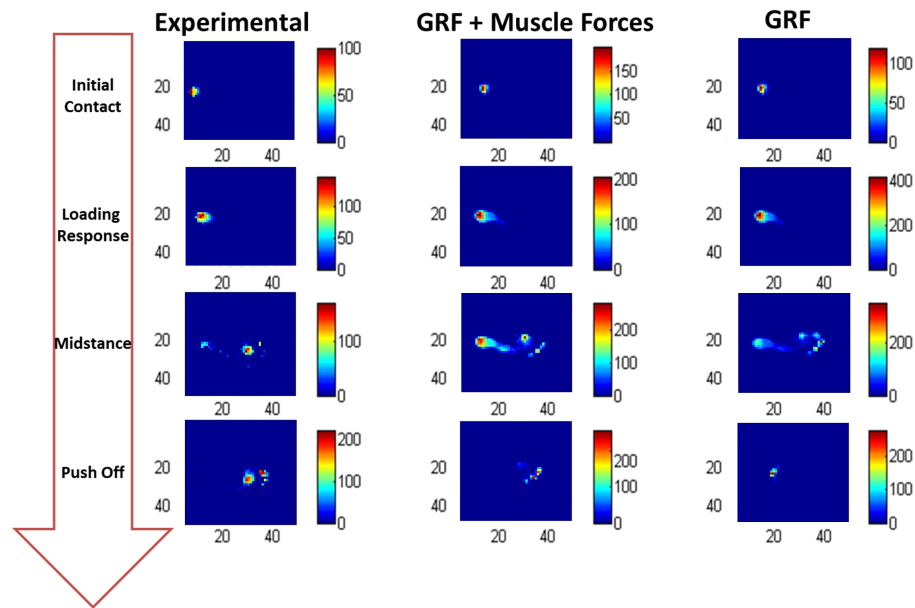


Figure 4.13 – The Figure shows the distribution of the HS’ plantar pressure on the platform, experimentally and simulated in C1 and C2.

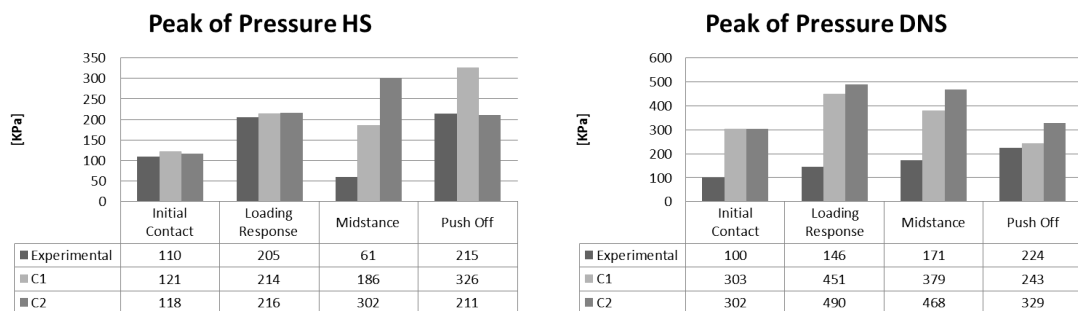


Figure 4.14 – On the left, the peak of pressure of the HS, experimental and simulated in C1 and C2. On the right, the peak of pressure of the DNS, experimental and simulated in C1 and C2.

## Chapter 4. Combining musculoskeletal models and finite element models

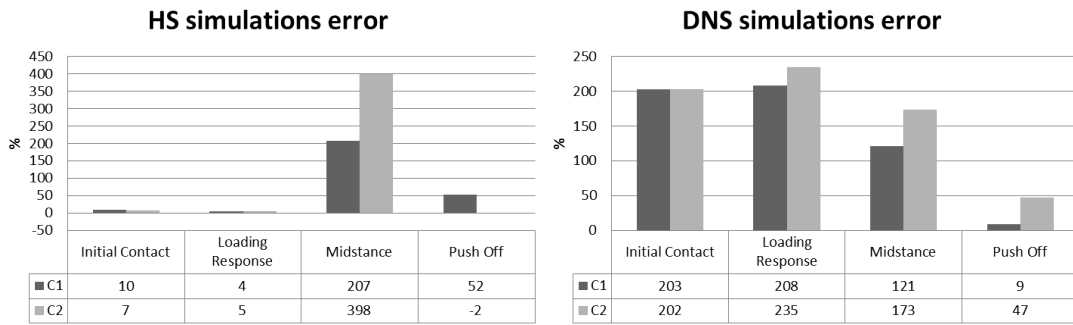


Figure 4.15 – On the left, the error calculated as the difference between simulated and experimental peak of pressure values and expressed in percentage of the experimental ones for both the condition C1 and C2 and for the HS. On the right, the error calculated as the difference between simulated and experimental peak of pressure values and expressed in percentage of the experimental ones for both the condition C1 and C2, and for the DNS.

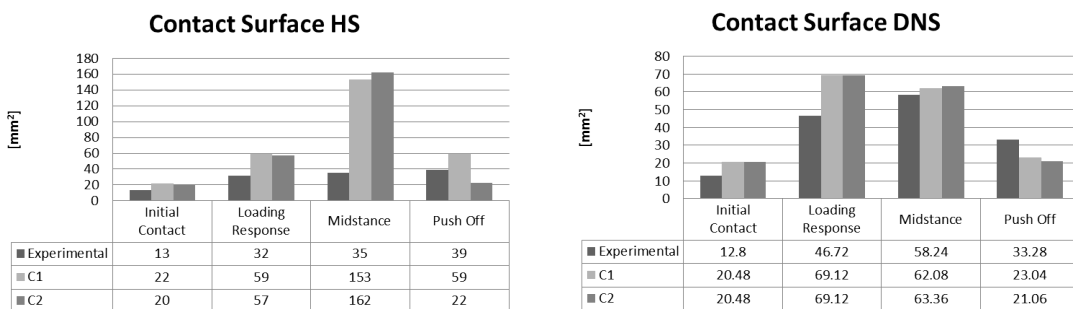


Figure 4.16 – On the left, the HS' contact surface experimentally acquired and in both the condition C1 and C2, for all the phases simulated, is reported. On the right, the DNS' contact surface experimentally acquired and in both the condition C1 and C2, for all the phases simulated, is reported.

### 4.3. Foot finite element models and muscle forces

imental contact surface values and expressed in percentage of the experimental ones for both the condition C1 and C2 for both subjects.

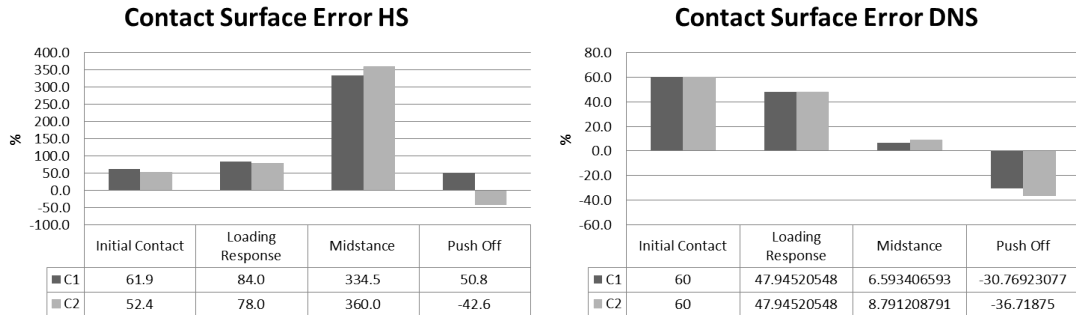


Figure 4.17 – On the left, the error calculated as the difference between simulated and experimental contact surface and expressed in percentage of the experimental ones for both the condition C1 and C2 and for the HS. On the right, the error calculated as the difference between simulated and experimental contact surface and expressed in percentage of the experimental ones for both the condition C1 and C2, and for the DNS.

#### 4.3.3.2 Internal Stresses

As attested before (see Section 1.2), FE analysis provides also information about the overall deformation and about stress and strain distributions of the structure under analysis. Von Mises stress, a parameter related to the strength of biological tissues of bone and plantar soft-tissue [54], was used to express the peak stress level calculated in the internal structure of the foot. The stress distribution is shown in Figure 4.18 for the DNS model and in Figure 4.19 for the HS, in both C1 and C2. The peak values relative to each simulated instant and for both the HSM and the DNSM were reported in Figure 4.18. Also a comparison between the two populations was made (see Figure 4.18).

In correspondence of the bone structure, peaks of stress were present at the Phalanges, Metatarsal and talus bones. The insertion points of the muscles at the Phalanges connection region experienced large stress.

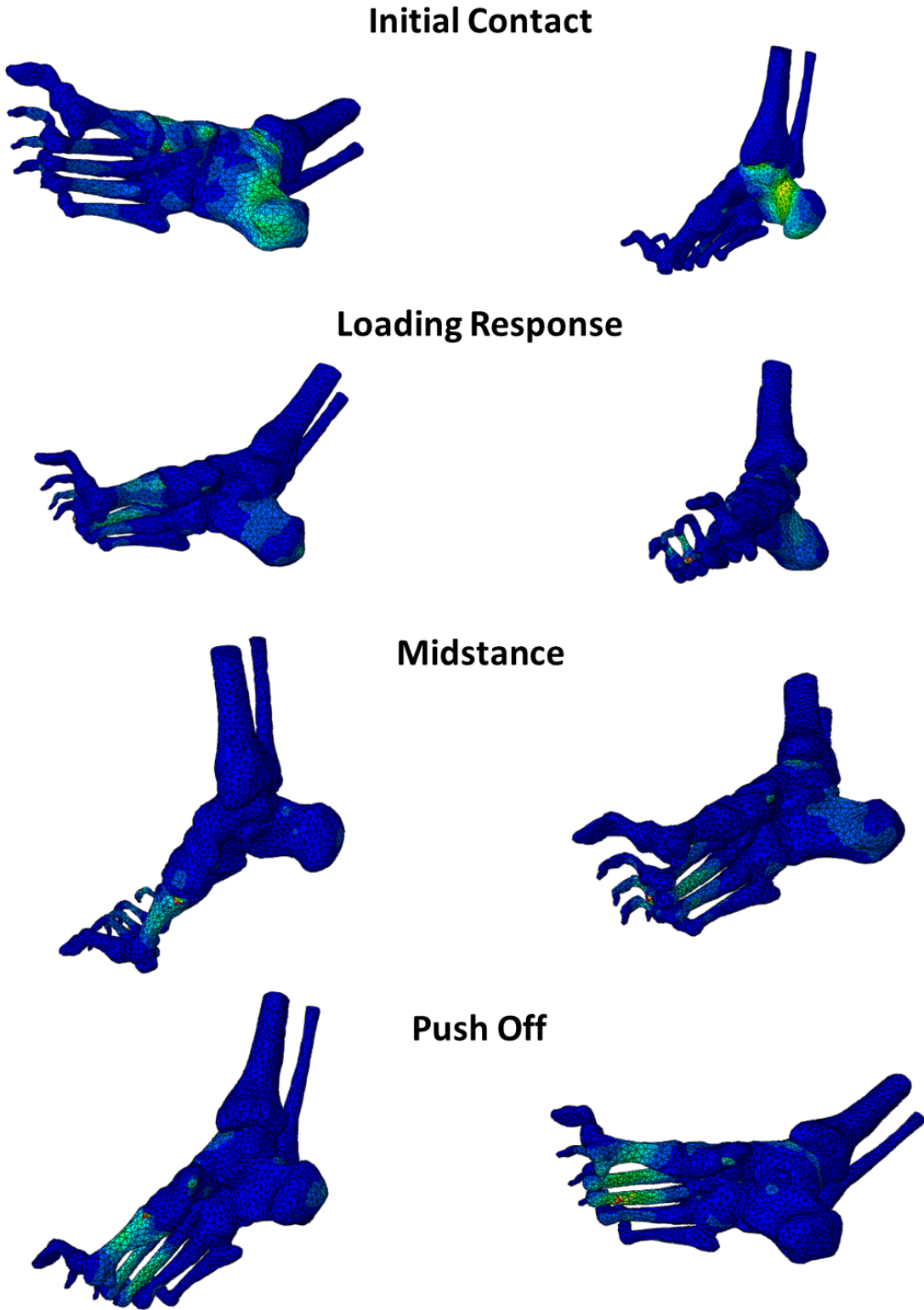


Figure 4.18 – The Figure shows the Von Mises stresses in the DNS’ bones during the different phases simulated. From the top to the bottom (INITIAL CONTACT, LOADING RESPONSE, MIDSTANCE and PUSH OFF). On the left column, results of C1 and on the right results of C2.

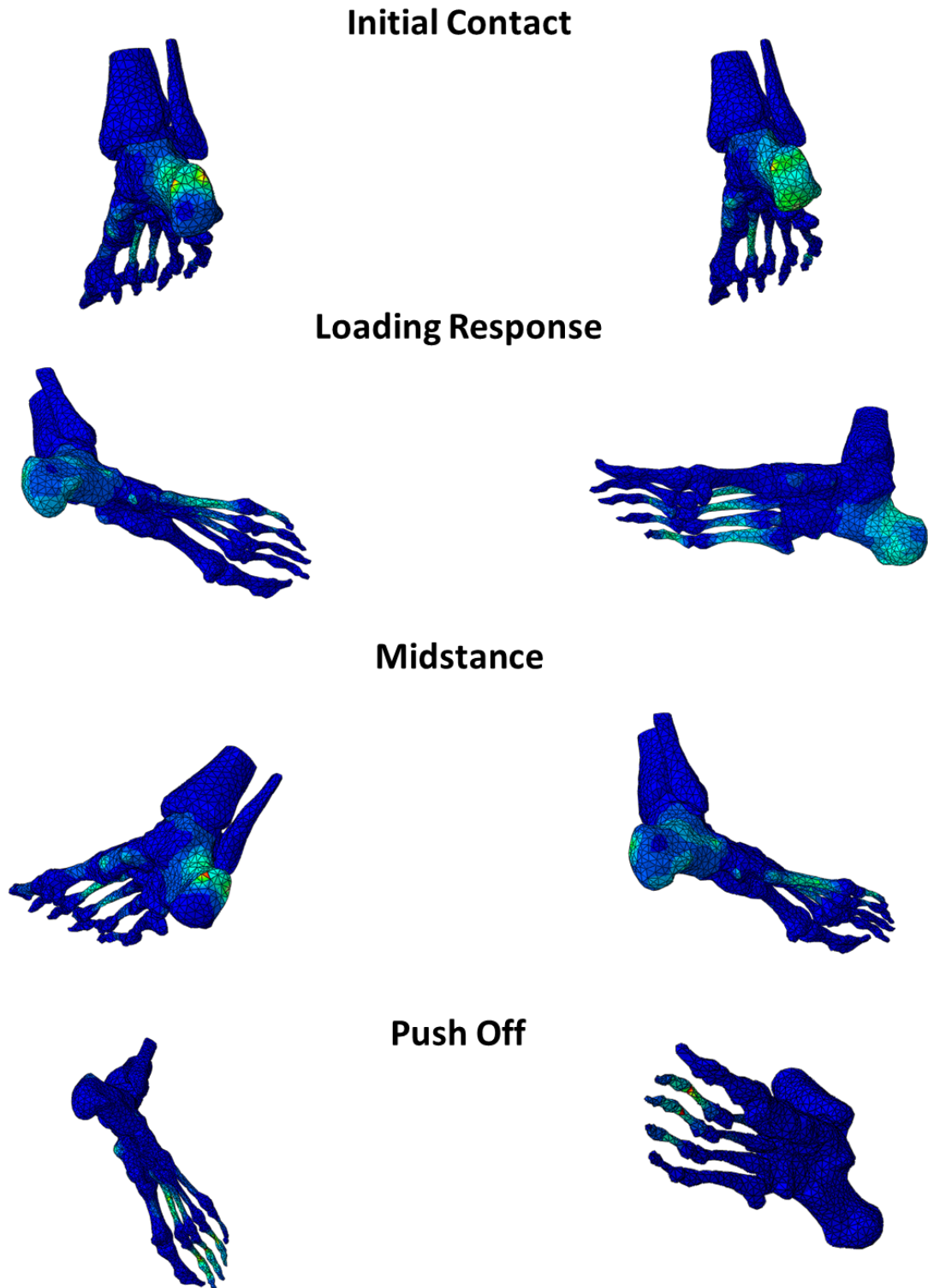


Figure 4.19 – The Figure shows the Von Mises stresses in the HS' bones during the different phases simulated. From the top to the bottom (INITIAL CONTACT, LOADING RESPONSE, MIDSTANCE and PUSH OFF). On the left column, results of C1 and on the right results of C2.

**Chapter 4. Combining musculoskeletal models and finite element models**

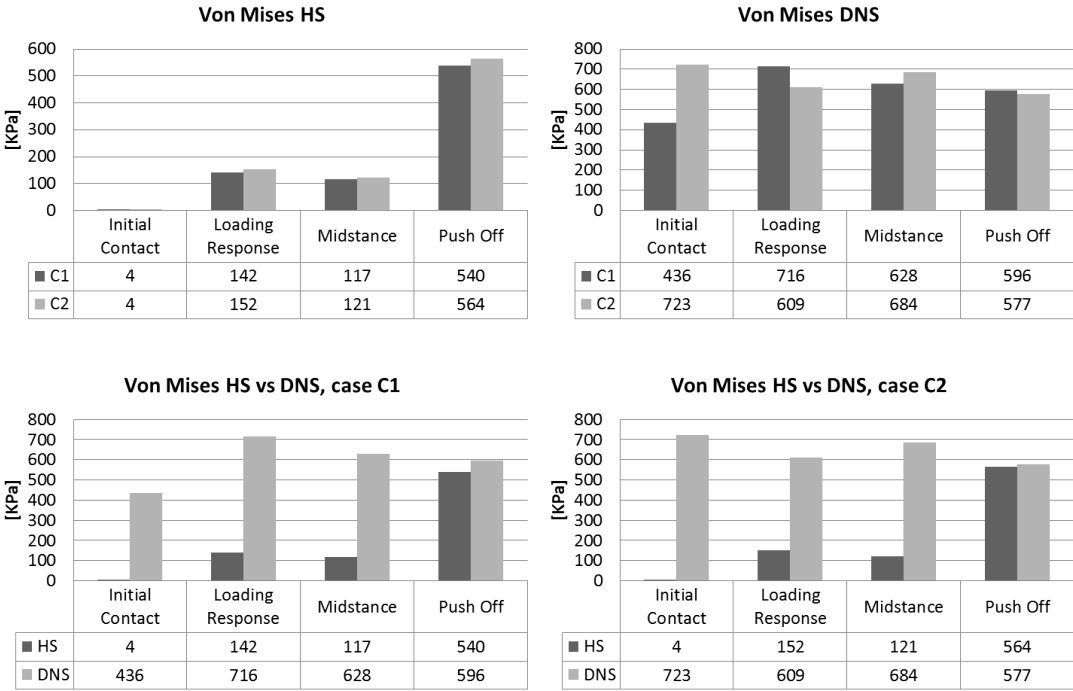


Figure 4.20 – The Figure shows the Von Mises stresses values in the DNS’ and HS’ bones during the different phases simulated and in the two conditions.

#### 4.3.4 Discussion

The work herein presented fits into the state of the art of the foot FE simulations. Image segmentation, mesh generation and the definition of the boundary conditions starting from the kinematics of the bones and the GRFS, was done according to the work of Guiotto et al. [78]. In addition to the original project, two important things were done:

- points of muscle insertion were identified in the MRI, starting from subject specific data and then exported in the FE model by means of transformation between reference systems;
- the presence of muscles, and relative subject-specific muscle forces obtained through musculoskeletal modeling in OpenSim, was taken into account.

The latter allows analyzing not only the contribution of the GRFs in the distribution of internal forces of the tissues, but also of the subject specific muscular strength. This evaluation would not have been possible without the application of an interdisciplinary approach that uses experimental data (kinematic and dynamic boundary conditions), data obtained through musculoskeletal modeling (muscle forces), and data extracted from the analysis of biomedical images (segmentation), for a FE analysis of the biomechanics of the foot. This approach was successfully pursued also by Philips et al. [194], who in 2007 published a study on the FE modeling of the pelvis including muscular and ligamentous boundary conditions computed with MSMs. An important aspect of the modeling approach lied on the possibility of comparing simulation results obtained with the FE analysis, with the experimental pressures collected during the gait evaluation. The validation of the model was indeed based on a comparison between the simulated peak of pressure and the experimental one [54], [41], [77] adding, as an element of innovation, the use of a subject specific gold standard as in Guiotto et al. [78]. The results obtained in this study can be compared to the results of Antunes et al. [43] who estimated a maximum pressure of 111 KPa in the heel, with a static test of balance. These pressures can be deemed to be comparable with those obtained in the model with muscles in midstance for the HS (186 KPa). The difference of intensity of the DNS subject (379KPa in C1 and 468 KPa in C2) may be due to the fact that the simulations were run in a quasi-static situation and that the weight of the patient was totally bore on one foot. Furthermore the DNS considered in this study, weighted 40kg more than the one reported in Antunes et al. [43]. The same applies to Chen WM et al. who found a peak pressure of 130.6 KPa [54], and to the values estimated by Chen WP et al. [68]. Furthermore in this work, as in the works mentioned above, the peak of pressure were always overestimated

## Chapter 4. Combining musculoskeletal models and finite element models

---

compared to experimental data. This should be considered as a good point given that it avoids the risk of under estimations of the peak of pressures. The improvement of the model with an inclusion of muscle forces in the boundary conditions was already reported in the study of Chen et al. who had shown that muscles, such as Soleus and Gastrocnemius, were crucial for an appropriate estimation of the peaks of pressure [75]. A clear improvement of the simulations that considered the muscular component has been demonstrated, thus highlighting the important role of the muscles at the modeling stage. In particular HS simulations showed a minor errors with respect to the DNS ones (less than 10% in initial contact and loading response), in all the phases except the midstance where the discrepancy was still really high. In the DNS' simulations, the push off phase gave the better results (error of only 8% in C1). These considerations should be integrated with the evaluations of the contact surface. For the HS' the larger error was again in the midstance where it was comparable to the one of DNS'. Furthermore FE analysis allows the evaluation of the internal stresses and strains. Von Mises stress predictions of the HSM at midstance were for the two conditions C1 and C2, respectively of 117KPa and 120KPa, while for the DNS ones they were 628KPa and 684KPa. The values of the DNS were comparable with the results of Gefen et al. (300-600 KPa in the heel pad) [180]. The bigger magnitude confirms the experimental studies that report higher internal stress and strains in the feet of diabetic people (see Section 2.6.4).

Anyway the difference between the experimental and the simulated pressures in some cases is still high. This can be due to different reason:

- material properties were taken from literature and were not subject specific. This is of paramount importance in the description of the diabetic tissues. A uniform soft tissue mass was indeed used to represent all foot structures except for bones and joint cartilage which were described as elastic materials. Considering all the changes due to the PVD (see Section 2.6.3), a more adequate integration of the internal structures of the plantar soft tissue, such as a formulation which includes the micro- and macro-chambers layers [195] or the skin [196] might be helpful to highlight interactions among different levels and should be considered as a future development. A two phase model was already successfully used in a 2D model of the plantar tissue [197] and its use could be extended in the 3D one.
- the fidelity of the model is highly depending on the number of degrees of freedom and a limitation of this study was the simplifications done grouping the bones in the forefoot, midfoot and hindfoot and the consideration of only the major joints. Typically when the focus is on the evaluation of the center of pressure and of the GRF, bones of the foot are grouped together into a rigid



### 4.3. Foot finite element models and muscle forces

---

body. This was done also in the current models, as in ([78], [51],[33]). The motion of the 30 bones of the foot was captured with motion analysis. However it should be considered that the stereophotogrammetric procedure is affected by errors associated with skin artifact ([186], [198]) and it is not able to capture the movement of individual foot bones. Several studies tried to overcome this problem, both with fluoroscopy ([199], [200], [201]) or with intracortical pins ([202], [203]).

- muscles represented in MSMs are a simplified version of the real ones also in the point of attachment, and this affect the muscle forces prediction [204]. In the future a sensitivity analysis on the individuation of the point of insertions of the muscles should be performed, together with an evaluation of the influence of their misplacement.
- the estimation of muscle forces was done by applying the static optimization. This techniques doesn't allow constraining the computation by considering the muscle activation experimentally recorded with superficial EMG. A study could thus be done to see the effect of using another approach like the CMC (see Section 1.1.2) in the muscle forces values and in the results of the FE simulations.
- muscles forces have been implemented as connectors in the FEM without taking into account the direction of application of the force. This can limit the degree of accuracy of the prediction and it will be object of future development. However, the same procedure was already applied in literature [194].

In conclusion, improvements will be made on different aspects as stated above: estimation of muscles insertions location and muscle forces, number of degrees of freedom of the model. The population under analysis will also be increased with more DNS and HS. This should be done in order to take into account also the effect of the foot shape in the results of the FE simulations which has demonstrated to play a significant role in the diabetic foot disease [83], [115] . Overall the study showed promising results, which are encouraging for the next steps towards the definition of a more complete model of the human foot.



## 5 Towards the definition of a parametric foot finite element model

*There have been many recent developments in patient-specific models with their potential to provide more information on the human pathophysiology and the increase in computational power. However they are not yet successfully applied in a clinical setting. One of the main challenges is the time required for mesh creation, which is difficult to automate. The development of parametric models by means of the Principle Component Analysis (PCA) represents an appealing solution. In this study PCA has been applied to the feet of a small cohort of diabetic and healthy subjects, in order to evaluate the possibility of developing parametric foot models, and to use them to identify variations and similarities between the two populations. Both the skin and the first metatarsal bones have been examined. Besides the reduced sample of subjects considered in the analysis, results demonstrated that the method adopted herein constitutes a first step towards the realization of a parametric foot models for biomechanical analysis. Furthermore the study showed that the methodology can successfully describe features in the foot, and evaluate differences in the shape of healthy and diabetic subjects.*

### 5.1 Background & Aims

Recently the development of Patient-specific models (PSMs) tailored to patient-specific data, has gained increasing attention in clinical applications ([205],[206],[207],[208]). PSMs could represent a solution to the growing awareness of personalized medicine [209]. PSMs have the potential of improving diagnosis and optimizing clinical treatments by predicting and comparing the outcomes of different approaches of intervention. Furthermore, they can provide information that cannot be directly measured, such as muscle forces, internal stresses, and strains of the bones. Given the considerable amount of diseases affecting motor ability, PSMs of the lower limbs have been broadly addressed in the literature [210]. One of the most popular techniques is the

## Chapter 5. Towards the definition of a parametric foot finite element model

---

finite element (FE) analysis due to its flexibility and adaptability to model biological geometries and materials, and to simulate complicated boundary and loading conditions. FE modeling constitutes a useful tool to provide an insight of the internal behavior of the human body. However, despite the increasing attention, FE modeling has not yet been successfully integrated into clinical practice [206]. One challenge for the development of FE models is the time required to generate personal-specific models, which often involve the segmentation of MRI or CT images. In addition, this process requires high levels of user intervention due to the complexity of the human anatomy. The excessive effort and time required to generate 3D FE models has motivated the development of more effective mesh generation techniques based on reconstructed image data [211]. This may provide an alternative to the image-based segmentation process. Common procedures used for this purpose are the Independent Component Analysis (ICA) and the Principal Component Analysis (PCA). Both are statistical techniques for analyzing multivariate data which identify features or variations within a population by highlighting their similarities and differences ([212],[213],[214],[215]). These features are ordered according to their relative significance and can be used to reconstruct the shape of different organs. PCA has been successfully used for several different applications like face recognition [212], [216] characterization of the adult human femur [217], [218] and sex determination from unidentified skeletal remains [219]. On the other hand, ICA has been extensively used in the ECG analysis ([220]). To the author's knowledge there are no studies focusing on the foot even though several 2 and 3-dimensional foot FE models have been proposed given their applicability in the design of therapeutic footwear and in the evaluation of the diabetic foot ([63], [78], [221], [222], [223], [172]). The latter is one of the most common consequences of diabetes and it implies the formation of ulcers which are major causes of disability in patients, often resulting in significant morbidity, extensive periods of hospitalization and mortality ([163], [116]). FE simulations can be used to predict the load distribution between the foot and different supports, and to provide additional information to the clinicians such as the internal stresses/strains of the ankle-foot complex [78]. Considering the complexity of the foot, the development of a parametric model would really benefit the field and make the translation into a clinical context easier. The aim of this preliminary study was to develop a new method for generating a parametric foot model based on PCA. The statistical technique was applied to 6 foot meshes for a preliminary feature analysis, 3 of which were of diabetic subjects and the rest were of healthy subjects. Such an approach can be useful for reducing current drawbacks of model generation, as well as allowing variations and similarities between the two populations to be identified. A similar method was applied on the meshes of the levator ani muscle [224] but never to a complex structure like the foot. It has the potential to markedly reduce the time required for FE model

generation, providing an opportunity for rapid generation of a large population of geometries that can be used for simulations.

## 5.2 Materials & Methods

### 5.2.0.1 Subjects

Three healthy subjects (HSs) and 3 diabetic subjects (DBs) were enrolled. Clinical and demographic characteristics are reported in Table 5.1. DBs were recruited among the patients attending the outpatient Clinic at the Department of Metabolic Disease of the University of Padova (Italy). The criteria of inclusion were type 1 or 2 diabetes, no history of neurological disorders (apart from neuropathy) or ulcers, orthopedic problems, lower limb surgery or cardiovascular disease. They should also have intact walking ability. HSs were enrolled among the personnel of the Department of Engineering Information of the University of Padova. Written informed consents were given by all subjects. The protocol was approved by the local Ethic Committee of the University Clinic of Padova. All the DBs underwent a neurological evaluation that included the assessment of symptoms, and signs compatible with peripheral nerve dysfunction. The Michigan Neuropathy Screening Instrument was used ([179],[225]). Furthermore they underwent a physical examination as in Sawacha et al, 2009 [119]. Each DBs had at least one urinary albumin-to-creatinine ratio measured (0–30 mg/g normal, 30–300 mg/g microalbuminuria, 4300 mg/g macroalbuminuria), one ophthalmologic examination, one 12-leads electrocardiogram collected in the three months preceding the study, and one carotid artery Doppler ultrasound examination and HbA1c values from the preceding ten years.

### 5.2.0.2 Data Acquisition

A right feet MRI was acquired with 1.5T devices on each HS and DB in a completely unloaded condition. More details are provided in Table 5.2. The grey scale images were then segmented with Simpleware-ScanIP software (v.5.0) into both the skin and 30 bones to represent the overall shape of the foot. The triangulated mesh was then generated from the bitmapped data with the Simpleware-ScanFE module (algorithm FE-Free, minimum and maximum edge length respectively of 6/8 mm, 0.4 mm target maximum error – smaller than the MRI resolution). First of all, only the geometry of the first metatarsal bone (FMTB) was extracted from each mesh to perform the PCA, as the area underneath it has been proven to be at a higher risk for the development of foot ulcers [116](Figure 5.1). In the chapter this will be referred to as Case A. In

## Chapter 5. Towards the definition of a parametric foot finite element model

Table 5.1 – Demographic and clinical data of the healthy and the neuropathic subjects.  
# = Number of subjects

	HS 1	HS 2	HS 3	DNS 1	DNS 2	DNS 3
<b>Gender</b>	Female	Female	Male	Male	Male	Male
<b>BMI [Kg/m<sup>2</sup>]</b>	20.15	21.48	22.94	25.10	24.50	37.00
<b>Age</b>	31	26	39	65	59	71
<b>Foot Size [EU size]</b>	40.5	38	43.50	42.5	42	43
<b>Cavus foot</b>	-	Right/Left	-	Right/Left	Right/Left	Right/Left
<b>Flat Foot</b>	Right	-	-	-	-	-
<b>Hallux Valgus</b>	-	Right	-	-	-	-
<b>Foot deformities</b>	-	-	-	Hammertoes/ Claw toes	Claw toes	Claw toes
<b>Plantar Callosity</b>	-	Under metatarsal head	-	-	Under metatarsal head	Under metatarsal head

order to analyze the geometrical variations of the whole foot, the outline of the skin of the feet was also extracted for every DBs and HSs. The toes were removed from the skin meshes due to large inter-subject variations. This allowed us to focus on the evaluation of features of the overall foot between DBs and HSs (Figure 5.2). In the paper this will be referred to as Case B.

Table 5.2 – Parameters of the MRI and data of the subjects. (HS= healthy subject, DB= diabetic subject)

	MRI scanner	Slice Thickness	Sequence	TE/TR
<b>HS1</b>	Philips Achieva (1.5 T)	1.2 mm	3D mFFE	9/33
<b>HS2</b>	Siemens Avanto (1.5 T)	1 mm	T2 3D MEDIC	14/32
<b>HS3</b>	Siemens Avanto (1.5 T)	1 mm	T1 3D MEDIC	3/27
<b>DB1</b>	Siemens Avanto (1.5 T)	1.5 mm	T2 3D MEDIC	14/32
<b>DB2</b>	Siemens Avanto (1.5 T)	1.5 mm	T2 3D MEDIC	14/32
<b>DB3</b>	Siemens Avanto (1.5 T)	1.5 mm	T2 3D MEDIC	14/32

### 5.2.0.3 Geometric Feature Extraction

The application of the PCA has two requirements: the meshes have to be aligned to eliminate spatial variations and they must have the same number of vertices. In order to achieve this, MeshLab (url) was used to control the number of elements coupled with NMSBuilder [207] for performing the mesh co-registration. NMSBuilder implements a standard rigid vertex-to-vertex iterative closest point (ICP) algorithm to align a moving

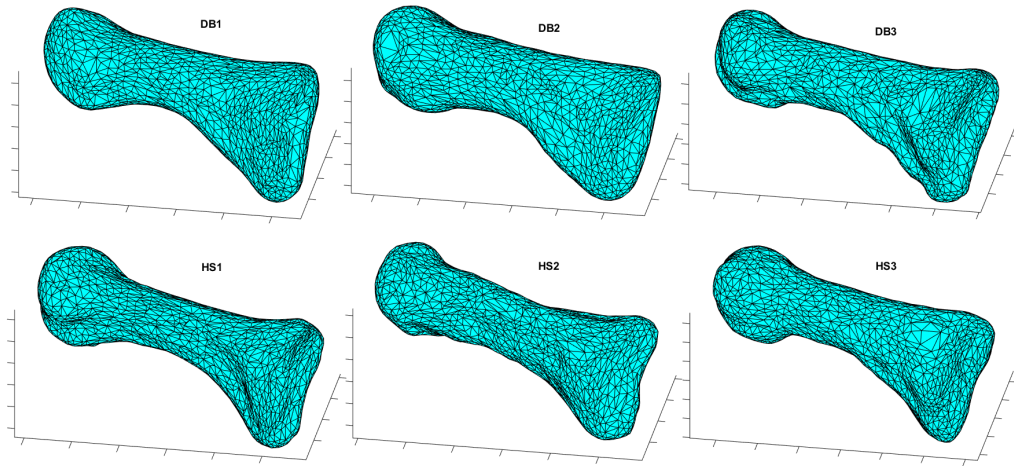


Figure 5.1 – Meshes of the first metatarsal bone of all the subjects used for the PCA. The first row shows the three diabetic subjects and the second one shows the three healthy subjects.

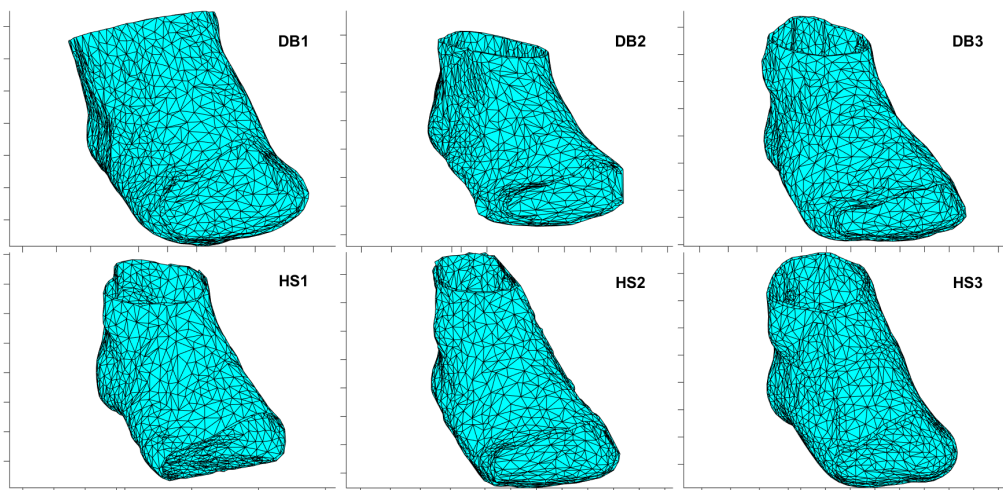


Figure 5.2 – Meshes of the skin without toes used for the PCA. The first row shows the three diabetic subjects and the second one the three healthy subjects.

mesh with a fixed one [226]. Then the elements of the meshes were reordered using k-nearest neighbor algorithm (k-NN). K-NN is a non-parametric method used for classification and regression. It solved the problem of finding the closest vertices given a reference so that the nodal numbers were consistent across all the meshes. Nodal coordinates of the meshes were then extracted to form a matrix  $M$  where each row corresponded to one individual. After this procedure was completed on all the meshes, PCA was performed by first computing the mean nodal coordinates  $M_{mean}$  across the population and then subtracting it from  $M$  to obtain  $M_{adjust} = M - M_{mean}$ . The covariance matrix of  $M_{adjust}$  was evaluated and an eigenvalue analysis was performed [212]. The eigenvalues ( $\lambda$ ) and associated eigenvectors ( $U$ ) were ordered according to their magnitudes, from largest to smallest. The eigenvalue gives a measure of variance of the associated mode (or eigenvector) so that the first (or the largest) one ( $\lambda_1$ ) and its corresponding eigenvector ( $U_1$ ) represent the most significant variation across the population. These shape changes were visualized by generating hypothesized models that contain features of the principal components, as shown in the following equation (5.1):

$$M_{new} = M_{mean} + U_i c \sqrt{\lambda_i} \quad (5.1)$$

Where  $M_{new}$  represents the new mesh and  $c$  is the scale factor that controls the amount of variation captured by the eigenvalues and eigenvectors ( $\lambda_i, U_i$ ) in both positive and negative directions [224]. All these steps were implemented using Matlab 2012a (7.14). A sketch of the workflow is shown in Fig.1. Once the new geometries were obtained, MeshLab was used to connect all the vertices of the point cloud in new meshes. The Poisson surface reconstruction approach is implemented in the software and was used for this purpose [227]. The procedure was applied first to the controls and the diabetic subjects separately (considering two distinct groups of 3 subjects each), and then by considering a whole group of 6 undifferentiated subjects. Finally in Case B the PCA was performed with the meshes of all the controls and by adding a different diabetic subject each time.

## 5.3 Results

### 5.3.0.1 Case A

In case A when the PCA was applied to two distinct groups, each containing 3 subjects (either DBs or Hs), only two modes were obtained. However, by considering the entire group of 6 undifferentiated subjects, 5 modes were observed. The eigenvalues were reported in Table 5.3. The hypothesized models (or shape variations) generated



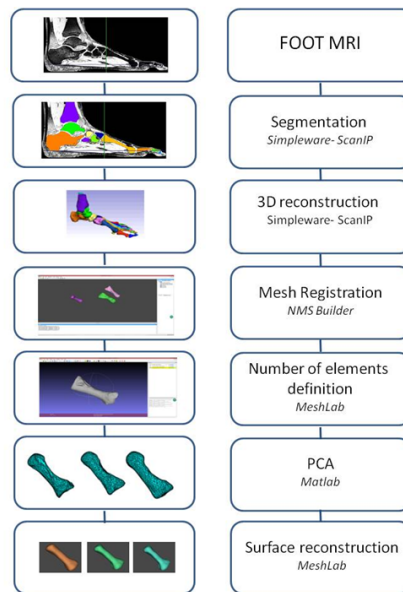


Figure 5.3 – Workflow of the computation of the PCA. The name of the software used for every step is indicated in italic.

by means of Equation 5.1 when considering all the subjects were shown in Figure 5.4. Results showed that the most obvious shape variations were located in the proximal and distal aspects of the bones, reflected by their thickness and length. The variations generated by means of Equation 5.1 when considering only the diabetic subjects or only the healthy ones were shown in Figures 5.5 and 5.6, respectively. For each population, only two modes were observed, resulting in two main shape variations. The models obtained when considering either HSs or DBs alone showed again the most substantial variations in the proximal and distal aspects of the bones. The HS's shape variations showed changes in the width of the bone, as well as the shape of the proximal and the distal ends whereas the DB's shape variations showed changes in both the length and the width of the bone. When all 6 individuals were analyzed together, the shape variations at the proximal and distal ends were more profound.

### 5.3.0.2 Case B

In case B when the PCA was applied to two distinct groups, each containing 3 subjects (either DBs or HSs), only the first two eigenvalues were significant. However, by considering a whole group of 6 undifferentiated subjects, 5 eigenvalues were significant. Eigenvalues were reported in Table 5.4. The shape variations generated by means of Equation 5.1 when the PCA was applied to the whole group are shown in figure 7. The first principal component identified a difference in the curvature of the superior

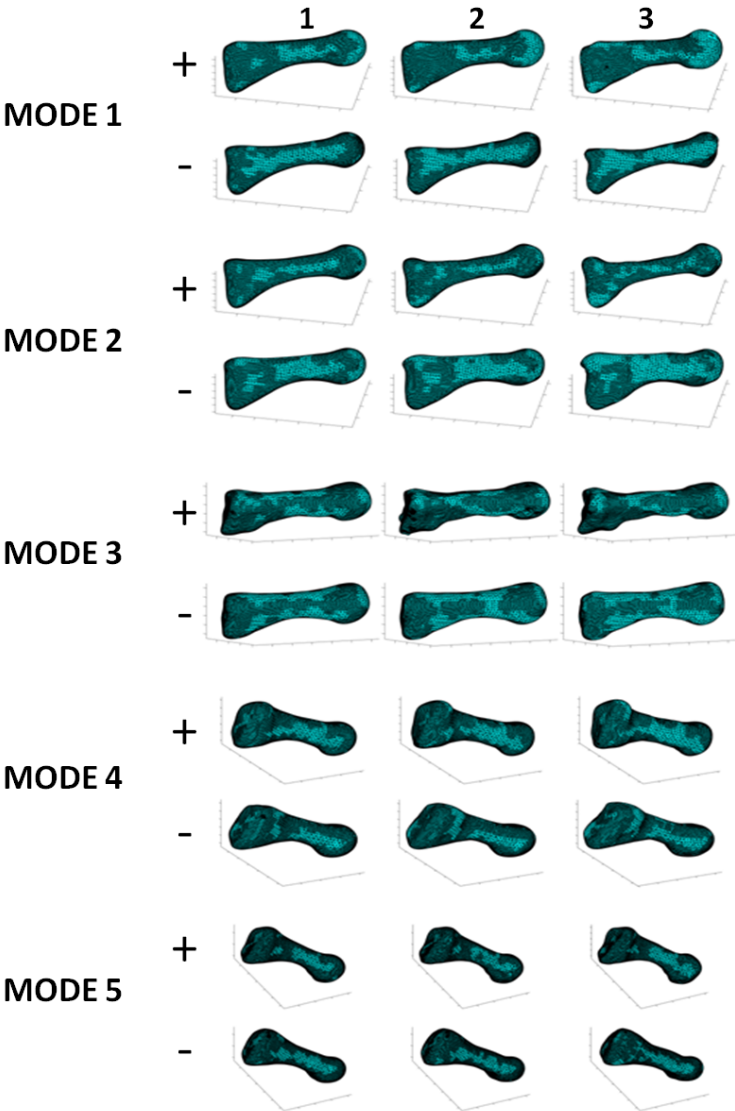


Figure 5.4 – FMTB hypothesized models generated by means of Equation 5.1 for all six subjects. For each principal mode, the variation was illustrated by varying the value of the constant  $c$  from  $-3$  to  $+3$ . Positive  $c$  values represent shape variation in the positive direction, whereas negative  $c$  values represent shape variation in the opposite direction. The larger the magnitude of constant  $c$ , the more substantial is the shape variation represented.

Table 5.3 – Eigenvalues computed with the PCA run on the meshes of the metatarsal bones (HS = healthy subjects, DB = diabetic subjects). First column shows the eigenvalues of PCA run on all the 6 meshes, second column shows the eigenvalues of PCA run on 3 HS, third column shows the eigenvalues of the PCA on 3 DB, fourth, fifth and sixth columns show the eigenvalues of the PCA run on 3 HS plus each time a different DB.

	3HS+3DS	3 HS	3 DS	3HS+DB1	3HS+DB2	3HS+1DB3
<b>Evalue 1</b>	9.67E+03	2.11E+04	1.35E+04	1.53E+04	1.50E+04	1.48E+04
<b>Evalue 2</b>	7.90E+03	9.14E+03	1.01E+04	9.88E+03	1.15E+04	1.03E+04
<b>Evalue 3</b>	5.51E+03	7.48E-11	4.41E-11	6.08E+03	6.00E+03	6.08E+03
<b>Evalue 4</b>	4.77E+03	4.86E-11	3.52E-11	4.38E-11	4.65E-11	4.62E-11
<b>Evalue 5</b>	3.54E+03	3.85E-11	2.48E-11	3.75E-11	3.79E-11	4.32E-11
<b>Evalue 6</b>	2.08E-11	2.88E-11	2.06E-11	1.93E-11	3.38E-11	4.11E-11

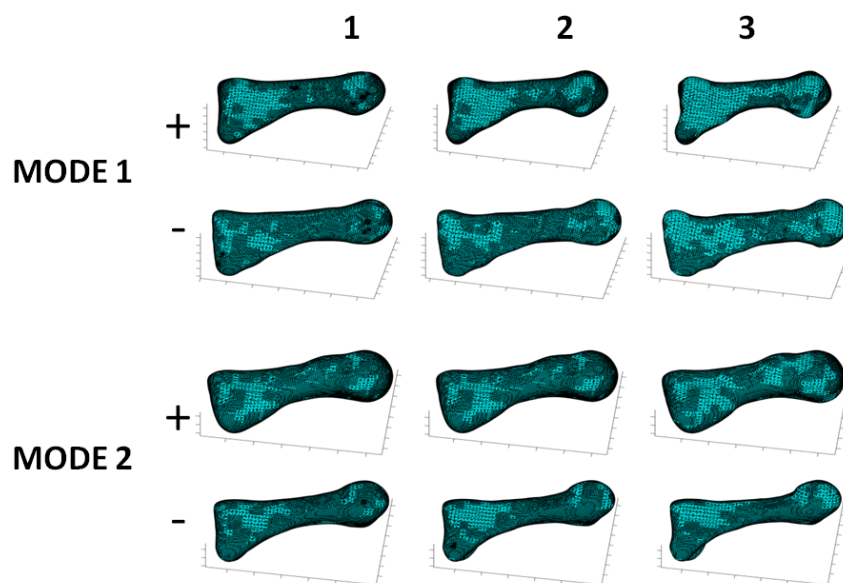


Figure 5.5 – FMTB shape variations generated by means of Equation 5.1 considering only the diabetic subjects. For each principal mode, the shape variations were shown by varying the constant  $c$  from -3 to +3.

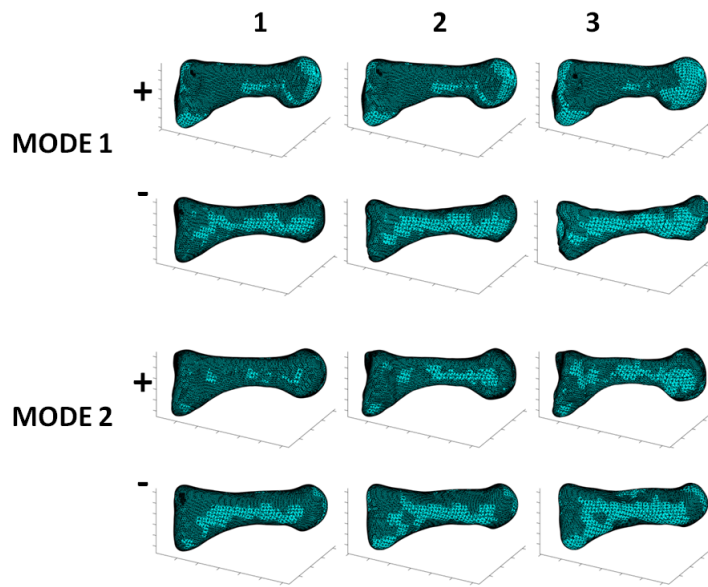


Figure 5.6 – FMTB shape variations generated by means of Equation 5.1 considering only the healthy subjects. For each principal mode, the shape variations were shown by varying the constant  $c$  from -3 to +3.

aspect of the foot. The second mode highlighted changes in the calcaneus while the third one in the anterior part of the foot. The last two components seemed to have a minor effect on the shape, mainly showing changes in the length and the width of the foot. The shape variations generated by means of Equation 5.1 when considering only the diabetic subjects or only the healthy ones were shown in Figures 5.8 and 5.9, respectively. As mentioned previously, for each subset of population, only two eigenvalues were significant, indicating 2 main shape variations. The first principal component in both groups showed a difference in the superior curvature of the foot. The second mode showed changes at the frontal part of the foot in the DBs, as opposed to the posterior part in the HSs. Finally the PCA was applied to all the HSs' meshes by adding each time a different DBs. Results were shown in figures 5.10, 5.11 and 5.12. Addition of DB1 showed a marked impact on the dominant shape variations predicted by the PCA. Since this foot was much larger with a more prevalent abnormal shape, the main shape changes predicted in this specific case were associated with the length and the width of various parts of the foot. Similar patterns can be observed in figures 5.11 and 5.12, where additional features were picked up by the PCA by introducing different DB individuals into the HS population.

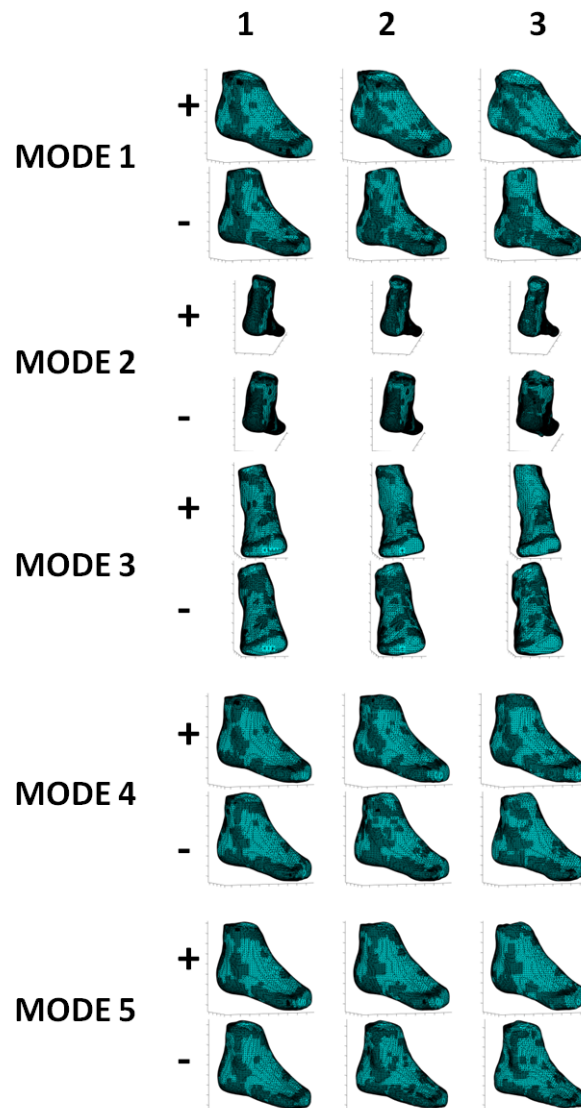


Figure 5.7 – hypothesized models generated by means of Equation 5.1 considering the meshes of the skin without toes of all the subjects. For each significant principal component 6 different models were obtained, according to the constant  $c$  which varied from -3 to +3.

## Chapter 5. Towards the definition of a parametric foot finite element model

Table 5.4 – Eigenvalues computed with the PCA run on the meshes of the skin without toes (HS = healthy subjects, DB = diabetic subjects). First column shows the eigenvalues of PCA run on all the 6 meshes, second columns the eigenvalues of PCA run on 3 HS, third column the eigenvalues of the PCA on 3 DB, fourth, fifth and sixth columns the eigenvalues of the PCA run on 3 HS plus each time a different DB.

	3HS+3DS	3 HS	3 DB	3HS+DB1	3HS+DB2	3HS+DB3
<b>Evalue 1</b>	2.33E+05	4.27E+05	4.32E+05	3.69E+07	5.06E+07	2.34E+05
<b>Evalue 2</b>	1.99E+05	3.21E+05	3.16E+05	3.13E+05	2.85E+05	1.64E+05
<b>Evalue 3</b>	1.67E+05	1.71E-09	3.24E-09	1.88E+05	2.10E+05	1.22E+05
<b>Evalue 4</b>	1.38E+05	1.24E-09	1.76E-09	1.00E-07	1.55E-07	9.69E-10
<b>Evalue 5</b>	1.06E+05	1.11E-09	1.70E-09	9.59E-08	1.16E-07	9.66E-10
<b>Evalue 6</b>	7.83E-10	8.28E-10	1.34E-09	6.80E-08	1.01E-07	6.01E-10

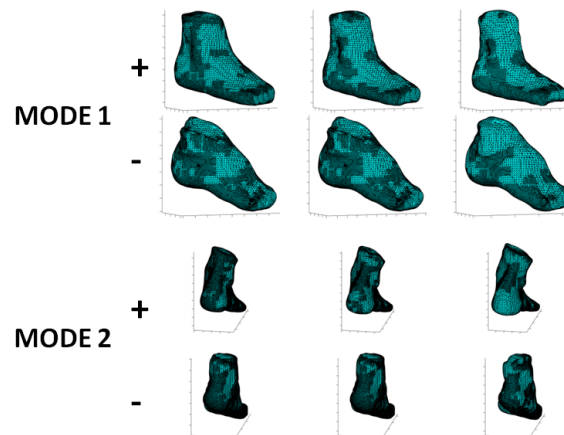


Figure 5.8 – hypothesized models generated by means of Equation 5.1 considering the meshes of the skin without toes of the diabetic subjects. For each significant principal component 6 different models were obtained, according to the constant  $c$  which varied from -3 to +3.

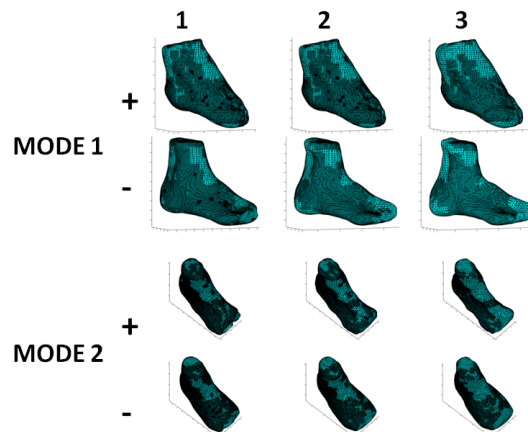


Figure 5.9 – hypothesized models generated by means of Equation 5.1 considering the meshes of the skin without toes of the healthy subjects. For each significant principal component 6 different models were obtained, according to the constant  $c$  which varied from -3 to +3.

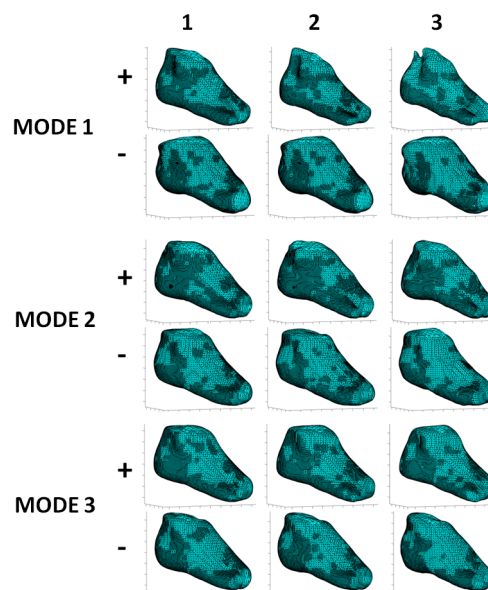


Figure 5.10 – hypothesized models generated by means of Equation 5.1 considering the meshes of the skin without toes of all the HSs plus the first DB subject. For each significant principal component 6 different models were obtained, according to the constant  $c$  which varied from -3 to +3.

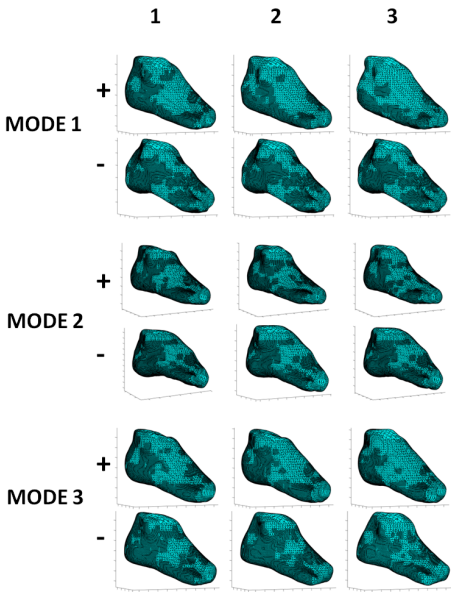


Figure 5.11 – hypothesized models generated by means of Equation 5.1 considering the meshes of the skin without toes of all the HSs plus the second DB subject. For each significant principal component 6 different models were obtained, according to the constant  $c$  which varied from -3 to +3.

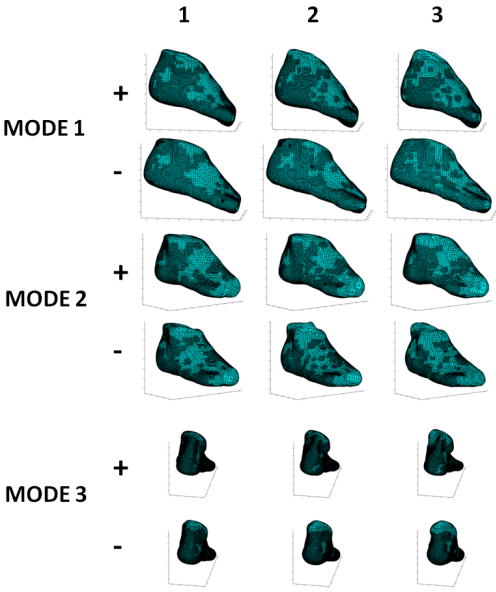


Figure 5.12 – hypothesized models generated by means of Equation 5.1 considering the meshes of the skin without toes of all the HSs plus the third DB subject. For each significant principal component 6 different models were obtained, according to the constant  $c$  which varied from -3 to +3.



## 5.4 Discussion

A PCA-based statistical modeling algorithm was proposed and qualitatively assessed on a small cohort of human foot anatomies derived from MRI. The aim of this study was to verify the possibility of generating parametric foot models and to evaluate the potential of PCA to pick up various shape changes in both the control and the diseased populations. A total number of 6 meshes was investigated: 3 of diabetic subjects and 3 of healthy subjects. The abnormal shape of diabetic feet has been examined by applying the PCA to both the meshes of the skin and the FMTB, the area underneath which was shown to be at high risk of developing foot ulcers [116]. PCA has been used for different purposes such as the quantification of sex differences in the femoral size and shape, as well as the bone density ([219], [228]). Furthermore, it has also been applied to the generation of hypothesized models [224]. The novelty of this study is the utilization of this technique on feet geometries. As shown in the results, the feasibility of this approach has been demonstrated, and different meshes of the foot and of the FMTB have been generated by means of the PCA. This represents a first step in a faster realization of PSMs of the feet, which could then be utilized in a clinical context for the evaluation of abnormalities in the biomechanics of gait. The realization of PSMs of lower limbs has recently been reported in literature and this study falls within the scope of the current state of the art ([205], [210]). Furthermore, the technique was able to discriminate differences between diabetic and healthy foot geometries. More data are required to capture the variations in the larger population, but the results are consistent with the literature [224]. In both Cases A and B, when the PCA was applied to the whole database, 5 eigenvalues were significant, compared with 2 eigenvalues when two separate groups were considered. Finally when considering all HSs combined with a single DB, an additional mode was often observed reflecting the main feature of the added individual. As we were expecting, looking at the shape of the FMTB, the main shape changes in case A were located at the proximal aspects of the bones. This can be related to the specific shape of the FMTBs, which in the case of diabetic subjects is also responsible for altering foot kinematics and plantar pressure during gait [126]. Other principal modes also showed variations in the thickness of the bones. The relation between diabetes and change in bone density and metabolism remains controversial but it has been proven under specific conditions ([229], [230]). These preliminary results suggest the possibility of using this technique for describing various foot shapes. The combination of PCA with other experimental parameters like weight, sex and shoe size may establish a tool to develop subject-oriented meshes, which can then be used for FE models and simulations in the future. The ability of recreating the geometries of different feet without the need of segmenting MRIs will constitute a step forward of the fast realization of personalized models, and the

## Chapter 5. Towards the definition of a parametric foot finite element model

---

potential of this approach has already been underlined in previous studies [224]. When the skin without toes of HSs was considered (case B), the first principal component identified a difference in the superior aspect of the foot. When considering only the diabetic subjects, this shape variation was more visible, mostly due to the influence of DB1 who had a particularly large foot. This finding is in line with the high incidence of cavus foot in diabetic feet reported in the literature [168]. This feature is correlated to diabetic pathology and may originate from the thickness of the plantar fascia which is typical of these patients [231]. The second PC highlights changes in the calcaneus, an area where the highest loads occur ([116]. The third PC highlights differences in the anterior part of the foot. These shape variations agreed qualitatively with what is described in the literature [168], [232]). Foot structure is important in predicting peak pressure and the development of ulcers as demonstrated by Bevans and Bowker [233], and this pilot study showed that PCA is able to detect the common shape variations typically observed in the diabetic subjects. Comparing the 2 case studies reported here, PCA seemed to work better for rigid structure (e.g. bone) than for soft tissue (e.g. skin), which tends to deform more readily and loses its shape. This is confirmed by the fact that in the literature PCA has traditionally been applied to bones like femur or patella [219], [228]. The methodology reported here will be further improved in order to analyze additional structural specificities of the foot, like the other bones, which can then be used for the creation of complete parametrized models. The biggest limitation of this study is the small sample size used for the PCA, which is unlikely to be representative of the larger population, due to its very limited statistical power [234]. This limitation has already been outlined in the literature [228]. However, the results showed that the methodology was able to isolate features with a small number of control and diabetic subjects. There is an on-going study to collect more data from the diabetic subjects. These will be used in another study to confirm the preliminary findings reported in this paper. The study is computationally expensive, however the costs can be reduced by adopting a Singular Value Decomposition (SVD) approach in order to calculate the eigenvalues, as shown in the work of Mahfouz et al [219]. SVD and PCA are two similar methods used to reduce a high-dimensional dataset into fewer dimensions while retaining important information. Their applications are comparable and often interchangeable. Another interesting technique which should be considered as a substitute or as a complement to the application of the PCA is the Independent Component Analysis (ICA) [235]. ICA is a computational method often used in the field of signal processing, for separating a multivariate signal into additive subcomponents. Multivariate data are usually represented as a linear transformation of the original data. ICA instead relies on the assumption that the subcomponents are non-Gaussian signals and they are statistically independent from each other, or as independent as possible. This representation proved its capability to

capture the essential structure of the data in many applications, such as the evaluation of electrocardiograms (ECGs). He et al, used ICA for online processing the ECG with the purpose to enhance the quality of the signal by reducing the noise and the artifacts [236]. Their technique proved to be successful in detecting and removing them and this might be useful in our applications when considering the variability of the toes. Furthermore the ability of PCA to reduce data dimensionality could be combined with the ICA for a better feature extraction. This was done by Chawla who proposed a combined PCA-ICA algorithm ([237], [238]). A similar application in this project could help in the identification of the most significant features that discriminate the two populations. Further studies are needed in order to detect changes in the geometrical shape of the foot with respect to clinically measurable subject-specific parameters such as the length of the foot, or the presence of bone abnormalities. Once a generic mesh of the foot has been generated (with a much larger dataset), it would be possible to verify its usability as a tool to improve the information available for the clinicians. The mesh could then be used for FE simulations, which could provide more information to the clinicians, useful to address treatments according to the features of each subject. In summary, the results of the present study indicate that the PCA is a useful method to describe features in the foot and to evaluate differences in the shape of healthy and diabetic subjects. The approach adopted herein can constitute a good starting point for the realization of a parametric foot model for further biomechanical analysis.

## 5.5 Acknowledgments

I acknowledge Gabriella Guarneri, MD and Prof Angelo Avogaro, MD for enrolling the subjects and performing the clinical screening. Furthermore I would like to acknowledge Dr. Xinshan Li from the *INSIGNEO Institute for in silico Medicine, Department of Mechanical Engineering, University of Sheffield*, for helping me with the application of the Principle Component Analysis.



## 6 Conclusion

### 6.1 Summary, achieved results and future developments

Lately the development of patient-specific models, tailored to patient-specific data, has been of great interest for the possible applications in a clinical context ([205],[206]). Until now a reductionist approach was applied in medicine: the human body was divided into sub parts and each one was considered by itself. Unfortunately this cannot work on diseases like diabetes which affects the whole body. The complications are the results of the interaction of different components, and they are often variable from subject to subject [107]. PSMs could represent a solution to the need of a personalized medicine which allows the realization of more effective rehabilitation treatments designed on each subject capabilities. They are believed to be competent for improving diagnosis and optimizing clinical treatments by predicting and comparing the outcomes of different approaches of intervention ([207],[208]). Furthermore they can provide information that cannot be directly measured, such as muscle forces or internal stresses and strains of the bones. Given the considerable amount of diseases affecting motor ability, PSMs of the lower limbs have been broadly addressed in literature. Two techniques are mostly used in this area: musculoskeletal (MS) modeling and finite element (FE) analysis.

The use of MS models has recently gained a lot of attention, as they can compute human internal variables, such as muscle activations and forces and joint contact forces ([28],[29]). FE analysis is chosen for its flexibility and adaptability to model biological geometries and materials and to simulate complicated boundary and loading conditions [239]. Several MS models and FE models of the lower limbs were published in literature ([78], [63], [77],[210], [240]). In the most recent, experimentally acquired data were chosen as boundary and loading conditions in order to reach the maximum possible subject specificity ([78], [63]). In this context, many gait analysis protocols have been proposed to assess the 3D kinetics, kinematics and plantar

## Chapter 6. Conclusion

---

pressure distribution. This evaluation has proved to be useful in characterizing the foot biomechanics in different pathologies like the diabetic foot. As mentioned above, diabetes is indeed a disease that could benefit of the use of PMSs for the large variety of complications that are typical of it. One of the most serious is represented by the diabetic foot which compromises the function and structure of the foot [107]. It can have a neuropathic or ischemic origin and in most subjects, especially at advanced age, it is results of both [112]. Subjects lose the ability to walk thanks to the decrease in the range of motion of the joints and to the increase of the stiffness in the tissues. Furthermore the foot structure changes, determining an alteration of the bearing surface of the foot that shrinks to some particular points thus subjected to very high pressures (usually metatarsal heads and heel) [116]. The body, in an attempt to defend itself from this excessive load, strengthens the more superficial layer of the skin with callosities. However the defense is weak and if there is not intervention the formation of ulcers is inevitable. Ulcers are major causes of disability in patients, often resulting in significant morbidity, extensive periods of hospitalization and mortality ([163], [116]). A close relationship between neuropathy and foot biomechanical alterations that leads to high pressures and thus ulcerations has been demonstrated by several authors ([165], [115], [166], [116],[167], [65], [126], [168], [169], [170]).

The present thesis represents a first effort towards the definition of a more complete PSM which combining both a MS model and a FE model, can increase the understanding of the diabetic foot pathology. To achieve this objective, several limitations and issues have been addressed. A deep evaluation of the background and of the pros and cons of each technique has been done and reported in the various chapters.

The first step towards the realization of the project was the development of MS models of diabetic and control subjects using OpenSim, in order to estimate muscle forces. The objective was to evaluate whether the diabetic population exhibit lower limb muscle strength deficits compared to the healthy one. A modified version of the IORgait protocol was used to perform a routine gait analysis on the subjects and to compute lower limb joints kinematics and kinetics. 3D lower limb joints kinematics and kinetics was also calculated with OpenSim. A comparison between the approaches was done. The use of OpenSim demonstrated to be complementary to the standard gait analysis performed as in [84]. It enabled the evaluation of muscles forces in the diabetic and control subjects, highlighting the differences between them. In particular OpenSim kinematics results identified a decreased mobility in the sagittal plane at the hip joint in DNS accompanied by a higher value of the pelvic rotation angle at the end of the gait cycle. At the same time both the activation and the force of the Iliacus and Gracilis were found significantly lower indicating the presence of differences in the hip flexor muscles for this specific population of subjects in agreement with the literature ([132], [148], [154], [122], [160], [147]). Significant differences between DNS and CS, were

## 6.1. Summary, achieved results and future developments

---

also found in the activation and in the force of the Tibialis Posterior. This muscle plays a key role in the ankle stabilization and it has a major role in supporting the medial arch of the foot [158] (See section 2.4). Its dysfunction can be cause of an irregular distribution of the load on the plantar surface. This will influence the localization of the ulcers as already reported in the literature [90]. Other differences between the two populations were also found in the Peroneus Longus and they were confirmed by the comparison with the SEMG signals. Overall this study proved the capability of the MS model to describe a pathology like the diabetes. In the future the use of CMC (see Section 1.1.2) for the estimation of the muscles forces should be evaluated, in order to have the possibility to constraint the outcomes with the SEMG signals. Furthermore it would be interesting to compare other parameters between the two populations such as muscles and tendons length.

The second step regarded the evaluation of the possibility to integrate FE models and MS models. This was done by first applying joint contact forces and then muscle forces as boundary conditions in the FE simulations. When applying joint contact forces also the importance of the subject-specificity was tested running the simulations not only with the subject specific data but with the data of 10 neuropathic and 10 healthy subjects as well. A better agreement was found between experimentally measured and simulated plantar pressure obtained with JCFs than with the GRFs as boundary conditions. The average error at the stance phase of gait, calculated as the difference between simulated and experimental values and expressed in percentage of the experimental ones, was of 17% in GRFs driven simulations while it was of -3.34% in the JFCs ones for the healthy model; it was respectively of 30% and 14% for the diabetic model. The results confirmed the aim to proceed with the insertions of muscle forces derived from MS in the FE models. Subject-specific integrated and synchronized kinematic-kinetic data acquired during gait analysis were again used for the development of the MSMs and for the computation of the muscle forces of two subjects, a healthy and a diabetic one. Muscle insertions were located in the MRI of the subject (used as well for the geometries of the FEM) and correspondent connectors were created in the FE model. FE subject-specific simulations were subsequently run with Abaqus by conducting a quasi-static analysis on 4 gait cycle phases and adopting 2 conditions: one including the muscle forces and one without. Once again the validation of the FE simulations was done by means of a comparison between simulated and experimentally measured plantar pressures. Results showed a marked improvement in the estimation of the peak pressure for the model that included the muscles. In particular the simulations with the healthy model showed an error (expressed in percentage of the experimental value) on the estimation of the peak of pressure as small as 4% in loading response, while in the diabetic model simulations the smallest error was of 9% in push off. Overall the possibility of integrate the two methodologies was proved.

## Chapter 6. Conclusion

---

Different aspects could be improved as future development:

- the formulation of the material should be improved and a more adequate integration of the internal structures of the plantar soft tissue should be pursued. A formulation which includes the micro-and macro-chambers layers [195] or the skin [196] could highlight interactions among different levels;
- given that the fidelity of the model is highly depending on the number of degrees of freedom, it could be increased. Bones should not be grouped in sub groups but an evaluation of the behavior of each one should be performed. Furthermore also the use of the fluoroscopy for the estimation of the kinematics boundaries should be attentively evaluated ([199], [200], [201]) in order to decrease skin artifact errors.
- estimation of the error in the location of the point of attachment of the muscles should be done together with a sensitivity analysis on the individuation of the point of insertions of the muscles.
- the direction of application of the muscle forces should be analyzed.

Finally the possibility of developing parametric models by means of PCA was evaluated. In this study it was applied to the feet of a small cohort of diabetic and healthy subjects. Both the skin and the first metatarsal bones were examined and besides the reduced sample of subjects considered in the analysis, results demonstrated that the method is promising as it is also able to highlight differences in the shape of healthy and diabetic subjects. Of course the populations needs to be increased as future development and other statistical methods rather than PCA could be tried in order to decrease the computational costs.

In conclusion, the aim of this thesis of analyzing and integrating different techniques to get a better understanding of the diabetic foot was successfully accomplished, besides all the improvements that can still be made.



# A Appendix

## A.1 Control of muscle insertions

In this appendix, the MRI images where the muscles insertions for the FEMs developed in section 4.3 were identified, are reported.

### Tibialis Anterior

**Insertion of origin:** lateral face of the tibia, the interosseous membrane and the crural fascia.

**Terminal insertion:** medial surface of the medial cuneiform bone and base of the first metatarsal bone.



## Appendix A. Appendix

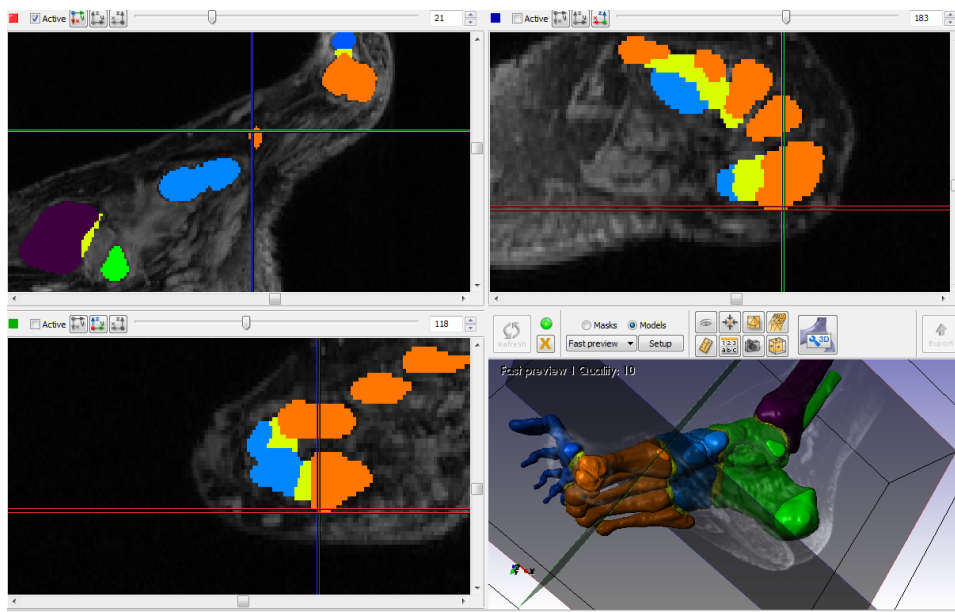


Figure A.1 – Insertion of the Tibialis Anterior on the first metatarsal bone. (ScanIP)

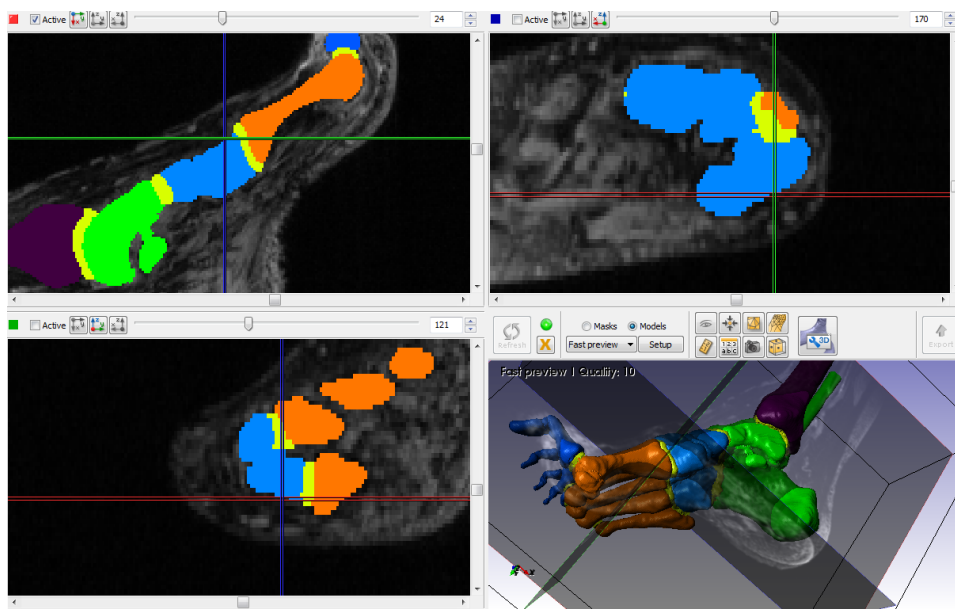


Figure A.2 – Insertion of the Tibialis Anterior on the medial cuneiform bone. (ScanIP)

## Extensor Hallucis

**Insertion of origin:** middle third of the medial aspect of the fibula and the interosseous membrane.

**Terminal insertion:** dorsal surface of the base of the phalanx of the big toe.

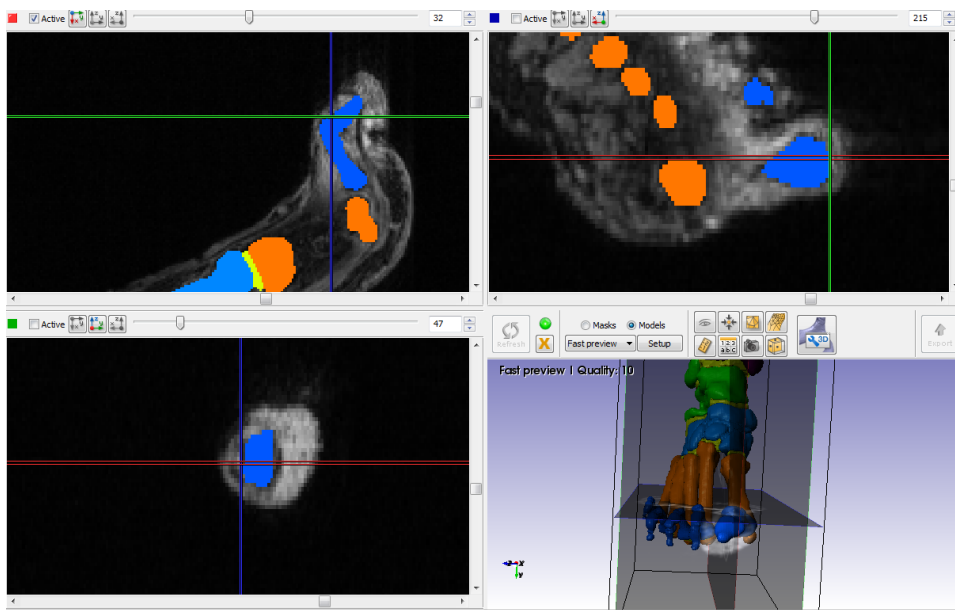
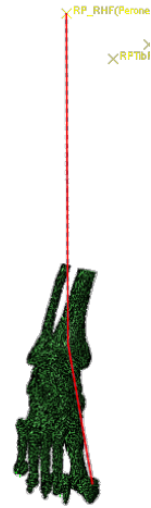


Figure A.3 – Insertion of Hallucis Extensor on the dorsal surface of the base of the phalanx of the hallux. (ScanIP)

## Extensor Digitorum

**Insertion of origin:** lateral condyle of the tibia, the interosseous membrane, the head and the front edge of the fibula and the crural fascia.

**Terminal insertion:** each of the secondary tendons of the four toes is divided into three parts of which, the middle one is inserted at the base of the middle phalanx, the others at the base of the distal phalanx.

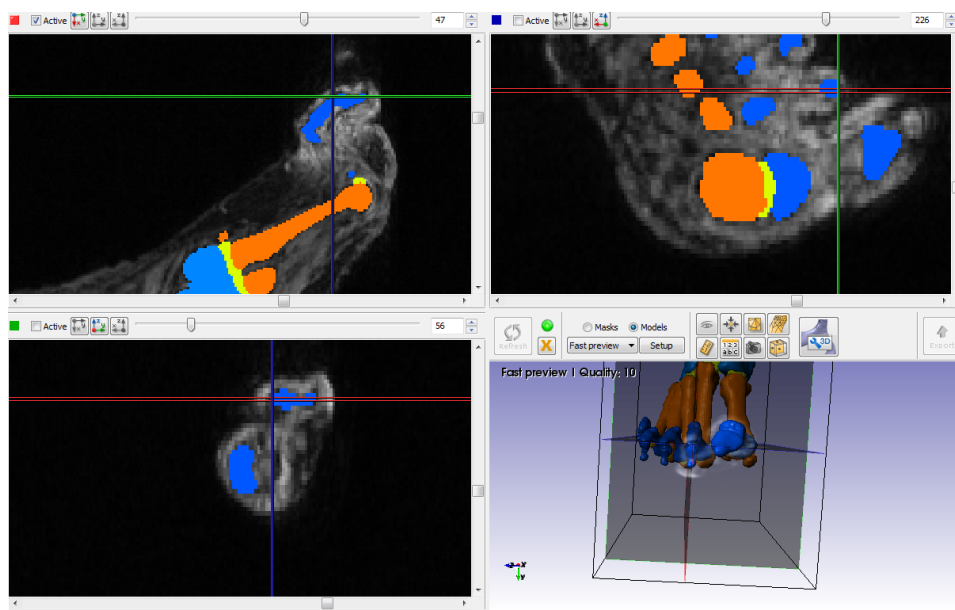


Figure A.4 – Insertion of the Extensor Digitorum on the base of the second distal phalanx. (ScanIP)

## A.1. Control of muscle insertions

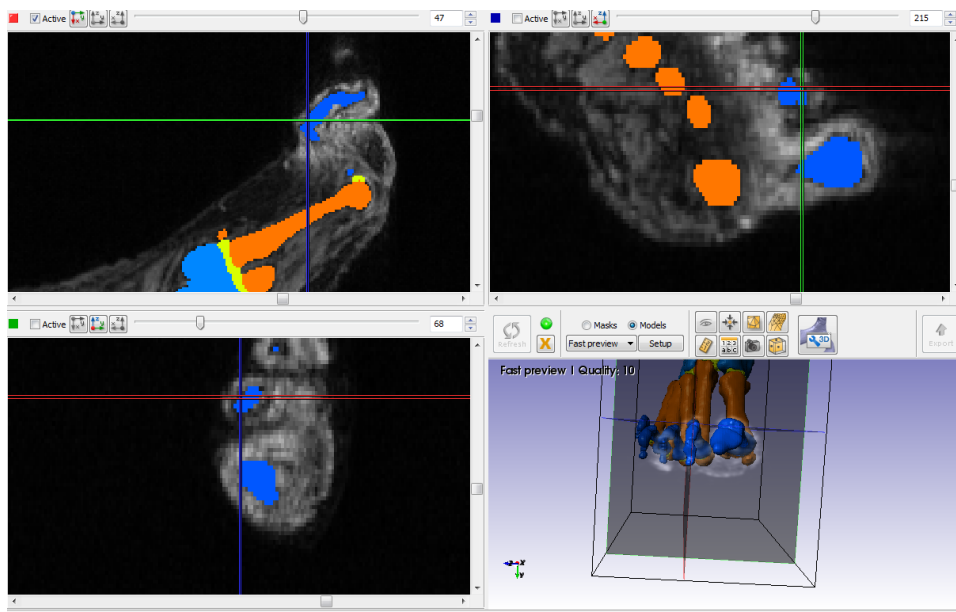


Figure A.5 – Insertion of the Extensor Digitorum on the base of the second medial phalanx. (ScanIP)

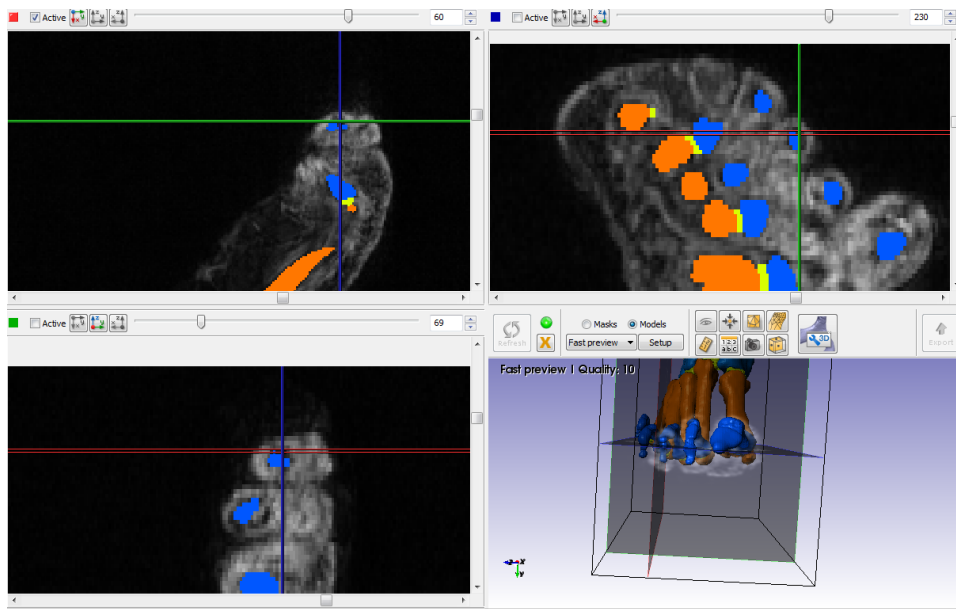


Figure A.6 – Insertion of the Extensor Digitorum on the base of the third distal phalanx. (ScanIP)

## Appendix A. Appendix

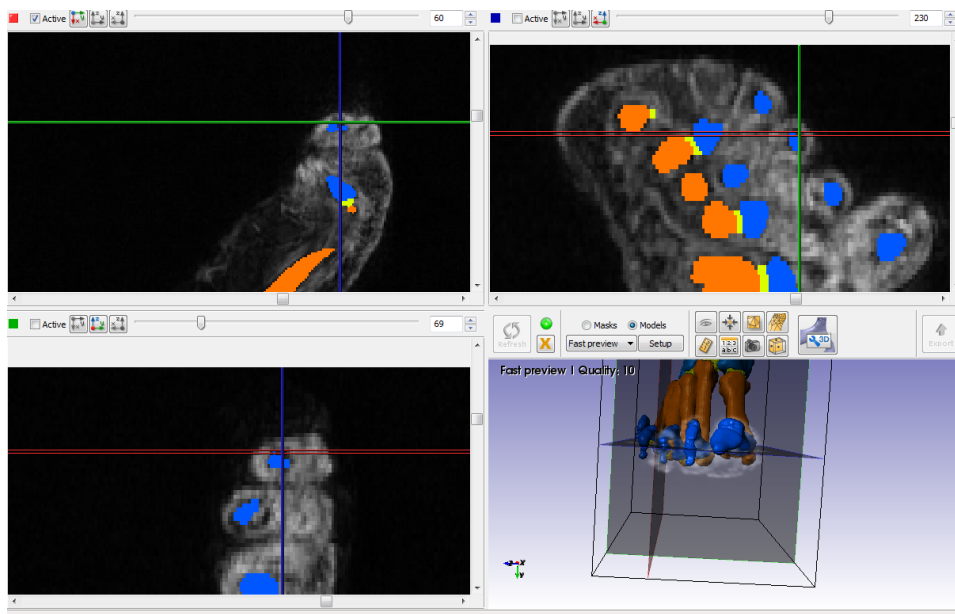


Figure A.7 – Insertion of the Extensor Digitorum on the base of the third medial phalanx. (ScanIP)

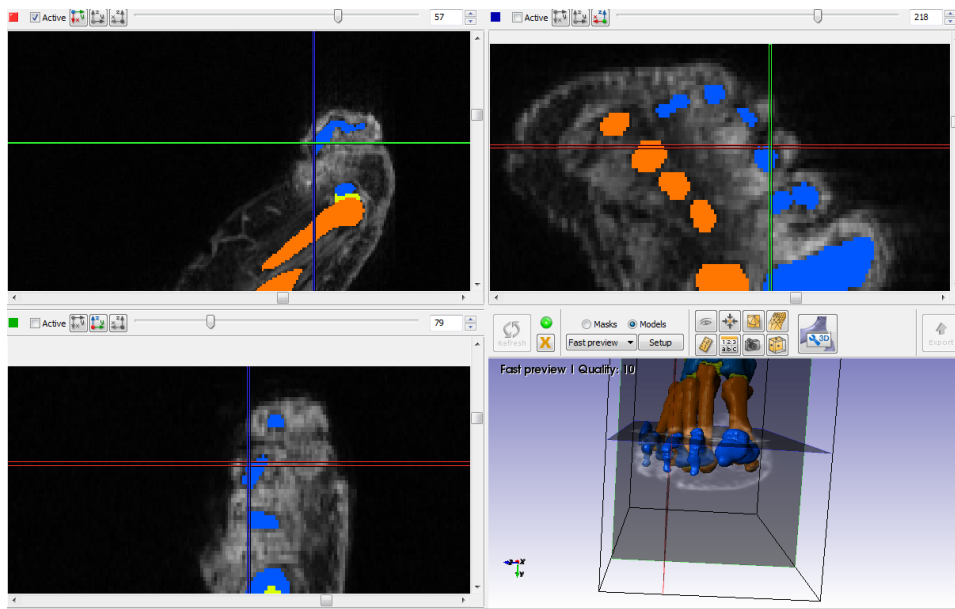


Figure A.8 – Insertion of the Extensor Digitorum on the base of the fourth distal phalanx. (ScanIP)

## A.1. Control of muscle insertions

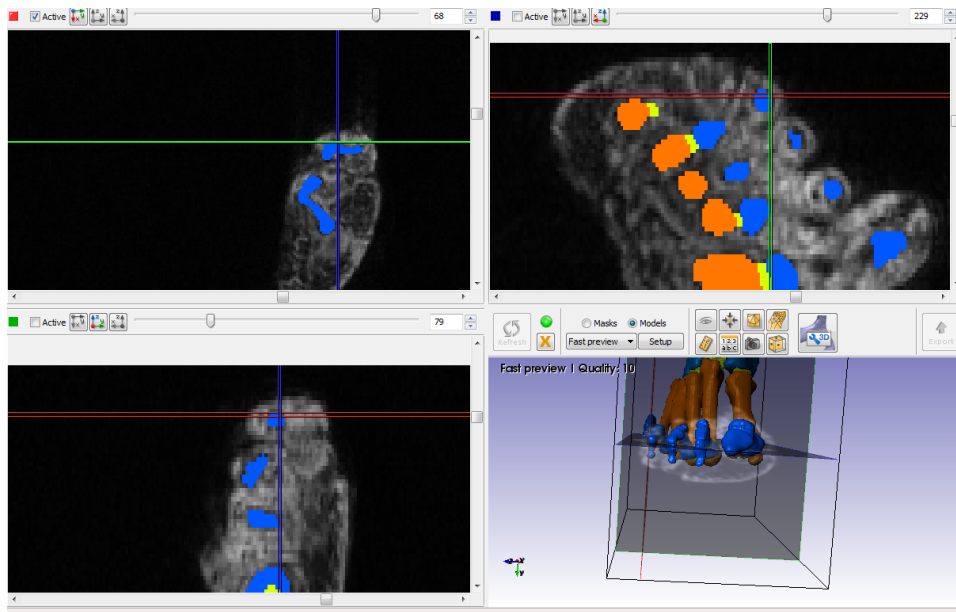


Figure A.9 – Insertion of the Extensor Digitorum on the base of the fourth medial phalanx. (ScanIP)

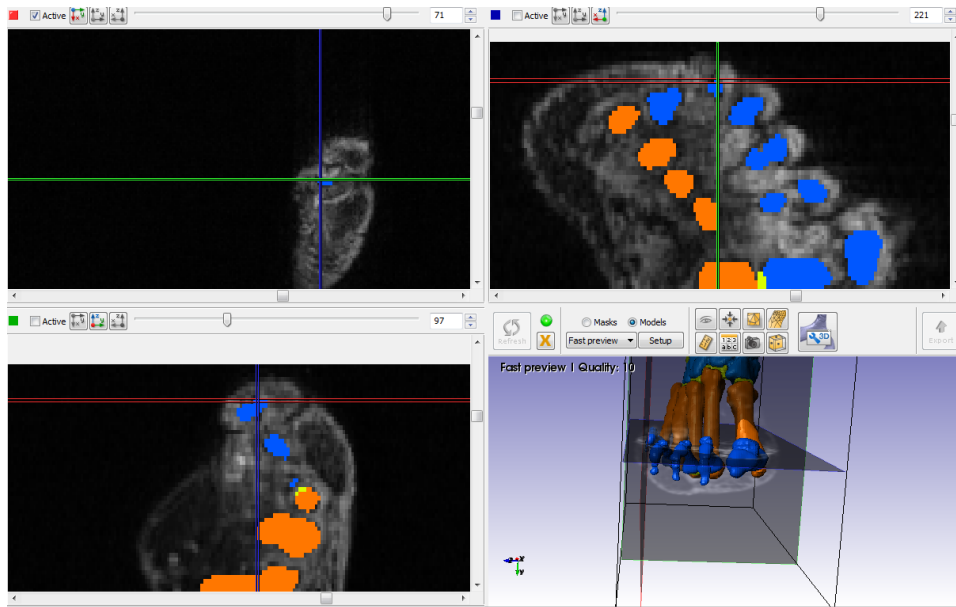


Figure A.10 – Insertion of the Extensor Digitorum on the base of the fifth distal phalanx. (ScanIP)

## Appendix A. Appendix

---

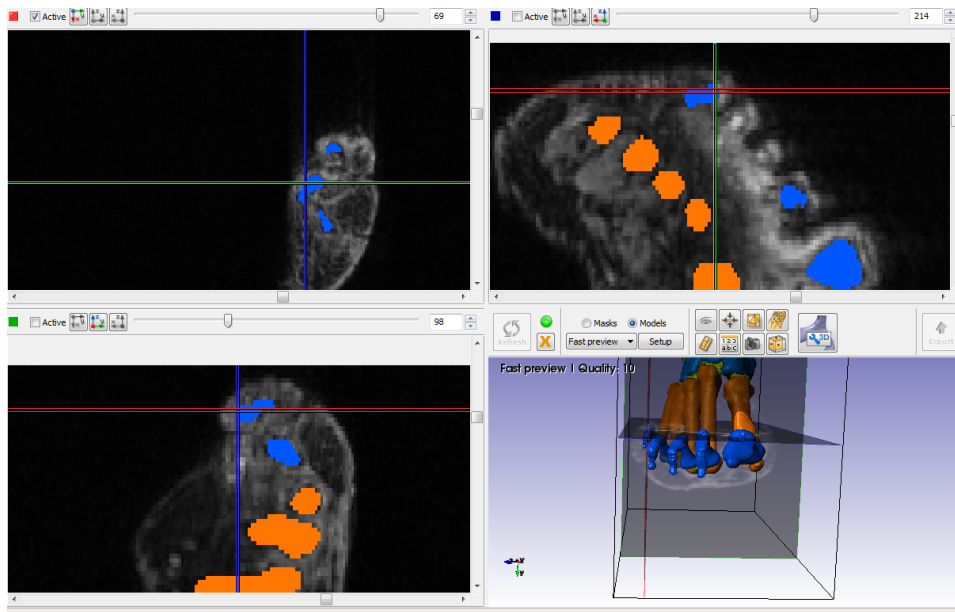


Figure A.11 – Insertion of the Extensor Digitorum on the base of the fifth medial phalanx. (ScanIP)



## Peroneus Longus

**Insertion of origin:** the head and the lateral face of the fibula.

**Terminal insertion:** medial cuneiform bone and tuberosity of the first metatarsal bone.

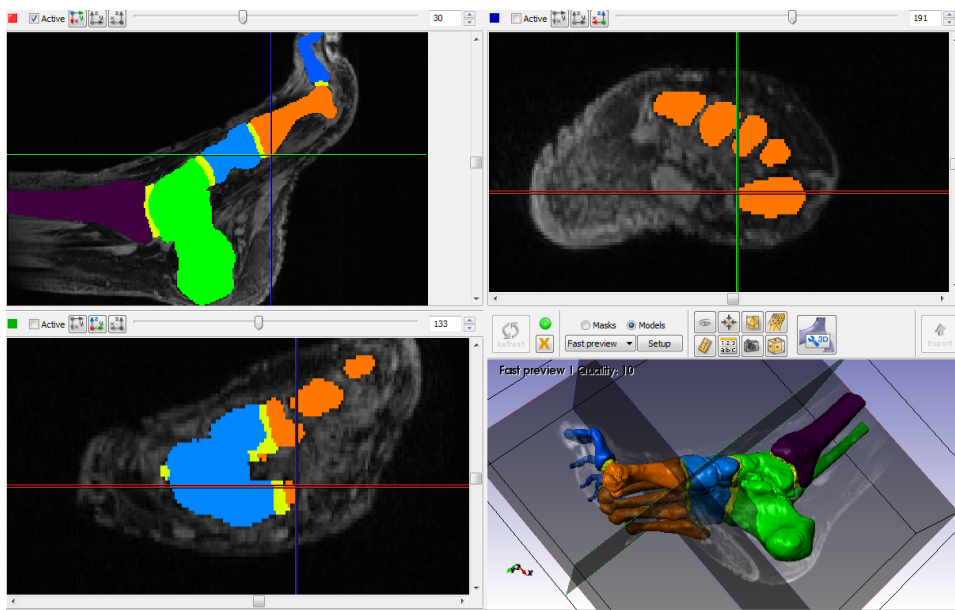
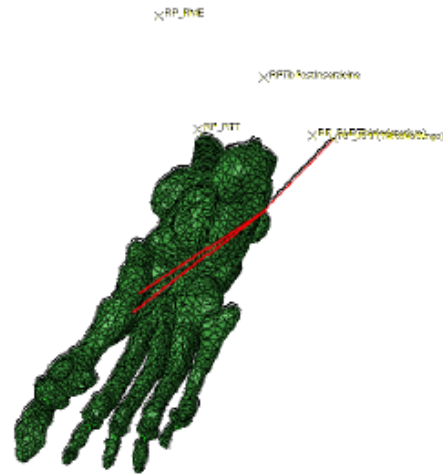


Figure A.12 – Insertions of the Peroneus Longus on the tuberosity of the first metatarsal bone. (ScanIP)

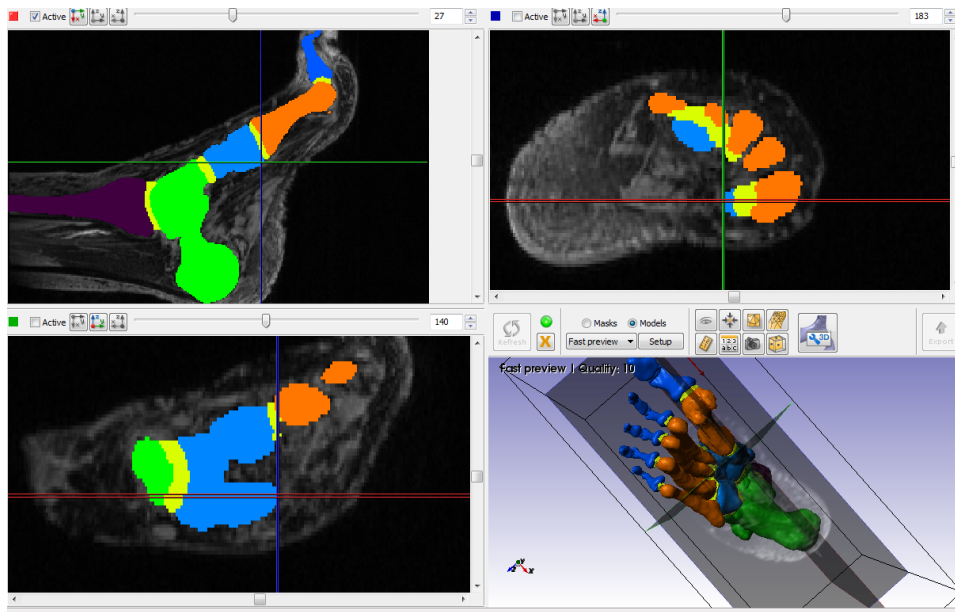


Figure A.13 – Insertion of the Peroneus Longus on the medial cuneiform bone. (ScanIP)

## Peroneus Brevis

**Insertion of origin:** the middle third of the lateral aspect of the fibula.

**Terminal insertion:** tuberosity of the fifth metatarsal bone.

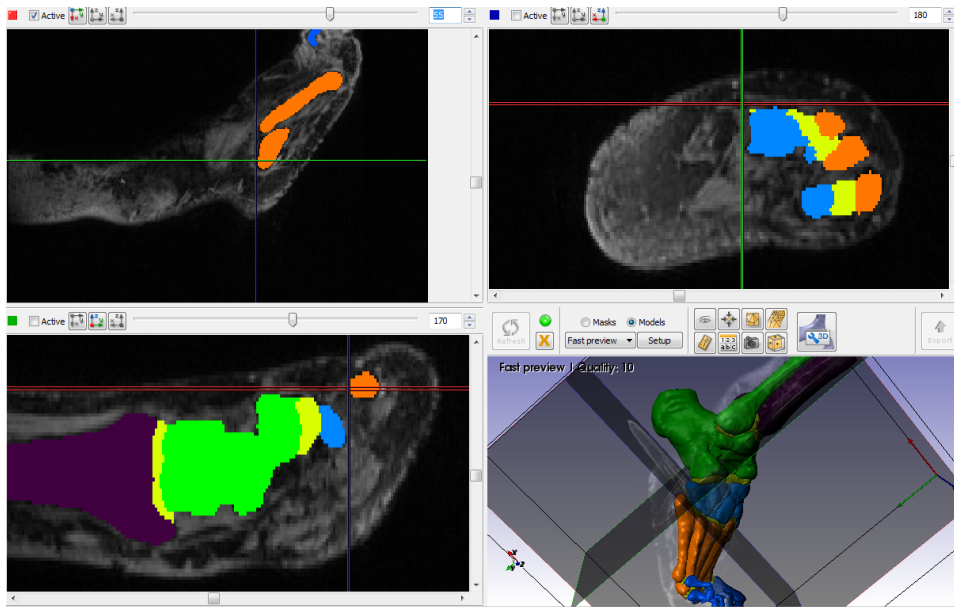


Figure A.14 – Insertions of the Peroneus Brevis on the tuberosity of the fifth metatarsal bone. (ScanIP)

## Soleus

**Insertion of origin:** from the head and the posterior face of the fibula, from the line of the soleus muscle of the posterior face of the tibia and from the fibrous archway stretched between the head of the fibula and the line of the soleus.

**Terminal insertion:** the tuberosity of the calcaneus via the Achilles tendon.



## Gastrocnemius

**Insertion of origin:** from the lateral and medial epicondyle and from the posterior surface of the medial condyle of the femur.

**Terminal insertion:** the tuberosity of the calcaneus via the Achilles tendon.



## A.1. Control of muscle insertions

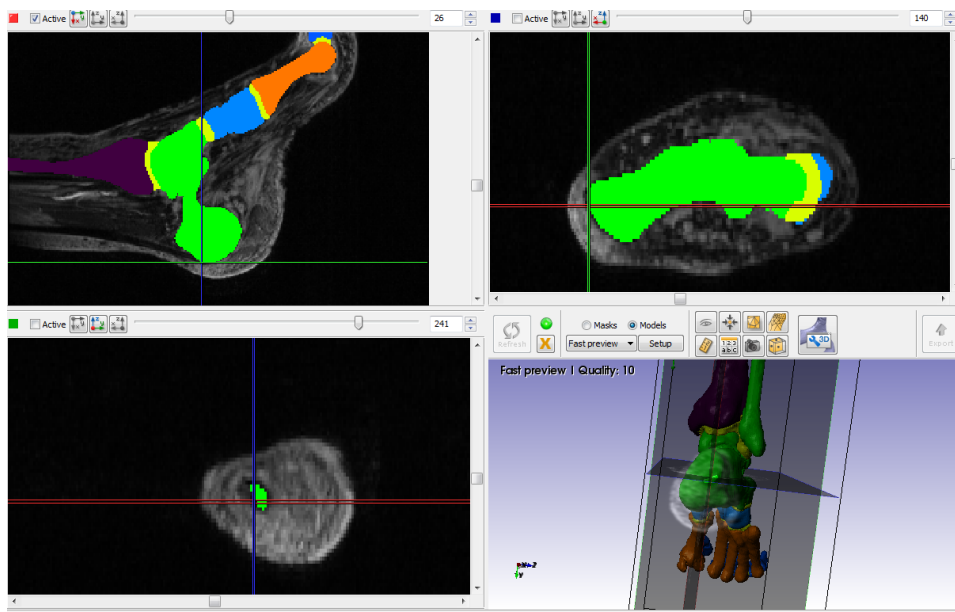


Figure A.15 – Insertion of the Achilles tendon on tuberosity of the calcaneus. (ScanIP)

## Tibialis Posterior

**Insertion of origin:** from the posterior face of the tibia, below the origin of the soleus, the interosseous membrane and the medial aspect of the fibula.

**Terminal insertion:** navicular tuberosity and the plantar surface of the three cuneiform bones.

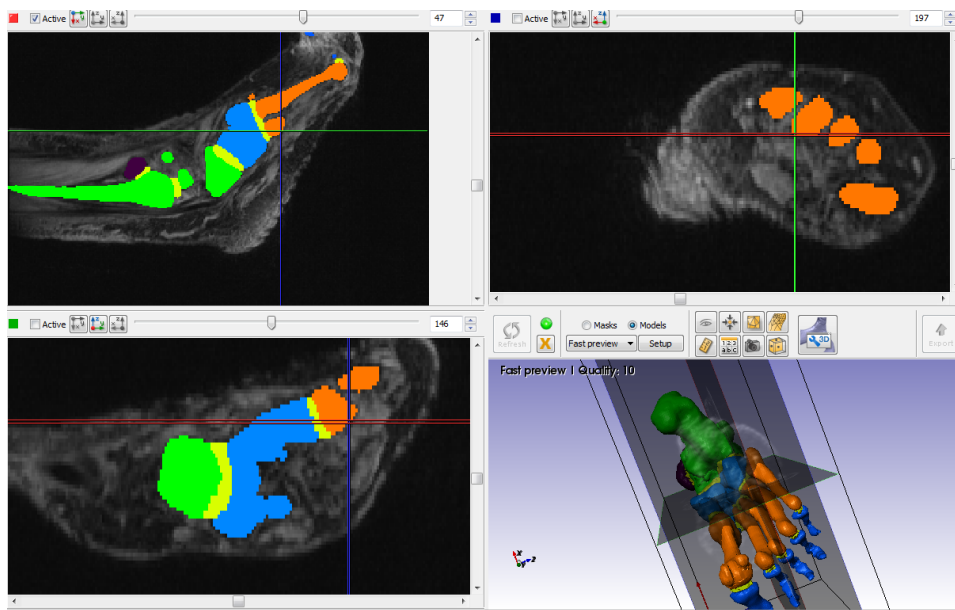
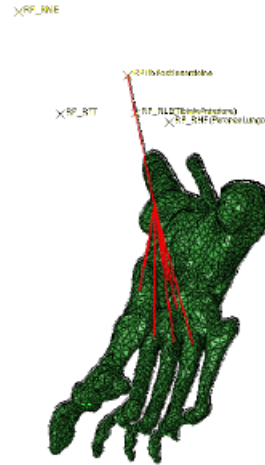


Figure A.16 – Insertion of the Tibialis Posterior on the fourth metatarsal bone. (ScanIP)

## A.1. Control of muscle insertions

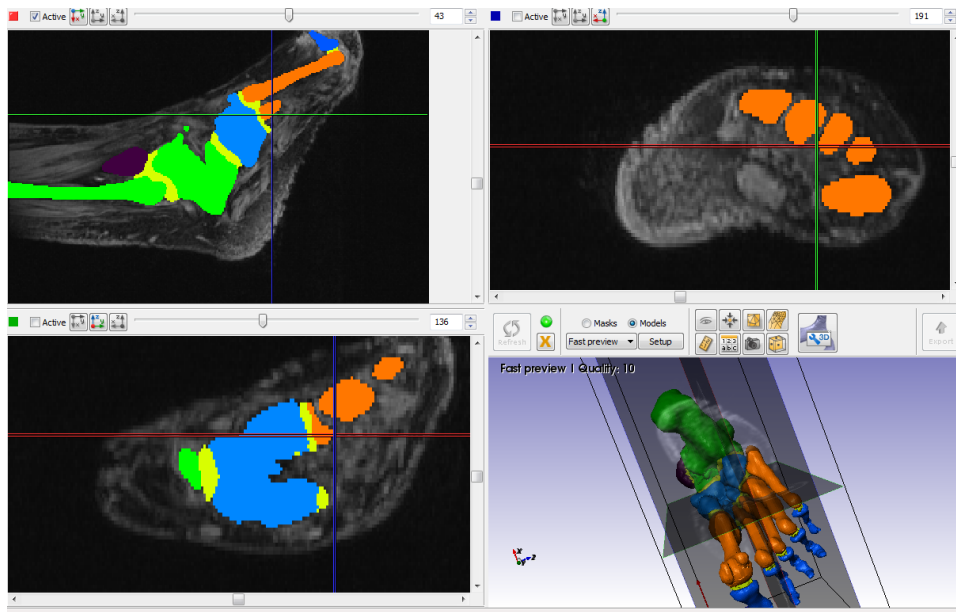


Figure A.17 – Insertion of the Tibialis Posterior on the third metatarsal bone. (ScanIP)

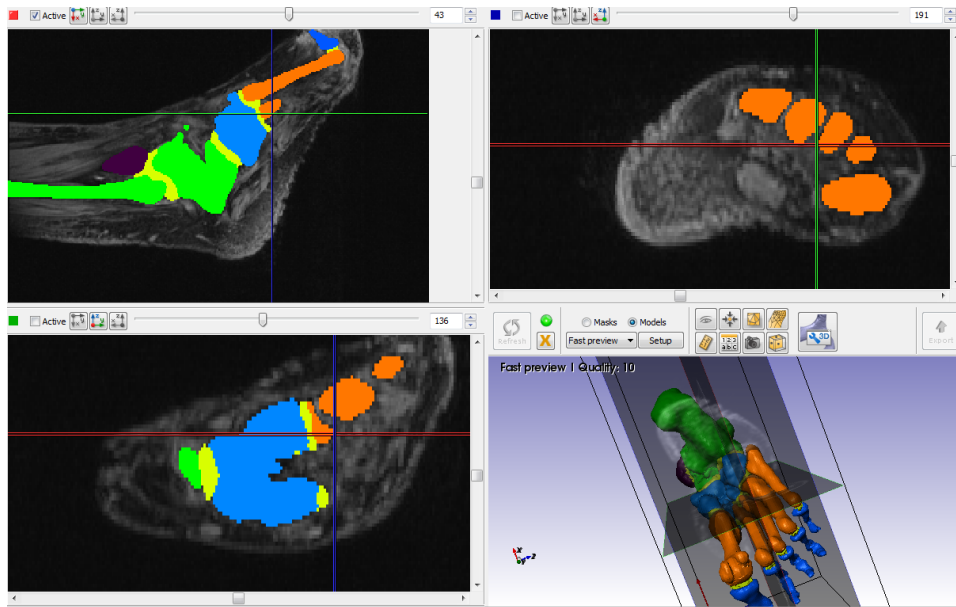


Figure A.18 – Insertion of the Tibialis Posterior on the second metatarsal bone. (ScanIP)

## Appendix A. Appendix

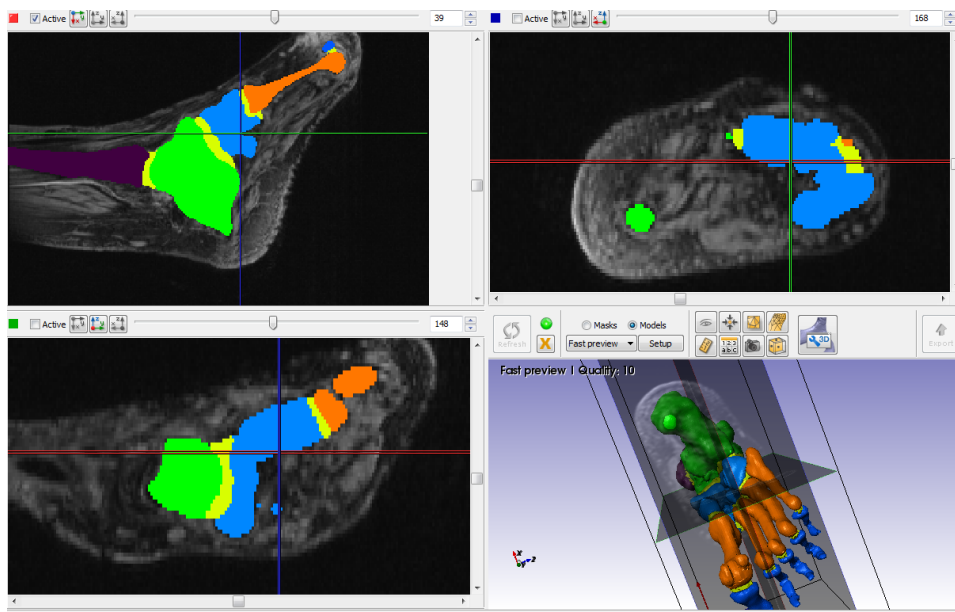


Figure A.19 – Insertion of the Tibialis Posterior on the third cuneiform bone. (ScanIP)

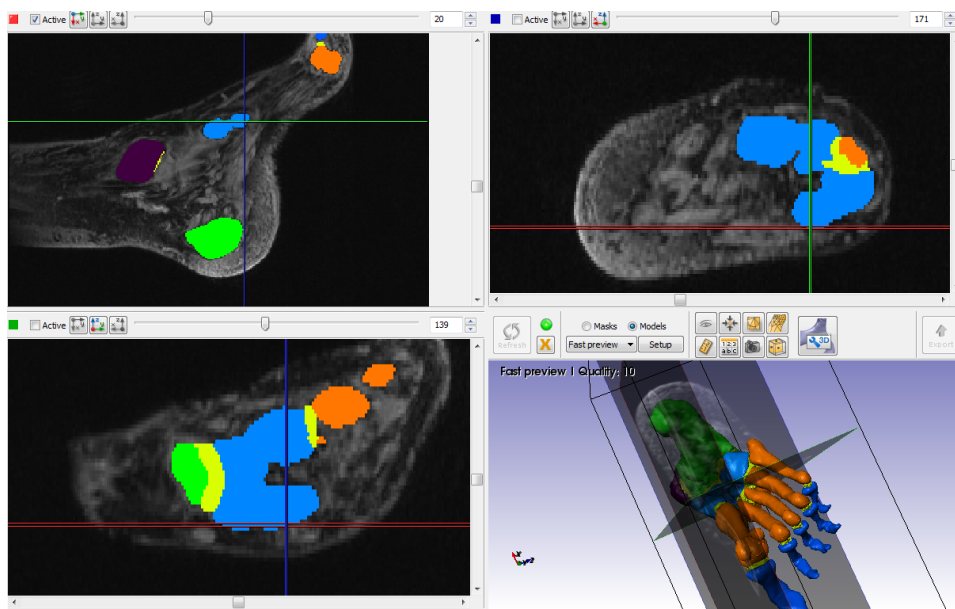


Figure A.20 – Insertion of the Tibialis Posterior on the second cuneiform bone. (ScanIP)



## A.1. Control of muscle insertions

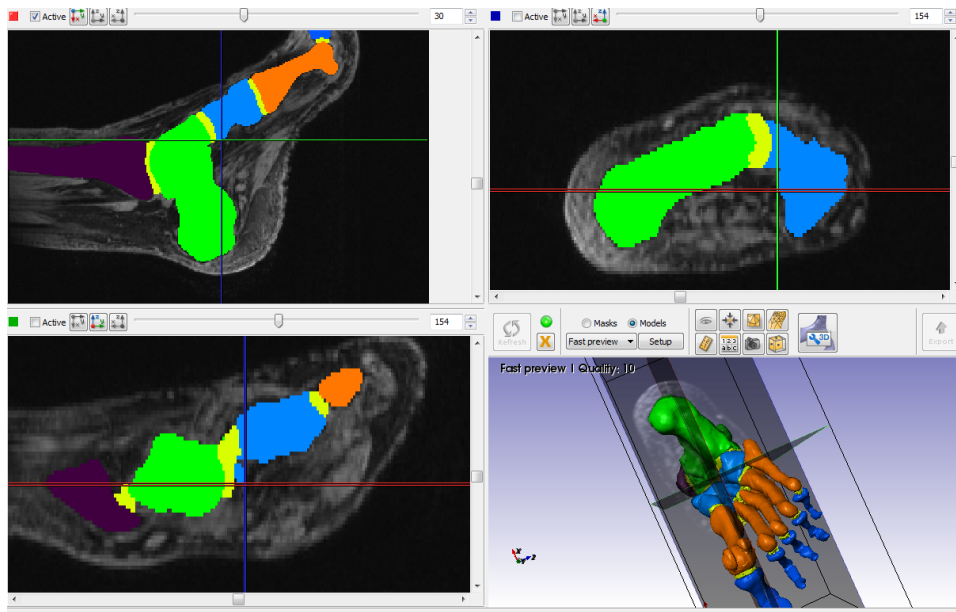


Figure A.21 – Insertion of the Tibialis Posterior on the first cuneiform bone. (ScanIP)

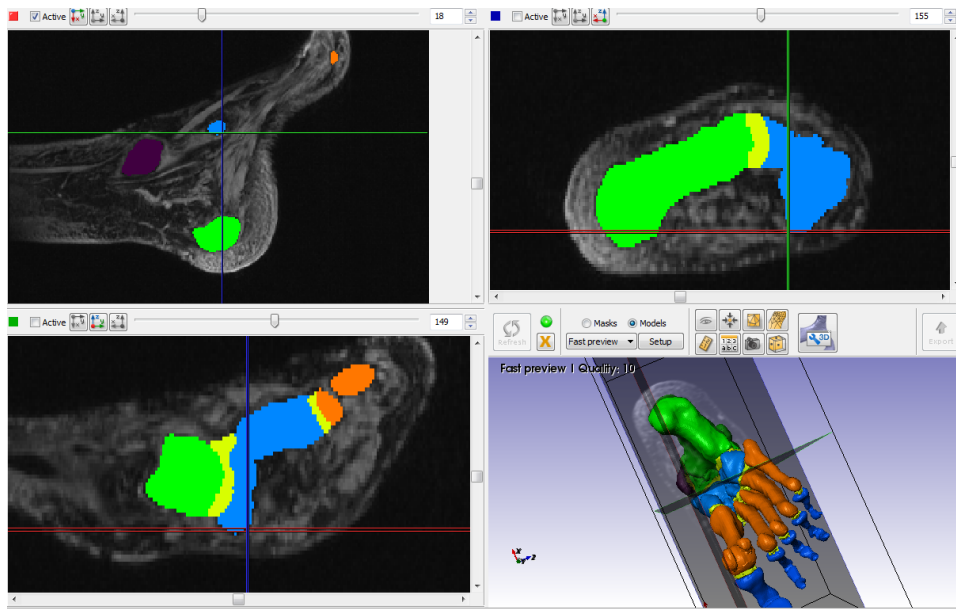


Figure A.22 – Insertion of the Tibialis Posterior on the navicular bone. (ScanIP)

## Plantar fascia

**Insertion of origin:** tuberosity of the heel.

**Terminal insertion:** on the toes at the metatarsal joints.

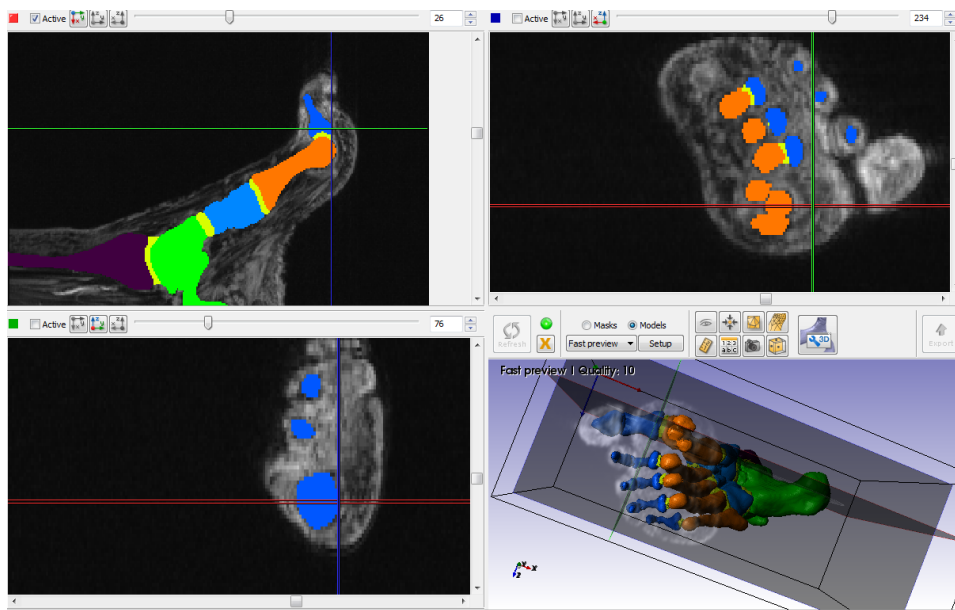


Figure A.23 – Insertion of the plantar fascia on the first phalanx. (ScanIP)

## A.1. Control of muscle insertions

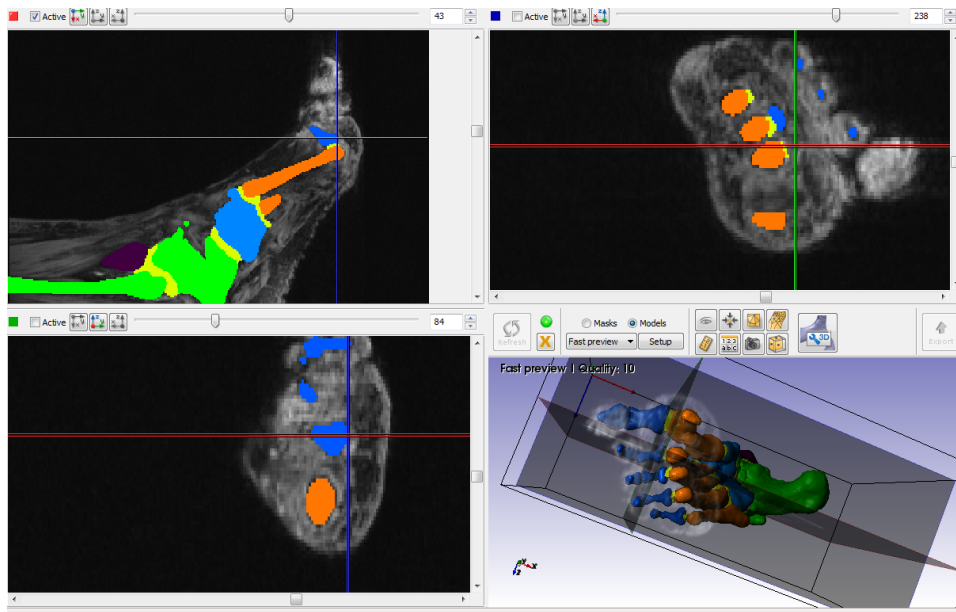


Figure A.24 – Insertion of the plantar fascia on the second phalanx. (ScanIP)

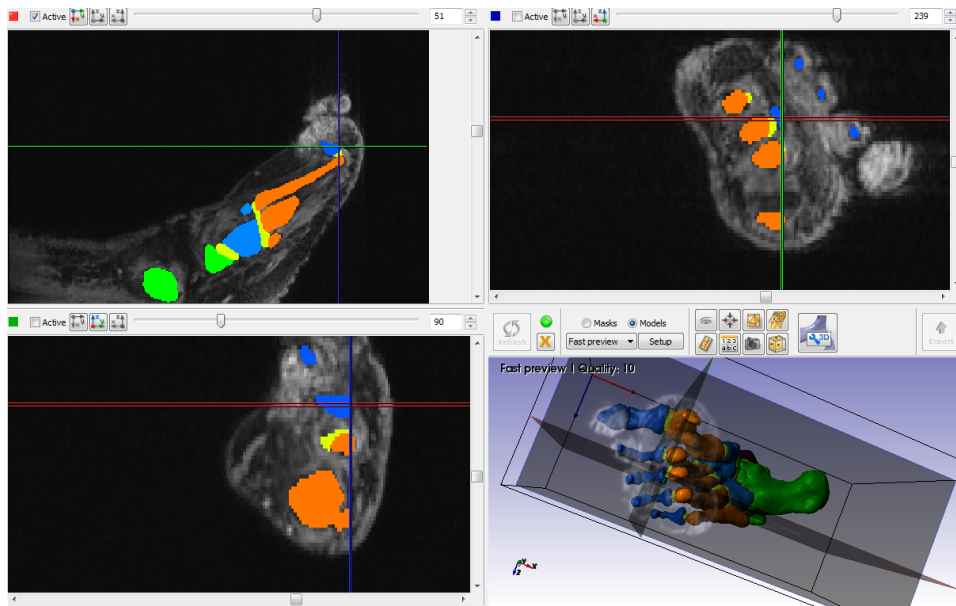


Figure A.25 – Insertion of the plantar fascia on the third phalanx. (ScanIP)

## Appendix A. Appendix

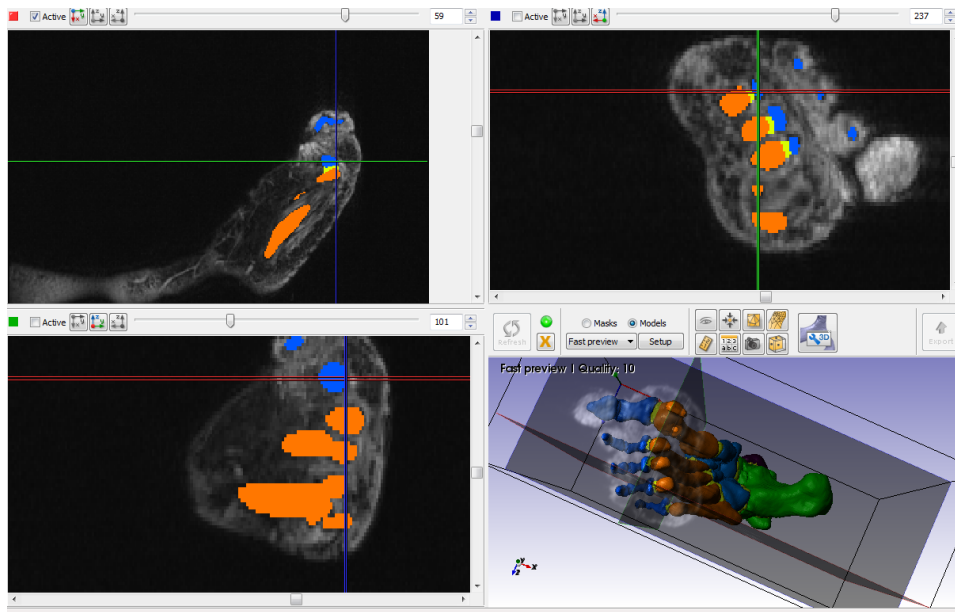


Figure A.26 – Insertion of the plantar fascia on the fourth phalanx. (ScanIP)

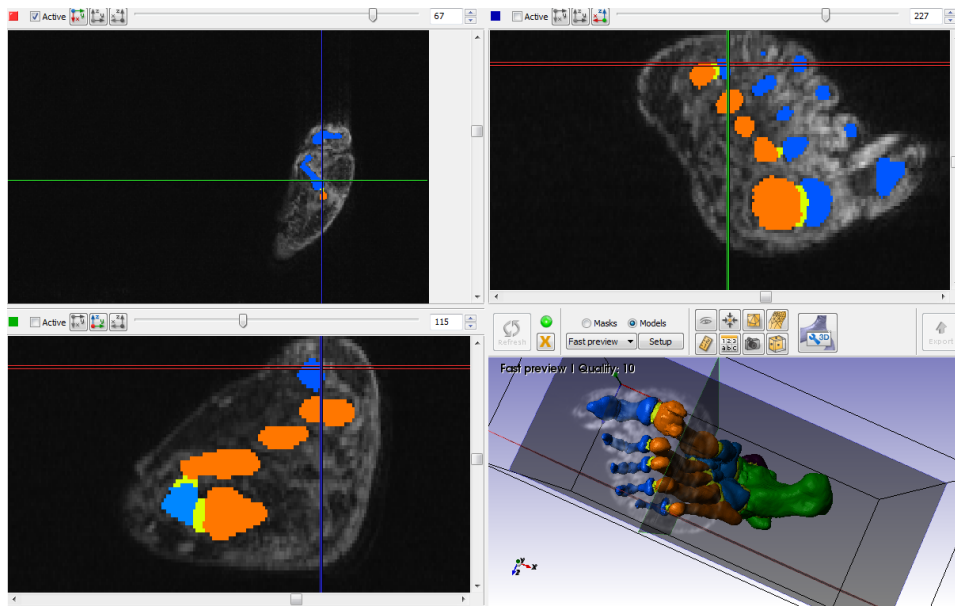


Figure A.27 – Insertion of the plantar fascia on the fifth phalanx. (ScanIP)

## A.1. Control of muscle insertions

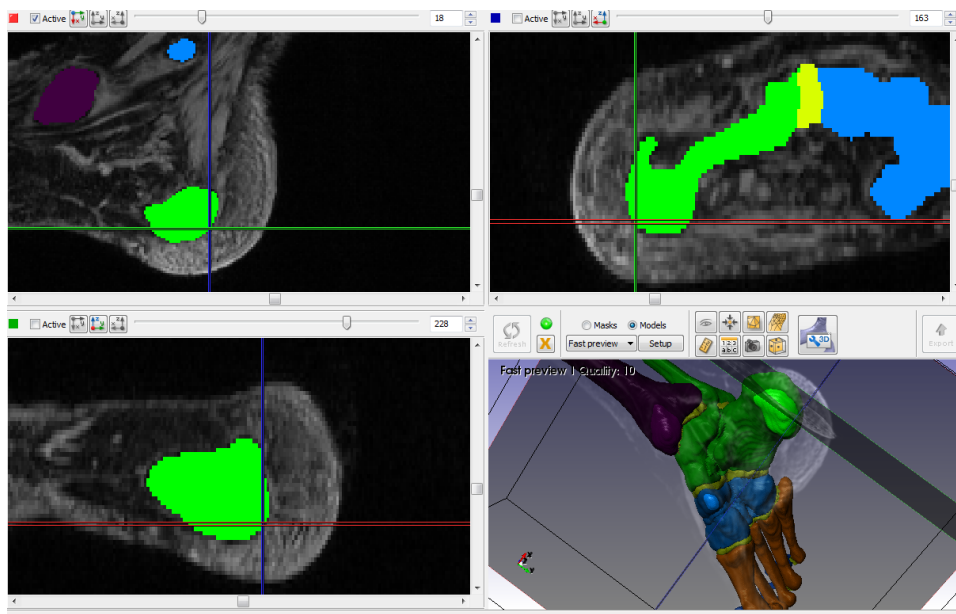
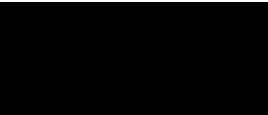


Figure A.28 – Insertion of the plantar fascia on the tuberosity of the calcaneus. (ScanIP)



- 
- [1] “Opensim user’s guide.”
- [2] A. H. Abdul Razak, A. Zayegh, R. K. Begg, and Y. Wahab, “Foot plantar pressure measurement system: a review,” *Sensors*, vol. 12, no. 7, pp. 9884–9912, 2012.
- [3] E. J. C. Dawe and J. Davis, “(vi) Anatomy and biomechanics of the foot and ankle,” *Orthopaedics and Trauma*, vol. 25, pp. 279–286, Aug. 2011.
- [4] Domenico Fedele, *Diabete e malattie del metabolismo*. Pacini editore medicina, 2009.
- [5] Princil., *Principles of Diabetes Mellitus*, DOI 10.1007/978-0-387-09841-8\_23, 357 C Springer Science+Business Media, LLC 2010 *ple of Diabetes Mellitus*. Poretsky.
- [6] D. G. Thelen and F. C. Anderson, “Using computed muscle control to generate forward dynamic simulations of human walking from experimental data,” *Journal of biomechanics*, vol. 39, no. 6, pp. 1107–1115, 2006.
- [7] J. T.-M. Cheung and M. Zhang, “A 3-dimensional finite element model of the human foot and ankle for insole design,” *Archives of Physical Medicine and Rehabilitation*, vol. 86, pp. 353–358, Feb. 2005.
- [8] A. Guiotto, A. Scarton, Z. Sawacha, G. Guarneri, A. Avogaro, and C. Cobelli, “Gait analysis driven 2d finite element model of the neuropathic hindfoot,” *Journal of Mechanics in Medicine and Biology*, p. 1650012, Mar. 2015.
- [9] A. Agić, V. Nikolić, B. Mijović, and U. Reischl, “Biomechanical model of the diabetic foot,” *Collegium Antropologicum*, vol. 32, pp. 881–886, Sept. 2008.
- [10] A. Erdemir, J. J. Saucerman, D. Lemmon, B. Loppnow, B. Turso, J. S. Ulbrecht, and P. R. Cavanagh, “Local plantar pressure relief in therapeutic footwear: design guidelines from finite element models,” *Journal of Biomechanics*, vol. 38, pp. 1798–1806, Sept. 2005.

## Bibliography

---

- [11] T.-X. Qiu, E.-C. Teo, Y.-B. Yan, and W. Lei, "Finite element modeling of a 3d coupled foot-boot model," *Medical Engineering & Physics*, June 2011.
- [12] J. W. Fernandez, M. Z. Ul Haque, P. J. Hunter, and K. Mithraratne, "Mechanics of the foot Part 1: a continuum framework for evaluating soft tissue stiffening in the pathologic foot," *International Journal for Numerical Methods in Biomedical Engineering*, vol. 28, pp. 1056–1070, Oct. 2012.
- [13] A. Guiotto, Z. Sawacha, G. Guarneri, A. Avogaro, and C. Cobelli, "3d finite element model of the diabetic neuropathic foot: a gait analysis driven approach," *Journal of Biomechanics*, vol. 47, pp. 3064–3071, Sept. 2014.
- [14] J. Perry and J. M. Burnfield, *Gait Analysis: Normal and Pathological Function*. SLACK, 2010.
- [15] T. Stöckel, R. Jacksteit, M. Behrens, R. Skripitz, R. Bader, and A. Mau-Moeller, "The mental representation of the human gait in young and older adults," *Frontiers in psychology*, vol. 6, 2015.
- [16] "Bertec corporation. Force plate user manual. Columbus OH, USA.."
- [17] "Imago s.n.c."
- [18] S. Del Din, E. Carraro, Z. Sawacha, A. Guiotto, L. Bonaldo, S. Masiero, and C. Cobelli, "Impaired gait in ankylosing spondylitis," *Medical & Biological Engineering & Computing*, vol. 49, pp. 801–809, Jan. 2011.
- [19] Z. Sawacha, G. Cristoferi, G. Guarneri, S. Corazza, G. Donà, P. Denti, A. Facchinetti, A. Avogaro, and C. Cobelli, "Characterizing multisegment foot kinematics during gait in diabetic foot patients," *Journal of NeuroEngineering and Rehabilitation*, vol. 6, pp. 37–37, 2009.
- [20] "Foot sub-segments." Accessed: 2016-01-12.
- [21] "Foot motions." Accessed: 2016-01-12.
- [22] F. H. Netter, *Atlas of human anatomy*. Elsevier Health Sciences, 2014.
- [23] "International diabetes federation, a letter from the chair of the idf diabetes atlas committee, 6th edition." Accessed: 2016-01-12.
- [24] "Piede diabetico." <http://lnx.endocrinologiaoggi.it/tag/piede-diabetico/>.



- [25] L. C. Rogers, R. G. Frykberg, D. G. Armstrong, A. J. M. Boulton, M. Edmonds, G. H. Van, A. Hartemann, F. Game, W. Jeffcoate, A. Jirkovska, E. Jude, S. Morbach, W. B. Morrison, M. Pinzur, D. Pitocco, L. Sanders, D. K. Wukich, and L. Uccioli, "The Charcot Foot in Diabetes," *Diabetes Care*, vol. 34, pp. 2123–2129, Sept. 2011.
- [26] J. W. Klaesner, M. K. Hastings, D. Zou, C. Lewis, and M. J. Mueller, "Plantar tissue stiffness in patients with diabetes mellitus and peripheral neuropathy," *Archives of Physical Medicine and Rehabilitation*, vol. 83, pp. 1796–1801, Dec. 2002.
- [27] C. H. M. van Schie, "A review of the biomechanics of the diabetic foot," *The International Journal of Lower Extremity Wounds*, vol. 4, pp. 160–170, Sept. 2005.
- [28] V. M. Zatsiorsky, *Kinetics of human motion*. Human Kinetics, 2002.
- [29] D. A. Winter, *Biomechanics and motor control of human movement*. John Wiley & Sons, 2009.
- [30] H. J. Chiel and R. D. Beer, "The brain has a body: adaptive behavior emerges from interactions of nervous system, body and environment," *Trends in neurosciences*, vol. 20, no. 12, pp. 553–557, 1997.
- [31] E. R. Kandel, J. H. Schwartz, T. M. Jessell, *et al.*, *Principles of neural science*, vol. 4. McGraw-Hill New York, 2000.
- [32] E. Bizzi and V. C. Cheung, "The neural origin of muscle synergies," *Frontiers in computational neuroscience*, vol. 7, 2013.
- [33] A. Huxley, "The origin of force in skeletal muscle," *Energy Transformation in Biological Systems*, vol. 992, p. 271, 2009.
- [34] F. E. Zajac, "Muscle coordination of movement: a perspective," *Journal of Biomechanics*, vol. 26, pp. 109–124, 1993.
- [35] V. C. Cheung, A. d'Avella, and E. Bizzi, "Adjustments of motor pattern for load compensation via modulated activations of muscle synergies during natural behaviors," *Journal of neurophysiology*, vol. 101, no. 3, pp. 1235–1257, 2009.
- [36] R. Balasubramaniam and A. G. Feldman, "Guiding movements without redundancy problems," in *Coordination dynamics: Issues and trends*, pp. 155–176, Springer, 2004.
- [37] N. A. Bernstein, "The co-ordination and regulation of movements," 1967.
- [38] P. V. Komi, "Relevance of in vivo force measurements to human biomechanics," *Journal of Biomechanics*, vol. 23, pp. 23–34, 1990.

## Bibliography

---

- [39] T. S. Buchanan, D. G. Lloyd, K. Manal, and T. F. Besier, "Neuromusculoskeletal modeling: estimation of muscle forces and joint moments and movements from measurements of neural command," *Journal of applied biomechanics*, vol. 20, no. 4, p. 367, 2004.
- [40] A. Erdemir, S. McLean, W. Herzog, and A. J. van den Bogert, "Model-based estimation of muscle forces exerted during movements," *Clinical Biomechanics*, vol. 22, no. 2, pp. 131–154, 2007.
- [41] F. C. Anderson and M. G. Pandy, "Static and dynamic optimization solutions for gait are practically equivalent," *Journal of biomechanics*, vol. 34, no. 2, pp. 153–161, 2001.
- [42] S. Heintz and E. M. Gutierrez-Farewik, "Static optimization of muscle forces during gait in comparison to emg-to-force processing approach," *Gait & posture*, vol. 26, no. 2, pp. 279–288, 2007.
- [43] B. Prilutsky, W. Herzog, and T. Allinger, "Forces of individual cat ankle extensor muscles during locomotion predicted using static optimization," *Journal of biomechanics*, vol. 30, no. 10, pp. 1025–1033, 1997.
- [44] R. T. Raikova and B. I. Prilutsky, "Sensitivity of predicted muscle forces to parameters of the optimization-based human leg model revealed by analytical and numerical analyses," *Journal of Biomechanics*, vol. 34, no. 10, pp. 1243–1255, 2001.
- [45] D. G. Lloyd and T. S. Buchanan, "Strategies of muscular support of varus and valgus isometric loads at the human knee," *Journal of biomechanics*, vol. 34, no. 10, pp. 1257–1267, 2001.
- [46] A. Jinha, R. Ait-Haddou, and W. Herzog, "Predictions of co-contraction depend critically on degrees-of-freedom in the musculoskeletal model," *Journal of biomechanics*, vol. 39, no. 6, pp. 1145–1152, 2006.
- [47] J. Van Dieen and I. Kingma, "Effects of antagonistic co-contraction on differences between electromyography based and optimization based estimates of spinal forces," *Ergonomics*, vol. 48, no. 4, pp. 411–426, 2005.
- [48] T. S. Buchanan, D. G. Lloyd, K. Manal, and T. F. Besier, "Estimation of muscle forces and joint moments using a forward-inverse dynamics model," *Medicine and Science in Sports and exercise*, vol. 37, no. 11, p. 1911, 2005.
- [49] M. Millard, J. McPhee, and E. Kubica, "Multi-step forward dynamic gait simulation," in *Multibody Dynamics*, pp. 25–43, Springer, 2009.

- [50] M. Reaz, M. Hussain, and F. Mohd-Yasin, "Techniques of emg signal analysis: detection, processing, classification and applications," *Biological procedures online*, vol. 8, no. 1, pp. 11–35, 2006.
- [51] C. Pizzolato, D. G. Lloyd, M. Sartori, E. Ceseracciu, T. F. Besier, B. J. Fregly, and M. Reggiani, "Ceinms: A toolbox to investigate the influence of different neural control solutions on the prediction of muscle excitation and joint moments during dynamic motor tasks," *Journal of biomechanics*, vol. 48, no. 14, pp. 3929–3936, 2015.
- [52] P. E. Di Prampero, A. Cappello, and A. Cappozzo, *Bioingegneria della postura e del movimento*. Patron, 2003.
- [53] S. L. Delp, F. C. Anderson, A. S. Arnold, P. Loan, A. Habib, C. T. John, E. Guendelman, and D. G. Thelen, "OpenSim: open-source software to create and analyze dynamic simulations of movement," *IEEE transactions on bio-medical engineering*, vol. 54, pp. 1940–1950, Nov. 2007.
- [54] M. Damsgaard, J. Rasmussen, S. T. Christensen, E. Surma, and M. de Zee, "Analysis of musculoskeletal systems in the anybody modeling system," *Simulation Modelling Practice and Theory*, vol. 14, no. 8, pp. 1100–1111, 2006.
- [55] M. Damsgaard, S. T. Christensen, and J. Rasmussen, "An efficient numerical algorithm for solving the muscle recruitment problem in inverse dynamics simulations," in *International Society of Biomechanics, XVIIIth Congress, July 8-13, 2001, Zurich, Switzerland*, 2001.
- [56] S. L. Delp, J. P. Loan, M. G. Hoy, F. E. Zajac, E. L. Topp, and J. M. Rosen, "An interactive graphics-based model of the lower extremity to study orthopaedic surgical procedures," *Biomedical Engineering, IEEE Transactions on*, vol. 37, no. 8, pp. 757–767, 1990.
- [57] A. Seth, "OpenSim: a musculoskeletal modeling and simulation framework for in silico investigations and exchange," 2011.
- [58] J. P. Hornak, "The basics of mri, 2008," URL <http://www.cis.rit.edu/htbooks/mri/index.html>, vol. 68, 2008.
- [59] P. Young, T. Beresford-West, S. Coward, B. Notarberardino, B. Walker, and A. Abdul-Aziz, "An efficient approach to converting three-dimensional image data into highly accurate computational models," *Philosophical Transactions of the Royal Society of London A: Mathematical, Physical and Engineering Sciences*, vol. 366, no. 1878, pp. 3155–3173, 2008.

## Bibliography

---

- [60] W. E. Lorensen and H. E. Cline, "Marching cubes: A high resolution 3d surface construction algorithm," in *ACM siggraph computer graphics*, vol. 21, pp. 163–169, ACM, 1987.
- [61] A. Malanthara and W. Gerstle, "Comparative study of unstructured meshes made of triangles and quadrilaterals," in *Proc. of 6th Intl. Meshing Roundtable*, pp. 437–447, Citeseer, 1997.
- [62] W.-M. Chen, T. Lee, P. V.-S. Lee, J. W. Lee, and S.-J. Lee, "Effects of internal stress concentrations in plantar soft-tissue—A preliminary three-dimensional finite element analysis," *Medical Engineering & Physics*, vol. 32, pp. 324–331, May 2010.
- [63] J. T.-M. Cheung and M. Zhang, "Parametric design of pressure-relieving foot orthosis using statistics-based finite element method," *Medical Engineering & Physics*, vol. 30, pp. 269–277, Apr. 2008.
- [64] X.-Q. Dai, Y. Li, M. Zhang, and J. T.-M. Cheung, "Effect of sock on biomechanical responses of foot during walking," *Clinical Biomechanics*, vol. 21, pp. 314–321, Mar. 2006.
- [65] J. T.-M. Cheung and M. Zhang, "A 3-dimensional finite element model of the human foot and ankle for insole design," *Archives of Physical Medicine and Rehabilitation*, vol. 86, pp. 353–358, Feb. 2005.
- [66] A. Gefen, M. Megido-Ravid, Y. Itzchak, and M. Arcan, "Biomechanical analysis of the three-dimensional foot structure during gait: a basic tool for clinical applications," *Journal of Biomechanical Engineering*, vol. 122, pp. 630–639, Dec. 2000.
- [67] P. Antunes, G. R. Dias, A. Coelho, F. Rebelo, and T. Pereira, "Nonlinear 3d foot fea modeling from ct scan medical images," 2011.
- [68] S. C. Tadepalli, A. Erdemir, and P. R. Cavanagh, "Comparison of hexahedral and tetrahedral elements in finite element analysis of the foot and footwear," *Journal of Biomechanics*, vol. 44, pp. 2337–2343, Aug. 2011.
- [69] N. M. Grosland, K. H. Shivanna, V. A. Magnotta, N. A. Kallemeyn, N. A. DeVries, S. C. Tadepalli, and C. Lisle, "Ia-femesh: An open-source, interactive, multiblock approach to anatomic finite element model development," *Computer methods and programs in biomedicine*, vol. 94, no. 1, pp. 96–107, 2009.

- [70] S. Banks, W. A. Hodge, *et al.*, “Accurate measurement of three-dimensional knee replacement kinematics using single-plane fluoroscopy,” *Biomedical Engineering, IEEE Transactions on*, vol. 43, no. 6, pp. 638–649, 1996.
- [71] A. Documentation, “Abaqus analysis user’s manual,” *Materials. Other plasticity models. Concrete*, 2010.
- [72] D. R. Carter and W. C. Hayes, “The compressive behavior of bone as a two-phase porous structure,” *The Journal of Bone & Joint Surgery*, vol. 59, no. 7, pp. 954–962, 1977.
- [73] R. L. Actis, L. B. Ventura, K. E. Smith, P. K. Commean, D. J. Lott, T. K. Pilgram, and M. J. Mueller, “Numerical simulation of the plantar pressure distribution in the diabetic foot during the push-off stance,” *Medical & Biological Engineering & Computing*, vol. 44, pp. 653–663, Aug. 2006.
- [74] S. Goske, A. Erdemir, M. Petre, S. Budhabhatti, and P. R. Cavanagh, “Reduction of plantar heel pressures: Insole design using finite element analysis,” *Journal of Biomechanics*, vol. 39, no. 13, pp. 2363–2370, 2006.
- [75] W. P. Chen, F. T. Tang, and C. W. Ju, “Stress distribution of the foot during mid-stance to push-off in barefoot gait: a 3-D finite element analysis,” *Clinical Biomechanics (Bristol, Avon)*, vol. 16, pp. 614–620, Aug. 2001.
- [76] R. Soames, “Foot pressure patterns during gait,” *Journal of biomedical engineering*, vol. 7, no. 2, pp. 120–126, 1985.
- [77] M. Brown, S. Rudicel, and A. Esquenazi, “Measurement of dynamic pressures at the shoe-foot interface during normal walking with various foot orthoses using the fscan system,” *Foot & ankle international*, vol. 17, no. 3, pp. 152–156, 1996.
- [78] W.-M. Chen, T. Lee, P. V.-S. Lee, J. W. Lee, and S.-J. Lee, “Effects of internal stress concentrations in plantar soft-tissue—A preliminary three-dimensional finite element analysis,” *Medical Engineering & Physics*, vol. 32, pp. 324–331, May 2010.
- [79] F. Wei, S. C. Hunley, J. W. Powell, and R. C. Haut, “Development and validation of a computational model to study the effect of foot constraint on ankle injury due to external rotation,” *Annals of Biomedical Engineering*, vol. 39, pp. 756–765, Feb. 2011.
- [80] M. R. Colville, R. A. Marder, J. J. Boyle, and B. Zarins, “Strain measurement in lateral ankle ligaments,” *The American journal of sports medicine*, vol. 18, no. 2, pp. 196–200, 1990.

## Bibliography

---

- [81] F. Wei, M. R. Villwock, E. G. Meyer, J. W. Powell, and R. C. Haut, "A biomechanical investigation of ankle injury under excessive external foot rotation in the human cadaver," *Journal of biomechanical engineering*, vol. 132, no. 9, p. 091001, 2010.
- [82] K. Tao, D. Wang, C. Wang, X. Wang, A. Liu, C. J. Nester, and D. Howard, "An in vivo experimental validation of a computational model of human foot," *Journal of Bionic Engineering*, vol. 6, no. 4, pp. 387–397, 2009.
- [83] A. E. Anderson, B. J. Ellis, and J. A. Weiss, "Verification, validation and sensitivity studies in computational biomechanics," *Computer methods in biomechanics and biomedical engineering*, vol. 10, no. 3, pp. 171–184, 2007.
- [84] K. Patil, L. Braak, and A. Huson, "Stresses in a simplified two dimensional model of a normal foot—a preliminary analysis," *Mechanics research communications*, vol. 20, no. 1, pp. 1–7, 1993.
- [85] D. Lemmon, T. Shiang, A. Hashmi, J. S. Ulbrecht, and P. R. Cavanagh, "The effect of insoles in therapeutic footwear—A finite element approach," *Journal of Biomechanics*, vol. 30, no. 6, pp. 615–620, 1997.
- [86] J. P. Halloran, M. Ackermann, A. Erdemir, and A. J. van den Bogert, "Concurrent musculoskeletal dynamics and finite element analysis predicts altered gait patterns to reduce foot tissue loading," *Journal of Biomechanics*, vol. 43, pp. 2810–2815, Oct. 2010.
- [87] S. P. Budhabhatti, A. Erdemir, M. Petre, J. Sferra, B. Donley, and P. R. Cavanagh, "Finite element modeling of the first ray of the foot: a tool for the design of interventions," *Journal of Biomechanical Engineering*, vol. 129, pp. 750–756, Oct. 2007.
- [88] T.-M. Chu, N. P. Reddy, and J. Padovan, "Stress distribution in the ankle-foot orthosis used to correct pathological gait," *Journal of rehabilitation research and development*, vol. 32, pp. 349–360, 1995.
- [89] W.-P. Chen, C.-W. Ju, and F.-T. Tang, "Effects of total contact insoles on the plantar stress redistribution: a finite element analysis," *Clinical Biomechanics (Bristol, Avon)*, vol. 18, pp. S17–24, July 2003.
- [90] J. T.-M. Cheung and B. M. Nigg, "Clinical applications of computational simulation of foot and ankle," *Sport-Orthopädie-Sport-Traumatologie-Sports Orthopaedics and Traumatology*, vol. 23, no. 4, pp. 264–271, 2008.

- [91] Y. Gu, X. Ren, J. Li, M. Lake, Q. Zhang, and Y. Zeng, "Computer simulation of stress distribution in the metatarsals at different inversion landing angles using the finite element method," *International orthopaedics*, vol. 34, no. 5, pp. 669–676, 2010.
- [92] J. M. Iaquinto and J. S. Wayne, "Computational model of the lower leg and foot/ankle complex: application to arch stability," *Journal of Biomechanical Engineering*, vol. 132, p. 021009, Feb. 2010.
- [93] Z.-h. Qian, L. Ren, Y. Ding, and L. Ren, "A three-dimensional musculoskeletal model of the human foot complex using finite element method," *ISB 2011-Bruxelles*, 2011.
- [94] G. D. PJ Antunes, "2. Nonlinear 3d foot FEA modeling from CT scan medical images," *Report paper*, 2008.
- [95] A. N. Natali, C. G. Fontanella, E. L. Carniel, and M. Young, "Biomechanical behaviour of heel pad tissue: experimental testing, constitutive formulation, and numerical modelling," *Proceedings of the Institution of Mechanical Engineers. Part H, Journal of Engineering in Medicine*, vol. 225, pp. 449–459, May 2011.
- [96] W.-M. Chen, J. Park, S.-B. Park, V. P.-W. Shim, and T. Lee, "Role of gastrocnemius-soleus muscle in forefoot force transmission at heel rise - A 3d finite element analysis," *Journal of Biomechanics*, vol. 45, pp. 1783–1789, June 2012.
- [97] M. J. Ackerman, "The visible human project: a resource for education.," *Academic Medicine*, vol. 74, no. 6, pp. 667–70, 1999.
- [98] J. Perry *et al.*, "Observational gait analysis handbook," *The Pathokinesiology Service and The Physical Therapy Department of Rancho Los Amigos Medical Center*, 1989.
- [99] M. Riberto, R. Liporaci, F. Vieira, and J. Volpon, "Setting up a human motion analysis laboratory: Camera positioning for kinematic recording of gait," *Int J Phys Med Rehabil*, vol. 1, no. 131, p. 2, 2013.
- [100] Z. Sawacha, G. Guarneri, G. Cristoferi, A. Guiotto, A. Avogaro, and C. Cobelli, "Integrated kinematics-kinetics-plantar pressure data analysis: a useful tool for characterizing diabetic foot biomechanics," *Gait & Posture*, vol. 36, pp. 20–26, May 2012.
- [101] R. B. Davis, S. Ounpuu, D. Tyburski, and J. R. Gage, "A gait analysis data collection and reduction technique," *Human movement science*, vol. 10, no. 5, pp. 575–587, 1991.

## Bibliography

---

- [102] A. Cappozzo, F. Catani, U. Della Croce, and A. Leardini, "Position and orientation in space of bones during movement: anatomical frame definition and determination," *Clinical Biomechanics*, vol. 10, pp. 171–178, June 1995.
- [103] A. Leardini, Z. Sawacha, G. Paolini, S. Ingrosso, R. Nativio, and M. G. Benedetti, "A new anatomically based protocol for gait analysis in children," *Gait & Posture*, vol. 26, pp. 560–571, Oct. 2007.
- [104] M. Harrington, A. Zavatsky, S. Lawson, Z. Yuan, and T. Theologis, "Prediction of the hip joint centre in adults, children, and patients with cerebral palsy based on magnetic resonance imaging," *Journal of biomechanics*, vol. 40, no. 3, pp. 595–602, 2007.
- [105] A. Leardini, A. Cappozzo, F. Catani, S. Toksvig-Larsen, A. Petitto, V. Sforza, G. Casanelli, and S. Giannini, "Validation of a functional method for the estimation of hip joint centre location," *Journal of biomechanics*, vol. 32, no. 1, pp. 99–103, 1999.
- [106] L. Uccioli, A. Caselli, C. Giacomozzi, V. Macellari, L. Giurato, L. Lardieri, and G. Menzinger, "Pattern of abnormal tangential forces in the diabetic neuropathic foot," *Clinical Biomechanics*, vol. 16, no. 5, pp. 446–454, 2001.
- [107] D. E. Lackey and J. M. Olefsky, "Regulation of metabolism by the innate immune system," *Nature Reviews Endocrinology*, vol. advance online publication, Nov. 2015.
- [108] R. A. DeFronzo and M. Abdul-Ghani, "Assessment and Treatment of Cardiovascular Risk in Prediabetes: Impaired Glucose Tolerance and Impaired Fasting Glucose," *The American Journal of Cardiology*, vol. 108, pp. 3B–24B, Aug. 2011.
- [109] P. Hossain, B. Kavar, and M. El Nahas, "Obesity and Diabetes in the Developing World — A Growing Challenge," *New England Journal of Medicine*, vol. 356, pp. 213–215, Jan. 2007.
- [110] n. Costa, D. I. Conget, and R. Gomis, "Impaired Glucose Tolerance," *Treatments in Endocrinology*, vol. 1, pp. 205–210, Aug. 2012.
- [111] E. Adeghate, P. Schattner, and E. Dunn, "An update on the etiology and epidemiology of diabetes mellitus," *Annals of the New York Academy of Sciences*, vol. 1084, pp. 1–29, Nov. 2006.
- [112] A. D. A. . N. B. S. Alex, ria, and V. . 1-800-Diabetes, "Statistics About Diabetes."



- [113] O. Sacks, *The man who mistook his wife for a hat and other clinical tales*. New York: Summit Books, 1985.
- [114] J. W. Klaesner, M. K. Hastings, D. Zou, C. Lewis, and M. J. Mueller, "Plantar tissue stiffness in patients with diabetes mellitus and peripheral neuropathy," *Archives of Physical Medicine and Rehabilitation*, vol. 83, pp. 1796–1801, Dec. 2002.
- [115] K. S. Maluf and M. J. Mueller, "Comparison of physical activity and cumulative plantar tissue stress among subjects with and without diabetes mellitus and a history of recurrent plantar ulcers," *Clinical Biomechanics*, vol. 18, pp. 567–575, Aug. 2003.
- [116] S. C. Wu, V. R. Driver, J. S. Wrobel, and D. G. Armstrong, "Foot ulcers in the diabetic patient, prevention and treatment," *Vascular Health and Risk Management*, vol. 3, no. 1, pp. 65–76, 2007.
- [117] J. S. Wrobel and B. Najafi, "Diabetic Foot Biomechanics and Gait Dysfunction," *Journal of Diabetes Science and Technology*, vol. 4, pp. 833–845, July 2010.
- [118] C. Giacomozzi, V. Macellari, A. Leardini, and M. G. Benedetti, "Integrated pressure-force-kinematics measuring system for the characterisation of plantar foot loading during locomotion," *Medical & Biological Engineering & Computing*, vol. 38, pp. 156–163, Mar. 2000.
- [119] H. M. Rathur and A. J. M. Boulton, "The diabetic foot," *Clinics in Dermatology*, vol. 25, pp. 109–120, Feb. 2007.
- [120] Z. Sawacha, G. Gabriella, G. Cristoferi, A. Guiotto, A. Avogaro, and C. Cobelli, "Diabetic gait and posture abnormalities: a biomechanical investigation through three dimensional gait analysis," *Clinical Biomechanics (Bristol, Avon)*, vol. 24, pp. 722–728, Nov. 2009.
- [121] D. G. Armstrong, E. J. Peters, K. A. Athanasiou, and L. A. Lavery, "Is there a critical level of plantar foot pressure to identify patients at risk for neuropathic foot ulceration?," *The Journal of Foot and Ankle Surgery: Official Publication of the American College of Foot and Ankle Surgeons*, vol. 37, pp. 303–307, Aug. 1998.
- [122] W. Clayton Jr and T. A. Elasy, "A review of the pathophysiology, classification, and treatment of foot ulcers in diabetic patients," *Clinical diabetes*, vol. 27, no. 2, p. 52, 2009.

## Bibliography

---

- [123] I. Sacco and A. Amadio, "Influence of the diabetic neuropathy on the behavior of electromyographic and sensorial responses in treadmill gait," *Clinical Biomechanics*, vol. 18, no. 5, pp. 426–434, 2003.
- [124] I. C. Sacco, P. M. Akashi, and E. M. Hennig, "A comparison of lower limb emg and ground reaction forces between barefoot and shod gait in participants with diabetic neuropathic and healthy controls," *BMC musculoskeletal disorders*, vol. 11, no. 1, p. 24, 2010.
- [125] Z. Sawacha, G. Guarneri, A. Avogaro, and C. Cobelli, "A New Classification of Diabetic Gait Pattern Based on Cluster Analysis of Biomechanical Data," *Journal of Diabetes Science and Technology*, vol. 4, pp. 1127–1138, Sept. 2010.
- [126] C. Giacomozzi, A. Caselli, V. Macellari, L. Giurato, L. Lardieri, and L. Uccioli, "Walking Strategy in Diabetic Patients With Peripheral Neuropathy," *Diabetes Care*, vol. 25, no. 8, pp. 1451–1457, 2002.
- [127] A. Guiotto, Z. Sawacha, G. Guarneri, G. Cristoferi, A. Avogaro, and C. Cobelli, "The role of foot morphology on foot function in diabetic subjects with or without neuropathy," *Gait & Posture*, vol. 37, pp. 603–610, Apr. 2013.
- [128] S. Rao, C. L. Saltzman, and H. J. Yack, "Relationships between segmental foot mobility and plantar loading in individuals with and without diabetes and neuropathy," *Gait & posture*, vol. 31, no. 2, pp. 251–255, 2010.
- [129] J. B. Dingwell and P. R. Cavanagh, "Increased variability of continuous over-ground walking in neuropathic patients is only indirectly related to sensory loss," *Gait & Posture*, vol. 14, no. 1, pp. 1–10, 2001.
- [130] C. Giacomozzi, E. D'Ambrogio, S. Cesinaro, V. Macellari, and L. Uccioli, "Muscle performance and ankle joint mobility in long-term patients with diabetes," *BMC musculoskeletal disorders*, vol. 9, no. 1, p. 99, 2008.
- [131] P. R. Cavanagh and S. A. Bus, "Off-loading the diabetic foot for ulcer prevention and healing," *Journal of the American Podiatric Medical Association*, vol. 100, no. 5, pp. 360–368, 2010.
- [132] J. E. Morley, "Diabetes, sarcopenia, and frailty," *Clinics in geriatric medicine*, vol. 24, no. 3, pp. 455–469, 2008.
- [133] Z. Sawacha, F. Spolaor, G. Guarneri, P. Contessa, E. Carraro, A. Venturin, A. Avogaro, and C. Cobelli, "Abnormal muscle activation during gait in diabetes patients with and without neuropathy," *Gait & Posture*, vol. 35, pp. 101–105, Jan. 2012.

- [134] C. D. Sartor, R. Watari, A. C. Pássaro, A. P. Picon, R. H. Hasue, and I. C. Sacco, "Effects of a combined strengthening, stretching and functional training program versus usual-care on gait biomechanics and foot function for diabetic neuropathy: a randomized controlled trial," *BMC Musculoskeletal Disorders*, vol. 13, p. 36, Mar. 2012.
- [135] C. D. Sartor, R. H. Hasue, L. P. Cacciari, M. K. Butugan, R. Watari, A. C. Pássaro, C. Giacomozzi, and I. C. Sacco, "Effects of strengthening, stretching and functional training on foot function in patients with diabetic neuropathy: results of a randomized controlled trial," *BMC musculoskeletal disorders*, vol. 15, no. 1, p. 137, 2014.
- [136] R. E. Climie, C. Moran, M. Callisaya, L. Blizzard, J. E. Sharman, A. Venn, T. G. Phan, R. Beare, J. Forbes, N. B. Blackburn, *et al.*, "Abdominal obesity and brain atrophy in type 2 diabetes mellitus," *PloS one*, vol. 10, no. 11, p. e0142589, 2015.
- [137] S. Balducci, M. Sacchetti, J. Haxhi, G. Orlando, V. D'Errico, S. Fallucca, S. Menini, and G. Pugliese, "Physical exercise as therapy for type 2 diabetes mellitus," *Diabetes/metabolism research and reviews*, vol. 30, no. S1, pp. 13–23, 2014.
- [138] S. Balducci, S. Zanuso, P. Cardelli, L. Salvi, A. Bazuro, L. Pugliese, C. Maccora, C. Iacobini, F. G. Conti, A. Nicolucci, *et al.*, "Effect of high-versus low-intensity supervised aerobic and resistance training on modifiable cardiovascular risk factors in type 2 diabetes; the italian diabetes and exercise study (ides)," 2012.
- [139] S. R. Colberg, R. J. Sigal, B. Fernhall, J. G. Regensteiner, B. J. Blissmer, R. R. Rubin, L. Chasan-Taber, A. L. Albright, and B. Braun, "Exercise and type 2 diabetes the american college of sports medicine and the american diabetes association: joint position statement," *Diabetes care*, vol. 33, no. 12, pp. e147–e167, 2010.
- [140] N. D. Eves and R. C. Plotnikoff, "Resistance training and type 2 diabetes considerations for implementation at the population level," *Diabetes Care*, vol. 29, no. 8, pp. 1933–1941, 2006.
- [141] S. E. Inzucchi, R. M. Bergenstal, J. B. Buse, M. Diamant, E. Ferrannini, M. Nauck, A. L. Peters, A. Tsapas, R. Wender, and D. R. Matthews, "Management of hyperglycemia in type 2 diabetes: a patient-centered approach position statement of the american diabetes association (ada) and the european association for the study of diabetes (easd)," *Diabetes care*, vol. 35, no. 6, pp. 1364–1379, 2012.
- [142] K. M. Madden, "Evidence for the benefit of exercise therapy in patients with type 2 diabetes," *Diabetes, metabolic syndrome and obesity: targets and therapy*, vol. 6, p. 233, 2013.

## Bibliography

---

- [143] S.-G. Sazlina, C. Browning, and S. Yasin, "Interventions to promote physical activity in older people with type 2 diabetes mellitus: a systematic review," *Frontiers in public health*, vol. 1, 2013.
- [144] E. L. Feldman, M. Stevens, P. Thomas, M. Brown, N. Canal, and D. Greene, "A practical two-step quantitative clinical and electrophysiological assessment for the diagnosis and staging of diabetic neuropathy," *Diabetes care*, vol. 17, no. 11, pp. 1281–1289, 1994.
- [145] A. Cappozzo, A. Cappello, U. D. Croce, and F. Pensalfini, "Surface-marker cluster design criteria for 3-d bone movement reconstruction," *Biomedical Engineering, IEEE Transactions on*, vol. 44, no. 12, pp. 1165–1174, 1997.
- [146] V. Camomilla, A. Cereatti, G. Vannozzi, and A. Cappozzo, "An optimized protocol for hip joint centre determination using the functional method," *Journal of biomechanics*, vol. 39, no. 6, pp. 1096–1106, 2006.
- [147] P. M. H. Akashi, I. C. N. Sacco, R. Watari, and E. Hennig, "The effect of diabetic neuropathy and previous foot ulceration in EMG and ground reaction forces during gait," *Clinical Biomechanics*, vol. 23, pp. 584–592, June 2008.
- [148] L. Allet, S. Armand, A. Golay, D. Monnin, R. A. de Bie, and E. D. de Bruin, "Gait characteristics of diabetic patients: a systematic review," *Diabetes/Metabolism Research and Reviews*, vol. 24, pp. 173–191, Apr. 2008.
- [149] L. Allet, S. Armand, R. A. de Bie, A. Golay, D. Monnin, K. Aminian, J. B. Staal, and E. D. de Bruin, "The gait and balance of patients with diabetes can be improved: a randomised controlled trial," *Diabetologia*, vol. 53, pp. 458–466, Mar. 2010.
- [150] A. Raspovic, "Gait characteristics of people with diabetes-related peripheral neuropathy, with and without a history of ulceration," *Gait & Posture*, vol. 38, pp. 723–728, Sept. 2013.
- [151] M. Fernando, R. Crowther, P. Lazzarini, K. Sangla, M. Cunningham, P. Buttner, and J. Golledge, "Biomechanical characteristics of peripheral diabetic neuropathy: A systematic review and meta-analysis of findings from the gait cycle, muscle activity and dynamic barefoot plantar pressure," *Clinical Biomechanics*, vol. 28, no. 8, pp. 831–845, 2013.
- [152] P. R. Cavanagh, J. A. Derr, J. S. Ulbrecht, R. E. Maser, and T. J. Orchard, "Problems with gait and posture in neuropathic patients with insulin-dependent diabetes mellitus," *Diabetic Medicine: A Journal of the British Diabetic Association*, vol. 9, pp. 469–474, June 1992.

- [153] J. B. Dingwell, J. P. Cusumano, D. Sternad, and P. R. Cavanagh, "Slower speeds in patients with diabetic neuropathy lead to improved local dynamic stability of continuous overground walking," *Journal of Biomechanics*, vol. 33, pp. 1269–1277, Oct. 2000.
- [154] M. J. Mueller, S. D. Minor, S. A. Sahrman, J. A. Schaaf, and M. J. Strube, "Differences in the gait characteristics of patients with diabetes and peripheral neuropathy compared with age-matched controls," *Physical therapy*, vol. 74, no. 4, pp. 299–308, 1994.
- [155] E. C. Katoulis, M. Ebdon-Parry, H. Lanshammar, L. Vileikyte, J. Kulkarni, and A. J. Boulton, "Gait abnormalities in diabetic neuropathy," *Diabetes care*, vol. 20, no. 12, pp. 1904–1907, 1997.
- [156] A. P. Picon, C. D. Sartor, M. I. Roveri, A. C. Pássaro, N. R. Ortega, and I. C. N. Sacco, "Diabetic patients with and without peripheral neuropathy reveal different hip and ankle biomechanical strategies during stair descent," *Revista Brasileira De Fisioterapia (São Carlos (São Paulo, Brazil))*, vol. 16, pp. 528–534, Dec. 2012.
- [157] I. C. N. Sacco and A. C. Amadio, "A study of biomechanical parameters in gait analysis and sensitive cronaxie of diabetic neuropathic patients," *Clinical Biomechanics*, vol. 15, pp. 196–202, Mar. 2000.
- [158] S. Rao, C. Saltzman, and H. J. Yack, "Ankle ROM and stiffness measured at rest and during gait in individuals with and without diabetic sensory neuropathy," *Gait & Posture*, vol. 24, pp. 295–301, Nov. 2006.
- [159] A. L. Rosenbloom, A. Grgic, and J. L. Frias, "Diabetes Mellitus, Short Stature and Joint Stiffness — a New Syndrome," *Pediatric Research*, vol. 8, pp. 441–441, Apr. 1974.
- [160] O.-Y. Kwon, S. D. Minor, K. S. Maluf, and M. J. Mueller, "Comparison of muscle activity during walking in subjects with and without diabetic neuropathy," *Gait & posture*, vol. 18, no. 1, pp. 105–113, 2003.
- [161] D. E. Kelley, J. He, E. V. Menshikova, and V. B. Ritov, "Dysfunction of mitochondria in human skeletal muscle in type 2 diabetes," *Diabetes*, vol. 51, no. 10, pp. 2944–2950, 2002.
- [162] V. Zatsiorsky, V. Seluyanov, and L. Chugunova, "Methods of determining mass-inertial characteristics of human body segments," *Contemporary problems of biomechanics*, vol. 272, p. 291, 1990.

## Bibliography

---

- [163] A. J. Boulton, L. Vileikyte, G. Ragnarson-Tennvall, and J. Apelqvist, "The global burden of diabetic foot disease," *The Lancet*, vol. 366, no. 9498, pp. 1719–1724, 2005.
- [164] C. A. Abbott, L. Vileikyte, S. Williamson, A. L. Carrington, and A. J. Boulton, "Multicenter study of the incidence of and predictive risk factors for diabetic neuropathic foot ulceration," *Diabetes Care*, vol. 21, pp. 1071–1075, July 1998.
- [165] S. A. Bus, J. S. Ulbrecht, and P. R. Cavanagh, "Pressure relief and load redistribution by custom-made insoles in diabetic patients with neuropathy and foot deformity," *Clinical Biomechanics*, vol. 19, no. 6, pp. 629–638, 2004.
- [166] M. J. Mueller, M. Hastings, P. K. Commean, K. E. Smith, T. K. Pilgram, D. Robertson, and J. Johnson, "Forefoot structural predictors of plantar pressures during walking in people with diabetes and peripheral neuropathy," *Journal of Biomechanics*, vol. 36, pp. 1009–1017, July 2003.
- [167] P. R. Cavanagh, G. G. Simoneau, and J. S. Ulbrecht, "Ulceration, unsteadiness, and uncertainty: the biomechanical consequences of diabetes mellitus," *Journal of Biomechanics*, vol. 26 Suppl 1, pp. 23–40, 1993.
- [168] W. R. Ledoux, J. B. Shofer, D. G. Smith, K. Sullivan, S. G. Hayes, M. Assal, and G. E. Reiber, "Relationship between foot type, foot deformity, and ulcer occurrence in the high-risk diabetic foot," *Journal of Rehabilitation Research and Development*, vol. 42, pp. 665–672, Oct. 2005.
- [169] K. M. Patil, L. H. Braak, and A. Huson, "Analysis of stresses in two-dimensional models of normal and neuropathic feet," *Medical & Biological Engineering & Computing*, vol. 34, pp. 280–284, July 1996.
- [170] G. Yarnitzky, Z. Yizhar, and A. Gefen, "Real-time subject-specific monitoring of internal deformations and stresses in the soft tissues of the foot: a new approach in gait analysis," *Journal of Biomechanics*, vol. 39, no. 14, pp. 2673–2689, 2006.
- [171] A. Guiotto, A. Scarton, Z. Sawacha, G. Guarneri, A. Avogaro, and C. Cobelli, "Gait analysis driven 2d finite element model of the neuropathic hindfoot," *Journal of Mechanics in Medicine and Biology*, p. 1650012, Mar. 2015.
- [172] E. Carson and C. Cobelli, "Finite element modelling in musculoskeletal biomechanics," in *Modeling Methodology for Physiology and Medicine*, Elsevier, 2013.
- [173] J. L. Hicks, T. K. Uchida, A. Seth, A. Rajagopal, and S. L. Delp, "Is my model good enough? best practices for verification and validation of musculoskeletal

- models and simulations of movement,” *Journal of biomechanical engineering*, vol. 137, no. 2, p. 020905, 2015.
- [174] P. Saraswat, M. S. Andersen, and B. A. MacWilliams, “A musculoskeletal foot model for clinical gait analysis,” *Journal of Biomechanics*, vol. 43, pp. 1645–1652, June 2010.
- [175] M. Błażkiewicz, L. Sundar, A. Healy, A. Ramachandran, N. Chockalingam, and R. Naemi, “Assessment of lower leg muscle force distribution during isometric ankle dorsi and plantar flexion in patients with diabetes: a preliminary study,” *Journal of Diabetes and its Complications*, vol. 29, no. 2, pp. 282–287, 2015.
- [176] L. Modenese, A. Gopalakrishnan, and A. Phillips, “A novel computational framework for deducing muscle synergies from experimental joint moments,” 2015.
- [177] J.-W. Seo, D.-W. Kang, J.-Y. Kim, S.-T. Yang, D.-H. Kim, J.-S. Choi, and G.-R. Tack, “Finite element analysis of the femur during stance phase of gait based on musculoskeletal model simulation,” *Bio-medical materials and engineering*, vol. 24, no. 6, pp. 2485–2493, 2014.
- [178] G. Valente, F. Taddei, and I. Jonkers, “Influence of weak hip abductor muscles on joint contact forces during normal walking: probabilistic modeling analysis,” *Journal of Biomechanics*, vol. 46, pp. 2186–2193, Sept. 2013.
- [179] E. L. Feldman, M. J. Stevens, P. K. Thomas, M. B. Brown, N. Canal, and D. A. Greene, “A practical two-step quantitative clinical and electrophysiological assessment for the diagnosis and staging of diabetic neuropathy,” *Diabetes Care*, vol. 17, pp. 1281–1289, Nov. 1994.
- [180] A. Gefen, M. Megido-Ravid, Y. Itzchak, and M. Arcan, “Biomechanical analysis of the three-dimensional foot structure during gait: a basic tool for clinical applications,” *Journal of biomechanical engineering*, vol. 122, no. 6, pp. 630–639, 2000.
- [181] G. Wu, S. Siegler, P. Allard, C. Kirtley, A. Leardini, D. Rosenbaum, M. Whittle, D. D D’Lima, L. Cristofolini, H. Witte, *et al.*, “Isb recommendation on definitions of joint coordinate system of various joints for the reporting of human joint motion—part i: ankle, hip, and spine,” *Journal of biomechanics*, vol. 35, no. 4, pp. 543–548, 2002.
- [182] J. T.-M. Cheung, M. Zhang, A. K.-L. Leung, and Y.-B. Fan, “Three-dimensional finite element analysis of the foot during standing—a material sensitivity study,” *Journal of Biomechanics*, vol. 38, pp. 1045–1054, May 2005.

## Bibliography

---

- [183] M. Cowley, E. Boyko, J. Shofer, J. Ahroni, and W. Ledoux, "Foot ulcer risk and location in relation to prospective clinical assessment of foot shape and mobility among persons with diabetes," *Diabetes Research and Clinical Practice*, vol. 82, no. 2, pp. 226–232, 2008.
- [184] C. Giacomozzi and F. Martelli, "Peak pressure curve: An effective parameter for early detection of foot functional impairments in diabetic patients," *Gait & Posture*, vol. 23, pp. 464–470, June 2006.
- [185] W. R. Ledoux, E. S. Rohr, R. P. Ching, and B. J. Sangeorzan, "Effect of foot shape on the three-dimensional position of foot bones," *Journal of Orthopaedic Research: Official Publication of the Orthopaedic Research Society*, vol. 24, pp. 2176–2186, Dec. 2006.
- [186] A. Leardini, L. Chiari, U. D. Croce, and A. Cappozzo, "Human movement analysis using stereophotogrammetry: Part 3. Soft tissue artifact assessment and compensation," *Gait & Posture*, vol. 21, pp. 212–225, Feb. 2005.
- [187] M. G. Pandy, "Computer modeling and simulation of human movement," *Annual Review of Biomedical Engineering*, vol. 3, pp. 245–273, 2001.
- [188] Z.-h. Qian, L. Ren, Y. Ding, and L. Ren, "A three-dimensional musculoskeletal model of the human foot complex using finite element method," *ISB 2011-Bruxelles*, 2011.
- [189] Y.-C. Hsu, Y.-W. Gung, S.-L. Shih, C.-K. Feng, S.-H. Wei, C.-h. Yu, and C.-S. Chen, "Using an Optimization Approach to Design an Insole for Lowering Plantar Fascia Stress—A Finite Element Study," *Annals of Biomedical Engineering*, vol. 36, pp. 1345–1352, Aug. 2008.
- [190] M. G. Pandy and T. P. Andriacchi, "Muscle and joint function in human locomotion," *Annual Review of Biomedical Engineering*, vol. 12, pp. 401–433, Aug. 2010.
- [191] John T. Hansen, *Interactive atlas of human anatomy*. italian edition 2006, masson spa, elsevier. ed.
- [192] "The muscles and fasciae of the foot."
- [193] J. T.-M. Cheung, M. Zhang, and K.-N. An, "Effect of Achilles tendon loading on plantar fascia tension in the standing foot," *Clinical Biomechanics (Bristol, Avon)*, vol. 21, pp. 194–203, Feb. 2006.



- [194] A. Phillips, P. Pankaj, C. Howie, A. Usmani, and A. Simpson, "Finite element modelling of the pelvis: inclusion of muscular and ligamentous boundary conditions," *Medical engineering & physics*, vol. 29, no. 7, pp. 739–748, 2007.
- [195] C.-C. Hsu, W.-C. Tsai, C.-L. Wang, S.-H. Pao, Y.-W. Shau, and Y.-S. Chuan, "Microchambers and macrochambers in heel pads: are they functionally different?," *Journal of Applied Physiology*, vol. 102, no. 6, pp. 2227–2231, 2007.
- [196] Y. Gu, J. Li, X. Ren, M. J. Lake, and Y. Zeng, "Heel skin stiffness effect on the hind foot biomechanics during heel strike," *Skin Research and Technology: Official Journal of International Society for Bioengineering and the Skin (ISBS) [and] International Society for Digital Imaging of Skin (ISDIS) [and] International Society for Skin Imaging (ISSI)*, vol. 16, pp. 291–296, Aug. 2010.
- [197] G. Sciumè, D. Boso, W. Gray, C. Cobelli, and B. Schrefler, "A two-phase model of plantar tissue: a step toward prediction of diabetic foot ulceration," *International journal for numerical methods in biomedical engineering*, vol. 30, no. 11, pp. 1153–1169, 2014.
- [198] A. Barré, B. M. Jolles, N. Theumann, and K. Aminian, "Soft tissue artifact distribution on lower limbs during treadmill gait: Influence of skin markers' location on cluster design," *Journal of biomechanics*, 2015.
- [199] A. Gefen, M. Megido-Ravid, and Y. Itzchak, "In vivo biomechanical behavior of the human heel pad during the stance phase of gait," *Journal of Biomechanics*, vol. 34, pp. 1661–1665, Dec. 2001.
- [200] L. Tersì and R. Stagni, "Effect of calibration error on bone tracking accuracy with fluoroscopy," *Journal of Biomechanical Engineering*, vol. 136, p. 054502, May 2014.
- [201] R. Stagni, S. Fantozzi, A. Cappello, and A. Leardini, "Quantification of soft tissue artefact in motion analysis by combining 3d fluoroscopy and stereophotogrammetry: a study on two subjects," *Clinical Biomechanics*, vol. 20, pp. 320–329, Mar. 2005.
- [202] B. Michaud, M. Jackson, A. Arndt, A. Lundberg, and M. Begon, "Determining in vivo sternoclavicular, acromioclavicular and glenohumeral joint centre locations from skin markers, ct-scans and intracortical pins: A comparison study," *Medical Engineering & Physics*, 2016.

## Bibliography

---

- [203] F. Dal Maso, Y. Blache, M. Raison, A. Lundberg, and M. Begon, “Glenohumeral joint kinematics measured by intracortical pins, reflective markers, and computed tomography: A novel technique to assess acromiohumeral distance,” *Journal of Electromyography and Kinesiology*, 2015.
- [204] L. Bosmans, G. Valente, M. Wesseling, A. Van Campen, F. De Groote, J. De Schutter, and I. Jonkers, “Sensitivity of predicted muscle forces during gait to anatomical variability in musculotendon geometry,” *Journal of biomechanics*, 2015.
- [205] P. J. Hunter, “The IUPS Physiome Project: a framework for computational physiology,” *Progress in Biophysics and Molecular Biology*, vol. 85, pp. 551–569, July 2004.
- [206] M. L. Neal and R. Kerckhoffs, “Current progress in patient-specific modeling,” *Briefings in Bioinformatics*, vol. 11, pp. 111–126, Jan. 2010.
- [207] S. Martelli, F. Taddei, D. Testi, S. L. Delp, and M. Viceconti, “NMSBuilder: an application to personalize NMS models,” (Brussels), 2011.
- [208] L. Antiga, M. Piccinelli, L. Botti, B. Ene-Iordache, A. Remuzzi, and D. A. Steinman, “An image-based modeling framework for patient-specific computational hemodynamics,” *Medical & Biological Engineering & Computing*, vol. 46, pp. 1097–1112, Nov. 2008.
- [209] Kent DM and Hayward RA, “Limitations of applying summary results of clinical trials to individual patients: The need for risk stratification,” *JAMA*, vol. 298, pp. 1209–1212, Sept. 2007.
- [210] G. Valente, *Subject-specific musculoskeletal models of the lower limbs for the prediction of skeletal loads during motion*. PhD thesis, Alma Mater Studiorum Università di Bologna, Bologna, Italy, Apr. 2013.
- [211] G. T. Charras and R. E. Guldborg, “Improving the local solution accuracy of large-scale digital image-based finite element analyses,” *Journal of Biomechanics*, vol. 33, pp. 255–259, Feb. 2000.
- [212] L. I. Smith, “A tutorial on Principal Components Analysis,” Feb. 2002.
- [213] M. Singhchawla, “A combined pcaica statistical approach and quadratic spline wavelets for detection of R-peaks and heart rate estimations in electrocardiograms,” *Journal of Mechanics in Medicine and Biology*, vol. 11, no. 03, 2011.
- [214] R. Bro and A. K. Smilde, “Principal component analysis,” *Analytical Methods*, vol. 6, no. 9, p. 2812, 2014.

- 
- [215] H. Abdi and L. J. Williams, "Principal component analysis," *Wiley Interdisciplinary Reviews: Computational Statistics*, vol. 2, pp. 433–459, July 2010.
- [216] V. Perlibakas, "Distance Measures for PCA-based Face Recognition," *Pattern Recogn. Lett.*, vol. 25, pp. 711–724, Apr. 2004.
- [217] M. R. Mahfouz, B. C. Merkl, E. E. A. Fatah, R. B. Jr, and J. N. Argenson, "Automatic methods for characterization of sexual dimorphism of adult femora: distal femur," *Computer Methods in Biomechanics and Biomedical Engineering*, vol. 10, pp. 447–456, Dec. 2007.
- [218] F. H. Low, L. P. Khoo, C. K. Chua, and N. N. Lo, "Determination of the major dimensions of femoral implants using morphometrical data and principal component analysis," *Proceedings of the Institution of Mechanical Engineers, Part H: Journal of Engineering in Medicine*, vol. 214, pp. 301–309, Mar. 2000.
- [219] A. B. Mohamed Mahfouz, "Patella sex determination by 3d statistical shape models and nonlinear classifiers," *Forensic science international*, vol. 173, no. 2-3, pp. 161–70, 2008.
- [220] M. Chawla, "Detection of indeterminacies in corrected ecg signals using parameterized multidimensional independent component analysis," *Computational and Mathematical Methods in Medicine*, vol. 10, no. 2, pp. 85–115, 2009.
- [221] R. L. Actis, L. B. Ventura, D. J. Lott, K. E. Smith, P. K. Commean, M. K. Hastings, and M. J. Mueller, "Multi-plug insole design to reduce peak plantar pressure on the diabetic foot during walking," *Medical & biological engineering & computing*, vol. 46, pp. 363–371, Apr. 2008.
- [222] R. L. Actis, L. B. Ventura, K. E. Smith, P. K. Commean, D. J. Lott, T. K. Pilgram, and M. J. Mueller, "Numerical simulation of the plantar pressure distribution in the diabetic foot during the push-off stance," *Medical & Biological Engineering & Computing*, vol. 44, pp. 653–663, Aug. 2006.
- [223] W.-M. Chen, T. Lee, P. V.-S. Lee, J. W. Lee, and S.-J. Lee, "Effects of internal stress concentrations in plantar soft-tissue—A preliminary three-dimensional finite element analysis," *Medical Engineering & Physics*, vol. 32, pp. 324–331, May 2010.
- [224] L. Xinshan, *Modelling Levator Ani Mechanics During the Second Stage of Labour*. PhD thesis, The Auckland Bionengineering Institute, The University of Auckland, Feb. 2011.

## Bibliography

---

- [225] “Peripheral Arterial Disease in People With Diabetes,” *Diabetes Care*, vol. 26, pp. 3333–3341, Dec. 2003.
- [226] P. J. Besl and N. D. McKay, “Method for registration of 3-d shapes,” in *Robotics-DL tentative*, pp. 586–606, International Society for Optics and Photonics, 1992.
- [227] M. Kazhdan, M. Bolitho, and H. Hoppe, “Poisson surface reconstruction,” in *Proceedings of the fourth Eurographics symposium on Geometry processing*, vol. 7, 2006.
- [228] L. Grassi, E. Schileo, C. Boichon, M. Viceconti, and F. Taddei, “Comprehensive evaluation of PCA-based finite element modelling of the human femur,” *Medical Engineering & Physics*, vol. 36, pp. 1246–1252, Oct. 2014.
- [229] R. Bouillon, “Diabetic bone disease,” *Calcified Tissue International*, vol. 49, pp. 155–160, May 1991.
- [230] M. E. Levin, V. C. Boisseau, and L. V. Avioli, “Effects of Diabetes Mellitus on Bone Mass in Juvenile and Adult-Onset Diabetes,” *New England Journal of Medicine*, vol. 294, pp. 241–245, Jan. 1976.
- [231] E. D’Ambrogi, L. Giurato, M. A. D’Agostino, C. Giacomozzi, V. Macellari, A. Caselli, and L. Uccioli, “Contribution of Plantar Fascia to the Increased Fore-foot Pressures in Diabetic Patients,” *Diabetes Care*, vol. 26, pp. 1525–1529, May 2003.
- [232] M. S. Cowley, E. J. Boyko, J. B. Shofer, J. H. Ahroni, and W. R. Ledoux, “Foot ulcer risk and location in relation to prospective clinical assessment of foot shape and mobility among persons with diabetes,” *Diabetes Research and Clinical Practice*, vol. 82, pp. 226–232, Nov. 2008.
- [233] J. S. Bevans and P. Bowker, “Foot structure and function: aetiological risk factors for callus formation in diabetic and non-diabetic subjects,” *The Foot*, vol. 9, pp. 120–127, Sept. 1999.
- [234] I. a. J. Radcliffe, P. Prescott, H. S. Man, and M. Taylor, “Determination of suitable sample sizes for multi-patient based finite element studies,” *Medical Engineering and Physics*, vol. 29, pp. 1065–1072, Dec. 2007.
- [235] A. Hyvärinen and E. Oja, “Independent component analysis: algorithms and applications,” *Neural networks*, vol. 13, no. 4, pp. 411–430, 2000.
- [236] T. He, G. Clifford, and L. Tarassenko, “Application of independent component analysis in removing artefacts from the electrocardiogram,” *Neural Computing & Applications*, vol. 15, no. 2, pp. 105–116, 2006.

- [237] M. P. S. Chawla, "Parameterization and R-Peak Error Estimations of ECG Signals Using Independent Component Analysis," *Computational and Mathematical Methods in Medicine*, vol. 8, no. 4, pp. 263–285, 2007.
- [238] M. Chawla, "Pca and ica processing methods for removal of artifacts and noise in electrocardiograms: A survey and comparison," *Applied Soft Computing*, vol. 11, no. 2, pp. 2216–2226, 2011.
- [239] G. Dhatt, E. Lefrançois, and G. Touzot, *Finite element method*. John Wiley & Sons, 2012.
- [240] D. Ascani, C. Mazzà, A. De Lollis, M. Bernardoni, and M. Viceconti, "A procedure to estimate the origins and the insertions of the knee ligaments from computed tomography images," *Journal of Biomechanics*, vol. 48, pp. 233–237, Jan. 2015.